# Performance Analysis of Energy Detector over Different Generalised Wireless Channels Based Spectrum Sensing in Cognitive Radio

By: Hussien Al-Hmood

A Thesis Submitted in Fulfilment of the Requirements

for the Degree of Doctor of Philosophy (PhD)

in

Communications

Department of Electronic and Computer Engineering,

College of Engineering, Design and Physical Sciences

Brunel University

London, United Kingdom

Supervised By: Professor Hamed Al-Raweshidy

July 2015

*Dedicated to master of martyrs,*
*my country (Iraq) martyrs,*
*my brother martyr (Ali),*
*my mother,*
*my father,*
*my wife,*
*my brother,*
*and my sisters.*

# Abstract

This thesis extensively analyses the performance of an energy detector which is widely employed to perform spectrum sensing in cognitive radio over different generalised channel models. In this analysis, both the average probability of detection and the average area under the receiver operating characteristic curve (AUC) are derived using the probability density function of the received instantaneous signal to noise ratio (SNR). The performance of energy detector over an $\eta - \mu$ fading, which is used to model the Non-line-of-sight (NLoS) communication scenarios is provided. Then, the behaviour of the energy detector over $\kappa - \mu$ shadowed fading channel, which is a composite of generalized multipath/shadowing fading channel to model the line-of-sight (LoS) communication medium is investigated. The analysis of the energy detector over both $\eta - \mu$ and $\kappa - \mu$ shadowed fading channels are then extended to include maximal ratio combining (MRC), square law combining (SLC) and square law selection (SLS) with independent and non-identically ($i.n.d$) diversity branches.

To overcome the problem of mathematical intractability in analysing the energy detector over $i.n.d$ composite fading channels with MRC and selection combining (SC), two different unified statistical properties models for the sum and the maximum of mixture gamma (MG) variates are derived. The first model is limited by the value of the shadowing severity index, which should be an integer number and has been employed to study the performance of energy detector over composite $\alpha - \mu$/gamma fading channel. This channel is proposed to represent the non-linear prorogation environment. On the other side, the second model is general and has been utilised to analyse the behaviour of energy detector over composite $\eta - \mu$/gamma fading channel.

Finally, a special filter-bank transform which is called slantlet packet transform (SPT) is developed and used to estimate the uncertain noise power. Moreover, signal denoising based on hybrid slantlet transform (HST) is employed to reduce the noise impact on the performance of energy detector. The combined SPT-HST approach improves the detection capability of energy detector with 97% and reduces the total computational complexity by nearly 19% in comparison with previously implemented work using filter-bank transforms. The aforementioned percentages are measured at specific SNR, number of selected samples and levels of signal decomposition.

# Acknowledgements

First of all, I would like to express my appreciation and gratefulness to the Martyrs Foundation for funding my PhD study.

I would like to thank my supervisor Professor Hamed Al-Raweshidy for his valuable advices and guidance during the PhD period. He has been very helpful and supportive for all these years.

I am thankful to my second supervisor Dr. Rajagopal Nilavalan for his encouragement and support. My gratitude goes to my colleagues in the Wireless Networks and Communications Centre (WNCC), who have been supportive throughout this period.

I would like to acknowledge the great attitude of all the staff members that I have interacted with at Brunel University and specifically in the department of Electronic and Computer Engineering.

I am very grateful to all my friends who always show their care and support. A special thank to my best friend Hayder Nsaeef and Falah Jassim whose support was precious.

Finally, to my brother, sisters and wife: thank you for being beside me as a source of care, love, motivation and encouragement, which travel the distance that separates us, and fill me with patience and commitment. Especially to my brother, who has always been my main inspiration and always urged me to pursue higher level of education and complete my PhD studies.

# Table of Contents

# List of Figures

# List of Tables

# List of Abbreviations

| Abbreviation | Definition |
|---|---|
| AWGN | additive white Gaussian noise |
| AMI | advanced metering infrastructure |
| ATSC | advanced television system committee |
| AF | amplify and forward |
| ADC | analog-to-digital converter |
| AUC | area under the receiver operating characteristics |
| ABEP | average bit error rate probability |
| | |
| BPF | band-pass filter |
| BS | base station |
| BPSK | binary phase shift keying |
| BER | bit error rate |
| | |
| CLT | central limit theorem |
| CSI | channel state information |
| CR | cognitive radio |
| CRU | cognitive radio user |
| CAUC | complementary area under the receiver operating characteristics |
| CROC | complementary receiver operating characteristics |
| CSS | cooperative spectrum sensing |
| CoMP | coordinated multiple point |
| CDF | cumulative distribution function |
| CFD | cyclostationary feature detection |
| | |
| DoF | degrees of freedom |
| DSP | digital signal processing |

| | |
|---|---|
| DWT | discrete Wavelet transform |
| DWPT | discrete Wavelet packet transform |
| | |
| ED | energy detector |
| EGC | equal gain combining |
| | |
| FFT | fast Fourier transform |
| FAN | field area networks |
| FC | fusion centre |
| FM | frequency modulation |
| | |
| GSM | global system for mobile communications |
| | |
| HAN | home/building area networks |
| HST | hybrid Slantlet transform |
| | |
| i.i.d | independent and identically distributed |
| i.n.d | independent and non-Identically distributed |
| | |
| LoS | line-of-sight |
| LTE | long-term evolution |
| | |
| MFD | matched filtering detection |
| MBAN | medical body area network |
| MG | mixture gamma |
| MGF | moment generating function |
| MIMO | multiple-input multiple-output |
| MRC | maximal ratio combining |
| | |
| NLoS | non-line-of-sight |

| | |
|---|---|
| OP | outage probability |
| | |
| PU | primary user |
| PU Tx | primary user receiver |
| PU Tx | primary user transmitter |
| PDF | probability density function |
| | |
| QPSK | quadrature phase shift keying |
| | |
| RF | radio frequency |
| ROC | receiver operating characteristics |
| RV | random variable |
| | |
| SDR | software-defined radio |
| SU | secondary user |
| SC | selection combining |
| SUN | smart utility network |
| SNR | signal-to-noise ratio |
| ST | Slantlet transform |
| SPT | Slantlet packet transform |
| SDR | software-defined radio |
| SS | spectrum sensing |
| SLC | square law combining |
| SLS | square law selection |
| | |
| TCC | total computational complexity |
| | |
| UWB | ultra-wide band |

WAN                      wide area network

WRAN                 wireless regional area network

# List of Symbols

‡ Basic arithmetic, and calculus notations have standard definitions.

## Elementary and Special Functions

| Notation | Definition |
|---|---|
| $\Gamma(.)$ | Gamma function |
| $\Gamma(.,.)$ | upper incomplete function |
| $G(.,.)$ | lower incomplete function |
| $I_a(.)$ | modified Bessel function of the first kind and $a$ order |
| $U(.;.;.)$ | confluent hypergeometric function of the second kind |
| $\ln(.)$ | natural logarithm |
| $\log_2(.)$ | logarithm to base 2 |
| ${}_1F_1(.;.;.)$ | confluent hypergeometric function of the first kind |
| ${}_2F_1(.,.;.;.)$ | Gaussian hypergeometric function |
| ${}_1\tilde{F}_1(.;.;.)$ | regularized confluent hypergeometric function of the first kind |
| $Q_u(.,.)$ | $u$th order generalized Marcum-Q function |
| $Q(.)$ | Gaussian-Q function |
| $U(.)$ | modified Bessel function of the second kind |
| $F_2(.;.;.)$ | double variables Appell hypergeometric function |
| $F_M(.;.;.)$ | triple variables Saran hypergeometric function |
| $(\varepsilon)_j$ | Pochhammer symbol |
| $\Phi_2^{(M)}(.;.;.)$ | confluent multivariate hypergeometric function |
| $\Phi_2(.;.;.)$ | confluent bivariate hypergeometric function |
| $\tilde{\Phi}_3(.;.;.,.)$ | regularized bivariate confluent hypergeometric function |
| $F_{C:D^1;...;D^{(n)}}^{A:B^1;...;B^{(n)}}\left(.\right)$ | Srivastava and Daoust hypergeometric function |
| $F_G(.)$ | another form of the triple variables Saran hypergeometric |

|  |  |
|---|---|
|  | function |
| $F_D^{(2)}$ | another model of the double variables Lauricella hypergeometric function |
| $F_D^{(M)}(.)$ | another form of the multivariate Lauricella hypergeometric function |
| $F_1(.)$ | another form of the double variables Appell hypergeometric function |
| $\mathbf{H}_4(.)$ | double variables Horn hypergeometric function |
| $X_{15}(.)$ | triple variables Exton hypergeometric function |
| $F_A^{(M)}(.)$ | another model of the multivariate Lauricella hypergeometric function |

## Probability and Statistics

| Notation | Definition |
|---|---|
| $\mathbb{E}\{.\}$ | expectation |
| $\mathbb{V}\mathrm{ar}\{.\}$ | variance |
| $f_\gamma(.)$ | probability density function of $\gamma$ |
| $F_\gamma(.)$ | cumulative distribution function of $\gamma$ |
| $\mathcal{M}_\gamma(.)$ | moment generating function of $\gamma$ |
| $\Pr(X)$ | probability of $X$ |

# List of Publications

1. **H. Al-Hmood**, and H. S. Al-Raweshidy, "Performance analysis of energy detector over $\eta - \mu$ fading channel: PDF-based approach," *Electronics Lett.*, vol. 51, no. 3, pp. 249-251, Feb. 2015.

2. R. S. Abbas, **H. Al-Hmood**, S. H. Amin, and H. S. Al-Raweshidy, "A distributed algorithm in WDM network to increase network capacity and minimize conversion range," *Int. J. of Advances in Eng. Science & Technol. (IJAEST)*, vol. 2, no. 2, pp. 137-143, Nov. 2013.

3. **H. Al-Hmood**, and H. S. Al-Raweshidy, "Signal denoising using hybrid slantlet transform based energy detector in cognitive radios," in *Proc. IEEE IFIP Wireless Days (WD)*, Nov. 2013, pp. 1-3.

4. **H. Al-Hmood**, and H. S. Al-Raweshidy, "Energy detection performance enhancement for cognitive radio using noise processing approach," in *Proc. IEEE Global Information Infrastructure Symp. (GIIS)*, Oct. 2013, pp. 1-6.

5. **H. Al-Hmood**, R. S. Abbas, A. Masrub, and H. S. Al-Raweshidy, "An estimation of primary user's SNR for spectrum sensing in cognitive radios," in *Proc. IEEE Int. Conf. Innovative Computing Technol. (INTECH)*, Aug. 2013, pp. 479-484.

6. A. Masrub, R. S. Abbas, **H. Al-Hmood**, M. Iqbal, and H. S. Al-Raweshidy, "Cooperative sensing for dynamic spectrum access in cognitive wireless mesh networks," in *Proc. IEEE Int. Symp. Broadband Multimedia Systems and Broadcasting (BMSB)*, June 2013, pp. 1-5.

# Chapter 1

# Introduction

## 1.1  Wireless Communications

*"Every day sees humanity more victorious in the struggle with space and time."*

*Guglielmo Marconi*

Since the late 19th century and the beginning of 20th century and the radio communications have witnessed rapid advances. This development has affected clearly on the life of people everywhere and at every moment. Therefore, to get maximum benefit from the radio frequency (RF) spectrum, governments have divided it into different bands and allocated each band for a certain application as shown in Fig. 1.1 (top of the next page). Moreover, this division alleviates the interference among adjacent bands and reduces the waste of the spectrum.

The rapid growth in wireless communications has increased the demand for the RF spectrum. To employ the RF spectrum efficiently and effectively, different technologies have been proposed. The features for some of these modern technologies are listed as follows.

- Cooperative communications: In this type of communications, multiple nodes are employed in transmitting the data to a receiver. This leads to high transmission reliability and high data rate. The cooperative communications can be implemented using different techniques such as relay, distributed antenna

1
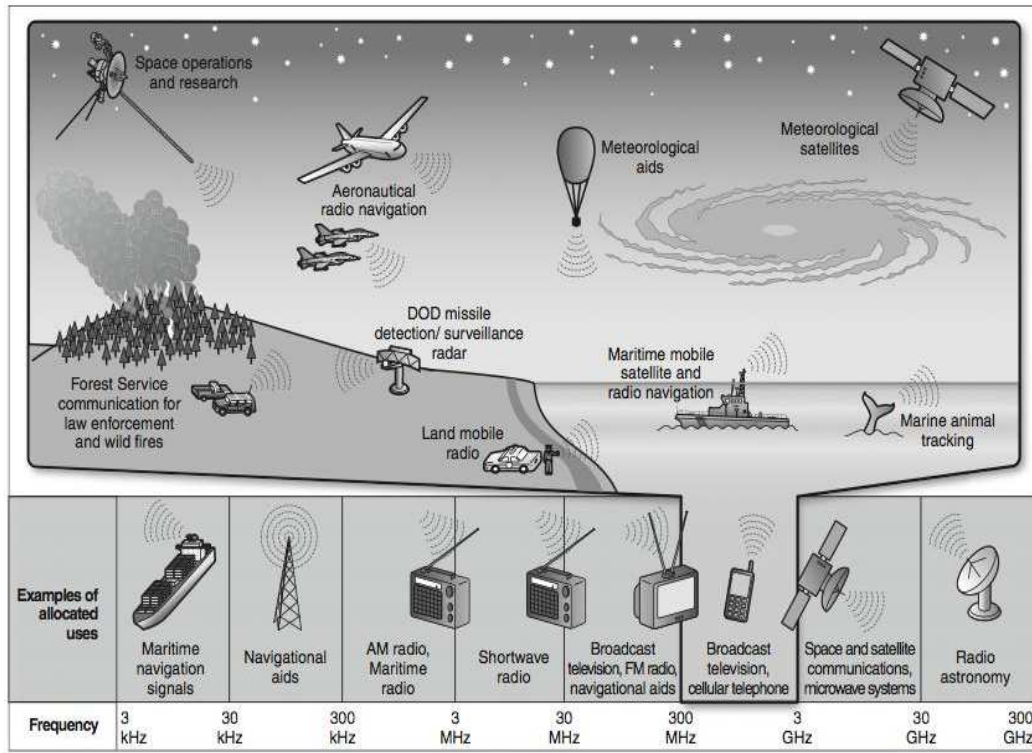
Figure 1.1: Examples of radio spectrum allocation for wireless communications [1].

systems (DAS), multi-cell coordination and group cell. In relay technique, a low power signal sends from the source to the destination with the help of a third party which is called relay node [2]. Distributed antenna systems or co-operative multiple-input multiple-output (MIMO) schemes are based on using a number of antennas for each user. The main usefulness of the distributed antenna system is to enhance the signal quality and the channel capacity by exploiting the advantages of both cooperative and MIMO systems. Unlike the relay technique in which the bandwidth is used by the transceiver and the relay, the distributed antenna system does not need more radio resources. In the open technical literature, the cooperative MIMO has been achieved in three schemes which are coordinated multiple point (CoMP) transmission and reception, fixed relay and mobile relay [3]. Multi-cell coordination technique has been used to alleviate the interference that is generated by multiple site transmission of the

2

cellular systems [4]. In group cell approach, in order to communicate with a certain user, the same resources are employed by some adjacent cells whereas they use various resources to communicate with various users [2].

- Massive MIMO: Massive MIMO systems or large scale antenna systems (LSAS) improve the throughput and the radiated energy efficiency by concentrating the power into ever smaller regions of space. Other advantages of massive MIMO include the use of simple signal processing and cheap low-power components. In massive MIMO, each base station (BS) is equipped with a few hundreds of antennas that simultaneously serve a large number of users in the same time-frequency resource [5]. In [6], a non-cooperative massive MIMO system with simple linear processing approach could provide a data rate of 17 Mb/s for each 40 users in a 20 MHz channel in both directions of links (uplink and downlink) with an overall spectral efficiency of 26.5 bps/Hz and an average throughput of 730 Mb/s per cell. Massive multi-user MIMO (MU-MIMO) systems exploit the multi-user diversity to achieve higher spectral efficiency than the point-to-point massive multi-user MIMO systems. Since the number of users in the massive MU-MIMO systems is supposed to be less than the number of antennas at the BS, a large number of degrees of freedom is available and can be employed to avoid the interference between the transmitted signals [7].

- Cognitive radio technology: In November 2002, the Federal Communication Commission (FCC) in the United States announced that the allocation for fixed spectrum causes inefficient use of radio spectrum. This is because most of the channels actively transmit the information (occupied the band) only for a short period while a certain part of the spectrum band (between 80% and 90%) is unused (called spectrum hole) when and where the licensed users are off as illustrated in Fig. 1.2 (top of the next page). Therefore, the problem of the lack of RF spectrum is not a result of scarcity of spectrum but a result of wasteful fixed spectrum assignments [8]. In order to mitigate this problem, cognitive radio (CR), inclusive of software-defined radio (SDR), has been suggested to be a tempting solution to the problem of spectral scarcity by defining opportunistic

3
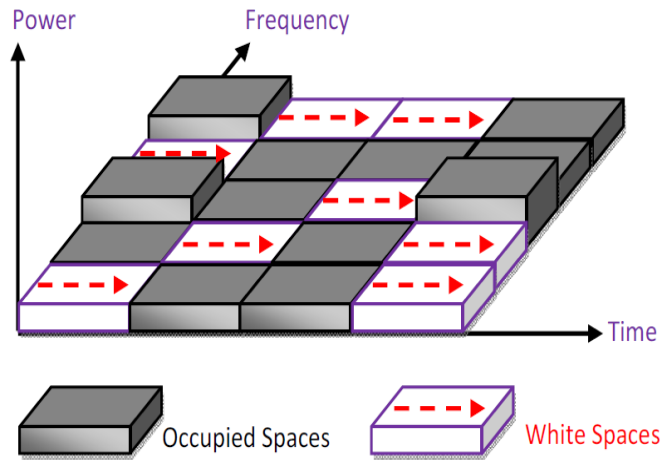
Figure 1.2: Scheme explains the occupied and the white spaces in the TV frequency bands.

usage of the RF bands that are not used by the licensed users such as TV bands [9-12]. The unoccupied TV spectrum bands by the authorized user is called TV white spaces. With the use of CR technology, the larger density of wireless employers can be accommodated without needing for a new RF spectrum band. Moreover, CR technique eases the spectrum sharing and leads to increase the spectrum efficiency with no harmful interference to the incumbent licensed users which include TV users and wireless microphone users.

In CR networks, there are two types of users: the primary users (PU)s which are licensed users and the secondary (cognitive) users (SU)s which are unlicensed users. The PU has the higher priority on the utilization of a specific part of the frequency band whereas the SU has the lower priority to occupy the same frequency band. The SUs can employ the frequency band of the PU when this user is absent (also called off, and vacant). Therefore, the SU should have the ability to sense the existence of the PU in specific time and/or geographical area and make correct decision in a timely and accurate manner [13]. Hence, the SU is equipped by cognitive capability and reconfigurability which are not available in the conventional radio systems. Cognitive capability means that the SU is able to identify the best unoccupied spectrum band via sensing and

collecting data from the surrounding environment, such as data about transmission bandwidth, frequency, power, etc. On the other hand, reconfigurability refers to rapid adaptation the operational parameters of the SU based on the sensing result in order to improve the performance [10].

## 1.2  Applications of Cognitive Radio

Cognitive radio technique can be utilised in different applications. Some of these applications are as follows

- Cellular networks: In recent years, new devices (e.g., smartphone) and services (e.g., media sites such as Youtube) are introduced and added to the already growing and high use of cellular networks. Consequently, the existing cellular networks are overloaded. Furthermore, the coverage in areas with low population density distribution (e.g., rural areas) is poor due to deploying the networks by cellular operators. To cope the overloading and coverage problems in the cellular networks, the TV white spaces can be employed by the cellular operator via the CR techniques [8]. Moreover, TV band spectrum that is not yet classified as white spaces may also be available to cellular operators [14]. However, some design considerations such as change the transmission requirements of the additional RF spectrum from that of the licensed cellular spectrum should be investigated.

- Public safety networks: Emergency responders such as police, fire, and medical services widely employ wireless communications systems to prevent or respond to accidents. The wireless services of the public safety networks are expanded from voice to email, web browsing, messaging, database access, video streaming, picture transfer, and other wideband services. Accordingly, reliability, delay requirements, and data rates differ from service to service. Hence, in many areas (especially urban), a high congestion in the allocated RF bands of the public safety services is generated and caused a delayed responder to citizens [14]. As the first National Emergency Communications Plan that is released by the

United State Department of Homeland Security and the National Broadband Plan [15], the CR can be used to overcome the above challenge. The CR increases the effectiveness and efficiency of spectrum usage in the public services by using the unlicensed RF spectrum (for instance, TV white spaces).

- Wireless medical networks: Nowadays, different devices are employed in hospitals to monitor vital signs (e.g., pressure, temperature, and blood oxygen) of patients. These signs are measured by on-body sensors and then sent by wires to a bedside monitor. Medical body area network (MBAN) is suggested as a good solution to reduce the cost of using wires by monitoring the vital signs wirelessly, collect many parameters at the same time, and get reliable result. However, available spectrum bands that are employed in medical applications such as medical device radiocommunications service and wireless medical telemetry service are limited bandwidth. Hence, the FCC has proposed solution to improve the quality of service of MBANs which utilize 2360-2390 MHz. This solution is based on allowing MBAN devices which are the SUs to coexist with the aeronautical mobile telemetry which represents the PU without interference by using principle work of CR technology [14].

- Smart grid networks: Recently, many governments have transferred the conventional power grid into a smart grid to address sustainability and power independence, emergency resilience cases and global warming. A smart grid networks consist of the home/building area networks (HANs), the advanced metering infrastructure (AMI) (or called field area networks (FANs)), and the wide area networks (WANs). The HANs that link the on-promises with smart meters can be implemented by Wi-Fi while the AMI/FAN transfers the information between comprises and a network gateway (accumulation point) via smart meter. The WANs that manage the communication between the network gateway and the utility data center can be achieved by the broadband cellular network infrastructure. On the other hand, appropriate technologies to implement the AMI/FAN are still under consideration. Because some requirements such as the distance between the promise and a gateway which could range from a few

hundred meters to a few kilometers and the required bandwidth which may not large enough when the number of connected devices increases should be taken into consideration in designing the AMI/FAN. Power line communication is utilised in some AMI but has several problems such as supporting small bandwidth and shorter distance and the safety issue that is associated with ground fault currents. The cellular networks are also used in AMI/FAN but they are already suffering from the problem of insufficient bandwidth. Therefore, CR is proposed to investigate the AMI/FAN with longer range, larger bandwidth, and lest cost as compared with power line communication and cellular networks [14]. Accordingly, Smart Utility Network (SUN) Task Group released different standard to deploy smart grid network in the TV white spaces [16].

## 1.3    Standards of Cognitive Radio

Many standardization activities have been released for different applications of CR technology. In the following, brief information about some standards is provided.

- ECMA 392: This standard is the first CR standard that describes physical and medium access control layers to allow personal/portable devices to occupy the TV white spaces. Both sensing and geolocation and database approaches are utilised in ECMA 392 to use the channel dynamically. The implementation of many new applications such as campus-wide wireless coverage is expected to achieve by ECMA 392 using TV white spaces [17].

- IEEE SCC41: The standards of IEEE SCC41 are released by five working group. For each working group, there is standard that describes specific topics for dynamic spectrum access. For example, the terminologies that are related to system functionality, spectrum management and for the dynamic spectrum access are defined and described by IEEE 1900.1 standard. Different cases for analysing the coexistence and interference between radio systems are presented in IEEE 1900.2 standard. For optimal usage of radio spectrum in heterogeneous wireless networks, several issues are addressed by IEEE 1900.4 standard. To

mange CR for dynamic spectrum access applications, some policy languages are defined by IEEE 1900.5 standard. The scenarios of exchange the data to achieve spectrum detection for dynamic spectrum access are defined in IEEE 1900.6 [18].

- IEEE 802.11: IEEE 802.11 standards include IEEE 802.11h, IEEE 802.11y, and IEEE 802.11af which are published in 2007, 2008, and 2010 respectively. The IEEE 802.11h standard depicts the dynamic selection of spectrum band and control on transmission power for coexistence with radar system working in the 5 GHz bandwidth. On the other hand, IEEE 802.11y standard is an extended of IEEE 802.11h to include the bands of satellite Earth stations [18]. The IEEE 802.11af standard is based on using the TV white spaces to increase the data rate and coverage range of the conventional Wi-Fi [19].

- IEEE 802.15: IEEE 802.15 standards include IEEE 802.15.4 and IEEE 802.15.2 which are published in May 2003 and June 2003, respectively. The former standard describes dynamic frequency choosing mechanisms for coexistence between wireless personal area networks (e.g., MBANs) devices that are operated in the unlicensed bands such as TV white spaces whereas the latter standard depicts the guidelines of this coexistence [18].

- IEEE 802.16: The standards that are covered by the IEEE 802.16 group are IEEE 802.16.2, IEEE 802.16a, and IEEE 802.16h. Some recommended practices to alleviate interference in fixed broadband wireless access networks are explained by IEEE 802.16.2 standard. The IEEE 802.16a standard describes the work of the wireless medium access network interface of broadband wireless access systems in unlicensed bands. The IEEE 802.16a standard is proposed to improve the coexistence of broadband wireless access networks operating in the unlicensed spectrum bands [18].

- IEEE 802.19: This standard provides the definition of coexistence metrics for all IEEE 802 systems operating in the PU's bands (e.g., the coexistence between IEEE 802.16h and IEEE 802.11y) [18].

- IEEE 802.22: IEEE 802.22 standard is the first international CR standard to specify wireless regional area network (WRAN) systems (e.g., large scale smart grid networks) operating in TV white spaces. Hence, it is sometimes called IEEE 802.22 wireless regional area network (WRAN) standard. The frequency range of IEEE 802.22 WRAN standard is wider than that of IEEE 802.11 standard [17]. Moreover, the physical and medium access control layers of IEEE 802.22 standard are similar to the layers of IEEE 802.16 with some amendments associated to the power levels for preventing the interference between adjacent bands and identifying of the PUs are investigated [18]. Further details about the IEEE 802.22 WRAN standard are provided in Section 2.10.

## 1.4   Spectrum Sensing Techniques

Spectrum sensing (SS) is a crucial step in CR network, because all the next steps such as spectrum sharing depend on the result of this process. In the open technical literature, many SS techniques have been proposed to detect whether the PU's signal is present or absent, such as

- Matched filtering detection (MFD): Matched filtering detection technique is an optimal method for SS when the transmitted PU signal in the additive white Gaussian noise (AWGN) environment is known by the SU [20]. It is classified as coherent detection, because the SU needs to know the perfect information about the PU signals such as the pilot, preamble and training sequence that are used for channel estimation and synchronization. The main benefit of MFD is the short sensing time to obtain a good detection performance. However, the complexity of this method is very high. Because the SU needs receivers for different PU signals. Another drawback of MFD is the estimation error for the PU signal becomes high when the signal-to-noise ratio (SNR) is low [21].

- Cyclostationary feature detection (CFD): The cyclostationary feature detection technique exploits the cyclostationary properties which are intentionally introduced to the modulated signals to help SS or they are caused by the periodicity

in the signal or in its statistics like mean and autocorrelation to detect the PU's signal [22]. Unlike the MFD, the CFD can distinguish primary users' signals from noise. This is because the noise is wide-sense stationary (WSS) with no correlation while the signals are cyclostationary with spectral correlation. However, the computational complexity of the CFD is much higher than the MFD. Other advantages of CFD are the differentiation between various kinds of transmissions and primary user signals, and the working at very low SNR values [23].

- Energy detection (ED): Energy detection technique has been widely used to provide SS in both CR and the ultra-wide band (UWB) systems. With ED, the energy of the received PU signal is measured and compared with a pref-defined threshold value to decide whether the PU is present or absent [24]. In contrast to the MFD and the CFD techniques, the ED is a non-coherent detection method where the SU receiver does not need any priori knowledge on the PUs' signals. Thus, the computational and implementation complexities of this technique are low in comparison with the aforementioned techniques. Moreover, it needs for short time to provide the sensing result [25].

## 1.5   Motivation

In spite of the ED technique having the accuracy, flexibility, low complexity, high speed and low power consumption which are the most important features that should be available in any SS technique, new challenges appear when it is used to detect the PU signal in CR networks. Therefore, the designing for a good ED requires overcoming on these challenges. One of these challenges is the difficulty in selecting the threshold value that depends on the noise floor and accordingly may change over time. This challenge has been treated by employing some approaches that can alleviate the effect of the noise uncertainty on the ED performance [21, 26]. Other challenges in the ED are the differentiation of the PU from other unknown signal sources and poor detection performance in low SNR regimes. To address these challenges, different

approaches are introduced in [13].

In addition to the aforementioned challenges in using the ED, this thesis shows another challenges that should be addressed to obtain good sensing results. The first challenge is analysing the behaviour of the energy detector in non-line-of-sight (NLoS) communication scenario by utilizing practical channel model without mathematical limitations and then proposing a method to enhance the performance of the ED by depending on this analysis.

The second challenge arises when the wireless signals concurrently undergo multipath and shadowing. In spite of few works that have been devoted to deal with this challenge, extensive study by using a practical channel model should be investigated to get clarifications about the impacts of shadowing on the performance of the energy detector. Accordingly, an optimal method to alleviate the effects of the shadowing can be developed.

Another challenge is the complexity of channel models' expressions that leads to intractable performance metrics especially when diversity reception schemes are used. This challenge can also be noticed in analysing the performance of communications systems.

The last challenge is improving the performance of the ED technique when the noise power is uncertain as well as this noise is very low. This case is attended when the ED technique is employed for SS in IEEE 802.22 standard.

Motived by these challenges, this thesis studies the behaviour of ED over different channels models for SS in CR network. Moreover, some techniques are utilised to improve the performance of ED under different communication scenarios.

## 1.6 Aim and Objectives

The main aim of this thesis is to analyse and enhance the performance of the energy detector for SS. The objectives of this thesis are highlighted in the following points:

1. Analysing the behaviour of the ED over an $\eta-\mu$ fading channel by using method

which gives non-limited analytic expressions for the performance metrics.

2. Studying the performance of the ED over a $\kappa - \mu$ shadowed fading channel which is a composite channel from generalized multipath fading channel and gamma distribution. Moreover, the behaviour of the ED over $\kappa - \mu$ extreme shadowed fading channel which models the wireless communication scenario in an enclosed area is considered.

3. Deriving unified expressions for the performance metrics of communications systems and the ED in diversity reception that can be applied for a variety of wireless channel models.

4. Improving the performance of the ED by diminishing the impacts of noise on the received PU's signal at the SU receiver.

## 1.7    Contributions

This thesis includes five contributions, **C1-C5**, related to spectrum sensing in cognitive radio networks via ED technique. These contributions are summarized as follows:

**C1:** The performance of an ED in non-line-of-sight (NLoS) communication environments has been analysed using $\eta - \mu$ multipath fading channels. The $\eta - \mu$ is general multipath fading channel model that gives results with better fitting to the practical measurements than the conventional channel models. To derive general exact analytic expressions for all measurements metrics, the probability density function (PDF) of the received signal to noise ratio (SNR) approach has been used rather than the moment generating function (MGF) approach that leads to limited expressions. Then, the analysis has been extended to include different diversity reception techniques that improve the ED performance. Two cases of fading channels which are independent and identically distributed ($i.i.d$) and independent and non-identically distributed ($i.n.d$) diversity receivers

have been investigated. Furthermore, the performance of cooperative spectrum sensing (CSS) which contains multiple SUs has been investigated.

**C2:** Since the multipath fading and the shadowing may occur simultaneously in practical communication channels, the behaviour of ED over $\kappa - \mu$ shadowed fading channel has been studied. The $\kappa - \mu$ fading channel was proposed as generalized multipath fading channel that can model the line-of-sight (LoS) communication environments. Similar to the $\eta - \mu$ fading channel, the $\kappa - \mu$ fading channel provides better fitting to the experimental data of realistic communications than the traditional distributions. General exact analytic expressions for the average detection probability and the area under the receiver operating characteristic curve (AUC) have been derived. To reduce the impacts of the multipath fading and the shadowing, various diversity reception techniques have been employed. Two cases for diversity branches which are fully $i.i.d$ and fully $i.n.d$ $\kappa - \mu$ shadowed fading channels have been assumed. Furthermore, the performance of CSS over a $\kappa - \mu$ shadowed fading channel has been shown. A method to improve the performance of CSS has been proposed. Finally, the $\kappa - \mu$ extreme shadowed fading channel, which is a special case of the $\kappa - \mu$ shadowed fading channel is utilized to model wireless channels for the communication scenarios in enclosed environments has been taken into consideration.

**C3:** Statistical characterizations of unified channel model for different diversity reception schemes with $i.n.d$ receivers have been derived. The mixture gamma (MG) distribution which is an approximated distribution that can model any intractable wireless channel with good accuracy has been utilized. Then, different performance metrics that are employed in analysing the diversity reception of communication systems and ED technique have been derived. This contribution has been tested over an $\alpha - \mu$/gamma fading channel. This channel is composite from $\alpha - \mu$ fading channel that is proposed to model the non-linear communication environments and gamma distribution that models the shadowing impacts.

**C4:** Since the derived statistical properties expressions in **C3** are limited by some conditions such as the shadowing severity index should be an integer number, this contribution provides the same expressions without limitations. Moreover, the $\eta - \mu$/gamma fading channel has been based on the analysis of both communication systems and ED technique. This channel has been chosen in this contribution because it has not been used with diversity reception in the literature.

**C5:** In spite of many methods that have been proposed and designed to estimate the noise variance and to enhance the performance of the ED technique, other digital signal processing approach that can provide both processes at low SNR regime should be employed. Therefore, the signal denoising approach based on hybrid slantlet transform (HST) which is special filter-bank transform has been firstly used to improve the performance of the ED. Then, new filter-bank transform has been employed to predict the uncertain noise power. This filter-bank transform is called slantlet packet transform (SPT) and it is firstly proposed and utilized in this thesis.

## 1.8 Thesis Outline

Chapter 2 gives background information on ED, different generalized channel models and various diversity receptions. Thereafter, chapters 3-7 explain how the contributions, **C1-C5**, are implemented. The chapters of this thesis are outlined as follows.

- **Chapter 2** explains the various models of energy detector that are widely employed in the literature. Furthermore, different generalized channel models that are considered throughout this thesis are given. Moreover, this chapter shows the principle work of maximal ratio combining (MRC), square law combining (SLC), square law selection (SLS), selection combining (SC) diversity reception schemes that are utilised in improving the performance of the ED. Background knowledge about the CSS approach using decision fusion rule is provided. In

14

addition, some signal processing approaches that are utilised to reduce the noise effects on the performance of the ED and are related to the work of this thesis are reviewed.

- **Chapter 3** includes contribution **C1** that studies the behaviour of the ED over generalised multipath fading channel, namely, $\eta - \mu$. The PDF of the received instantaneous SNR is employed in this study. The performance of the ED with different diversity reception techniques is analysed over $i.n.d$ and $i.i.d$ $\eta - \mu$ fading channels. Both, the complementary receiver operating characteristic (CROC) curve and the average complementary AUC curve (CAUC) are presented for different scenarios.

- **Chapter 4** presents contribution **C2** of this thesis in which the behaviour of energy detector over composite generalised multipath shadowed fading channel namely $\kappa - \mu$ shadowed fading channel is analysed. The PDF of the received instantaneous SNR is also employed in this analysis. Similar to chapter 3, the MRC, SLC and SLS diversity reception approaches are used over $i.n.d$ and $i.i.d$ $\kappa - \mu$ shadowed fading channels. The effect of the shadowing index on the detectability of ED is explained by the CROC and the average CAUC.

- **Chapter 5** demonstrates contribution **C4** where the equivalent parameters of MG distribution for composite $\alpha - \mu$/gamma fading channel are introduced. Furthermore, chapter 5 provides the statistical characterizations, i.e., PDF, CDF and MGF of the sum and the maximum of $i.n.d$ MG distribution random variables (RV)s. Then, different performance metrics with MRC and SC diversity reception such as the outage probability (OP), the average channel capacity ($C$) and the average bit error rate probability (ABEP) that are mainly employed in analysing the communication systems are derived. In addition, the performance metrics of special model of ED based SS are given.

- **Chapter 6** explains the equivalent parameters of MG distribution for composite $\eta - \mu$/gamma fading channel. In spite of the derived expressions in chapter 5 that are unified and expressed in simple functions, these expressions are limited

by some conditions such as the value of shadowing index should be an integer number. Thus, in chapter 6, the same statistical properties of chapter 5 are derived in general closed-form expressions. Moreover, the performance same metrics of chapter 5 are provided.

- **Chapter 7** illustrates some approaches that can be applied to improve the performance of the ED as pointed out in contribution **C5**. In the first approach, HST based signal denoising technique which is one of most useful methods to reduce noise impacts on the received signals is utilized. The HST is a filter-bank transform that is constructed from filters with special characteristics. In the second approach, the uncertain noise power that is included in the PU signal is estimated by using HST. This approach is based on employing SPT which is firstly proposed in this thesis. The two approaches are used together to improve the performance of the ED when it is used to provide SS in IEEE 802.22 WRAN standard. A comparison of results with previous work is presented in chapter 7.

- **Chapter 8** summarises the contributions and results obtained from this thesis. Moreover, it lists some problems that need to be treated in future work.

# Chapter 2

# Background

This chapter provides background knowledge about the related topics for this thesis. Firstly, available models of an energy detector are shown. Secondly, different types of test statistical distributions for the energy detector based spectrum sensing that are used in this thesis are provided. Thirdly, brief mathematical information about some generalised distributions that are utilised throughout this thesis to model the multipath fading channels are presented. Then, the principle work of different types of diversity reception schemes and cooperative spectrum sensing are given. Finally, the characteristics of some special filter-bank transforms that are employed in improving the performance of energy detector and the limitations of spectrum sensing in the IEEE 802.22 standard are explained.

## 2.1 Energy Detector Models

In the ED technique, a device which called an energy detector is employed to sense the primary user's signal. The principle work of the energy detector is based on filtering the received signal by an ideal band-pass filter (BPF) to limit the noise power as well as to normalize the noise variance. The signal is then squared and integrated over particular time interval by using square law device and an integrator, respectively to evaluate the test statistic (or it is sometimes called decision statistic). The block diagram for this model which is known as analog energy detector is illustrated in Fig.
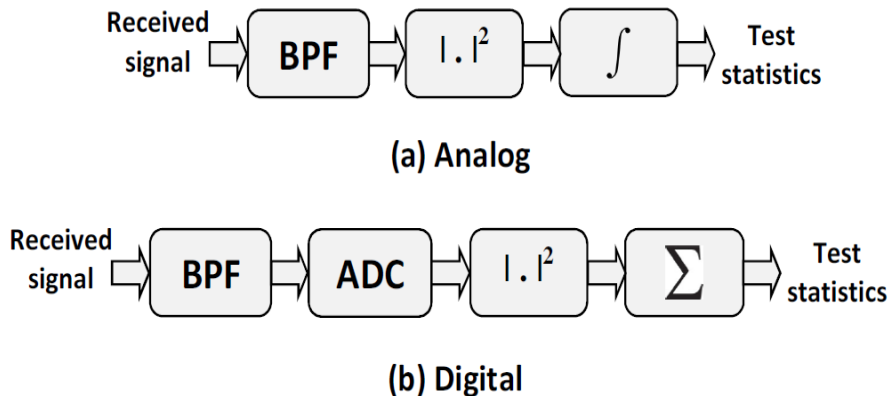
Figure 2.1: Energy detector models.

2.1(a) [24].

The process of evaluating the test statistic can be carried out digitally. In this case, the energy detector is called digital energy detector. In this model, the received signal is firstly filtered by BPF. Secondly, the continuous signal is transformed digital signal by the analog-to-digital converter (ADC) device. Thereafter, the discrete signal is squared and summed by utilizing a square law device and a summing device to compute the test statistic. The block diagram for this model is shown in Fig. 2.1(b) [27].

Both previous models are followed by a comparator device that compares the test statistic with a specific threshold value generated by threshold device. Then, the final result about whether the the primary user signal is present or absent is made by decision device.

## 2.2 Test Statistic of an Energy Detector

According to the result of the comparison between the test statistic and the threshold value, the received signal, $r(t)$, at the SU side follows a binary hypothesis: $\mathcal{H}_0$ and $\mathcal{H}_1$ which represent the signal is absent and the signal is present, respectively

[24, 27-30].

$$r(m) = \begin{cases} w(m) & : \mathcal{H}_0 \\ hs(m) + w(m) & : \mathcal{H}_1 \end{cases} \qquad (2.1)$$

where $w(m)$, $h$ and $s(m)$ are the additive white Gaussian noise (AWGN) signal at the SU's receiver, the wireless channel gain which is assumed to be fixed during the sensing time, the sent signal by PU's transmitter, respectively. The noise is assumed to be circularly symmetric complex Gaussian RV with zero mean and $2\sigma_w^2$ variance, i.e., $\mathbb{E}\{w(m)\} = 0$ and $\mathbb{Var}\{w(m)\} = 2\sigma_w^2$ where $\mathbb{E}\{.\}$ and $\mathbb{Var}\{.\}$ stand for expectation (mean) and variance operations, respectively.

As mentioned previously about the principle work of the analog energy detector, the received signal is filtered first by an ideal BPF with bandwidth $W$. The signal is then squared and integrated over $T$ time interval (i.e., sensing time) to evaluate the test statistic $\Xi$, i.e., [28-30]

$$\Xi = \frac{1}{T} \int_t^{t+T} |r(t)|^2 dt \qquad (2.2)$$

where $|.|$ denotes the amplitude of the signal that may be complex signal, i.e., $r(t) = r_r(t) + r_i(t)$ where $r_r(t)$ and $r_i(t)$ stand for real part and imaginary part, receptively.

It can be noted that a reliable detection result is obtained when the sensing time, $T$, is high. However, this reduces the throughput for CR network. Hence, the sensing time differs from standard to standard and its value depends on the SNR, i.e., when SNR is very low, long sensing time is needed to obtain good detection result [27]. For example, the required sensing time to achieve a performance target on detection parameters in IEEE 802.22 standard is no larger than 2 s at SNR = -20 dB [31]. In the released of the FCC in 2010 [32], it is shown that a minimum time interval to detect TV white spaces and unused wireless microphone signals by TV band devices is 30 s [1]. In [33], the sensing time to achieve good trade-off between reliability in PU

---

[1]According to advanced television system committee (ATSC) standard in the United States, the

detection and throughput loss due to sensing for 200 MHz radio bandwidth at SNR = -5 dB is chosen less than 50 ms. In [27], the optimal sensing time to fulfil high throughput and good detection performance for 6 MHz bandwidth at SNR = -20 dB should be smaller 14.2 ms.

When digital energy detector is employed to sense the received signal, the test statistic in (2.2) is expressed as follows [27]

$$\Xi = \sum_{m=1}^{M} |r(m)|^2 \tag{2.3}$$

where $M \approx 2u$ and $u = TW$ stand for the number of samples and the time-bandwidth product respectively[2].

To decide whether the unknown PU signal is present or absent, the test statistic, $\Xi$, is compared with a pre-defined threshold value $\lambda$. This threshold defines the detection sensitivity of the SU and depends on the ratio between bandwidths and broadcast powers of SUs and PUs. Moreover, PU's resilience, interference among PUs, multipath, shadowing, and the accumulation of interference of multiple SUs are also impact on the detection threshold. To cope the effect of each factor that is not fully available at the SU side, a safety margin, a conservative PU interference margin, a multipath margin, a hidden node margin, and an aggregate interference margin are added, respectively, to the latter value of the threshold [34].

The threshold value, $\lambda$, is usually chosen to achieve the target value of the performance metric of interest (e.g., high probability of detection). However, this achievement may not always provide good detection performance because other performance metrics that are related to $\lambda$ are changed simultaneously (as it is explained in the next of this section). Hence, for each standard, there is a certain detection threshold. For instance, in IEEE 802.22 standard, the required sensing thresholds for digital TV, analog TV, and wireless microphone signals are -116 dBm, -94 dBm, and -107 dBm,

---

channel bandwidth of digital TV signals is 6 MHz while for the analog TV is 100 kHz. The maximum channel bandwidth of wireless microphone signals that are usually FM modulated is 200 kHz [14].

[2]Both $T$ and $W$ should be selected to give integer $2u$.

respectively [31]. The sensitive sensing thresholds for mobile station and macro-base station receiver for global system for mobile communications (GSM) are -102 dBm and -114 dBm, respectively while for long-term evolution (LTE) are -106.4 dBm and -123.4 dBm, respectively [34].

The comparison between $\Xi$ and $\lambda$ leads to three different cases that use as performance metrics to study the behaviour of an energy detector. These cases are described as follows:

- Probability of false alarm ($P_f(\lambda)$): it represents the probability of case $\mathrm{Pr}\{\Xi > \lambda \mid \mathcal{H}_0\}$ where $\mathrm{Pr}\{.\}$ stands for an event probability. In other words, this probability is present when $\Xi > \lambda$ and $\mathcal{H}_0$ are true. Thus, the SU doesn't utilise the spectrum bands of the PU. Consequently, to get an efficient spectrum usage, $P_f(\lambda)$ should be small (e.g., in IEEE 802.22 standard, $P_f(\lambda) = 0.1$ for all signal types [31]). The main factors that cause the $P_f(\lambda)$ are multipath fading, hidden node (harsh shadowing), and the aggregation of mutual interference of multiple SUs.

  The $P_f(\lambda)$ can be computed by [27-30]

  $$P_f(\lambda) = \mathrm{Pr}\{\Xi > \lambda | \mathcal{H}_0\} = \int_{\lambda}^{\infty} f_\Xi(y) dy \qquad (2.4)$$

  where $f_\Xi(y)$ is the PDF of test statistic $\Xi$.

- Probability of detection ($P_d(\gamma, \lambda)$): it represents the probability of case $\mathrm{Pr}\{\Xi > \lambda \mid \mathcal{H}_1\}$. In another meaning, this probability is present when both $\mathcal{H}_1$ and $\Xi > \lambda$ are true. Thus, it is sometimes called the probability of correct detection. In this case, the spectrum holes of the PU can be utilised by the SU. Hence, large $P_d(\gamma, \lambda)$ leads to reliable SS with high protection for PU from the interference by the SU. The $P_d(\gamma, \lambda)$ can be evaluated by [27-30]

  $$P_d(\gamma, \lambda) = \mathrm{Pr}\{\Xi > \lambda | \mathcal{H}_1\} = \int_{\lambda}^{\infty} f_\Xi(y) dy \qquad (2.5)$$

- Probability of missed-detection ($P_{md}(\gamma, \lambda) = 1 - P_d(\gamma, \lambda)$): it is the comple-

mentary probability of $P_d(\gamma, \lambda)$, i.e., the probability of case $\Pr\{\Xi < \lambda \mid \mathcal{H}_1\}$ [30]. In another words, incorrect decision on the presence of the PU is made by the SU and that causes mutual interference between both users. Therefore, small $P_{md}(\gamma, \lambda)$ means reliable sensing results and subsequently keeping the PU from the interference. The main parameters that generate the $P_{md}(\gamma, \lambda)$ are low SNR, multipath fading, shadowing, and interference between multiple PUs. In IEEE 802.22 standard and for all signal types, the typical value of $P_{md}(\gamma, \lambda)$ that achieves high protection for the PU is 0.1 [31].

## 2.3 Models of Detection and False Alarm Probabilities

Depending on the available information about the distribution of $s(m)$, the test statistic, $\Xi$, follows different distributions. Hence, in the open technical literature, different expressions for both $P_d(\gamma, \lambda)$ and $P_f(\lambda)$ which are the complementary CDFs of $\Xi$ are employed to study the behaviour of the energy detector. In the following subsections, the used expressions in this thesis are reviewed.

### 2.3.1 Exact Models

This thesis provides two different exact mathematical expressions for $P_d(\gamma, \lambda)$ and $P_f(\lambda)$ (**E1** and **E2**) that are used widely in the previous works as follows:

**E1:** In this model, the signal $s(m)$ is considered to be transmitted over a flat band-limited Gaussian noise channel and the received signal $r(m)$ has a Gaussian distribution. Thus, the test statistic, $\Xi$, represents a sum of squares of $M$ Gaussian RVs that are independent but arbitrarily distributed. Hence, $\Xi$ follows a central chi-square distribution with $2u$ degrees of freedom (DoF)s under hypothesis $\mathcal{H}_0$. Moreover, it follows a non-central chi-square distribution with $2u$ DoFs under hypothesis $\mathcal{H}_1$ with non-centrality parameter, $2\gamma$. Accordingly,

the PDFs of $\Xi$, $f_\Xi(y)$ under both hypothesis are given by [29, 30]

$$
f_\Xi(y) = \begin{cases} \dfrac{1}{(2\sigma_w^2)^u \Gamma(u)} y^{u-1} e^{-\frac{y}{2\sigma_w^2}} & : \mathcal{H}_0 \\[3ex] \dfrac{1}{2\sigma_w^2}\left(\dfrac{y}{2\gamma}\right)^{\frac{u-1}{2}} e^{-\frac{2\gamma+y}{2\sigma_w^2}} I_{u-1}\left(\dfrac{\sqrt{2\gamma y}}{\sigma_w^2}\right) & : \mathcal{H}_1 \end{cases} \tag{2.6}
$$

where $\Gamma(.)$ and $I_a(.)$ are the gamma function and the modified Bessel function of the first kind of order $a$, respectively.

Now, the $P_f(\lambda)$ and the $P_d(\gamma, \lambda)$ over AWGN channel can be calculated by substituting (2.6) into (2.4) and (2.5), respectively[3]. Accordingly, the following expressions yield

$$
P_f(\lambda) = \frac{\Gamma\left(u, \frac{\lambda}{2\sigma_w^2}\right)}{\Gamma(u)} \tag{2.7}
$$

$$
P_d(\gamma, \lambda) = Q_u\left(\sqrt{\frac{2\gamma}{\sigma_w^2}}, \sqrt{\frac{\lambda}{\sigma_w^2}}\right) \tag{2.8}
$$

where $\gamma = \frac{|h|^2 E_s}{2\sigma_w^2}$ is the instantaneous SNR, $E_s$ is the transmitted signal energy, $\Gamma(.,.)$ is the upper incomplete gamma function, and $Q_u(.,.)$ is the generalized Marcum-$Q$ function given by [35, eq.(29)][4]

$$
Q_\rho(x, y) = e^{-\frac{x^2}{2}} \sum_{k=0}^{\infty} \frac{\Gamma(k+\rho, \frac{y^2}{2})}{\Gamma(1+k)\Gamma(k+\rho)} \left(\frac{x^2}{2}\right)^k \tag{2.9}
$$

This model is employed in analysing the performance of energy detector in Chapters 3, 4 and 6 of this thesis.

**E2:** In this model, the signal sample also has a Gaussian distribution but it's assumed

---

[3]To evaluate $P_f(\lambda)$, the PDF of $\Xi$ under hypothesis $\mathcal{H}_0$ is used whereas the PDF of $\Xi$ under hypothesis $\mathcal{H}_1$ is applied to calculate $P_d(\gamma, \lambda)$.

[4]The generalized Marcum-Q function is a standard built in function available in MATLAB software package.

to be as single RV with $\mathbb{E}\{s(m)\} = 0$ and $\mathbb{V}\text{ar}\{s(m)\} = 2\sigma_s^2$. In this case, the received signal $r(m)$ also has a Gaussian distribution with $\mathbb{E}\{r(m)\} = 0$ and $\mathbb{V}\text{ar}\{r(m)\} = 2\sigma_w^2(1 + \gamma)$. Consequently, the test statistic, $\Xi$, represents a sum of squares of $M$ Gaussian RVs that are independent and identically distributed and follows central chi-square distributions with $2u$ DoFs under hypothesis $\mathcal{H}_0$ and $\mathcal{H}_1$. The PDFs of $\Xi$, $f_\Xi(y)$, under both hypotheses for model **E2** are expressed by [36, 37]

$$
f_\Xi(y) = \begin{cases} \dfrac{1}{(2\sigma_w^2)^u \Gamma(u)} y^{u-1} e^{-\frac{y}{2\sigma_w^2}} & : \mathcal{H}_0 \\[4mm] \dfrac{1}{(2\sigma_w^2(1+\gamma))^u \Gamma(u)} y^{u-1} e^{-\frac{y}{2\sigma_w^2(1+\gamma)}} & : \mathcal{H}_1 \end{cases}
\tag{2.10}
$$

By following a similar procedure in (2.7) and (2.8), the expressions of the $P_f(\lambda)$ and the $P_d(\gamma, \lambda)$ for this model are deduced as follows[5],

$$
P_f(\lambda) = \frac{\Gamma\left(u, \frac{\lambda}{2\sigma_w^2}\right)}{\Gamma(u)}
\tag{2.11}
$$

$$
P_d(\gamma, \lambda) = \frac{\Gamma\left(u, \frac{\lambda}{2\sigma_w^2(1+\gamma)}\right)}{\Gamma(u)}
\tag{2.12}
$$

This model is used in studying the behaviour of the energy detector in Chapter 5 of this thesis.

### 2.3.2 Approximated Models

This model more accurately approximates the distribution of the test statistic, $\Xi$, in (2.3) to a normal distribution by using principle of the central limit theorem (CLT). This approximation can be applied for any type of received signal model when

---

[5]Without loss of generality, $\sigma_w^2$ is set to a unity (0 dB) when model **E1** and model **E2** are used anywhere in this thesis.

the number of samples, $M$, is large enough. Consequently, the exact models **E1** in (2.6) and **E2** in (2.10) can be approximated as follows:

**P1:** This model is the result of applying the CLT on the model **E1**. In this model, the test statistic, $\Xi$, follows Gaussian distributions with $\frac{M}{2}$ DoFs under both hypotheses $\mathcal{H}_0$ and $\mathcal{H}_1$. Hence, $\Xi$ follows $\mathcal{N}(\sigma_w^2 M, 2M\sigma_w^4)$ and $\mathcal{N}(\sigma_w^2(1 + \gamma)M, 2M(1 + 2\gamma)\sigma_w^4)$ under $\mathcal{H}_0$ and $\mathcal{H}_1$, respectively. Therefore, the PDFs of $\Xi$, $f_\Xi(y)$, under both hypothesis are expressed by [38, 39],

$$
f_\Xi(y) \approx \begin{cases} -\dfrac{1}{\sqrt{4\pi M \sigma_w^2}} e^{-\frac{(y - \sigma_w^2 M)^2}{4M(\sigma_w^2)^2}} & : \mathcal{H}_0 \\[4ex] -\dfrac{1}{\sqrt{4\pi(1 + \gamma)M \sigma_w^2}} e^{-\frac{(y - \sigma_w^2(1+2\gamma)M)^2}{4(\sigma_w^2)^2(1+2\gamma)M}} & : \mathcal{H}_1 \end{cases} \tag{2.13}
$$

Similar to (2.7) and (2.8), the $P_f(\lambda)$ and the $P_d(\gamma, \lambda)$ for model **P1** are given by

$$
P_f(\lambda) \approx Q\left(\frac{\lambda - \sigma_w^2 M}{\sqrt{2M}\sigma_w^2}\right) \tag{2.14}
$$

$$
P_d(\gamma, \lambda) \approx Q\left(\frac{\lambda - \sigma_w^2(1 + \gamma)M}{\sqrt{2(1 + 2\gamma)M}\sigma_w^2}\right) \tag{2.15}
$$

where $Q(.)$ is the standard Gaussian $Q$ function defined in [27, eq. (6)].

**P2:** This model is produced when model **E2** is approximated by the CLT. Similar to **P1**, the distributions of the decision statistic, $\Xi$, under both hypotheses $\mathcal{H}_0$ and $\mathcal{H}_1$ are Gaussian distributions with $\frac{M}{2}$ DoFs. However, $\Xi$ follows $\mathcal{N}(\sigma_w^2 M, 2M\sigma_w^4)$ and $\mathcal{N}(\sigma_w^2(1 + \gamma)M, 2M(1 + \gamma)\sigma_w^4)$ under $\mathcal{H}_0$ and $\mathcal{H}_1$, respectively. Accordingly, the PDFs of $\Xi$, $f_\Xi(y)$, under both hypothesis are expressed by [39, 40],

$$f_\Xi(y) \approx \begin{cases} -\dfrac{1}{\sqrt{4\pi M \sigma_w^2}} e^{-\frac{(y-\sigma_w^2 M)^2}{4M(\sigma_w^2)^2}} & : \mathcal{H}_0 \\[3em] -\dfrac{1}{\sqrt{4\pi(1+\gamma)M\sigma_w^2}} e^{-\frac{(y-\sigma_w^2(1+\gamma)M)^2}{4(\sigma_w^2)^2(1+\gamma)M}} & : \mathcal{H}_1 \end{cases} \tag{2.16}$$

Using (2.4), (2.5) and (2.16), the $P_f(\lambda)$ and the $P_d(\gamma, \lambda)$ for this model are given by

$$P_f(\lambda) \approx Q\left(\frac{\lambda - \sigma_w^2 M}{\sqrt{2M}\sigma_w^2}\right) \tag{2.17}$$

$$P_d(\gamma, \lambda) \approx Q\left(\frac{\lambda - \sigma_w^2(1+\gamma)M}{\sqrt{2(1+\gamma)M}\sigma_w^2}\right) \tag{2.18}$$

The model **P2** is employed by Chapter 7 of this thesis.

## 2.4 Area under the Receiver Operating Characteristics Curve (AUC)

In some cases, when two systems are compared using the receiver operating characteristics (ROC) curve which is a plot of the $P_d(\gamma, \lambda)$ versus $P_f(\lambda)$, the intersection between both curves may happen in a certain value of the $P_f(\lambda)$. Accordingly, the result about the superiority of each one on the other is ambiguous. Therefore, a comparison using single figure of merit is necessary to explain which scheme has better detection capability than the other. Hence, the AUC is proposed by [41, 42] to measure the total area under the ROC curve and to show the difference between two schemes versus the SNR.

The unfaded AUC (in AWGN channel) can be computed by [41]

$$A(\gamma) = -\int_0^\infty P_d(\gamma, \lambda)\frac{\partial P_f(\lambda)}{\partial \lambda}d\lambda \tag{2.19}$$

where $\frac{\partial P_f(\lambda)}{\partial \lambda}$ is the partial derivative of $P_f(\lambda)$ with respect to $\lambda$.

For both models **E1** and **E2**, $\frac{\partial P_f(\lambda)}{\partial \lambda}$ is given by

$$\frac{\partial P_f(\lambda)}{\partial \lambda} = -\frac{\lambda^{u-1}}{2^u \Gamma(u)} e^{-\frac{\lambda}{2}} \tag{2.20}$$

Substituting (2.8) and (2.20) into (2.19), the unfaded AUC for model **E1** is obtained as [41]

$$A(\gamma) = 1 - \sum_{n=0}^{u-1} \frac{1}{2^n n!} \gamma^n e^{-\frac{\gamma}{2}} + \sum_{n=1-u}^{u-1} \frac{\Gamma(u+n)}{2^{u+n}\Gamma(u)} e^{-\gamma} {}_1\tilde{F}_1\left(u+n; 1+n; \frac{\gamma}{2}\right) \tag{2.21}$$

where ${}_1\tilde{F}_1(.)$ is the regularized confluent hypergeometric function defined by [41, eq. (27)].

For **E2**, the unfaded AUC expression can be computed by plugging (2.12) and (2.20) into (2.19) with the aid of [43, eq. (6.4551)]. Thus, this yields

$$A(\gamma) = \frac{\Gamma(2u)}{u[\Gamma(u)]^2}\left(\frac{1+\gamma}{(2+\gamma)^2}\right)^u {}_2F_1\left(1, 2u; 1+u; \frac{1+\gamma}{2+\gamma}\right) \tag{2.22}$$

where ${}_2F_1(.)$ is the confluent hypergeometric function defined by [44, eq. (1.2.23)].

The unfaded AUC expressions for both **P1** and **P2** models cannot be derived in closed-form due to containing mathematically intractable integral.

## 2.5  Generalized Fading Distributions

In the open technical literature, the fading models of the wireless channel have been represented by various distributions. For example, the log-normal distribution is the best choice to model the large-scale signal variation that occurs due to the shadowing impact by barriers such as buildings. On the other side, the small-scale signal variation which occurs in enclosed areas is characterized by many other distributions such as Rayleigh, Nakagami-$m$ ($m$ is the number of the multipaths) and Nakagami-$n$ (Rician) [45-48]. However, these distributions which can be called conventional (tra-

Table 2.1: Conventional Distributions Derived from the $\kappa - \mu$ distribution [51].

| Conventional Distributions | Parameters of the $\kappa - \mu$ Distribution |
|---|---|
| One-Sided Gaussian | $\kappa \to 0,\ \mu = 0.5$ |
| Rayleigh | $\kappa \to 0,\ \mu = 1$ |
| Nakagami-$m$ with shaping parameter $m$ | $\kappa \to 0,\ \mu = m$ |
| Rician (Nakagami-$n$) with shaping parameter $K$ | $\kappa = K,\ \mu = 1$ |

ditional) distributions do not give better fitting to the experimental measurements than the generalized fading distributions that are introduced in [49-55]. Nevertheless, some of the conventional distributions can be obtained from these generalized fading distributions by setting the fading parameters to certain values as it's explained later. Another feature that can be noticed in these generalized fading distributions is the Nakagami-$m$ distribution considers a common distribution between them and it can be applied for integer and non-integer $m$. But, the traditional Nakagami-$m$ is limited by integer $m$. These distributions are described in the following subsections.

## 2.5.1 $\kappa - \mu$ Distribution

The $\kappa - \mu$ distribution has been proposed by [50] to model the line-of-sight (LoS) communications scenarios with better fitting to the practical data than the traditional distributions. In addition to that, some of these distributions such as One-Sided Gaussian, Rayleigh, Nakagami-$m$ and Rician distributions are special cases of the $\kappa - \mu$ distribution as explained in Table 2.1.

In the $\kappa - \mu$ distribution, $\kappa$ shows the ratio between the total power of the dominant components and the scattered waves and it is computed by $\kappa = \frac{d^2}{2n\sigma^2}$ where $\sigma^2 = \mathbb{E}\{X_l^2\} = \mathbb{E}\{Y_l^2\}$, $d^2 = \sum_{l=1}^{n}(p_l^2 + q_l^2)$, $X_l$ with mean value $p_l$ and $Y_l$ with mean value $q_l$ are the quadrature and in-phase complements of the multipath waves of cluster (path) $l$, respectively and $n$ is the number of multipath clusters[6]. The parameter

---

[6]A cluster is a group of multipath waves that have similar delay and directions at transmitter and receiver.

$\mu$ represents the real extension of the number of the multipath clusters and it is evaluated by $\mu = \frac{(1+2\kappa)}{(1+\kappa)^2} \frac{(d^2+2n\sigma^2)}{(4\sigma^2 d^2 + 4n\sigma^2)}$. It can be noted that $\mu$ may be non-integer due to either the correlation between the quadrature and in-phase components is non-zero or the correlation among the clusters of multipath components is non-zero (see [51] and the references therein).

The PDF of the received instantaneous SNR, $\gamma$, over $\kappa - \mu$ distribution is given by [51],

$$f_\gamma(\gamma) = \frac{\mu(1+\kappa)^{\frac{\mu+1}{2}} \gamma^{\frac{\mu-1}{2}}}{\kappa^{\frac{\mu-1}{2}} e^{\kappa\mu} \bar{\gamma}^{\frac{\mu+1}{2}}} e^{-\frac{\mu(1+\kappa)}{\bar{\gamma}}\gamma} I_{\mu-1}\left(2\mu\sqrt{\frac{\kappa(1+\kappa)}{\bar{\gamma}}\gamma}\right) \tag{2.23}$$

where $\bar{\gamma}$ is the average SNR.

The CDF of the received instantaneous SNR, $\gamma$, that is computed by $F_\gamma(\gamma) = \int_0^\gamma f_\gamma(\gamma) d\gamma$ over $\kappa - \mu$ distribution is expressed as follows [51],

$$F_\gamma(\gamma) = 1 - Q_\mu\left(\sqrt{2\kappa\mu}, \sqrt{\frac{2\mu(1+\kappa)\gamma}{\bar{\gamma}}}\right) \tag{2.24}$$

The MGF of the received instantaneous SNR, $\gamma$, $(\mathcal{M}_\gamma(\gamma))$ which is Laplace transform of the PDF, i.e., $\mathcal{M}_\gamma(\gamma) = \mathcal{L}\{f_\gamma(\gamma); s\} = \int_0^\infty e^{-s\gamma} f_\gamma(\gamma) d\gamma$ over $\kappa - \mu$ distribution is expressed as follows [56][7],

$$\mathcal{M}_\gamma(s) = \left(\frac{\mu(1+\kappa)}{\mu(1+\kappa) + s\bar{\gamma}}\right)^\mu e^{\frac{\mu^2\kappa(1+\kappa)}{\mu(1+\kappa)+s\bar{\gamma}} - \mu\kappa} \tag{2.25}$$

The $\kappa - \mu$ distribution is employed by Chapter 4 of this thesis.

## 2.5.2 $\eta - \mu$ Distribution

This distribution has been employed to embody the non-line-of-sight (NLoS) communications scenarios. As in the $\kappa - \mu$ distribution, the $\eta - \mu$ includes two parameters which are $\eta$ and $\mu$. The definition of $\eta$ depends on the type of format (format 1 or format 2) as it will be shown later. However, $\mu$ has unified definition in all for-

---

[7]Here $\mathcal{L}$ stands for Laplace transform.

mats and it is similar to $\mu$ of the $\kappa - \mu$ distribution. However, it is expressed by $\mu = \frac{n(1+\eta)^2}{4(1+\eta^2)}\left[1 + \left(\frac{H}{h}\right)^2\right]$.

The PDF of the received instantaneous SNR, $\gamma$, over $\eta - \mu$ distribution is given by [51],

$$f_\gamma(\gamma) = \frac{2\sqrt{\pi}\mu^{\mu+\frac{1}{2}}h^\mu \gamma^{\mu-\frac{1}{2}}}{\Gamma(\mu)H^{\mu-\frac{1}{2}}\bar{\gamma}^{\mu+\frac{1}{2}}}e^{-\frac{2\mu h}{\bar{\gamma}}\gamma}I_{\mu-\frac{1}{2}}\left(\frac{2\mu H}{\bar{\gamma}}\gamma\right) \tag{2.26}$$

where $h$ and $H$ are parameters related to $\eta$.

The CDF of the the received instantaneous SNR, $\gamma$, over $\eta - \mu$ distribution is expressed by [57],

$$F_\gamma(\gamma) = \frac{\left(1 - \left(\frac{H}{h}\right)^2\right)^\mu \left(\frac{2h\mu\gamma}{\bar{\gamma}}\right)^{2\mu}}{\Gamma(1+2\mu)}$$
$$\times \Phi_2\left(\mu, \mu; 1 + 2\mu; -\left(1 + \frac{H}{h}\right)\frac{2h\mu\gamma}{\bar{\gamma}}, -\left(1 - \frac{H}{h}\right)\frac{2h\mu\gamma}{\bar{\gamma}}\right) \tag{2.27}$$

where $\Phi_2(.)$ is the confluent bivariate Lauricella hypergeometric function defined in [44, eq. (1.3.17)].

The MGF of the received instantaneous SNR, $\gamma$, over $\eta - \mu$ distribution is given by [56],

$$\mathcal{M}_\gamma(s) = \left(\frac{4\mu^2 h}{(2(h-H)\mu + s\bar{\gamma})(2(h+H)\mu + s\bar{\gamma})}\right)^\mu \tag{2.28}$$

As mentioned in [39], $\eta$ differs from format 1 to format 2. These formats are defined as follows:

- Format 1: In this format, $\eta$ represents the power ratio between the in-phase and quadrature scattered components in each multipath cluster with $0 < \eta < \infty$ i.e., $\eta = \sigma_X^2/\sigma_Y^2$ where $\sigma_X^2 = \mathbb{E}\{X_l^2\}$, $\sigma_Y^2 = \mathbb{E}\{Y_l^2\}$. The particular $H$ and $h$ are expressed by

$$H = \frac{\eta^{-1} - \eta}{4} \quad \text{and} \quad h = \frac{2 + \eta^{-1} + \eta}{4}$$

Table 2.2: Conventional Distributions Derived from the $\eta - \mu$ Distribution [51].

| Conventional | Parameters of the $\eta - \mu$ Distribution | |
|---|---|---|
| distributions | Format 1 | Format 2 |
| One-sided Gaussian | $\eta \to 0$ or $\eta \to \infty$, $\mu = 0.5$ or $\eta \to 1$, $\mu = 0.25$ | $\eta \to 0$, $\mu = 0.25$ or $\eta \to \pm 1$, $\mu = 0.5$ |
| Rayleigh | $\eta \to 0$ or $\eta \to \infty$, $\mu = 1$ or $\eta \to 1$, $\mu = 0.5$ | $\eta \to 0$, $\mu = 0.5$ or $\eta \to \pm 1$, $\mu = 1$ |
| Nakagami-$m$ with shaping parameter $m$ | $\eta \to 0$ or $\eta \to \infty$, $\mu = m$ or $\eta \to 1$, $\mu = 0.5m$ | $\eta \to 0$, $\mu = 0.5m$ or $\eta \to \pm 1$, $\mu = m$ |
| Hoyt (Nakagami-$q$) with shaping parameter $q$ | $\eta = q^2$, $\mu = 0.5$ | $\eta = -q$, $\mu = 0.5$ |

- Format 2: In this format, $\eta$ stands for the correlation coefficient between the in-phase and quadrature scattered components in each multipath cluster with $-1 < \eta < 1$ i.e., $\eta = \mathbb{E}\{X_l Y_l\}/\sigma^2$ where $\sigma^2 = \mathbb{E}\{X_l^2\} = \mathbb{E}\{Y_l^2\}$ and $\mathbb{E}\{X_l\} = \mathbb{E}\{Y_l\} = 0$. The respective $H$ and $h$ are given by

$$H = \frac{\eta}{1 - \eta^2} \quad \text{and} \quad h = \frac{1}{1 - \eta^2}$$

Interestingly, $\eta$ of format 1 ($\eta_{\text{Format1}}$) and $\eta$ of format 2 ($\eta_{\text{Format2}}$) are related together by similar mathematical relationship as follows:

$$\eta_{\text{Format1(2)}} = \frac{1 - \eta_{\text{Format2(1)}}}{1 + \eta_{\text{Format2(1)}}}$$

Hence, the performance analysis of communications systems and even the energy detector using one format is enough where the results for the other format can be evaluated by applying the bilinear transformation method. Consequently, the $\eta - \mu$ with format 1 is utilised in Chapters 2 and 6 of this thesis.

The possible traditional distributions that can be extracted from the $\eta - \mu$ distribution by setting $\eta$ and $\mu$ for certain values are One-Sided Gaussian, Rayleigh, Nakagami-$m$ and Hoyt distributions as illustrated in Table 2.2.

31

## 2.5.3  $\alpha - \mu$ Distribution

The $\alpha - \mu$ distribution has been suggested by [52, 53] to model a signal that is propagated in a multipath non-homogeneous environment. Unlike the envelopes of the $\kappa - \mu$ and $\eta - \mu$ distributions that have linear function with the modulus of the sum of the multipath components, this relationship is non-linear in the $\alpha - \mu$ distribution. Accordingly, in the $\alpha - \mu$ distribution, the parameter $\alpha$ indicates the non-linearity of the propagation medium that is evaluated practically (see [53] and references therein for further details). On the other hand, $\mu$ can be calculated analytically by $\mu = \frac{\mathbb{E}^2\{R^\alpha\}}{\mathbb{Var}\{R^\alpha\}}$ where $R^\alpha = \sum_{l=1}^{n}(X_l^2 + Y_l^2)$ is the envelope of the fading signal.

The PDF of the the received instantaneous SNR, $\gamma$, over $\alpha - \mu$ distribution is expressed by [52]

$$f_\gamma(\gamma) = \frac{\alpha \mu^\mu \gamma^{\alpha\mu-1}}{\Gamma(\mu)\bar{\gamma}^{\alpha\mu}} e^{-\frac{\mu^\alpha}{\bar{\gamma}^\alpha}\gamma^\alpha} \tag{2.29}$$

The CDF of the the received instantaneous SNR, $\gamma$, over $\alpha - \mu$ distribution is expressed by [53],

$$F_\gamma(\gamma) = \frac{G(\mu, \frac{\mu}{\bar{\gamma}^\alpha}\gamma^\alpha)}{\Gamma(\mu)} \tag{2.30}$$

where $G(.,.)$ is the lower incomplete gamma function [43, eq. (8.350.1)].

The MGF of the the received instantaneous SNR, $\gamma$, over $\alpha - \mu$ distribution is given by [58],

$$\mathcal{M}_\gamma(s) = \frac{\alpha \mu^\mu k^{\frac{1}{2}} l^{\frac{\alpha\mu-1}{2}}}{2\Gamma(\mu)\bar{\gamma}^{\frac{\alpha\mu}{2}}(2\pi)^{\frac{l+k-2}{2}} s^{\frac{\alpha\mu}{2}}} G_{l,k}^{k,l}\left(\left(\frac{\mu}{\bar{\gamma}^{\frac{\alpha}{2}}}\right)^k \frac{l^l}{s^l k^k}\middle| \begin{array}{c} I(l, 1-\frac{\alpha\mu}{2}) \\ I(k, 0) \end{array}\right) \tag{2.31}$$

where $G_{l,k}^{k,l}(.)$ is the Meijer's G-function [43, eq. (9.301)], $I(a,b) = b/a, (b+1)/a, \cdots, (b+a-1)/a$ and $\alpha/2 = l/k$ with $\gcd(l,k) = 1$ where gcd stands for great common divisor.

The well-known distributions that are special cases of the $\alpha - \mu$ distribution are demonstrated in Table 2.3 (top of the next page).

The analysis of Chapter 5 of this thesis is based on the $\alpha - \mu$ distribution.

Table 2.3: Conventional Distributions Derived from the $\alpha - \mu$ Distribution [53].

| Conventional distributions | Parameters of the $\alpha - \mu$ Distribution |
|---|---|
| Negative Exponential | $\alpha = 1$, $\mu = 1$ |
| One-sided Gaussian | $\alpha = 2$, $\mu = 0.5$ |
| Rayleigh | $\alpha = 2$, $\mu = 1$ |
| Nakagami-$m$ with shaping parameter $m$ | $\alpha = 2$, $\mu = m$ |
| Gamma with shaping parameter $a$ | $\alpha = 1$, $\mu = a$ |
| Weibull with shaping parameter $k$ | $\alpha = k$, $\mu = 1$ |

## 2.6 Mixture Gamma Distribution

The performance of communication systems and energy detector over composite multipath/shadowing fading channels has been studied by few works. This is because the statistical characterizations, namely, PDF, CDF, and MGF of these channels are mathematically intractable. This problem rises when the analysis is extended to diversity reception techniques. To overcome this problem, an approximate unified distribution with high accuracy is proposed by [59]. This distribution is based on mixing number of gamma distributions to obtain an accurate approximation, hence it is called MG distribution. In [60], the MG distribution has been used to model the SNR of various distributions such as Nakagami-$m$, $\kappa - \mu$ and $\eta - \mu$ distributions.

The PDF of the received instantaneous SNR, $\gamma$, over any fading channel can be expressed by using the MG distribution as follows [60][8]

$$f_\gamma(\gamma) = \sum_{i=1}^{N} w_i f_i(\gamma) = \sum_{i=1}^{N} \boldsymbol{\alpha}_i \gamma^{\beta_i - 1} e^{-\zeta_i \gamma} \tag{2.32}$$

where $f_i(\gamma) = \frac{\zeta_i^{\beta_i} \gamma^{\beta_i - 1} e^{-\zeta_i \gamma}}{\Gamma(\beta_i)}$ is a standard Gamma distribution, $w_i = \frac{\alpha_i \Gamma(\beta_i)}{\zeta_i^{\beta_i}}$, $\boldsymbol{\alpha}_i = \zeta_i^{\beta_i}$, $\beta_i$ is the shape parameter, $\zeta_i$ is the rate parameter, and $N$ is the number of terms,

---

[8]Bold $\boldsymbol{\alpha}$ is used here to distinguish between $\alpha$ of the $\alpha - \mu$ fading channel and $\alpha$ of the MG distribution.

i.e., number of gamma distributions.

The CDF of the received instantaneous SNR, $\gamma$, using the MG is given by [60]

$$F_\gamma(\gamma) = \sum_{i=1}^{N} \boldsymbol{\alpha}_i \zeta_i^{-\beta_i} G(\beta_i, \zeta_i \gamma) \tag{2.33}$$

The MGF of the received instantaneous SNR, $\gamma$, is expressed by [60]

$$\mathcal{M}_\gamma(s) = \sum_{i=1}^{N} \frac{\boldsymbol{\alpha}_i \Gamma(\beta_i)}{(s + \zeta_i)^{\beta_i}} \tag{2.34}$$

The MG distribution is used to analyse the performance of communication systems and energy detector with diversity reception over composite $\alpha - \mu/$gamma and $\eta - \mu/$gamma fading channels in Chapters 5, and 6, respectively.

## 2.7    Diversity Reception Techniques

Diversity reception techniques are employed at the receiver (secondary user in energy detection) side to improve the received instantaneous SNR. But, some diversity combing techniques require additional information, thus leading to increase the design complexity of the system. In this thesis, four diversity reception techniques which are MRC, SLC, SLS and SC schemes are mainly used. These techniques are explained as follows.

### 2.7.1    Maximal Ratio Combining

MRC is a coherent combining scheme which requires for the instantaneous channel state information (CSI). Therefore, the implementation complexity of MRC is higher than the other techniques [47].

In MRC reception, each diversity branch is weighted via multiplying it by factor as illustrated in Fig. 2.2 (top of the next page). This factor is relative to the complex fading coefficient of the branch. Accordingly, the combined signal, $R(m)$, of $L$ diversity receivers under both hypothesis $\mathcal{H}_0$ and hypothesis $\mathcal{H}_1$ can be expressed by
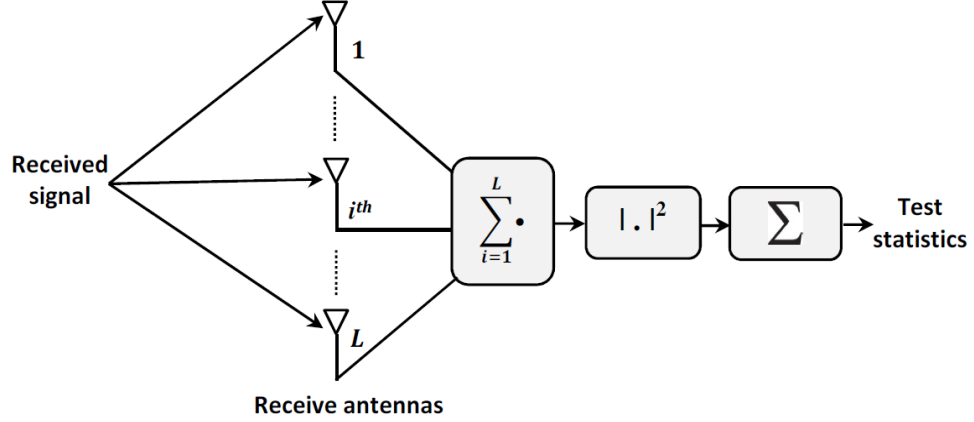
Figure 2.2: Energy detection with maximal ratio combining.

[61]

$$R(m) = \begin{cases} W(m) & : \mathcal{H}_0 \\ \mathsf{H}s(m) + W(m) & : \mathcal{H}_1 \end{cases} \tag{2.35}$$

where $W(m) = \sum_{i=1}^{L} w_i(m)$ is the noise sample and $\mathsf{H} = \sum_{i=1}^{L} |h_i(m)|^2$ is the wireless channel gain and $w_i(m)$ and $h_i(m)$ are the noise and the channel coefficient of the $i$th branch, respectively.

Based on (2.34), the test statistic, $\Xi^{MRC}$, at the output of the MRC is given as

$$\Xi^{MRC} = \sum_{m=1}^{M} |R(m)|^2 \tag{2.36}$$

In addition, the instantaneous SNR at the output of the MRC combiner is evaluated by $\gamma^{MRC} = \sum_{i=1}^{L} \gamma_i$ [47] where $\gamma_i$ is the received instantaneous SNR at the $i$th branch. Since, in the MRC, the combining is performed before energy calculation, the probability of false alarm over AWGN for all models does not change. In contrast, the probability of the detection over AWGN with MRC can be calculated by replacing $\gamma$ in (2.8), (2.11), (2.14), (2.17) by $\gamma^{MRC}$.

35

## 2.7.2 Square Law Combining

SLC is a non coherent combining technique, thus it does not require the CSI. The principle work of this scheme is based on evaluating the energy of the received signal ($\Xi$) by each branch as shown in Fig. 2.3. Thereafter, the test statistic, $\Xi^{SLC}$, is the sum of all test statistics, i.e.,

$$\Xi^{SLC} = \sum_{i=1}^{L} \Xi_i \tag{2.37}$$

where $\Xi_i$ is the test statistic of the $i$th branch.

Substituting (2.3) into (2.36), one can deduce that $\Xi^{SLC}$ follows a central chi-square distribution with $2Lu$ DoFs for **E1** and **E2** models and $\frac{LM}{2}$ DoFs for **P1** and **P2** models under hypothesis $\mathcal{H}_0$. Furthermore, it follows $2Lu$ DoFs for **E1** and **E2** models and $\frac{LM}{2}$ DoFs for **P1** and **P2** models under hypothesis $\mathcal{H}_1$ with non-centrality parameter $\gamma^{SLC} = \sum_{i=1}^{L} \gamma_i$.

It can be noticed that the difference between MRC and SLC is $u$. Hence, the performance metrics of ED with SLC can be evaluated by replacing $u$ or $M$ of the expressions with MRC by $Lu$ or $LM$, respectively [30].
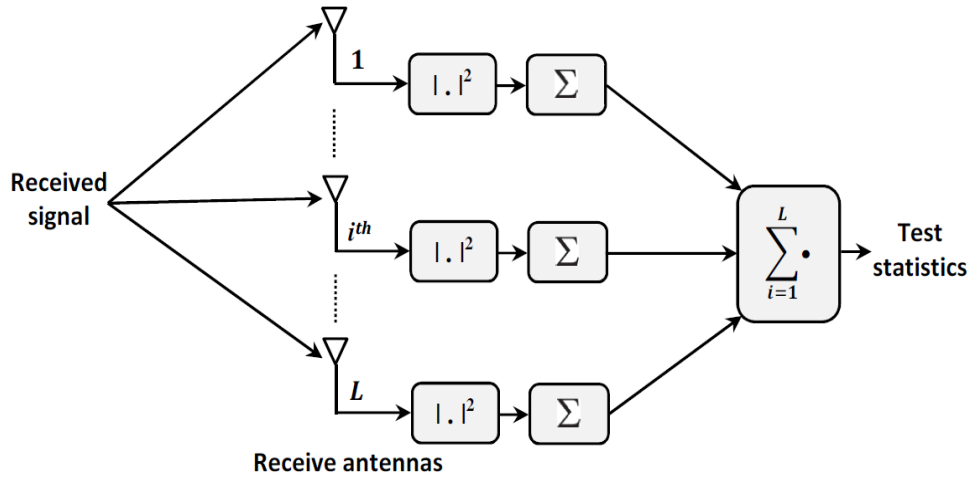


Figure 2.3: Energy detection with square law combining.

### 2.7.3    Square Law Selection

SLS is also a non coherent combining approach based on selecting the branch with highest energy as the output of the combiner. In another words, the test statistic of ED with SLS, $\Xi^{SLS}$, is given by $\Xi^{SLS} = \max\{\Xi_1, \Xi_2, \ldots, \Xi_L\}$ as demonstrated in Fig. 2.4. Accordingly, the $P_f(\lambda)$ and the $P_d(\gamma, \lambda)$ in AWGN are given by [30]

$$P_f^{SLS}(\lambda) = 1 - \left[1 - P_f(\lambda)\right]^L \tag{2.38}$$

$$P_d^{SLS}(\gamma, \lambda) = 1 - \prod_{i=1}^{L} \left[1 - P_d(\gamma_i, \lambda)\right] \tag{2.39}$$

where $P_f(\lambda)$ and $P_d(\gamma_i, \lambda)$ are given in (2.7), (2.10), (2.13) and (2.16) and (2.8), (2.11), (2.14) and (2.17), respectively.
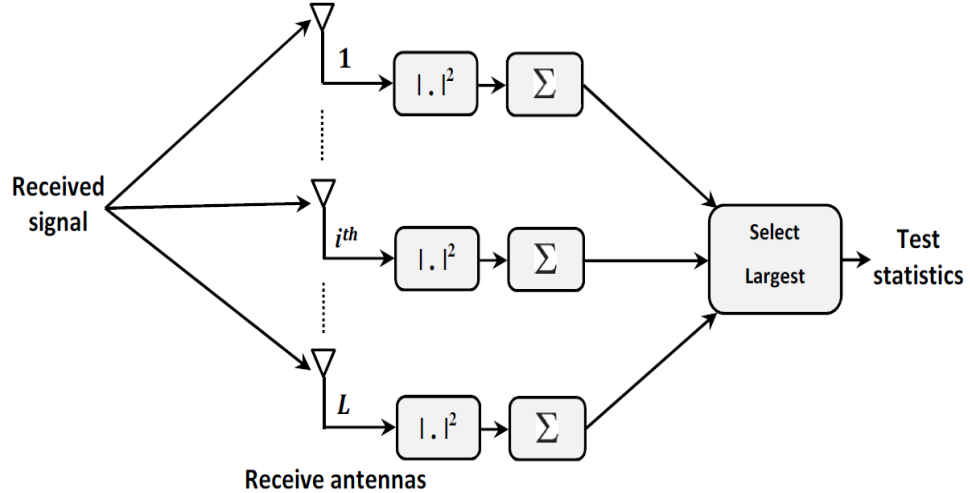


Figure 2.4: Energy detection with square law selection.

### 2.7.4    Selection Combining

SC has simplest implementation in comparison with MRC, SLC and SLS. In contrast to SLS, the combiner in SC chooses the receiver with maximal SNR among all diversity branches [47]. In another meaning, the instantaneous SNR at the output

of the SC combiner is given by $\gamma^{SC} = \max\{\gamma_1, \gamma_2, \cdots, \gamma_L\}$ as explained in Fig. 2.5. Then, the computed test statistic for this branch is considered as the test statistic of the SC combiner, $\Xi^{SC}$. Since, in the SC, the energy is evaluated after the combining, the $P_f(\lambda)$ in AWGN for all models is the same. But, the $P_d(\gamma, \lambda)$ in AWGN with MRC can be computed by replacing $\gamma$ in (2.8), (2.11), (2.14), (2.17) by $\gamma^{SC}$.
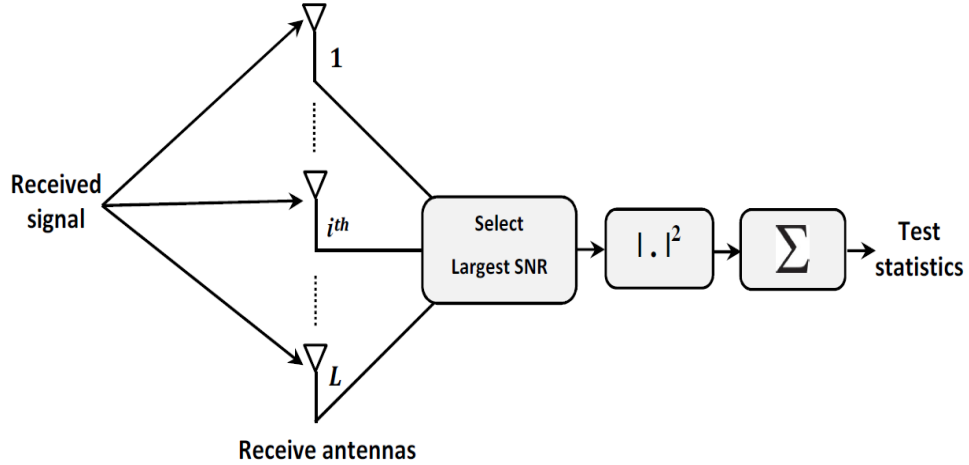


Figure 2.5: Energy detection with selection combining.

## 2.8  Cooperative Spectrum Sensing

Sometimes, an obstacle in the sensing channel which is the link between the PU Tx and the SU causes shadowing degrades the detection capability of the ED as shown in Fig. 2.6 (top of the next page)[62]. From this figure, one can observe that the link from PU transmitter (PU Tx) to SU1 is shadowed by a huge building. Accordingly, the result of decision that is made by SU1 is inaccurate, i.e., $P_f(\lambda)$ and $P_{md}(\gamma, \lambda)$ are high. This leads to high interference between SU1 and PU Rx as well as SU1 and other SUs. Cooperation between number of SUs is employed to mitigate this problem and to improve the detection performance of the CR network by introducing spatial diversity [63]. Moreover, the problem of hidden PU is solved by using cooperation among SUs which greatly reduces the required sensing time at each individual SU [64, 65].
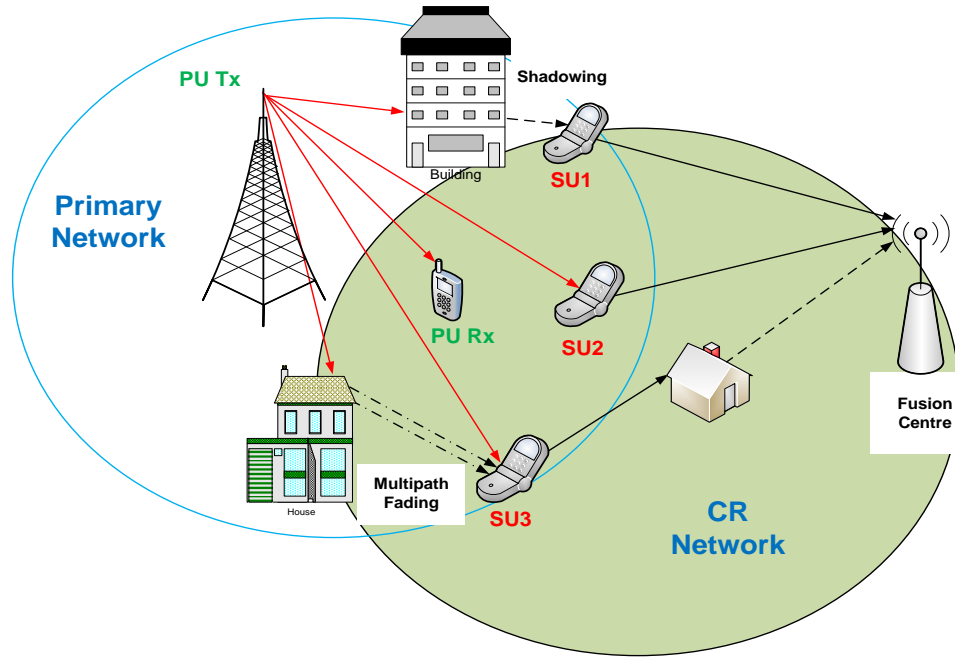
Figure 2.6: Cooperative spectrum sensing.

There are three methods to implement CSS:

- Centralized CSS: In centralized CSS, each SU senses independently the PU and sends the sensing results to the fusion centre (FC) (sometimes, SU is chosen as FC and it is called the head) which fuses the SU decisions, makes a final decision and broadcasts it to other SUs. For example, in Fig. 2.6, the sensing channel of SU2 is not affected by channel impairments such as shadowing and multipath fading. However, the sensing channels of SU1 and SU3 are influenced by shadowing and multipath fading, respectively. Moreover, the reporting channels which are the links between the SU and the FC for SU1 and SU2 are imperfect channels (error free channels) [62-65]. But, the reporting channel for SU3 includes error rate which is a result from the shadowing by barrier (e.g., house) [66-68].

  At the FC, the final decision about the case of the PU is made by using one of the decision rules which are decision fusion (hard decision) and data fusion (soft decision). In the former, the decision that is made by the SU is sent by

using one bit (either 1 which means the PU is ON or 0 which implies the PU is OFF) or more whereas in the latter, the data of the PU Tx is processed and then sent to the FC [62]. Hence, the required bandwidth for reporting channels in soft decision is larger than that in hard decision. Moreover, in both fusion scenarios, the bandwidth of reporting channels increases, when the number of SUs becomes large. To overcome this problem, only the SUs with good reporting channel (e.g., high SNR) are allowed to send their local sensing result to the FC. This can be done by using double thresholding rather than single thresholding at each unreliable SU [13].

The decision fusion approach includes different rules which are AND rule, OR rule and Majority rule. All these rules are generalized in one rule which is called the "$k$-out-of-$n$" rule where $k$ is the number of SUs who participate in the final decision and $n$ is the total number of PUs. The "$k$-out-of-$n$" rule represents AND rule, OR rule, and Majority rule when $k = n$, $k = 1$, and $k = \lceil n/2 \rceil$, respectively [62-68][9]. The false alarm probability, $Q_f$, and the detection probability, $Q_d$, at the FC using hard decision and "$k$-out-of-$n$" rule are expressed by [68],

$$Q_f = \sum_{i=k}^{n} \binom{n}{i} (P_{f_i}(1-P_e)+(1-P_{f_i})P_e)^i (1-(P_{f_i}(1-P_e)+(1-P_{f_i})P_e))^{n-i} \quad (2.40)$$

$$Q_d = \sum_{i=k}^{n} \binom{n}{i} (P_{d_i}(1-P_e)+(1-P_{d_i})P_e)^i (1-(P_{d_i}(1-P_e)+(1-P_{d_i})P_e))^{n-i} \quad (2.41)$$

where $\binom{a}{b}$ is the binomial expansion defined as $\binom{a}{b} = \frac{a!}{b!(a-b)!}$, $P_{f_i}$ and $P_{d_i}$ are the false alarm and the detection probabilities at $i$th SU, respectively and $P_e$ is the error rate probability at the FC which can be evaluated as a bit error rate probability (BEP) over reporting channel.

- Distributed CSS: In distributed CSS, SUs share their local sensing information among themselves but the decision is made separately by each SU as to which

---

[9]The function $\lceil x \rceil$ represents the smallest integer greater than or equal to x.

portion of the spectrum this SU can employ. Distributed CSS does not require a backbone structure and it has low cost in comparison with centralised CSS. In [64], distributed CSS using the amplify-and-forward protocol is investigated to sense the PU. In this protocol, SUs are divided into pairs by using some available algorithms. Then, in each pair, one SU is assigned as a relay which amplifies and forwards the signal received from the other SU without doing any additional processing. For instance, in Fig. 2.6, SU1 and SU2 can be considered as pair and the relay is SU2. Because both sensing and reporting channels of this user are better than that of SU2. In [69], transmit and relay diversity approaches are employed to alleviate the impact of the imperfect reporting channel on the performance of CSS. In transmit diversity, each two closely located SUs are viewed as virtual antenna array. Some coding techniques such as space time coding and space frequency coding are then applied on these distributed antenna arrays to enhance the detection performance of CSS. In relay diversity approach, the decision of the SU who is experienced heavy shadowing in the reporting channel is sent to the nearest SU who has a good reporting channel. Thereafter, both the decisions at the SU who is worked as relay are sent at the same time by using two orthogonal channels.

- External CSS: In the case of external CSS, an external sensor node accomplishes the sensing process and sends the result to SUs. External CSS can solve the problems of hidden PU and the uncertainty that are resulted by fading and shadowing in both sensing and reporting channels. Moreover, since the sensing time by the SUs is zero, spectrum efficiency using an external CSS is better than that in centralised CSS and distributed CSS. In addition, the problem of the consumed power of internal sensing which is performed internally by the SU transceivers is addressed in an external CSS. This is because the sensing network is not necessarily powered by batteries [70]. External CSS is one of the approaches suggested for identifying PUs in IEEE 802.22 standard as well.

## 2.9 Energy Detection with Filter-Bank Transform

A great number of filter-bank transforms have been widely utilized in different digital signal processing (DSP) such as signal denoising [71-78]. One of extensively used filter-bank transform is the discrete wavelet transform (DWT) which is a set of digital low-pass filters (LPF)s and high-pass filters (HPF)s [79]. These filters have high accuracy of separating the noise from the non stationary PU signals. Moreover, the coefficients of theses filters are not constant and depend on the type of the wavelet basis function, e.g., Haar, Daubechies 2 ($D2$) and Daubechies 4 ($D4$). Fig. 2.7 shows the forward and backward filter-bank structure of DWT that are employed for signal analysis (decomposition) and signal synthesis (reconstruction), respectively. In (a) of this figure, H(z) and F(z) stand for the LPF and the HPF, respectively. However, in (b) of this figure, IH(z) and IF(z) stand for the inverse LPF and the inverse HPF, respectively. When the signal is analysed by the DWT, the coefficients that are created by filtering the input signal by H(z) and F(z) are called the scaling (approximation) coefficients and the wavelet (details) coefficients, respectively.
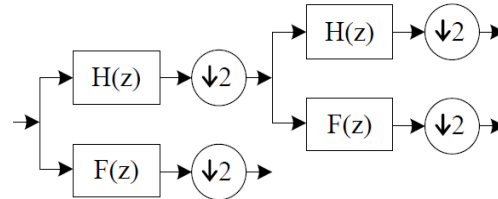
↓2 means selecting the second sample from each two samples.

**(a) Two-level DWT (Signal analysis)**
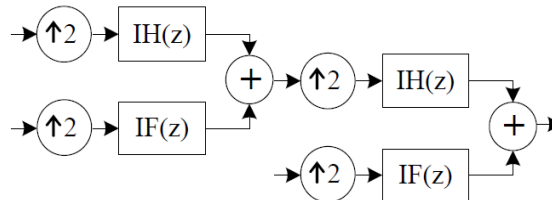
↑2 means making each one sample as two samples by adding zero.

**(b) Two-level IDWT (Signal synthesis)**

Figure 2.7: Filter-bank structure of discrete wavelet transform [80].

When the analysed signal contains noise, this noise is concentrated in the details of the coefficients [79]. Hence, the analysis of the second scale is applied on the outputs of the H(z) filters.

In the open technical literature, DWT has been extensively used in signal denoising technique to improve the performance of the ED technique [79-85]. For instance, in [80-82], DWT is used to reduce the noise impact on the PU's signal before employing the energy detector in both single and CSS scenarios.

Some applications that use the DWT need to analyse both the wavelet and the scaling coefficients, e.g., noise estimation. In this case, the DWT is called discrete wavelet packet transform (DWPT) as illustrated in Fig. 2.8 [79]. This transform has been also employed to enhance the behaviour of energy detector via estimating the uncertain noise power [86-88] which is considered as one of the main reasons in



**(a) Two-level DPWT (Signal analysis)**



**(b) Two-level IDPWT (Signal synthesis)**
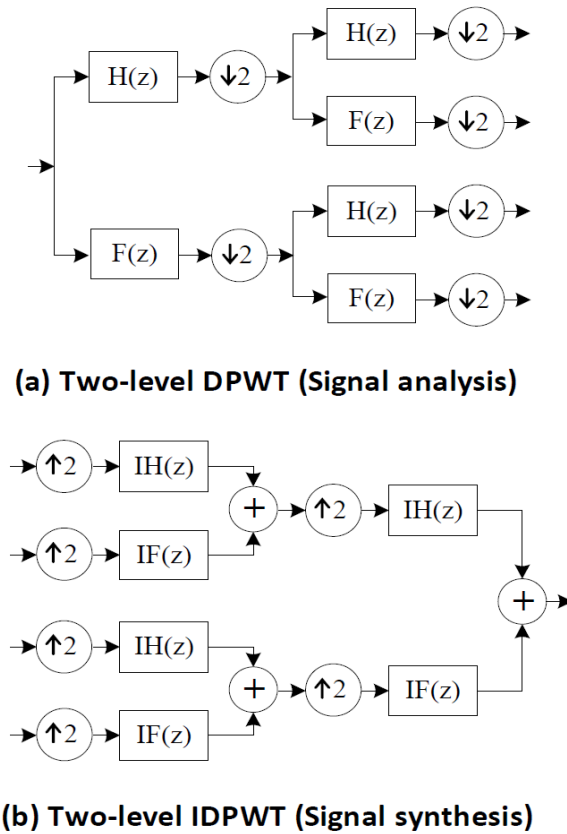
Figure 2.8: Filter-bank structure of discrete wavelet packet transform [86].

43

degrading the performance of energy detector as mentioned in Section 1.5.

## 2.10 IEEE 802.22 Standard

The IEEE 802.22 WRAN is the first standard for CR network [31, 18, 89]. In this standard, the use of licensed digital TV, analog TV and wireless microphones white spaces for broadband access with no-interference to the PU is permitted. The availability of TV white spaces in IEEE 802.22 WRAN is performed by using either geolocation and database approach or one of SS techniques [31]. In the geolocation and database approach, information knowledge about all channels at the sensing receiver is required. Hence, the complexity of this approach is high as well as the unrecorded channels can not be checked. On the other side, as mentioned in Chapter 1, some SS techniques are non coherent and they can detect the white spaces with low complexity such as ED [90].

In IEEE 802.22 WRAN, the SS is limited by some requirements such as the false alarm and the detection probabilities are 0.1 and 0.9, respectively for all signal types at high, moderate and very low SNR (e.g., -20 dB) [31]. However, the sensing at very low SNR region needs long detection latency which includes sensing time and the time to achieve specific processing such as signal denoising before decision making [21, 26]. To meet this demand, a large number of selected PU's signal samples is required, which means that the transmission time is reduced.

# Chapter 3

# Energy Detection over $\eta - \mu$ Fading Channel: PDF Based Approach

This chapter studies the behaviour of an energy detector over $\eta - \mu$ fading channel. The PDF approach is employed rather than the MGF approach to derive general exact analytic expressions for both the average probability of detection and the average AUC. The study is then extended to include MRC, SLC and SLS diversity reception techniques. Two cases of fading channels which are $i.i.d$ and $i.n.d$ $\eta - \mu$ fading channels are studied. Furthermore, the CSS with diversity reception at the fusion centre is investigated with calculated error rate at the reporting channel.

## 3.1 Introduction

The performance of ED has been comprehensively analysed over different channel models. In [24], analytic expressions for the detection and the false alarm probabilities over a flat, band-limited Gaussian noise channel are derived. Depending on [24], these probabilities are evaluated over Nakagami-$m$, Rayleigh and Rice fading channels in [28]. Then, different diversity receptions such as SLC, SLS and SC are used in [29, 30]. Only, one case has been studied in [30] with $i.n.d$ diversity branches which is dual receivers over $i.n.d$ Rayleigh fading channels. The analysis of an energy detector over $i.i.d$ Nakagami-$m$ with various diversity schemes is repeated by [91, 92], but

with simple analytic expressions. In [61], an extensive analysis for energy detector over $i.i.d$ Nakagami-$m$ and Rician fading channels with MRC, SC and equal gain combining (EGC) is investigated. Due to the intersection in a specific point when the ROC is employed in the comparison between two systems, the AUC is suggested by [41, 40, 93] as a single figure of merit.

To obtain on better fitting to the field measurements, the performance of an energy detector over $\kappa - \mu$, $\eta - \mu$ and $\alpha - \mu$ fading channels is evaluated in [94-96]. Since this chapter studies the behaviour of energy detector over $\eta - \mu$ fading channel, the literature review for employing this channel is performed. In [93, 94], the performance of energy detector over $\eta - \mu$ is studied by deriving the average $P_d$ and the AUC, receptively using the MGF of the received instantaneous SNR. However, these expressions are limited by some conditions such as the MGF should be a rational function and powers of the poles are integer numbers, i.e., the fading parameters such as $\mu$ should be integer numbers. Although similar unified approach is recently proposed by [97-102] to overcome this problem, it is still restricted with the expression of the MGF which should be in closed-form. Furthermore, it produces expressions with too complicated integral that can not be solved analytically. In addition to that, in some cases, it is difficult to derive the exact expression of the MGF such as SLS with $i.n.d$ diversity branches. To cope with the aforementioned problems, the PDF has been employed in [95, 96] to analyse the performance of energy detector over $\kappa - \mu$ and $\alpha - \mu$ fading channels. Therefore, the analysis of the performance of energy detector over $\eta - \mu$ fading channel in this chapter is based on using the PDF approach. Accordingly, this analysis has led to several contributions which are summarized as follows:

- Deriving exact analytic expression for the average probability of detection, $\overline{P_d}$, over $\eta - \mu$ fading channel. Moreover, exact expressions for $\overline{P_d}$ with different diversity reception approaches with $i.n.d$ and $i.i.d$ diversity branches are provided.

- Deriving exact analytic expression for the average AUC, $\bar{A}$, over $\eta - \mu$ fading channel. Similar to the contribution in the previous point, the expressions of $\bar{A}$

for different diversity reception techniques are given.

- Studying the general case of CSS over $\eta - \mu$ fading channel. The "$k$-out-of-$n$" decision fusion rule with non-identically distributed SUs is used here. In addition, the error rate at the reporting channel is calculated and reduced via employing diversity combining at the FC.

## 3.2 Performance Analysis with No Diversity

### 3.2.1 Average Probability of Detection

The average probability of detection, $\overline{P_d}(\lambda)$, over $\eta - \mu$ fading channel can be calculated by averaging the $P_d(\gamma, \lambda)$ of (2.8) over the PDF of the instantaneous SNR $\gamma$ (2.26), i.e., [61]

$$\overline{P_d}(\lambda) = \int_0^\infty P_d(\gamma, \lambda) f_\gamma(\gamma) d\gamma \tag{3.1}$$

After some mathematical manipulations, the exact analytic expression of $\overline{P_d}(\lambda)$ over $\eta - \mu$ fading channel is given by

$$\overline{P_d}(\lambda) = \frac{2\sqrt{\pi}\Gamma(2\mu)}{\Gamma(\mu)\Gamma(\mu + \frac{1}{2})} \left( \frac{\mu^2 h}{(\bar{\gamma} + 2\mu h)^2} \right)^\mu \left[ \mathbf{H}_4 \left( 2\mu, 1; \mu + \frac{1}{2}, 1; \left( \frac{\mu H}{2\mu h + \bar{\gamma}} \right)^2, \frac{\bar{\gamma}}{2\mu h + \bar{\gamma}} \right) \right.$$
$$\left. - \frac{\lambda^u}{2^u u!} X_{15} \left( 2\mu, u; u, 1 + u, \mu + \frac{1}{2}; \left( \frac{\mu H}{2\mu h + \bar{\gamma}} \right)^2, \frac{\bar{\gamma}\lambda}{2(2\mu h + \bar{\gamma})}, -\frac{\lambda}{2} \right) \right] \tag{3.2}$$

where $\mathbf{H}_4(.)$ and $X_{15}(.)$ denote the double variables Horn hypergeometric function [44, eq. (1.3.12)] and the triple variables Exton hypergeometric function [44, eq. (3.3.39a)], respectively.

*Proof:* See Appendix A.1. ∎

### 3.2.2 Average Area under the ROC (AUC) Curve

The average AUC curve, $\bar{A}$, over $\eta - \mu$ fading channel can be evaluated by integrating (2.21) over (2.26) as follows [41]

$$\bar{A} = \int_0^\infty A(\gamma) f_\gamma(\gamma) d\gamma \tag{3.3}$$

After some mathematical operations, the $\bar{A}$ over $\eta - \mu$ fading is yielded as

$$\bar{A} = 1 - \frac{2\sqrt{\pi}\Gamma(2\mu)(\mu^2 h)^\mu}{\Gamma(\mu)\Gamma(\mu + \frac{1}{2})}\left[\frac{2^{2\mu}}{(4\mu h + \bar{\gamma})^{2\mu}}\sum_{n=0}^{u-1}\frac{(2\mu)_n}{n!}\left(\frac{\bar{\gamma}}{4\mu h + \bar{\gamma}}\right)^n\right.$$

$$\times {}_2F_1\left(\mu + \frac{n}{2}, \mu + \frac{n}{2} + \frac{1}{2}; \mu + \frac{1}{2}; \left(\frac{2\mu H}{4\mu h + \bar{\gamma}}\right)^2\right) - \frac{1}{2^u(2\mu h + \bar{\gamma})^{2\mu}}\sum_{n=1-u}^{u-1}\frac{(u)_n}{n!}\left(\frac{1}{2}\right)^n$$

$$\left.\times \mathbf{H}_4\left(2\mu, u + n; \mu + \frac{1}{2}, 1 + n; \left(\frac{2\mu H}{2\mu h + \bar{\gamma}}\right)^2, \frac{\bar{\gamma}}{2(2\mu h + \bar{\gamma})}\right)\right] \tag{3.4}$$

where $(.)_n$ is the Pochhammer symbol.

*Proof:* See Appendix A.2. ∎

## 3.3 Performance Analysis with MRC

In spite of the MRC needs the instantaneous CSI between the PU and the SU that makes the analysis of the ED's performance with MRC is not desirable, many efforts have been achieved to study this scenario as in [61, 41, 91, 92, 94, 99-101].

The PDF of the received SNR over $i.n.d$ $\eta - \mu$ fading channels with MRC diversity branches is given by [103][1]

$$f_{\gamma,i.n.d}^{MRC}(\gamma) = \left(\prod_{i=1}^L\left(\frac{4\mu_i^2 h_i}{\bar{\gamma}_i^2}\right)^{\mu_i}\right)\frac{\gamma^{2\sum_{i=1}^L \mu_i - 1}}{\Gamma\left(2\sum_{i=1}^L \mu_i\right)}\Phi_2^{(2L)}\left(\mu_1, \mu_1, ..., \mu_L, \mu_L; 2\sum_{i=1}^L \mu_i;\right.$$

$$\left. -\frac{2\mu_1(h_1 - H_1)\gamma}{\bar{\gamma}_1}, -\frac{2\mu_1(h_1 + H_1)\gamma}{\bar{\gamma}_1}, ..., -\frac{2\mu_L(h_L - H_L)\gamma}{\bar{\gamma}_L}, -\frac{2\mu_L(h_L + H_L)\gamma}{\bar{\gamma}_L}\right) \tag{3.5}$$

---

[1]It can be noted that the term $\prod_{i=1}^L\left(\frac{4\mu_i^2 h_i}{\bar{\gamma}_i^2}\right)^{\mu_i}$ is written in incorrect form in [103].

where $\Phi_2^{(M)}$ is the confluent multivariate Lauricella hypergeometric function [44, eq. (1.4.8)].

When the variates of the $\eta - \mu$ fading channel are *i.i.d* with MRC diversity receivers, the PDF is easily deduced from (3.5) as follows

$$f_{\gamma,i.i.d}^{MRC}(\gamma) = \left(\frac{4\mu^2 h}{\bar{\gamma}^2}\right)^{L\mu} \frac{\gamma^{2L\mu-1}}{\Gamma(2L\mu)} \Phi_2\left(L\mu, L\mu; 2L\mu; -\frac{2\mu(h-H)\gamma}{\bar{\gamma}}, -\frac{2\mu(h+H)\gamma}{\bar{\gamma}}\right) (3.6)$$

### 3.3.1 Average Probability of Detection

The average probability of detection with MRC diversity combining, $\overline{P}_{d_{i.n.d}}^{MRC}(\lambda)$ can be evaluated by substituting (2.8) and (3.5) into (3.1). Thus, after some mathematical manipulations, this yields

$$\overline{P}_{d_{i.n.d}}^{MRC}(\lambda) = \left(\prod_{i=1}^{L} \left(\frac{4\mu_i^2 h_i}{\bar{\gamma}_i^2}\right)^{\mu_i}\right)\left[\mathcal{K}_{1,i.n.d} - \frac{\lambda^u}{u!2^u}\mathcal{K}_{2,i.n.d}\right] \tag{3.7}$$

with

$$\mathcal{K}_{1,i.n.d} = F_{1:0;\cdots;0;0}^{\overbrace{1:1;\ldots;1;0}^{2L+1}}\left(\begin{matrix}[2\sum_{i=1}^{L}\mu_i : 1, ..., 1, 1] : [\mu_1 : 1]; [\mu_1 : 1]; ...; [\mu_L : 1]; [\mu_L : 1]; -; \\ \\ [2\sum_{i=1}^{L}\mu_i : 1, ..., 1, 0] : \underline{\quad\quad}; \underline{\quad\quad}; ...; \underline{\quad\quad}; \underline{\quad\quad}; -;\end{matrix}\right.$$

$$\left.-\frac{2\mu_1(h_1 - H_1)}{\bar{\gamma}_1}, -\frac{2\mu_1(h_1 + H_1)}{\bar{\gamma}_1}, ..., -\frac{2\mu_L(h_L - H_L)}{\bar{\gamma}_L}, -\frac{2\mu_L(h_L + H_L)}{\bar{\gamma}_L}, 1\right)$$

and

$$\mathcal{K}_{2,i.n.d} = F^{\overbrace{2:1;\,...;\,1;\,0;\,0}^{2L+2}}_{2:0;\,\cdots;\,0;\,0;\,1} \left( \begin{array}{c} [2\sum_{i=1}^{L}\mu_i : 1,...,1,1,0], \quad [u:0,...,0,1,1] \quad : [\mu_1:1];[\mu_1:1];...; \\[2mm] [2\sum_{i=1}^{L}\mu_i : 1,...,1,0,0], [1+u:0,...,0,1,1] : \underline{\quad}; \underline{\quad}; ...; \end{array} \right.$$

$$[\mu_L:1];[\mu_L:1]; \underline{\quad}; \underline{\quad};$$

$$-\frac{2\mu_1(h_1-H_1)}{\bar{\gamma}_1}, -\frac{2\mu_1(h_1+H_1)}{\bar{\gamma}_1}, ...,$$

$$\underline{\quad}; \underline{\quad}; \underline{\quad}; [u:1];$$

$$\left. -\frac{2\mu_L(h_L-H_L)}{\bar{\gamma}_L}, -\frac{2\mu_L(h_L+H_L)}{\bar{\gamma}_L}, -\frac{\lambda}{2}, \frac{\lambda}{2} \right)$$

where $F^{A:B^1;...;B^{(n)}}_{C:D^1;...;D^{(n)}}\left(\cdot\right)$ is the Srivastava and Daoust hypergeometric function defined in [44, eq. (1.4.21)], $[2\sum_{i=1}^{L}\mu_i : 1,...,1,1,1] = (2\sum_{i=1}^{L}\mu_i)_{k_1+j_1+...+k_L+j_L+n}$, $[2\sum_{i=1}^{L}\mu_i : 1,...,1,1,1] = (2\sum_{i=1}^{L}\mu_i)_{k_1+j_1+...+k_L+j_L}$, $[\mu_1:1] = (\mu_1)_{k_1}$, $[\mu_L:1] = (\mu_L)_{k_L}$, $\underline{\quad} = (.)_0$, i.e, $\underline{\quad} = 1$ and it is used in the Srivastava and Daoust hypergeometric function to make the number of terms in the dominator is equal to the number of terms in the numerator and vice versa[2].

*Proof:* See Appendix A.3. ∎

**Corollary 1** *When the diversity branches are i.i.d, the average probability of detection $\overline{P}_{d_{i.i.d}}^{MRC}(\lambda)$ can be computed by inserting (2.8) and (3.6) into (3.1) to yield (3.8).*

$$\overline{P}_{d_{i.i.d}}^{MRC}(\lambda) = \left(\frac{4\mu^2 h}{\bar{\gamma}^2}\right)^{L\mu}\left[\mathcal{K}_{1,i.i.d} - \frac{\lambda^u}{u!2^u}\mathcal{K}_{2,i.i.d}\right] \tag{3.8}$$

where

$$\mathcal{K}_{1,i.i.d} = F_G\left(2L\mu, 2L\mu, 2L\mu, L\mu, L\mu, 1; 1, 2L\mu, 2L\mu; -\frac{2\mu(h-H)}{\bar{\gamma}}, -\frac{2\mu(h+H)}{\bar{\gamma}}, 1\right)$$

---

[2]For further details about all these notations, please refer to (A.13) and [44, eq. (1.4.21)].

and

$$
\mathcal{K}_{2,i.i.d} = F_{2:0;0;1;0}^{2:1;1;0;0}\left(\begin{array}{c}
[2L\mu:1,1,1,0], \quad [u:0,0,1,1] \; : [L\mu:1];[L\mu:1];\underline{\quad\quad};\underline{\quad}; \\[3mm]
[2L\mu:1,1,0,0],[1+u:0,0,1,1]:\underline{\quad\quad}\;;\;\underline{\quad\quad};[u:1];\underline{\quad}; \\[6mm]
-\frac{2\mu(h-H)}{\bar{\gamma}},\; -\frac{2\mu(h+H)}{\bar{\gamma}},\; -\frac{\lambda}{2},\frac{\lambda}{2}
\end{array}\right)
$$

where $F_G(.)$ is another form of the triple variables Saran hypergeometric function [44, eq. (1.5.3)].

    *Proof:* See Appendix A.3. ∎

### 3.3.2 Average Area under the ROC (AUC) Curve

    The average AUC over $i.n.d$ $\eta - \mu$ fading channels with MRC diversity reception, $\bar{A}_{i.n.d}^{MRC}$ can be calculated by averaging (2.21) over (3.5) using (3.3). Accordingly, the result is

$$
\bar{A}_{i.n.d}^{MRC} = 1 - \left(\prod_{i=1}^{L}\left(\frac{4\mu_i^2 h_i}{\bar{\gamma}_i^2}\right)^{\mu_i}\right)\left[\sum_{n=0}^{u-1}2^{2\sum\limits_{i=1}^{L}\mu_i}\frac{\left(2\sum\limits_{i=1}^{L}\mu_i\right)_n}{n!}\mathcal{F}_{1,i.n.d}\right.
$$
$$
\left. -\sum_{n=1-u}^{u-1}\frac{(u)_n}{2^{(u+n)}n!}\mathcal{F}_{2,i.n.d}\right] \quad (3.9)
$$

with

$$
\mathcal{F}_{1,i.n.d} = F_D^{(2L)}\left(n+2\sum_{i=1}^{L}\mu_i;\mu_1,\mu_1,...,\mu_L,\mu_L;2\sum_{i=1}^{L}\mu_i;-\frac{4\mu_1(h_1-H_1)}{\bar{\gamma}_1},\right.
$$
$$
\left. -\frac{4\mu_1(h_1+H_1)}{\bar{\gamma}_1},....,-\frac{4\mu_1(h_L-H_L)}{\bar{\gamma}_L},-\frac{4\mu_1(h_L+H_L)}{\bar{\gamma}_L}\right)
$$

and

$$
\mathcal{F}_{2,i.n.d} = F^{\overbrace{1:1;\,...;\,1;\,1}^{2L+1}}_{1:0;\,...;\,0;\,1}\left(\begin{array}{c} [2\sum\limits_{i=1}^{L}\mu_i:1,...,1,1]:[\mu_1:1];[\mu_1:1];...;[\mu_L:1];[\mu_L:1];[u+n:1]; \\[4mm] [2\sum\limits_{i=1}^{L}\mu_i:1,...,1,0]:\underline{\quad};\underline{\quad};...;\underline{\quad};\underline{\quad};[1+n:1]; \\[6mm] -\dfrac{4\mu_1(h_1+H_1)}{\bar{\gamma}_1},\,-\dfrac{4\mu_1(h_1-H_1)}{\bar{\gamma}_1},\,...,\,-\dfrac{4\mu_1(h_L-H_L)}{\bar{\gamma}_L},\,-\dfrac{4\mu_1(h_L+H_L)}{\bar{\gamma}_L},\,\dfrac{1}{2} \end{array}\right)
$$

where $F_D^{(2L)}(.)$ is the multivariate Lauricella hypergeometric function [44, eq. (1.4.4)].

   *Proof:* See Appendix A.4. ■

**Corollary 2** *When the diversity branches are i.i.d, the AUC curve, $\bar{A}_{i.i.d}^{MRC}$, can be evaluated by integrating (2.21) over the PDF in (2.6) to yield (3.10).*

$$
\overline{A}_{i.i.d}^{MRC} = 1 - \left(\frac{4\mu^2 h}{\bar{\gamma}^2}\right)^{L\mu}\left[\sum_{n=0}^{u-1}2^{2L\mu}\frac{(2L\mu)_n}{n!}\mathcal{F}_{1,i.i.d} - \sum_{n=1-u}^{u-1}\frac{(u)_n}{2^{(u+n)}n!}\mathcal{F}_{2,i.i.d}\right] \tag{3.10}
$$

with

$$
\mathcal{F}_{1,i.i.d} = F_D^{(2)}\left(n+2L\mu;L\mu,L\mu;2L\mu;-\frac{4\mu(h-H)}{\bar{\gamma}},-\frac{4\mu(h+H)}{\bar{\gamma}}\right)
$$

and

$$
\mathcal{F}_{2,i.i.d} = F_G\left(2L\mu,2L\mu,2L\mu,L\mu,L\mu,u+n;n+1,2L\mu,2L\mu;\right.
$$
$$
\left.-\frac{2\mu(h-H)}{\bar{\gamma}},-\frac{2\mu(h+H)}{\bar{\gamma}},\frac{1}{2}\right)
$$

where $F_D^{(2)}$ is another model of the double variables Lauricella hypergeometric function [43, eq. (9.180.1)] [3].

   *Proof:* See Appendix A.4. ■

---

[3]It can be observed that $F_D^{(2)}$ is a special case of $F_D^{(M)}$ with $M=2$.

52

## 3.4 Performance Analysis with SLC

As mentioned in Subsection 2.7.2, the only difference between the MRC and the SLC is in the time-bandwidth product. Thus, the average probability of detection over $\eta - \mu$ fading channels with $i.n.d$ and $i.i.d$ SLC diversity receivers calculated by (3.7) and (3.8), respectively after replacing $u$ by $Lu$. Similarly, the average AUC curve for $i.n.d$ and $i.i.d$ $\eta - \mu$ fading channels with SLC diversity receivers are obtained from (3.9) and (3.10), respectively.

## 3.5 Performance Analysis with SLS

### 3.5.1 Average Detection Probability

The average probability of detection for $i.n.d$ SLS diversity reception $\overline{P}_{d,i.n.d}^{SLS}(\lambda)$ is given by [30]

$$\overline{P}_{d,i.n.d}^{SLS}(\lambda) = 1 - \prod_{i=1}^{L} \int_{0}^{\infty} \left[1 - Q_u(\sqrt{2\gamma_i}, \sqrt{\lambda})\right] f_{\gamma_i}(\gamma_i) d\gamma_i \tag{3.11}$$

Similar to deriving (3.1) in Appendix A.1, the $\overline{P}_{d,i.n.d}^{SLS}(\lambda)$ over $i.n.d$ $\eta - \mu$ fading channels can be computed by substituting (2.26) in (3.11) to yield

$$\overline{P}_{di.n.d}^{SLS}(\lambda) = 1 - \prod_{i=1}^{L} \left[ 1 - \frac{2\sqrt{\pi}\Gamma(2\mu_i)}{\Gamma(\mu_i)\Gamma(\mu_i + \frac{1}{2})} \left( \frac{\mu_i^2 h_i}{(\bar{\gamma}_i + 2\mu_i h_i)^2} \right)^{\mu_i} \right.$$
$$\times \left\{ \mathbf{H}_4 \left( 2\mu_i, 1; \mu_i + \frac{1}{2}, 1; \frac{(\mu_i H_i)^2}{(2\mu_i h_i + \bar{\gamma}_i)^2}, \frac{\bar{\gamma}_i}{2\mu_i h_i + \bar{\gamma}_i} \right) \right.$$
$$\left. \left. - \frac{\lambda^u}{u!2^u} X_{15} \left( 2\mu_i, u; u, 1 + u, \mu_i + \frac{1}{2}; \frac{(\mu_i H_i)^2}{(2\mu_i h_i + \bar{\gamma}_i)^2}, \frac{\bar{\gamma}_i \lambda}{2(2\mu_i h_i + \bar{\gamma}_i)}, -\frac{\lambda}{2} \right) \right\} \right] \tag{3.12}$$

For the case of $i.i.d$ SLS diversity branches, the $\overline{P}_{d,i.i.d}^{SLS}(\lambda)$ over $\eta - \mu$ fading channels

can be deduced from (3.12) as follows

$$
\overline{P}_{d.i.i.d}^{SLS}(\lambda) = 1 - \Bigg[ 1 - \frac{2\sqrt{\pi}\Gamma(2\mu)}{\Gamma(\mu)\Gamma(\mu+\frac{1}{2})} \left( \frac{\mu^2 h}{(\bar{\gamma}+2\mu h)^2} \right)^{\mu}
$$
$$
\times \Bigg\{ \mathbf{H}_4 \left( 2\mu, 1; \mu+\frac{1}{2}, 1; \frac{(\mu H)^2}{(2\mu h+\bar{\gamma})^2}, \frac{\bar{\gamma}}{2\mu h+\bar{\gamma}} \right)
$$
$$
- \frac{\lambda^u}{u!2^u} X_{15} \left( 2\mu, u; u, 1+u, \mu+\frac{1}{2}; \frac{(\mu H)^2}{(2\mu h+\bar{\gamma})^2}, \frac{\bar{\gamma}\lambda}{2(2\mu h+\bar{\gamma})}, -\frac{\lambda}{2} \right) \Bigg\} \Bigg]^{L} \quad (3.13)
$$

### 3.5.2 Average Area under the ROC (AUC)

It is obvious from (2.38) and (2.39) that the unfaded AUC curve for both $i.i.d$ and $i.n.d$ SLS diversity scheme over any fading channel can not be calculated by using (2.21). Accordingly, the exact analytic expression of the unfaded AUC curve for $i.n.d$ SLS diversity reception is firstly derived as shown in Appendix A.5. Then, the exact expression for the AUC curve with $i.n.d$ SLS diversity branches, $\bar{A}_{i.n.d}^{SLS}$, over $\eta-\mu$ fading channels is deduced as follows

$$
\bar{A}_{i.n.d}^{SLS} = \frac{\Gamma(1+Lu)}{[\Gamma(1+u)]^L} \Bigg[ F_A^{(L-1)}(Lu; u, ..., u; 1+u, ..., 1+u; -1, ..., -1) - \frac{\mathcal{G}(Lu)_{Lu}}{[\Gamma(1+u)]^L}
$$

$$
\times F_L^{2L+1:\overbrace{0;\cdots;0}^{L};\overbrace{1;\cdots;1}^{L};\overbrace{0;\cdots;0}^{2L-1}}_{\quad\;\; :2;\cdots;2;1;\cdots;1;1;\cdots;1} \Bigg( \begin{array}{c} [P_1 : \vartheta_1^{(1)}, ..., \vartheta_1^{(3L-1)}], [P_2 : \vartheta_2^{(1)}, ..., \vartheta_2^{(L)}], [P_3 : \vartheta_3^{(1)}, ..., \vartheta_3^{(L)}] : \\[4pt] [C : \vartheta_2^{(1)}, ..., \vartheta_2^{(L)}] \end{array} \Big|
$$

$$
\underline{\qquad} \; ; ...; \; \underline{\qquad} \; ; [p_1^{(1)} : \phi_1^{(1)}] ; ...; [p_1^{(2L-1)} : \phi_1^{(2L-1)}]; \quad \underline{\qquad} \; ; ...; \; \underline{\qquad} \; ;
$$

$$
[c_1^{(1)} : \psi_1^{(1)}]; ...; [c_1^{(L)} : \psi_1^{(L)}]; [c_2^{(1)} : \psi_2^{(1)}]; ...; [c_2^{(2L-1)} : \psi_2^{(2L-1)}]; [c_3^{(1)} : \psi_3^{(1)}]; ...; [c_3^{(L)} : \psi_3^{(L)}];
$$

$$
\frac{\bar{\gamma}_1}{2\mu_1 h_1+\bar{\gamma}_1}, \; ..., \; \frac{\bar{\gamma}_L}{2\mu_L h_L+\bar{\gamma}_L}, \frac{(\mu_1 H_1)^2}{(2\mu_1 h_1+\bar{\gamma}_1)^2}, \; ..., \; \frac{(\mu_L H_L)^2}{(2\mu_L h_L+\bar{\gamma}_L)^2}, -1, ..., -1 \Bigg) \Bigg]
$$

$$
(3.14)
$$

where $F_A^{(L-1)}(.)$ is another model of the multivariate Lauricella hypergeometric function defined in [44, eq. (1.4.1)], $\mathcal{G} = \prod_{i=1}^{L} \frac{2\sqrt{\pi}\Gamma(2\mu_i)}{\Gamma(\mu_i)\Gamma(\mu_i+\frac{1}{2})} \left( \frac{\mu_i^2 h_i}{(2\mu_i h_i + \bar{\gamma})^2} \right)^{\mu_i}$, $\vartheta_1 = [1, 1, \cdots, 1]$, $P_1 = 2Lu$, $P_2 = [u, \cdots, u]$, $P_3 = [2\mu_1, \cdots, 2\mu_L]$, and $C = [1+u, \cdots, 1+u]$. Moreover, $\vartheta_2 = \vartheta_3$ with $L \times L$ dimensions where

$$\vartheta_2 = \begin{bmatrix} 1 & 1 & 0 & 0 & \cdots & 0 & 0 \\ 0 & 0 & 1 & 1 & \cdots & 0 & 0 \\ \vdots & \vdots & \vdots & \vdots & \ddots & \vdots & \vdots \\ 0 & 0 & 0 & 0 & \cdots & 1 & 1 \end{bmatrix}$$

$d_1^{(i)} = \phi_1^{(i)} = 0 \;\; \forall \;\; i \in \{1, \cdots, L\}$, $d_1^{(i)} = u$ and $\phi_1^{(i)} = 1 \;\; \forall \;\; i \in \{L+1, \cdots, 2L-1\}$, $c_1^{(i)} = u$ and $\psi_1^{(i)} = 1 \;\; \forall \;\; i \in \{1, \cdots, L\}$, $c_2^{(i)} = \psi_2^{(i)} = 0 \;\; \forall \;\; i \in \{1, \cdots, L\}$, $c_2^{(i)} = 1 + u$ and $\psi_2^{(i)} = 1 \;\; \forall \;\; i \in \{L+1, \cdots, 2L-1\}$, and $c_3^{(i)} = \mu_i + \frac{1}{2}$ and $\psi_3^{(i)} = 1 \;\; \forall \;\; i \in \{1, \cdots, L\}$.

*Proof:* See Appendix A.5. ∎

## 3.6    Numerical Results

This section provides the numerical results of the performance of energy detector over $\eta - \mu$ fading channel[4]. These results are generated for different cases through the complementary ROC (CROC) curves, i.e., $\overline{P_{md}}$ against $P_f$ and the complementary AUC (CAUC), $1 - \overline{A}$, versus average SNR, $\bar{\gamma}$, curves using MATLAB software package.

Fig. 3.1 (top of the next page) illustrates the CROC curves of energy detector over $\eta - \mu$ fading channel with $\bar{\gamma} = 5$ dB and $u = 1$ and for different values of $\eta$ and $\mu$. From this figure, it can be noticed that when $\eta$ or/and $\mu$ increase, the performance of energy detector becomes better. This is because higher $\eta$ and $\mu$ correspond to high power rate, i.e., the total power of the in-phase components is higher than the total

---

[4]In this thesis, Format 1 is employed and the results for Format 2 can be easily obtained from Format 1 by applying the bilinear transformation as described in [51].
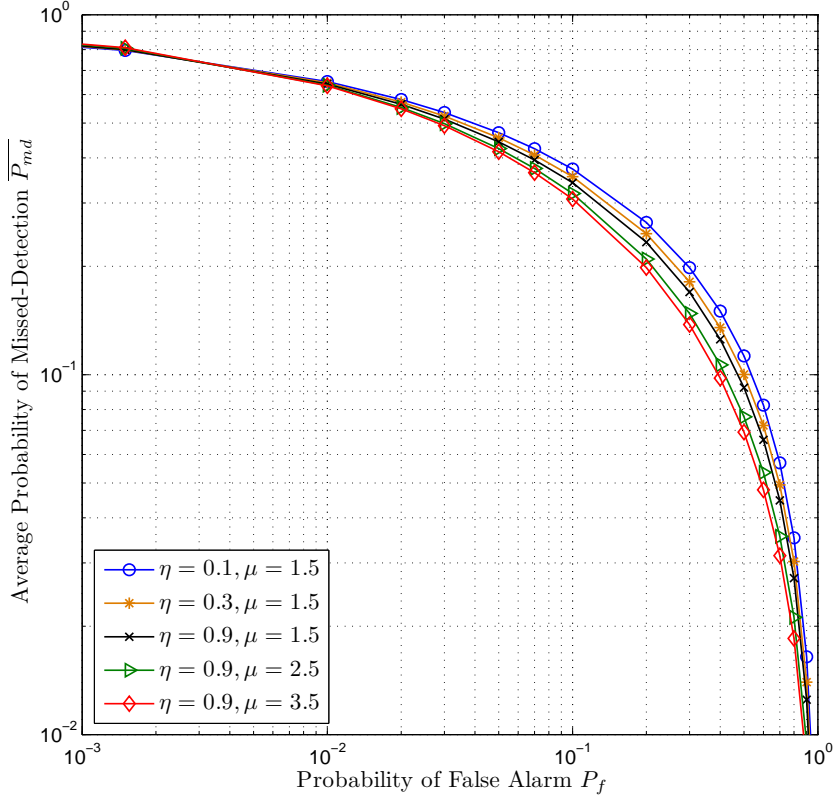
Figure 3.1: Complementary ROC curves of energy detector over $\eta - \mu$ fading channel with $\bar{\gamma} = 5$ dB and $u = 1$ and for different values of $\eta$ and $\mu$ (Format 1).

power of the quadrature components and large number of the multipath clusters, respectively. For example, when $P_f = 0.1$, $\eta = 0.9$ (fixed), the $\overline{P_{md}}$ for $\mu = 3.5$ is nearly 10% less than for $\mu = 1.5$. In the same context, when $\eta$ increases from 0.1 to 0.9 with $\mu$ is fixed at 1.5, the $\overline{P_{md}}$ reduces for about 8% from its original value. From previous results, one can observe that $\mu$ has higher impact on the energy detector performance than $\eta$.

Fig. 3.2 (top of the next page) shows the CAUC of energy detector over $\eta - \mu$ fading channel versus the average SNR, $\bar{\gamma}$, with $u = 1$ and for different values of $\eta$ and $\mu$. The results in this figure confirm the results of Fig. 3.1. However, the differences between the compared curves in Fig. 3.2 are clearer than Fig. 3.1. This case explains one of the AUC curve's advantages. For example, for the case of $\bar{\gamma} = 7$ dB, $\eta = 0.9$

56
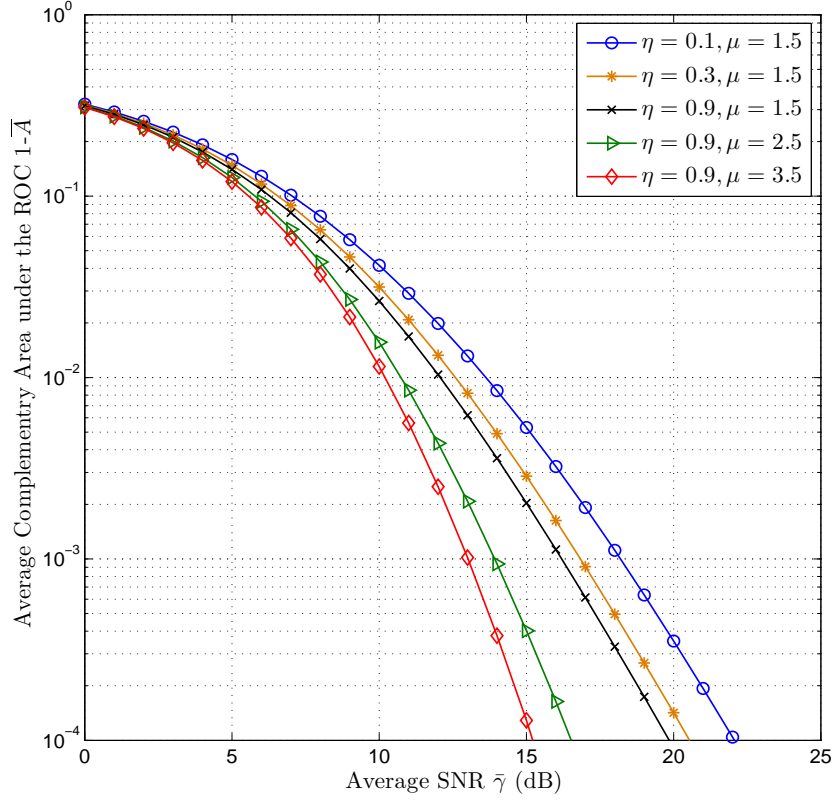
Figure 3.2: Complementary AUC of energy detector over $\eta - \mu$ fading channel versus the average SNR, $\bar{\gamma}$, with $u = 1$ and for different values of $\eta$ and $\mu$ (Format 1).

(fixed), the CAUC for $\mu = 3.5$ is roughly 27% less than for $\mu = 1.5$. In the same context, when $\mu = 1.5$ (fixed), the CAUC for $\eta = 0.9$ is about 20% less than for the case of $\eta = 0.1$.

Fig. 3.3 (top of the next page) depicts the CROC curves of energy detector for different diversity schemes over $i.n.d$ $\eta - \mu$ fading channels with $u = 1$. In this figure, three diversity scenarios which are single-branch, three-branches and five-branches for MRC, SLC and SLS diversity reception are employed. In all these scenarios, the simulation parameters for each branch are set to $(\eta_1, \mu_1, \bar{\gamma}_1) = (0.5, 0.7, 0$ dB$)$, $(\eta_2, \mu_2, \bar{\gamma}_2) = (1.2, 1.5, 1$ dB$)$, $(\eta_3, \mu_3, \bar{\gamma}_3) = (2.3, 3.1, 2$ dB$)$, $(\eta_4, \mu_4, \bar{\gamma}_4) = (3.4, 4.6, 5$ dB$)$ and $(\eta_5, \mu_5, \bar{\gamma}_5) = (4.7, 5.2, 10$ dB$)$. As expected, the overall detection capability of energy detector with diversity reception is better than the case of no-diversity. This
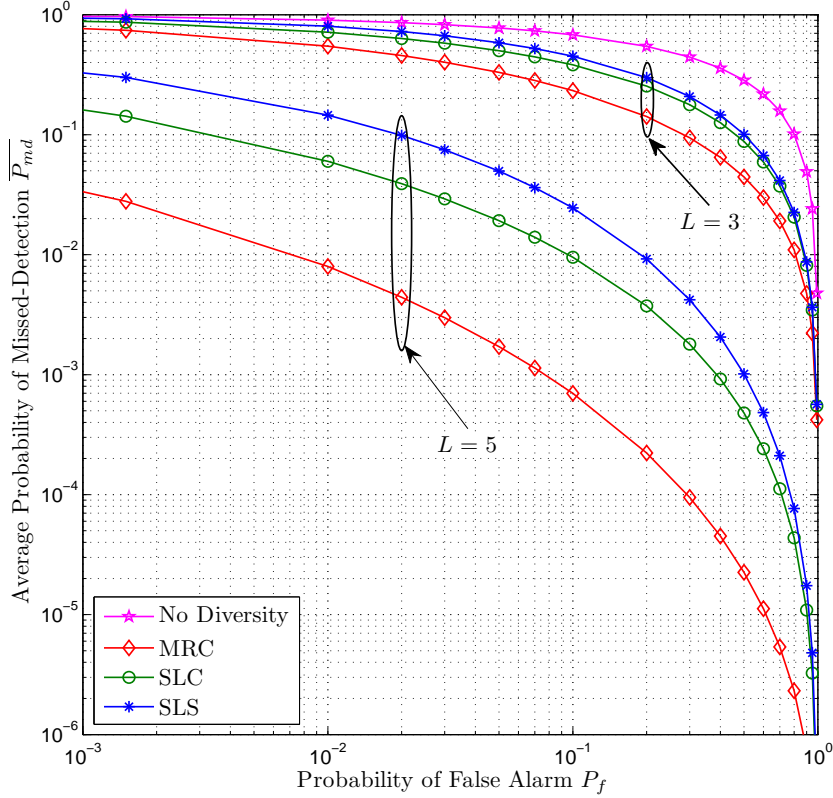
Figure 3.3: Complementary ROC curves of energy detector for different diversity receptions over *i.n.d* $\eta - \mu$ fading channels with $(\eta_1, \mu_1, \bar{\gamma}_1) = (0.5, 0.7, 0$ dB$)$, $(\eta_2, \mu_2, \bar{\gamma}_2) = (1.2, 1.5, 1$ dB$)$, $(\eta_3, \mu_3, \bar{\gamma}_3) = (2.3, 3.1, 2$ dB$)$, $(\eta_4, \mu_4, \bar{\gamma}_4) = (3.4, 4.6, 5$ dB$)$, $(\eta_5, \mu_5, \bar{\gamma}_5) = (4.7, 5.2, 10$ dB$)$ (Format 1) and $u = 1$.

refers to the increase in either the average SNR (in MRC diversity receivers) or the calculated energy (in both SLC and SLS diversity receivers) at the SU side which increases the test statistic $\Xi$. For example, the value of $\overline{P_{md}}$ for $P_f = 0.1$ (fixed) and $L = 1$ is nearly 34%, 44% and 66% larger than for SLS, SLC and MRC, respectively with $L = 3$. Obviously, these gains rise when $L = 5$ due to the increase in all fading parameters for the fourth and the fifth branches as well as the number of the diversity branches, i.e., the total average SNR or the evaluated energy.

The results in Fig. 3.3 are also confirmed by Fig. 3.4 (top of the next page) which explains the CAUC for different SNR values and for the same scenarios of Fig. 3.3.
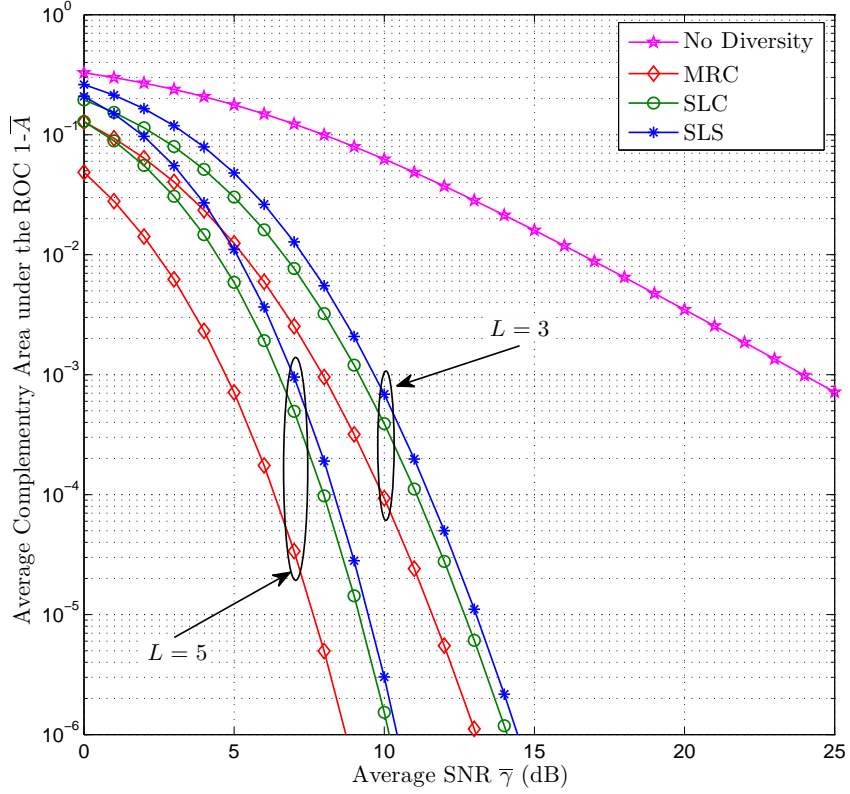
Figure 3.4: Complementary AUC versus average SNR, $\bar{\gamma}$, for different diversity receptions over $i.n.d$ $\eta - \mu$ fading channels with $(\eta_1, \mu_1) = (0.5, 0.7)$, $(\eta_2, \mu_2) = (1.2, 1.5)$, $(\eta_3, \mu_3) = (2.3, 3.1)$, $(\eta_4, \mu_4) = (3.4, 4.6)$, $(\eta_5, \mu_5) = (4.7, 5.2)$ (Format 1) and $u = 1$.

The results in Fig. 3.4 show different gains between the performed scenarios than in Fig. 3.3. For instance, when $\bar{\gamma} = 5$ dB (fixed) and $L = 1$, the value of CAUC is roughly 73%, 83% and 93% higher compared with the corresponding cases of SLS, SLC and MRC, respectively with $L = 3$.

Fig. 3.5 (top of the next page) demonstrates the effect of the number of diversity branches, $L$, on the behaviour of energy detector over $i.i.d$ $\eta - \mu$ fading channels. The simulation parameters are set to $\eta = 0.7$, $\mu = 1.2$, $\bar{\gamma} = 3$ dB, $P_f = 0.01$ and $u = 3$. One can observe a significant effect for $L$ on both the $\overline{P_d}$ and the $\bar{A}$ and for all diversity techniques. For example, for $L = 7$, it can be seen that the amplitudes of $\overline{P_d}$
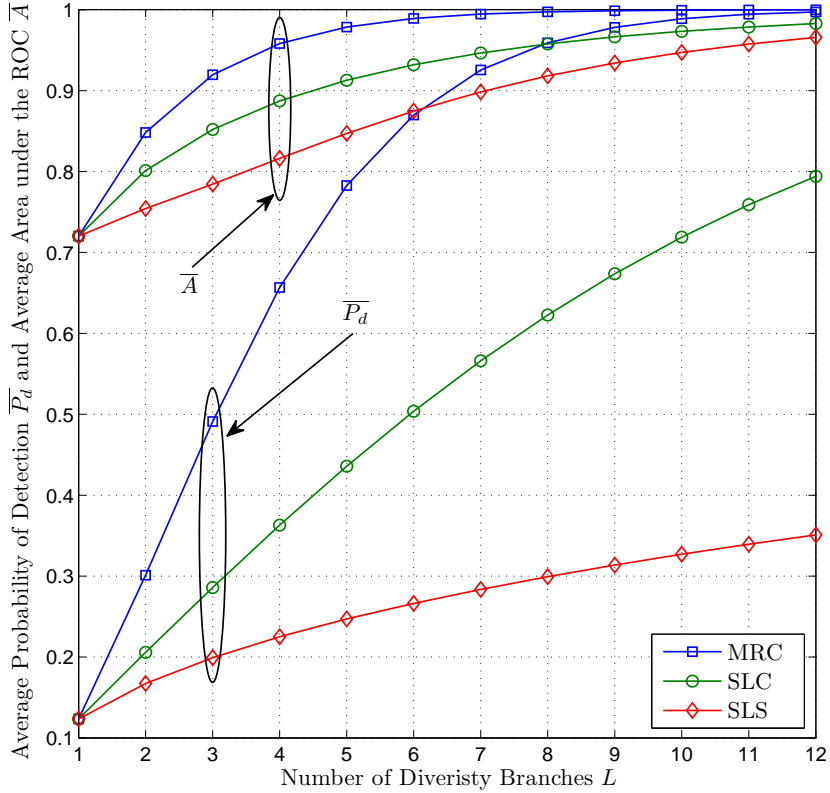
Figure 3.5: Average probability of detection, $\overline{P_d}$ and average AUC curves, $\bar{A}$, versus the number of diversity branches for different $i.i.d$ combining schemes with $\eta = 0.7$, $\mu = 1.2$ (Format 1), $\bar{\gamma} = 3$ dB, $P_f = 0.01$ and $u = 3$.

are approximately 41%, 56% and 26% higher compared with the corresponding case of $L = 4$ for MRC, SLC and SLS, respectively. In the same context, the values of $\bar{A}$ for $L = 4$ are lower by about 4%, 6% and 9% for MRC, SLC and SLS respectively than for $L = 7$.

Fig. 3.6 (top of the next page) portrays the CROC curves of energy detector for different CSS scenarios with non-identical SUs over $\eta - \mu$ fading channels. The simulation parameters for each user are chosen as $(\eta_3, \mu_3, \bar{\gamma}_3, P_{f_3}) = (0.1, 0.8, 5$ dB, $[0.01, 0.99]$ with $\Delta = 0.035)$, $(\eta_4, \mu_4, \bar{\gamma}_4, P_{f_4}) = (0.3, 1.5, 4$ dB, $[0.01, 0.99]$, with $\Delta = 0.035)$, $(\eta_5, \mu_5, \bar{\gamma}_5, P_{f_5}) = (0.6, 1.9, 3$ dB, $[0.02, 1]$, with $\Delta = 0.035)$, $(\eta_6, \mu_6, \bar{\gamma}_6, P_{f_6}) = (0.9, 2.6, 2$ dB, $[0.025, 0.99]$, with $\Delta = 0.034)$, $(\eta_7, \mu_7, \bar{\gamma}_7, P_{f_7}) = (1.3,$
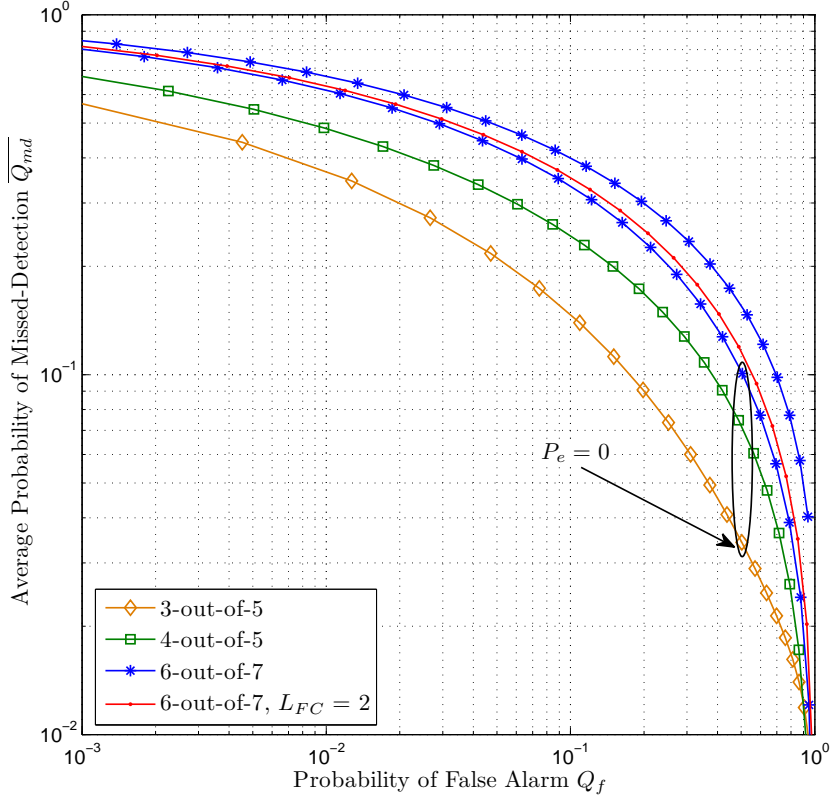
Figure 3.6: Complementary ROC curves for different CSS scenarios with non-identical SUs over $\eta - \mu$ fading channels (Format 1).

3.5, 1.5 dB, $[0.026, 0.99]$, with $\Delta = 0.034$) and $(\eta_{FC}, \mu_{FC}, \bar{\gamma}_{FC}) = (0.5, 3.5, 2.5$ dB$)$[5]. Furthermore, the reporting channel is assumed to be error-rate channel. This error is evaluated as an ABEP over $\eta - \mu$ fading channel by using [56, eq. (10)] for a signal with binary phase shift keying (BPSK) modulation. As explained in Fig. 3.6, substantial enhancements in the behaviour of energy detector occur when the number of collaborated SUs increases. This refers to decreasing in the sensing error probabilities (missed-detection and false alarm probabilities) at the FC. However, a large number of participant SUs makes the sensing time high in comparison with small number of SUs. For example, for the case with no-diversity at the FC and the

---

[5]The notations [,] and $\Delta$ indicate for the closed interval and step size, respectively.

reporting channel with free error-rate, i.e., $P_e = 0$, the value of $\overline{Q_{md}}$ $(\overline{Q_{md}} = 1 - \overline{Q_d})$ for 4-out-of-5 is larger than for 3-out-of-5 by 66% at $Q_f = 0.1$. In the same context, the $\overline{Q_{md}}$ for 6-out-of-7 is higher than for 4-out-of-5 by 37%. When the reporting channel is assumed to be error-rate channel, the value of $\overline{Q_{md}}$ increases by 20% for 6-out-of-7 with $Q_f = 0.1$ and no-diversity at the FC. This is because the $P_e$ increases both the missed-detection and false alarm probabilities and makes their increase faster than for error-free channel. This impact can be minimized by employing one of diversity combining techniques at the FC. Since the reporting channel case is known by the FC, the MRC scheme is the best choice to reduce $P_e$. For simplicity, dual diversity receivers over $i.n.d$ $\eta - \mu$ fading channels are employed. For both branches, the channel parameters are set to $(\eta_{FC_1}, \mu_{FC_1}, \bar{\gamma}_{FC_1}) = (0.5, 3.5, 2.5 \text{ dB})$ and $(\eta_{FC_2}, \mu_{FC_2}, \bar{\gamma}_{FC_2}) = (0.7, 2.1, 0.8 \text{ dB})$. As expected, an improvement in the detection capability of energy detector is obtained by using the diversity technique. For instance, for the case of 6-out-of-7 and $Q_f = 0.1$, the value of $\overline{Q_{md}}$ is degraded by 13% when the diversity reception is utilised.

## 3.7    Conclusions

In this chapter, the behaviour of the energy detector over $\eta - \mu$ fading channels was analysed by deriving exact analytic expressions for both the average probability of detection and the average AUC by using the PDF approach. The analysis was also carried out over $i.n.d$ $\eta - \mu$ fading channels with MRC, SLC, SLS diversity schemes and CSS scenarios. From the provided results, it was noticed that the performance of the energy detector improves when $\eta$ or/and $\mu$ increase. Furthermore, the parameter $\mu$ has a higher impact on the detectability of energy detector in comparison with $\eta$. This superiority becomes more clear by using the average CAUC versus the average SNR rather than the CROC curves. Moreover, the MRC was better than the SLC and the SLS diversity receivers. However, it requires for a CSI between the PU and the SU, i.e., information about the sensing channel. It was also observed that an improvement in the performance of energy detector in CSS is achieved when the number of SUs who participate in the decision increases. The reason is as follows, when $Q_f$ is fixed,

$P_e = 0$ and by using (2.41), one can see that $Q_{md}^{k\text{-out-of-}n} = Q_{md}^{k+1\text{-out-of-}n} - \binom{n}{k} P_{d_k}^k (1 - P_{d_k})^{n-k}$. Moreover, when the reporting channel is assumed to be an error channel, the performance of CSS is degraded due to the increase in the total error rate probability, i.e., $Q_{md} + Q_f$ at the FC.

# Chapter 4

# Performance Analysis of an Energy Detector over $\kappa - \mu$ Shadowed

This chapter analyses the performance of an energy detector over $\kappa - \mu$ shadowed fading channel. Exact analytic expressions for the average detection probability and the average AUC curve are derived first. Thereafter, different diversity reception techniques such as MRC, SLC, and SLS schemes are employed to improve the detectability of the SU. Two cases of diversity branches which are fully $i.i.d$ and fully $i.n.d$ $\kappa - \mu$ shadowed fading channels are investigated. Moreover, different CSS scenarios over $\kappa - \mu$ shadowed fading for both the sensing and the reporting channels are shown. The case of FC with MRC diversity receivers to reduce the error rate probability is analysed. Finally, the behaviour of an energy detector over $\kappa - \mu$ extreme shadowed fading channel which is a special case of the $\kappa - \mu$ shadowed fading is explained.

## 4.1   Introduction

The wireless signal is also affected by shadowing which is a part of fading that can not be ignored. This impact has been studied, in the open technical literature, by few works with limited contributions [104-110]. In [104-107], the performance of energy detector over $K$ and $K_G$ which are mixture of Rayleigh/gamma distributions and Nakagami-$m$/gamma distributions, respectively is analysed. The authors in [104]

have assumed the multipath fading parameters are identical for all branches whereas the shadowing parameters are supposed to be identical and non-identical over MRC and SC diversity receptions. In contrast to [104], the behaviour of energy detector over $K_G$ is investigated in [105] by using closed-from expression for the average probability of detection. The study in [106] is based on deriving the average AUC curves over fully $i.i.d$ $K_G$ fading channels with MRC, SLC and SC diversity schemes. A learning approach is proposed by [107] to provide spectrum sensing over $K_G$ fading with $i.i.d$ branches for both MRC and SLC systems. In [108], the approximated MGF expression for the Nakagami-lognormal is employed to derive the average probability of detection for both SLC and SLS receivers with $i.i.d$ branches. Both the average probability of detection and the average AUC curves over gamma shadowed Rician fading channel are given in [109] for no diversity scheme. The previous work is then extended by the same authors in [110] to include MRC, EGC, and SC schemes under condition of $i.i.d$ diversity receivers.

Recently, the so-called $\kappa - \mu$ shadowed fading distribution is introduced in [111] as a composite generalised distribution which includes both multipath fading and shadowing. In this distribution, the $\kappa - \mu$ and Nakagami-$m$ distributions are utilised to model the multipath fading and shadowing, respectively. As explained in Section 2.5 regarding the features of the generalised distributions, the $\kappa - \mu$ shadowed fading channel gives better fitting to the experimental data of realistic communications than composite conventional channel models that are used in the literature. Furthermore, this channel includes special cases of previously used composite fading channel, such as Rician fading channel with Nakagami-$m$ shadowing [109]. Thus, this channel is very useful to obtain practical comprehensive analysis for the performance of energy detector over fading channel with both multipath and shadowing. From aforementioned advantages for the $\kappa - \mu$ shadowed fading channel as well as from the open technical literature that shows this channel has not been yet employed in studying the behaviour of energy detector, this channel is used in this chapter. This study has led to several novel contributions which are summarized as follows:

- Providing exact analytic expression for both the average probability of detection

65

and the average AUC curve over $\kappa - \mu$ shadowed fading channel.

- Extending the expressions in the previous point to include MRC, SLC, and SLS schemes with $i.n.d$ and $i.i.d$ diversity branches.

- Studying the behaviour of energy detector over $\kappa - \mu$ extreme shadowed fading channel which is a special case of $\kappa - \mu$ shadowed fading channel to model the wireless channels of the communication scenarios in enclosed environments.

- Analysing different general scenarios of CSS with non-identical SUs using energy detector over $\kappa - \mu$ shadowed fading channel for both sensing and reporting channels. Similar to Chapter 3, the error rate at the reporting channel is evaluated and reduced by employing MRC scheme with dual branches.

## 4.2 $\kappa - \mu$ Shadowed Fading Channel

In the $\kappa - \mu$ shadowed fading channel, the shadowing is represented by Nakagami-$m$ distribution because it provides simple statistical characteristics expressions, i.e., PDF, CDF, and MGF in comparison with other distributions such as lognormal distribution. Therefore, this channel has three parameters which are: $\kappa$, $\mu$, and $m$ which stands for the shadowing severity parameter.

The PDF of the instantaneous SNR, $\gamma$, over $\kappa - \mu$ shadowed fading channel is expressed by [111],

$$f_\gamma(\gamma) = \frac{\mu^\mu m^m (1+\kappa)^\mu \gamma^{\mu-1}}{\Gamma(\mu)\bar{\gamma}^\mu(\mu\kappa+m)^m} e^{-\frac{\mu(1+\kappa)\gamma}{\bar{\gamma}}} {}_1F_1\left(m;\mu;\frac{\mu^2\kappa(1+\kappa)}{(\mu\kappa+m)}\frac{\gamma}{\bar{\gamma}}\right) \tag{4.1}$$

where ${}_1F_1(.;.;.)$ is another model of the confluent hypergeometric function defined in [44, eq. (1.2.23)]

## 4.3 Performance Analysis with No Diversity

### 4.3.1 Average Probability of Detection

The average probability of detection, $\overline{P_d}(\lambda)$, over $\kappa - \mu$ shadowed fading channel can be computed by inserting $P_d(\gamma, \lambda)$ of (2.8) and the PDF of the instantaneous SNR $\gamma$ of (4.1) in (3.1). After some mathematical operations, the exact expression for $\overline{P_d}(\lambda)$ is given as follows

$$
\overline{P_d}(\lambda) = \frac{\mu^\mu m^m (1+\kappa)^\mu}{(\mu(1+\kappa) + \bar{\gamma})^\mu (\mu\kappa + m)^m}
$$
$$
\times \left[ F_2\left( \mu, m, 1; \mu, 1; \frac{\mu^2\kappa(1+\kappa)}{(\mu\kappa + m)(\mu(1+\kappa) + \bar{\gamma})}, \frac{\bar{\gamma}}{(\mu(1+\kappa) + \bar{\gamma})} \right) \right.
$$
$$
- \frac{\lambda^u}{u! 2^u} F_M\left( m, u, u, \mu, u, \mu; \mu, 1+u, 1+u; \right.
$$
$$
\left. \left. \frac{\mu^2\kappa(1+\kappa)}{(\mu\kappa + m)(\mu(1+\kappa) + \bar{\gamma})}, \frac{\bar{\gamma}\lambda}{2(\mu(1+\kappa) + \bar{\gamma})}, -\frac{\lambda}{2} \right) \right] \quad (4.2)
$$

where $F_2(.)$ and $F_M(.)$ denote the double variables Appell hypergeometric function [43, eq. (9.180.2)] and the triple variables Saran hypergeometric function [44, eq. (1.5.5)], respectively.

*Proof:* See Appendix B.1. ∎

It is noted that, for the special case of $\kappa - \mu$ shadowed fading channel, when $m \to \infty$ and after some mathematical operations, (4.2) becomes identical to the previously derived expression [95, eq. (15)]. Moreover, when $m \to \infty$ and $\kappa \to 0$, (4.2) is identical to the $\overline{P_d}(\lambda)$ over Nakagami-$m$ fading channel [30, eq. (7)], [61, eq. (8)] and Rayleigh fading channel [30, eq. (9)] with $\mu = m$ and $m = 1$, respectively. The Rician shadowed fading channel is obtained by setting the channel parameters as follows: $m \to \infty$ and $\kappa = K$ where $K$ is the Rician factor. Accordingly, (4.2) is equivalent to [109, eq. (12)].

## 4.3.2 Average Area under the ROC (AUC)

The average AUC, $\bar{A}$, can be calculated by averaging the unfaded AUC of (2.21) over the PDF of the received SNR $\gamma$ of (4.1) using (3.3). Accordingly, this yields

$$
\bar{A} = 1 - \frac{\mu^\mu m^m (1+\kappa)^\mu}{(\mu\kappa + m)^m} \left[ \frac{2^\mu}{(2\mu(1+\kappa)+\bar{\gamma})^\mu} \sum_{n=0}^{u-1} \frac{(\mu)_n}{n!} \left( \frac{\bar{\gamma}}{(2\mu(1+\kappa)+\bar{\gamma})} \right)^n \right.
$$
$$
\times {}_2F_1\left( m, \mu+n; \mu; \frac{2\mu^2\kappa(1+\kappa)}{(\mu\kappa+m)(2\mu(1+\kappa)+\bar{\gamma})} \right) - \frac{1}{2^u(\mu(1+\kappa)+\bar{\gamma})^\mu} \sum_{n=1-u}^{u-1} \frac{(u)_n}{n!} \left( \frac{1}{2} \right)^n
$$
$$
\left. \times F_2\left( \mu, m, u+n; \mu, 1+n; \frac{\mu^2\kappa(1+\kappa)}{(\mu\kappa+m)(\mu(1+\kappa)+\bar{\gamma})}, \frac{\bar{\gamma}}{2(\mu(1+\kappa)+\bar{\gamma})} \right) \right] \tag{4.3}
$$

*Proof:* See Appendix B.2. ∎

It is noted that, when $m \to \infty$ and $\kappa \to 0$ (Nakagami-$m$ fading channel) with some straightforward mathematical operations, (4.3) becomes equal to [41, eq. (13)] with $\mu = m$. In addition, when $\mu = 1$, (4.3) is identical to expression of $\bar{A}$ over Rician shadowed fading channel [109, eq. (20)].

## 4.4 Performance Analysis with MRC

The PDF of the sum of $i.n.d$ $\kappa - \mu$ shadowed fading variates that can be employed for MRC is given by [111]

$$
f_{\gamma,i.n.d}^{MRC}(\gamma) = \left( \prod_{i=1}^{L} \frac{\mu_i^{\mu_i} m_i^{m_i} (1+\kappa_i)^{\mu_i}}{(\mu_i\kappa_i + m_i)^{m_i}} \left( \frac{1}{\bar{\gamma}_i} \right)^{\mu_i} \right) \frac{\gamma^{\sum_{i=1}^{L}\mu_i - 1}}{\Gamma\left( \sum_{i=1}^{L}\mu_i \right)}
$$
$$
\times \Phi_2^{(2L)}\left( \mu_1 - m_1, ..., \mu_L - m_L, m_1, ..., m_L; \sum_{i=1}^{L}\mu_i; -\frac{\mu_1(1+\kappa_1)\gamma}{\bar{\gamma}_1}, ..., -\frac{\mu_L(1+\kappa_L)\gamma}{\bar{\gamma}_L}, \right.
$$
$$
\left. -\frac{\mu_1(1+\kappa_1)}{\bar{\gamma}_1} \frac{m_1\gamma}{\mu_1\kappa_1 + m_1}, ..., -\frac{\mu_L(1+\kappa_L)}{\bar{\gamma}_L} \frac{m_L\gamma}{\mu_L\kappa_L + m_L} \right) \tag{4.4}
$$

When the $\kappa - \mu$ shadowed fading variates are $i.i.d$, the PDF is expressed by [111]

$$f_{\gamma,i.i.d}^{MRC}(\gamma) = \frac{1}{\Gamma(L\mu)} \frac{\mu^{L\mu} m^{Lm} (1+\kappa)^{L\mu}}{(\mu\kappa+m)^{Lm}} \left(\frac{1}{\bar{\gamma}}\right)^{L\mu} \gamma^{L\mu-1}$$
$$\times \Phi_2\left(L\mu - Lm, Lm; L\mu; -\frac{\mu(1+\kappa)\gamma}{\bar{\gamma}}, -\frac{\mu(1+\kappa)}{\bar{\gamma}} \frac{m\gamma}{\mu\kappa+m}\right) \quad (4.5)$$

## 4.4.1 Average Probability of Detection

The average probability of detection over $i.n.d$ $\kappa-\mu$ shadowed fading channels with MRC receivers, $\overline{P}_{d_{i.n.d}}^{MRC}(\lambda)$, that is given in (4.6) can be computed through averaging (2.8) by the PDF of SNR in (4.4) with some mathematical manipulations.

$$\overline{P}_{d_{i.n.d}}^{MRC}(\lambda) = \left(\prod_{i=1}^{L} \frac{\mu_i^{\mu_i} m_i^{m_i} (1+\kappa_i)^{\mu_i}}{(\mu_i\kappa_i+m_i)^{m_i}} \left(\frac{1}{\bar{\gamma}_i}\right)^{\mu_i}\right) \left[\mathcal{I}_{1,i.n.d} - \frac{\lambda^u}{u!2^u}\mathcal{I}_{2,i.n.d}\right] \quad (4.6)$$

where

$$\mathcal{I}_{1,i.n.d} =$$

$$F^{\overbrace{1:1;\,...;\,1;\,0}^{2L+1}}_{1:0;\,\cdots;\,0;\,0}\left(\begin{array}{c} [\sum_{i=1}^{L}\mu_i : 1,...,1,1] : [\mu_1 - m_1 : 1]; ...; [\mu_L - m_L : 1]; [m_1 : 1]; ...; [m_L : 1]; \underline{\phantom{x}}; \\[2mm] [\sum_{i=1}^{L}\mu_i : 1,...,1,0] : \underline{\phantom{xxxx}}; ...; \underline{\phantom{xxxx}}; \underline{\phantom{xx}}; ...; \underline{\phantom{xx}}; \underline{\phantom{x}}; \end{array}\right.$$

$$\left. -\frac{\mu_1(1+\kappa_1)}{\bar{\gamma}_1}, ..., -\frac{\mu_L(1+\kappa_L)}{\bar{\gamma}_L}, -\frac{\mu_1(1+\kappa_1)m_1}{\bar{\gamma}_1(\mu_1\kappa_1+m_1)}, ..., -\frac{\mu_L(1+\kappa_L)m_L}{\bar{\gamma}_L(\mu_L\kappa_L+m_L)}, 1 \right)$$

and

$$\mathcal{I}_{2,i.n.d} =$$

$$F^{\overbrace{2:1;\,...;\,1;\,0;\,0}^{2L+2}}_{2:0;\,\cdots;\,0;\,0;\,1}\left([\sum_{i=1}^{L}\mu_i:1,...,1,1,0],\quad[u:0,...,0,1,1]\quad:[\mu_1-m_1:1];...;[\mu_L-m_L:1];\right.$$

$$[\sum_{i=1}^{L}\mu_i:1,...,1,0,0],[1+u:0,...,0,1,1]:\underline{\qquad};...;\underline{\qquad};$$

$$[m_1:1];...;[m_L:1];\underline{\qquad};\underline{\qquad};$$

$$-\frac{\mu_1(1+\kappa_1)}{\bar{\gamma}_1},\,...,\,-\frac{\mu_L(1+\kappa_L)}{\bar{\gamma}_L},$$

$$\underline{\qquad};...;\underline{\qquad};\underline{\qquad};[u:1];$$

$$\left.-\frac{\mu_1(1+\kappa_1)}{\bar{\gamma}_1}\frac{m_1}{\mu_1\kappa_1+m_1},\,\cdots,\,-\frac{\mu_L(1+\kappa_L)}{\bar{\gamma}_L}\frac{m_L}{\mu_L\kappa_L+m_L},\,-\frac{\lambda}{2},\frac{\lambda}{2}\right)$$

*Proof:* See Appendix B.3. ∎

**Corollary 3** *Substituting (2.8) and (4.5) in (3.1) and doing some mathematical calculations, the average probability of detection over i.i.d $\kappa-\mu$ shadowed fading channels with MRC branches, $\overline{P}_{d_{i.i.d}}^{MRC}$, is calculated as follows*

$$\overline{P}_{d_{i.i.d}}^{MRC}(\lambda) = \frac{\mu^{L\mu}m^{Lm}(1+\kappa)^{L\mu}}{\bar{\gamma}^{L\mu}(\mu\kappa+m)^{Lm}}\left[\mathcal{I}_{1,i.i.d}-\frac{\lambda^u}{u!2^u}\mathcal{I}_{2,i.i.d}\right] \tag{4.7}$$

*where*

$$\mathcal{I}_{1,i.i.d} = F_G\left(L\mu, L\mu, L\mu, L\mu-Lm, Lm, 1; 1, L\mu, L\mu;\right.$$

$$\left.-\frac{\mu(1+\kappa)}{\bar{\gamma}}, -\frac{m}{(\mu\kappa+m)}\frac{\mu(1+\kappa)}{\bar{\gamma}}, 1\right)$$

and

$$\mathcal{I}_{2,i.i.d} = F_{2:0;0;1;0}^{2:1;1;0;0}\left(\begin{array}{l} [L\mu:1,1,1,0], \quad [u:0,0,1,1] \quad : [L\mu - Lm:1];[Lm:1];\underline{\quad\quad};\underline{\quad}; \\[2em] [L\mu:1,1,0,0],[1+u:0,0,1,1]:\underline{\quad\quad\quad}\;;\;\underline{\quad\quad\quad}\;;[u:1];\underline{\quad}; \\[2em] \qquad\qquad -\frac{\mu(1+\kappa)}{\bar{\gamma}}, \; -\frac{m}{(\mu\kappa+m)}\frac{\mu(1+\kappa)}{\bar{\gamma}}, \; -\frac{\lambda}{2}, \frac{\lambda}{2} \end{array}\right)$$

*Proof:* See Appendix B.3. ∎

## 4.4.2    Average Area under the ROC (AUC)

Similar to (3.9) in Subsection 3.3.2, the average AUC over $i.n.d$ $\kappa - \mu$ shadowed fading channels with MRC diversity reception, $\bar{A}_{i.n.d}^{MRC}$, can be evaluated by substituting (2.21) and (4.4) into (3.3) and doing some calculations. Accordingly, this yields

$$\bar{A}_{i.n.d}^{MRC} = 1 - \left( \prod_{i=1}^{L} \frac{\mu_i^{\mu_i} m_i^{m_i}(1+\kappa_i)^{\mu_i}}{(\mu_i\kappa_i + m_i)^{m_i}} \left(\frac{1}{\bar{\gamma}_i}\right)^{\mu_i} \right)$$

$$\left[ \sum_{n=0}^{u-1} 2^{\sum_{i=1}^{L}\mu_i} \frac{\left(\sum_{i=1}^{L}\mu_i\right)_n}{n!} \mathcal{B}_{1,i.n.d} - \sum_{n=1-u}^{u-1} \frac{(u)_n}{2^{(u+n)}n!}\mathcal{B}_{2,i.n.d} \right] \quad (4.8)$$

with

$$\mathcal{B}_{1,i.n.d} =$$
$$F_D^{(2L)}\left( n + \sum_{i=1}^{L}\mu_i; \mu_1 - m_1,...,\mu_L - m_L, m_1,...,m_L; \sum_{i=1}^{L}\mu_i; -\frac{2\mu_1(1+\kappa_1)}{\bar{\gamma}_1}, \right.$$
$$\left. ..., -\frac{2\mu_L(1+\kappa_L)}{\bar{\gamma}_L}, -\frac{2\mu_1(1+\kappa_1)}{\bar{\gamma}_1}\frac{m_1}{\mu_1\kappa_1 + m_1}, ..., -\frac{2\mu_L(1+\kappa_L)}{\bar{\gamma}_L}\frac{m_L}{\mu_L\kappa_L + m_L} \right)$$

71

and

$$\mathcal{B}_{2,i.n.d} =$$

$$F_{1:0;\,...;\,0;\,1}^{\overbrace{1:1;\,...;\,1;\,1}^{2L+1}}\left(\begin{array}{c}[\sum\limits_{i=1}^{L}\mu_i:1,...,1,1]:[\mu_1-m_1:1];...;[\mu_L-m_L:1];\\[\sum\limits_{i=1}^{L}\mu_i:1,...,1,0]:\underline{\qquad};...;\underline{\qquad};\end{array}\right.$$

$$[m_1:1];...;[m_L:1];[u+n:1];$$
$$-\frac{\mu_1(1+\kappa_1)}{\bar{\gamma}_1},\,...,\,-\frac{\mu_L(1+\kappa_L)}{\bar{\gamma}_L},$$
$$\underline{\qquad};...;\underline{\qquad};[1+n:1];$$

$$\left.-\frac{\mu_1(1+\kappa_1)}{\bar{\gamma}_1}\frac{m_1}{\mu_1\kappa_1+m_1},\,\cdots\,,\,-\frac{\mu_L(1+\kappa_L)}{\bar{\gamma}_L}\frac{m_L}{\mu_L\kappa_L+m_L},\frac{1}{2}\right)$$

*Proof:* See Appendix B.4. ∎

**Corollary 4** *When the MRC receivers are i.i.d, the average AUC over $\kappa-\mu$ shadowed fading channels, $\bar{A}_{i.i.d}^{MRC}$, can be computed by averaging (2.21) over (4.5) utilising (3.3). Consequently, $\bar{A}_{i.i.d}^{MRC}$ is given by*

$$\overline{A}_{i.i.d}^{MRC} = 1 - \frac{\mu^{L\mu}m^{Lm}(1+\kappa)^{L\mu}}{\bar{\gamma}^{L\mu}(\mu\kappa+m)^{Lm}}\left[\sum_{n=0}^{u-1}2^{L\mu}\frac{(L\mu)_n}{n!}\mathcal{B}_{1,i.i.d} - \sum_{n=1-u}^{u-1}\frac{(u)_n}{2^{(u+n)}n!}\mathcal{B}_{2,i.i.d}\right] \quad (4.9)$$

with

$$\mathcal{B}_{1,i.i.d} = F_D^{(2)}\left(n+L\mu;L\mu-Lm,Lm;L\mu;-\frac{2\mu(1+\kappa)}{\bar{\gamma}},-\frac{2\mu(1+\kappa)}{\bar{\gamma}}\frac{m}{\mu\kappa+m}\right)$$

and

$$\mathcal{B}_{2,i.i.d} = F_G\left(L\mu,L\mu,L\mu,L\mu-Lm,Lm,u+n;n+1,L\mu,L\mu;\right.$$
$$\left.-\frac{\mu(1+\kappa)}{\bar{\gamma}},-\frac{\mu(1+\kappa)}{\bar{\gamma}}\frac{m}{\mu\kappa+m},\frac{1}{2}\right)$$

*Proof:* See Appendix B.4. ∎

## 4.5  Performance Analysis with SLC

Similar to Section 3.4, the average probability of detection with $i.n.d$ and $i.i.d$ SLC branches over $\kappa - \mu$ shadowed fading channels can be evaluated by substituting $Lu$ rather than $u$ in (4.6) and (4.7), respectively. In similar manner, the average AUC for $i.n.d$ and $i.i.d$ $\kappa - \mu$ shadowed fading channels with SLC branches can be deduced from (4.8) and (4.9), respectively.

## 4.6  Performance Analysis with SLS

### 4.6.1  Average Detection Probability

The average probability of detection for SLS over $i.n.d$ $\kappa - \mu$ shadowed fading channels, $\overline{P}^{SLS}_{d,i.n.d}(\lambda)$, can be evaluated by inserting (4.1) in (3.2) and following the same steps in Appendix B.1. Accordingly, this produces:

$$
\overline{P}^{SLS}_{d,i.n.d}(\lambda) = 1 - \prod_{i=1}^{L} \left[ 1 - \frac{{\mu_i}^{\mu_i} {m_i}^{m_i} (1+\kappa_i)^{\mu_i}}{(\mu_i(1+\kappa_i)+\bar{\gamma}_i)^{\mu_i}(\mu_i\kappa_i+m_i)^{m_i}} \right.
$$
$$
\times \left\{ F_2\left(\mu_i, m_i, 1; \mu_i, 1; \frac{{\mu_i}^2\kappa_i(1+\kappa_i)}{(\mu_i\kappa_i+m_i)(\mu_i(1+\kappa_i)+\bar{\gamma}_i)}, \frac{\bar{\gamma}_i}{(\mu_i(1+\kappa_i)+\bar{\gamma}_i)}\right) \right.
$$
$$
- \frac{\lambda^u}{u!2^u} F_M\big(m_i, u, u, \mu_i, u, \mu_i; \mu_i, 1+u, 1+u;
$$
$$
\left. \left. \frac{{\mu_i}^2\kappa_i(1+\kappa_i)}{(\mu_i\kappa_i+m_i)(\mu_i(1+\kappa_i)+\bar{\gamma}_i)}, \frac{\bar{\gamma}_i\lambda}{2(\mu_i(1+\kappa_i)+\bar{\gamma}_i)}, -\frac{\lambda}{2}\big)\right\}\right] \tag{4.10}
$$

When the diversity receivers are $i.i.d$, $\overline{P}^{SLS}_{d,i.i.d}(\lambda)$ over $\kappa - \mu$ shadowed fading chan-

nels can be obtained from (4.10) as follows

$$
\overline{P}_{d_{i.i.d}}^{SLS}(\lambda) = 1 - \left[ 1 - \frac{\mu^{\mu} m^m (1+\kappa)^{\mu}}{(\mu(1+\kappa)+\bar{\gamma})^{\mu}(\mu\kappa+m)^m} \right.
$$
$$
\times \left\{ F_2\left( \mu, m, 1; \mu, 1; \frac{\mu^2 \kappa (1+\kappa)}{(\mu\kappa+m)(\mu(1+\kappa)+\bar{\gamma})}, \frac{\bar{\gamma}}{(\mu(1+\kappa)+\bar{\gamma})} \right) \right.
$$
$$
- \frac{\lambda^u}{u! 2^u} F_M\left( m, u, u, \mu, u, \mu; \mu, 1+u, 1+u; \right.
$$
$$
\left. \left. \left. \frac{\mu^2 \kappa (1+\kappa)}{(\mu\kappa+m)(\mu(1+\kappa)+\bar{\gamma})}, \frac{\bar{\gamma}\lambda}{2(\mu(1+\kappa)+\bar{\gamma})}, -\frac{\lambda}{2} \right) \right\} \right]^L \qquad (4.11)
$$

## 4.6.2 Average Area under the ROC (AUC)

The exact representation for the AUC with $i.n.d$ SLS diversity branches, $\bar{A}_{i.n.d}^{SLS}$, over $\kappa - \mu$ shadowed fading channels can be computed by averaging $\bar{A}^{SLS}(\gamma)$ of (A.30) over (4.1). The final result is as follows

$$
\bar{A}_{i.n.d}^{SLS} = \frac{\Gamma(1+Lu)}{[\Gamma(1+u)]^L} \left[ F_A^{(L-1)}(Lu; u, ..., u; 1+u, ..., 1+u; -1, ..., -1) - \frac{\mathcal{G}(Lu)_{Lu}}{[\Gamma(1+u)]^L} \right.
$$

$$
\times F_{L}^{2L+1:\overbrace{0;\cdots;0}^{L};\overbrace{1;\cdots;1}^{L};\overbrace{1;1;\cdots;1}^{2L-1}}_{\quad\ :2;\cdots;2;1;\cdots;1;1;\cdots;1} \left( \begin{array}{c} [B_1 : \theta_1^{(1)}, ..., \theta_1^{(3L-1)}], [B_2 : \theta_2^{(1)}, ..., \theta_2^{(L)}], [B_3 : \theta_3^{(1)}, ..., \theta_3^{(L)}] : \\ \\ [C : \theta_2^{(1)}, ..., \theta_2^{(L)}] \qquad\qquad\qquad : \end{array} \right.
$$

$$
\underline{\qquad} \;;...;\; \underline{\qquad} \; ; [b_1^{(1)} : \phi_1^{(1)}];...;[b_1^{(2L-1)} : \phi_1^{(2L-1)}]; [b_2^{(1)} : \phi_2^{(1)}];...;[b_2^{(L)} : \phi_2^{(L)}];
$$

$$
[c_1^{(1)} : \varphi_1^{(1)}];...;[c_1^{(L)} : \varphi_1^{(L)}]; [c_2^{(1)} : \varphi_2^{(1)}];...;[c_2^{(2L-1)} : \varphi_2^{(2L-1)}]; [c_3^{(1)} : \varphi_3^{(1)}];...;[c_3^{(L)} : \varphi_3^{(L)}];
$$

$$
\frac{\bar{\gamma}_1}{\mu_1(1+\kappa_1)+\bar{\gamma}_1}, \; ..., \; \frac{\bar{\gamma}_L}{\mu_L(1+\kappa_L)+\bar{\gamma}_L}, \frac{\mu_1^2 \kappa_1 (1+\kappa_1)}{(\mu_1\kappa_1+m_1)(\mu_1(1+\kappa_1)+\bar{\gamma}_1)}, \; ...,
$$

$$
\left. \left. \frac{\mu_L^2 \kappa_L (1+\kappa_L)}{(\mu_L\kappa_L+m_L)(\mu_L(1+\kappa_L)+\bar{\gamma}_L)}, -1, ..., -1 \right) \right]
$$

$$
(4.12)
$$

where $\mathcal{G} = \prod\limits_{i=1}^{L} \frac{\mu_i{}^{\mu_i} m_i{}^{m_i}(1+\kappa_i)^{\mu_i}}{(\mu_i(1+\kappa_i)+\bar{\gamma}_i)^{\mu_i}(\mu_i\kappa_i+m_i)^{m_i}}$, $B_1 = 2Lu$, $B_2 = [u, \cdots, u]$, $B_3 = [\mu_1, \cdots, \mu_L]$, $\theta_1 = [1, 1, \cdots, 1]$ and $C = [1+u, \cdots, 1+u]$. Moreover, $\theta_2 = \theta_3$ with $L \times L$ dimensions where

$$\theta_2 = \begin{bmatrix} 1 & 1 & 0 & 0 & \cdots & 0 & 0 \\ 0 & 0 & 1 & 1 & \cdots & 0 & 0 \\ \vdots & \vdots & \vdots & \vdots & \ddots & \vdots & \vdots \\ 0 & 0 & 0 & 0 & \cdots & 1 & 1 \end{bmatrix}$$

$b_1^{(i)} = \phi_1^{(i)} = 0$ $\forall$ $i \in \{1, \cdots, L\}$, $b_1^{(i)} = u$ and $\phi_1^{(i)} = 1$ $\forall$ $i \in \{L+1, \cdots, 2L-1\}$, $b_2^{(i)} = m_i$ and $\phi_2^{(i)} = 1$ $\forall$ $i \in \{1, \cdots, L\}$, $c_1^{(i)} = [u \quad \mu_i]$ and $\varphi_1^{(i)} = [1 \quad 1]$ $\forall$ $i \in \{1, \cdots, L\}$, $c_2^{(i)} = \varphi_2^{(i)} = 0$ $\forall$ $i \in \{1, \cdots, L\}$, $c_2^{(i)} = 1+u$ and $\varphi_2^{(i)} = 1$ $\forall$ $i \in \{L+1, \cdots, 2L-1\}$, and $c_3^{(i)} = \mu_i$ and $\varphi_3^{(i)} = 1$ $\forall$ $i \in \{1, \cdots, L\}$.

*Proof:* See Appendix B.5. ∎

## 4.7 $\kappa - \mu$ Extreme Shadowed Fading Channel

The $\kappa - \mu$ shadowed fading channel converts to another case which is called $\kappa - \mu$ extreme shadowed fading when its parameters arrive at the extreme value, i.e., the power of the dominant components is very high ($\kappa \to \infty$) and the number of the multipaths is too small ($\mu \to 0$) [112]. The $\kappa - \mu$ extreme shadowed fading channel describes the harsh channel conditions that occur in enclosed areas. Thus, this channel can be utilized to model the wireless fading channel for indoor communication scenarios. The fading severity index for $\kappa - \mu$ extreme shadowed fading channel is represented by Nakagami-**m** parameter as follows, [113][1].

$$\mathbf{m} = \frac{\mu(1+\kappa)^2}{1+2\kappa} \tag{4.13}$$

Using (4.13), $\kappa \to \infty$ and $\mu \to 0$, we can express $\kappa\mu \approx 2\mathbf{m}$. Thus, the performance

---

[1]Bold **m** is used here to distinguish between the severity index of $\kappa - \mu$ extreme shadowed fading channel and the shadowing severity index $m$.

analysis of energy detector over $\kappa - \mu$ extreme shadowed fading channel can be found by applying the previously mentioned assumptions on all derived expressions of the $\kappa - \mu$ shadowed fading channel.

## 4.8   Numerical Results

In this section, the numerical results that show the behaviour of energy detector over $\kappa - \mu$ shadowed fading channel are presented. These results that include the CROC curves and the average complementary CAUC versus average SNR for different scenarios are obtained by using MATLAB software package. The impact of the shadowing severity index $m$ on the values of $\overline{P_d}$ and $\overline{A}$ is explained. The impacts of $\kappa$, $\mu$ and $\mathbf{m}$ on $\overline{P_d}$ are given in [95].

Fig. 4.1 (top of the next page) shows the CROC curves of energy detector over $\kappa - \mu$ shadowed fading channel with SNR = 10 dB and $u = 1$ and for various values of $\kappa$, $\mu$ and $m$. One can see an improvement in the behaviour of energy detector when $\kappa$, $\mu$ or/and $m$ increase. This is because higher $\kappa$, $\mu$ and $m$ refer to the power rate is high, i.e., the total power of the scattered waves is less than the total power of the dominant components, the average number of the multipath clusters is large and the shadowing has low effects, respectively. For example, when $P_f = 0.1$, $\kappa = 1$ and $m = 2.5$ ($\kappa$ and $m$ are fixed), the $\overline{P_{md}}$ for $\mu = 0.5$ is approximately 72% higher than for $\mu = 2.5$. In the same context, when $\kappa$ decreases from 3 to 1 with $\mu$ and $m$ are constant at 0.8 and 2.5, respectively, the $\overline{P_{md}}$ increases by 23% from its original value. It can be noted that the previous two cases are consistent with the results in [96, Fig. 1]. Furthermore, the increase in $m$ from 0.5 to 2.5 at $P_f = 0.1$, $\mu = 2.5$ and $\kappa = 1$ ($\mu$ and $\kappa$ are fixed) leads to nearly 31% dropping in the $\overline{P_{md}}$.
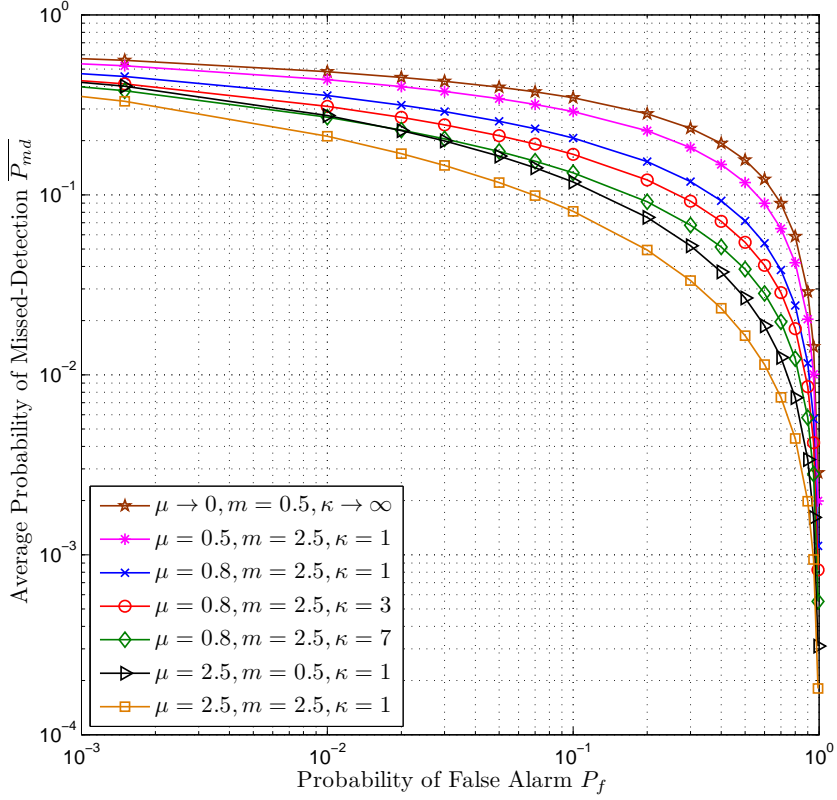
Figure 4.1: Complementary ROC curves of energy detector over $\kappa - \mu$ shadowed fading channel with $\bar{\gamma} = 10$ dB and $u = 1$ and for different values of $\kappa$, $\mu$ and $m$.

Fig. 4.2 (top of the next page) illustrates the CAUC of energy detector over $\kappa - \mu$ shadowed fading channel versus the average SNR, $\bar{\gamma}$, with $u = 1$ and for the same scenarios of Fig. 4.1. Similar to Chapter 3, the results in Fig. 4.1 are affirmed by Fig 4.2 and for wide range of SNR regardless of values of the $P_f$. For example, when $\bar{\gamma} = 10$ dB, $\kappa = 1$ and $m = 2.5$ ($\kappa$ and $m$ are fixed), the CAUC for $\mu = 2.5$ is roughly 77% less than for $\mu = 0.5$. In the same context, when $\mu = 0.8$ and $m = 2.5$ ($\mu$ and $m$ are fixed), the CAUC for $\kappa = 3$ is about 20% less than for the case $\kappa = 1$. In addition to that, the CAUC reduces by 32% from its original value when the value of $m$ rises from 0.5 to 2.5 with $\mu = 2.5$ and $\kappa = 1$ ($\mu$ and $\kappa$ are fixed).
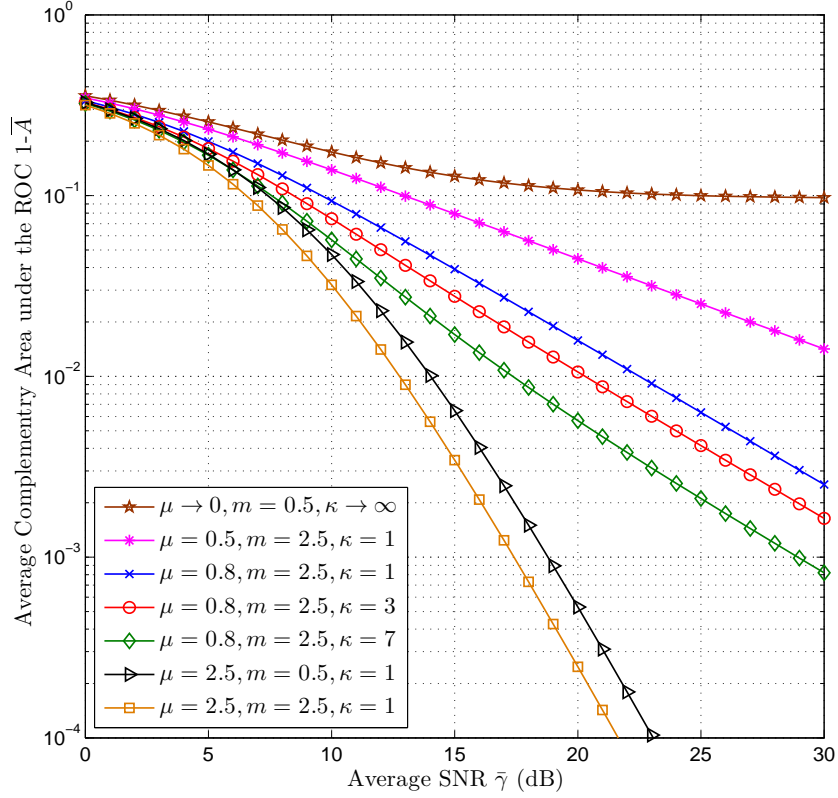
Figure 4.2: Complementary AUC of energy detector over $\eta - \mu$ fading channel versus the average SNR, $\bar{\gamma}$, with $u = 1$ and for different values of $\kappa$, $\mu$ and $m$.

Fig. 4.3 (top of the next page) and Fig. 4.4 (top of the page 80) repeat Fig. 4.1 and Fig. 4.2, respectively for various combining techniques over $i.n.d \; \kappa - \mu$ shadowed fading channels with $u = 1$. In these figures, MRC, SLC and SLS are employed with single receiver (no-diversity), three receivers and five receivers for each scheme. The simulation parameters for each receiver set to $(\kappa_1, \mu_1, m_1, \bar{\gamma}_1) = (0.9, 0.5, 0.6, 5 \text{ dB})$, $(\kappa_2, \mu_2, m_2, \bar{\gamma}_2) = (1.4, 1.2, 0.6, 7 \text{ dB})$, $(\kappa_3, \mu_3, m_3, \bar{\gamma}_3) = (2.3, 1.7, 1.1, 10 \text{ dB})$, $(\kappa_4, \mu_4, m_4, \bar{\gamma}_4) = (2.5, 1.9, 1.5, 11 \text{ dB})$ and $(\kappa_5, \mu_5, m_5, \bar{\gamma}_5) = (2.8, 2.1, 1.6, 12 \text{ dB})$. The results in these figures are consistent with the results in Fig 3.3 and Fig 3.4 and for the same reasons. For instance, when $\bar{\gamma} = 5$ dB (fixed), the values of CAUC for SLS, SLC and MRC with $L = 5$ are approximately 99%, 96% and 86%, respectively lower than $L = 1$.
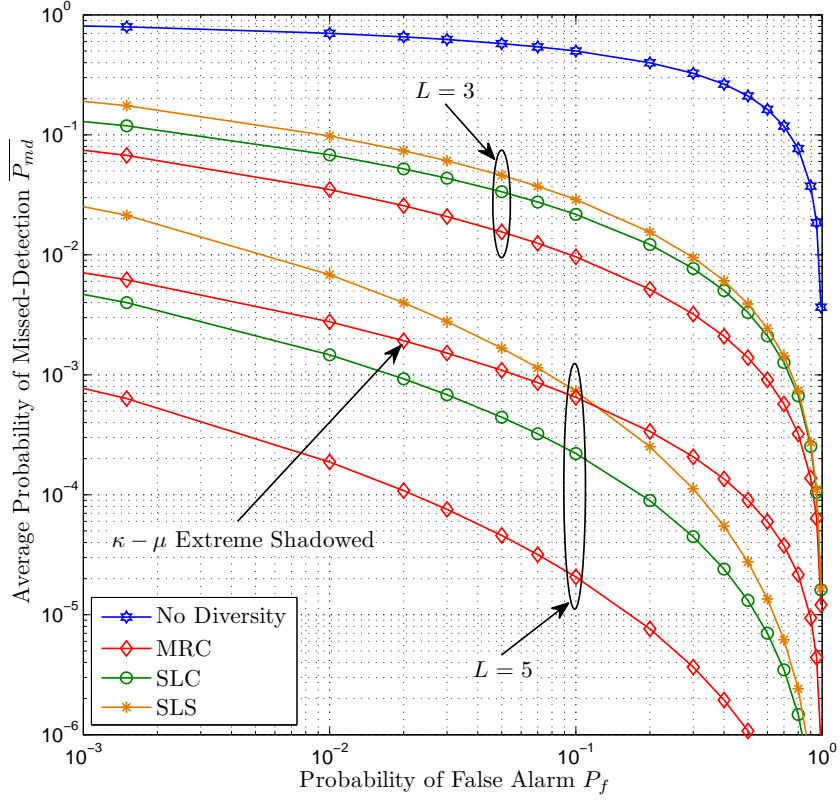
Figure 4.3: Complementary ROC curves of energy detector for different diversity reception over $i.n.d$ $\eta - \mu$ fading channels with $(\kappa_1, \mu_1, m_1, \bar{\gamma}_1) = (0.9, 0.5, 0.6, 5$ dB), $(\kappa_2, \mu_2, m_2, \bar{\gamma}_2) = (1.4, 1.2, 0.6, 7$ dB), $(\kappa_3, \mu_3, m_3, \bar{\gamma}_3) = (2.3, 1.7, 1.1, 10$ dB), $(\kappa_4, \mu_4, m_4, \bar{\gamma}_4) = (2.5, 1.9, 1.5, 11$ dB), $(\kappa_5, \mu_5, m_5, \bar{\gamma}_5) = (2.8, 2.1, 1.6, 12$ dB) and $u = 1$.

Fig. 4.5 (top of the page 81) demonstrates the CROC curves of energy detector for different CSS scenarios with non-identically distributed SUs over $\kappa - \mu$ shadowed fading channels. The simulation parameters for each user are set to $(\kappa_4, \mu_4, m_4, \bar{\gamma}_4, P_{f_4}) = (3.9, 0.8, 0.6, 4$ dB, $[0.01, 0.99]$ with $\Delta = 0.035)$, $(\kappa_5, \mu_5, m_5, \bar{\gamma}_5, P_{f_5}) = (4.4, 1.2, 1.1, 3$ dB, $[0.02, 1]$, with $\Delta = 0.035)$, $(\kappa_6, \mu_6, m_6, \bar{\gamma}_6, P_{f_6}) = (6.3, 1.9, 1.9, 2$ dB, $[0.025, 0.99]$ with $\Delta = 0.034)$, $(\kappa_7, \mu_7, m_7, \bar{\gamma}_7, P_{f_7}) = (8.5, 2.6, 3.3, 1.5$ dB, $[0.026, 0.99]$ with $\Delta = 0.034)$ and $(\kappa_{FC}, \mu_{FC}, m_{FC}, \bar{\gamma}_{FC}) = (5, 2.9, 1.7, 3$ dB$)$. The BER probability for the reporting channel is calculated over $\kappa - \mu$ shadowed fading

79
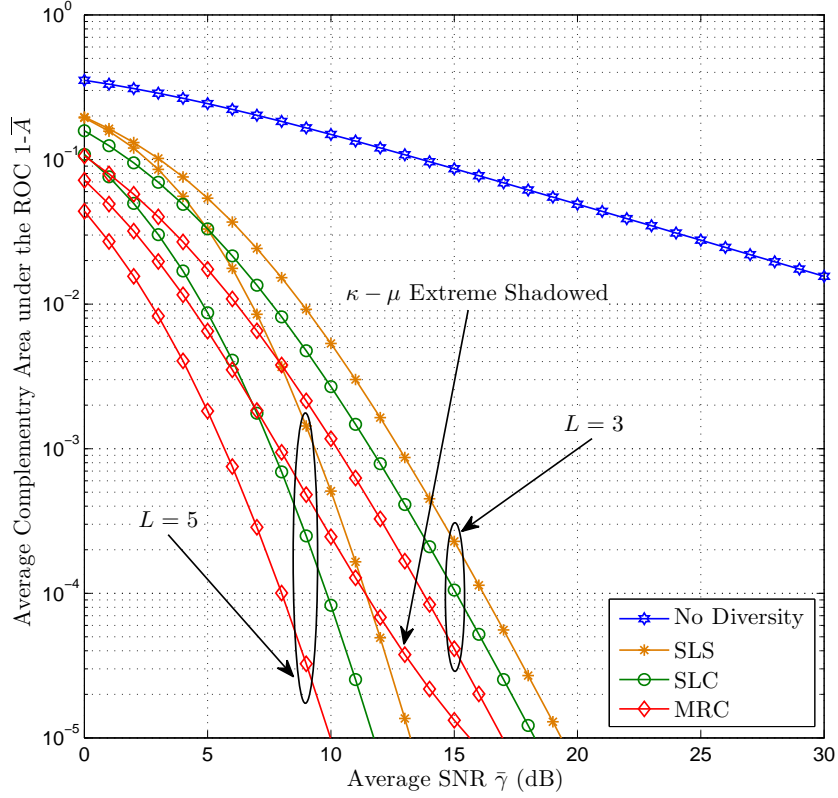
Figure 4.4: Complementary AUC curves versus average SNR, $\bar{\gamma}$, over $i.n.d$ $\kappa - \mu$ shadowed fading channels with $(\kappa_1, \mu_1, m_1) = (0.9, 0.5, 0.6)$, $(\kappa_2, \mu_2, m_2) = (1.4, 1.2, 0.6)$, $(\kappa_3, \mu_3, m_3) = (2.3, 1.7, 1.1)$, $(\kappa_4, \mu_4, m_4) = (2.5, 1.9, 1.5)$, $(\kappa_5, \mu_5, m_5)= (2.8, 2.1, 1.6)$ and $u = 1$.

channel by using [111, eq. (21)] for a signal with BPSK modulation. As expected, the performance of energy detector becomes better when the number of secondary users who participate in the final decision at the FC increases. For example, for the case of $\kappa - \mu$ shadowed, no-diversity at the FC, $Q_f = 0.01$ and the reporting channel is an error rate channel (i.e., $P_e$ is calculated), the value of $\overline{Q_{md}}$ for 5-out-of-7 is higher than for 4-out-of-7 by 15%. Furthermore, when the reporting channel is free error-rate channel, the value of $\overline{Q_{md}}$ for 4-out-of-7 at $Q_f = 0.01$ drops by 21% in comparison with the evaluated error rate case.

Similar to Fig. 3.6, the effect of error at the reporting channel can be reduced by
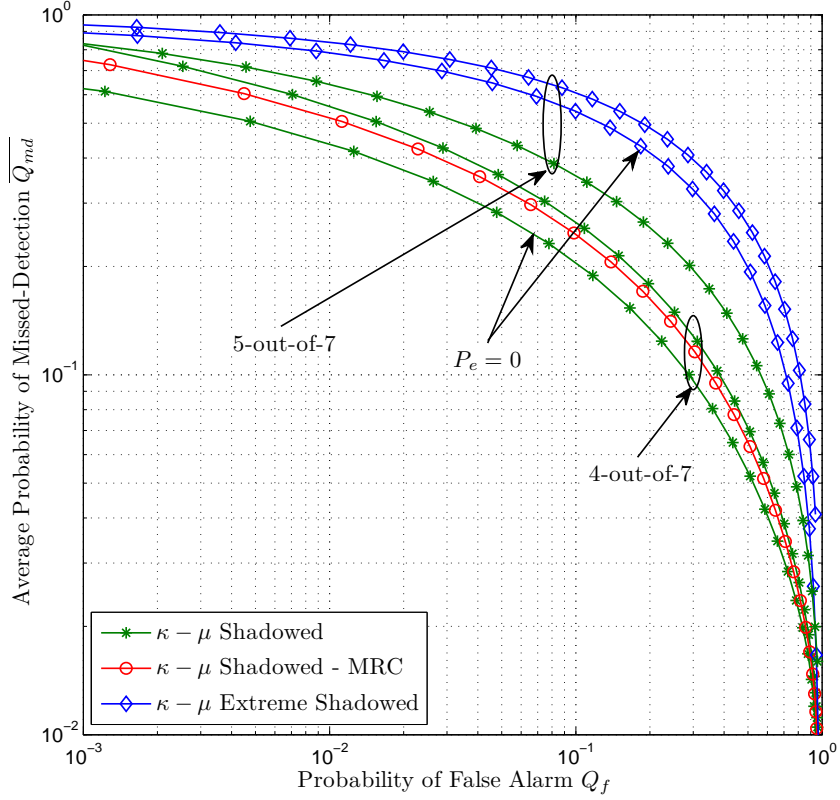
Figure 4.5: Complementary ROC curves for different CSS scenarios with non-identical SUs over $\kappa - \mu$ shadowed fading channels.

utilising dual MRC branches at the FC. For both branches, the channel parameters set to $(\kappa_{FC_1}, \mu_{FC_1}, m_{FC_1}, \bar{\gamma}_{FC_1}) = (0.9, 0.5, 0.6, 1 \text{ dB})$ and $(\kappa_{FC_2}, \mu_{FC_2}, m_{FC_2}, \bar{\gamma}_{FC_2}) = (1.4, 1.2, 0.8, 3 \text{ dB})$.

One can see that Figures 4.1 - 4.5 also explain the behaviour of energy detector over $\kappa - \mu$ extreme shadowed fading channel. Clearly, this channel gives good explanation about the performance of energy detector in enclosed area where $\kappa \to \infty$ and $\mu \to 0$. It can be noted that $\mu$ has higher impact on the behaviour of energy detector than $\kappa$ at constant $m$. This is due to very few number (roughly 0) of clusters that arrive to the receiver (SU or FC).

In Fig. 4.6 (top of the next page), $\overline{P_d}$ and $\bar{A}$ versus $m$ for different average SNR, $\bar{\gamma}$ values with $\kappa = 2$, $\mu = 0.7$, $P_f = 0.1$ and $u = 1$ are presented. As it can be noticed,
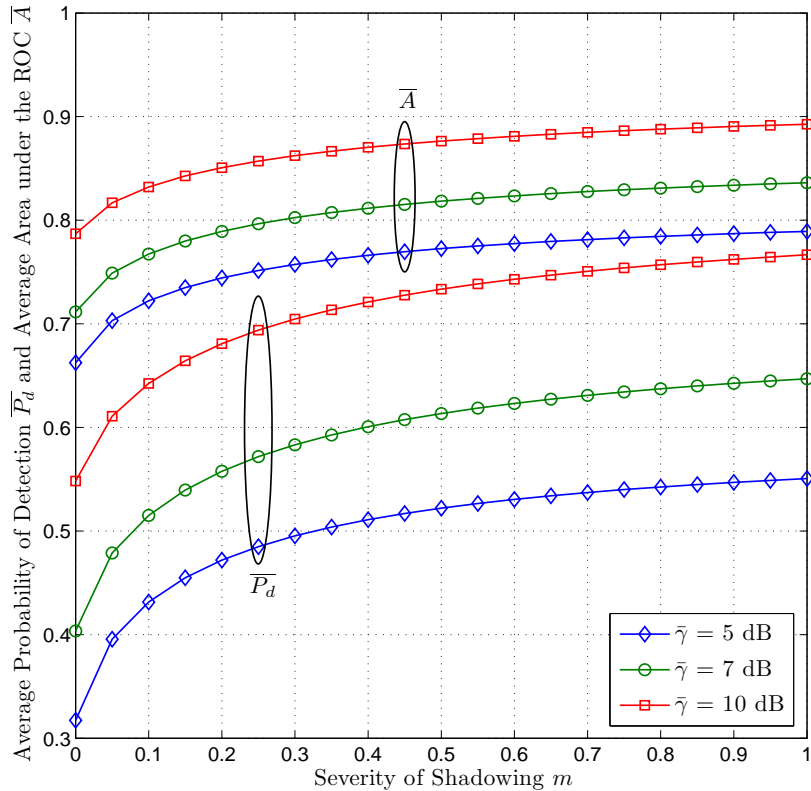
Figure 4.6: Average probability of detection, $\overline{P_d}$ and average AUC, $\bar{A}$, versus the severity of shadowing index, $m$, for different SNR, $\bar{\gamma}$, with $\kappa = 2$, $\mu = 0.7$, $P_f = 0.1$ and $u = 1$.

when $m$ increases, a substantial enhancement in the performance of energy detector is achieved. For instance, when $\bar{\gamma} = 5$ dB and $m = 0.1$, $\overline{P_d} = 0.4314$ and $\bar{A} = 0.7222$. But, when $m = 0.2$ and in the same context, $\overline{P_d} = 0.4719$ and $\overline{A} = 0.7443$.

## 4.9 Conclusions

The behaviour of an energy detector over $\kappa - \mu$ shadowed fading channel was studied in this chapter. Exact analytic expressions for both the average probability of detection and the average AUC were derived. This study also included MRC, SLC and SLS schemes over over $i.n.d$ $\kappa - \mu$ shadowed fading channels. Different CSS

scenarios over $\kappa - \mu$ shadowed fading channels for both sensing and reporting channels were analysed. The given results explained that the parameters $\kappa$ and $m$ have lower impacts on the performance of energy detector than $\mu$ as in $\kappa - \mu$ extreme shadowed fading channel. In all results, the effects of reaching the multipath fading parameters for their extreme values were also demonstrated.

# Chapter 5

# Diversity Combining over Composite $\alpha - \mu$/Gamma Fading Channels using MG Distribution

This chapter evaluates the performance of communications systems with different diversity combining schemes over fully $i.n.d$ composite $\alpha - \mu$/gamma fading channels. A MG distribution is employed to approximate with high accuracy the SNR of composite $\alpha - \mu$/gamma fading channel. The equivalent parameters of MG distribution for $\alpha - \mu$/gamma fading are calculated first. The statistics for the sum and the maximum of $i.n.d$ MG variates are then derived. Thereafter, analytic expressions of the OP, the ABEP and the average channel capacity for MRC and SC schemes are provided. Moreover, the performance of an energy detector is analysed by deriving the average detection probability and the average AUC.

## 5.1 Introduction

The $\alpha - \mu$ fading channel has been widely employed to model the non-linearity of medium propagation. The statistical characterizations for single RV of the $\alpha - \mu$ fading are introduced in [53, 58] with applications to the OP and ABEP.

Several efforts have been dedicated, in the open technical literature, to derive

the statistics of the multivariate $\alpha - \mu$ fading channels which are used to study the performance of communications systems with diversity reception. In [114], highly accurate approximation to the sum of $i.i.d$ $\alpha - \mu$ variates by using another $\alpha - \mu$ variate is proposed and used to calculate the OP and the ABEP for MRC, SC and EGC systems. However, this approximation is solely applicable under specific conditions, e.g., when the sum of $\alpha - \mu$ RVs is another $\alpha - \mu$ variate. The joint PDF and the joint CDF for $i.n.d$ multivariate $\alpha - \mu$ fading are approximately derived by [115] using gamma distribution. These statistics are expressed in infinite series, general and exact form and employed to evaluate the OP of the SC for different scenarios. Another work is achieved by [116] to simplify the joint PDF and the joint CDF of [115]. But, they are also included an infinite series. In [117], the CDF for the sum of two $\alpha - \mu$ variates is presented in simple formulation with finite series.

Based on the statistical properties in [114-117] and the references therein, different performance metrics of communications systems in $\alpha - \mu$ fading channels and diversity reception have been derived. In [118], the average capacity of SC diversity receivers over $\alpha - \mu$ fading channel with $i.i.d$ branches is presented. The average channel capacity and the ABEP for multi-user MIMO systems over $i.i.d$ $\alpha - \mu$ fading scenario is given in [119]. Closed-form exact analytic expressions for the average symbol error-rate probability (ASEP) of MRC and EGC schemes for different digital modulation schemes over $\alpha - \mu$ fading channel with $i.n.d$ branches have been recently derived in [120] using Mellin transform.

The performance analysis of energy detector over $i.i.d$ $\alpha - \mu$ fading channels with SC reception is analysed in [96, 121] with infinite series representation for the average probability of detection. A unified approach is proposed by [102] to derive the average probability of detection for many diversity combining techniques over different $i.n.d$ fading channels. But, the derived expressions are in integral form that needs to be solved numerically.

Since wireless channels that are modelled by the $\alpha - \mu$ fading channel undergo shadowing at the same time, this case is recently studied by [122] for single diversity receiver. Although the shadowing effect which is also represented by the $\alpha - \mu$ fading to perform immense amount of composite fading models, the provided results are

based on assuming that $\alpha$ of both multipath and shadowing are co-prime integer numbers.

In this chapter, different performance metrics for both the MRC and the SC over *i.n.d* composite $\alpha - \mu$/gamma fading channels are derived using a MG distribution. This distribution is recently utilised in [123] to compute the ASEP and the average channel capacity over *i.i.d* $K_G$ fading channels with MRC and SC receivers. However, there are some issues that are not addressed by [123]. Motivated by these as well as by the aforementioned problems in [96, 102, 114-122], the main contributions of this chapter are summarized as follows:

- In contrast to [123], the sum and the maximum of MG variates are derived under condition *i.n.d* RVs. Thus, these expressions can be employed in analysing the performance of communications systems with *i.n.d* diversity receivers. In [123, eq. (9)] and [123, eq. (14)], the derived results are for $K_G$ with *i.i.d* branches for both MRC and SC. Furthermore, one case which is the SC with dual branches over *i.n.d* $K_G$ variates is introduced in [123, eq. (19)].

- In [123], the derived results can be only used for $K_G$ fading channel. On the other side, the provided expressions in this chapter can be applied to a variety of distributions after substituting the equivalent parameters of MG distribution. Hence, the composite $\alpha - \mu$/gamma fading channel is used as an example because it has not been yet studied.

- The ABEP expressions in [123] are given in an integral form that can not be calculated analytically. However, this chapter provides these expressions in exact and closed-form.

## 5.2 MG Distribution for Composite $\alpha - \mu$/gamma Fading Channel

The PDF of the instantaneous SNR, $\gamma$, over composite $\alpha - \mu$/gamma fading channel can be calculated by averaging (2.29) over gamma distribution [104, eq. (4)]

as follows

$$f_\gamma(\gamma) = \frac{\alpha\mu^\mu\gamma^{\frac{\alpha\mu}{2}-1}}{2\Gamma(\mu)\Gamma(k)\Omega^k} \int_0^\infty y^{k-\frac{\alpha\mu}{2}-1} e^{-\frac{\mu\gamma^{\alpha/2}}{y^{\alpha/2}}-\frac{y}{\Omega}} dy \tag{5.1}$$

where $k$ is the shaping parameter, $\Omega = \frac{\bar{\gamma}}{kE_s/N_0}$ is the mean power.

Substituting $x = \frac{\mu\gamma^{\alpha/2}}{y^{\alpha/2}}$ in (5.1), this yields

$$f_\gamma(\gamma) = \vartheta_{\alpha-\mu}\gamma^{k-1} \int_0^\infty e^{-x} g(x) dx \tag{5.2}$$

where $\vartheta_{\alpha-\mu} = -\frac{\mu^{2k/\alpha}}{\Gamma(\mu)\Gamma(k)\Omega^k}$ and $g(x) = x^{\mu-\frac{2}{\alpha}k-1}e^{-\frac{\mu^{2/\alpha}}{x^{2/\alpha}\Omega}\gamma}$.

The integral in (5.2), $\mathcal{S} = \int_0^\infty e^{-x} g(x) dx$, can be approximated as a Gaussian-Laguerre quadrature sum as $\mathcal{S} \approx \sum_{i=1}^N w_i g(x_i)$ where $x_i$ and $w_i$ are the abscissas and weight factors at $i^{th}$ point, respectively for the Gaussian-Laguerre integration [124, pp. 923]. Accordingly, the MG distribution parameters for composite $\alpha - \mu$/gamma fading channel are expressed by

$$\boldsymbol{\alpha}_i = \frac{\theta_i}{\sum_{l=1}^N \theta_l\Gamma(\beta_l)\zeta_l^{-\beta_l}}, \quad \beta_i = k, \quad \zeta_i = \frac{\mu^{2/\alpha}}{\Omega x_i^{2/\alpha}}, \quad \theta_i = \vartheta_{\alpha-\mu}w_i x_i^{\mu-\frac{2k}{\alpha}-1} \tag{5.3}$$

## 5.3 Statistics of The MG Distribution with I.N.D Variates

In this section, the statistics, namely, PDF, CDF and MGF of the sum and the maximum of $i.n.d$ MG variates are derived. These functions are then employed to study the performance of wireless communications systems and the energy detector with MRC and SC schemes over composite $\alpha - \mu$/gamma fading channels.

### 5.3.1 Statistics of the Sum of $i.n.d$ MG Variates

The statistics of the sum of variates that represent the instantaneous SNRs in a fading channel is very important in analysing the performance of MRC diversity reception and space-time block code system.

Assume $\gamma_j$ to be a MG variate with average $\bar{\gamma}_j$ and shaping parameters $\alpha_{i_j}$, $\beta_{i_j}$ and $\zeta_{i_j}$ for $j = 1, \cdots, L$, where $L$ is the number of the RVs which are $i.n.d.$ The MGF of the sum $\gamma^{Sum} = \sum_{j=1}^{L} \gamma_j$ of $i.n.d$ MG variates, $\mathcal{M}_{\gamma^{Sum}}(s)$, can be expressed by

$$\mathcal{M}_{\gamma^{Sum}}(s) = \prod_{j=1}^{L} \mathcal{M}_{\gamma_j}(s) = \prod_{j=1}^{L} \left[ \sum_{i_j=1}^{N_j} \frac{\alpha_{i_j} \Gamma(\beta_{i_j})}{(s + \zeta_{i_j})^{\beta_{i_j}}} \right] \tag{5.4}$$

It can be noted that (5.4) can be written in multiple summations form as follows,

$$\mathcal{M}_{\gamma^{Sum}}(s) = \sum_{i_1=1}^{N_1} \cdots \sum_{i_L=1}^{N_L} \prod_{j=1}^{L} \frac{\alpha_{i_j} \Gamma(\beta_{i_j})}{(s + \zeta_{i_j})^{\beta_{i_j}}} \tag{5.5}$$

Assuming all values of $\beta_{i_j}$, i.e., $k$ in composite $\alpha - \mu/$gamma fading are integer numbers and following the same steps in [125, Appendix C] and [126, Appendix C], an exact closed-form analytic expression for $f_{\gamma^{Sum}}(\gamma)$ is yielded

$$f_{\gamma^{Sum}}(\gamma) = \sum_{i_1=1}^{N_1} \cdots \sum_{i_L=1}^{N_L} \left( \prod_{j=1}^{L} \alpha_{i_j} \Gamma(\beta_{i_j}) \right) \sum_{j=1}^{L} \sum_{r=1}^{\beta_{i_j}} \frac{b_{j_r} \gamma^{r-1}}{(r-1)!} e^{-\zeta_{i_j}\gamma} \tag{5.6}$$

where

$$b_{j_r} = \left[ \sum_{n_1=0}^{\beta_{i_j}-r-1} \binom{\beta_{i_j}-r-1}{n_1} \mathcal{C}_j^{(\beta_{i_j}-r-1-n_1)} \sum_{n_2=0}^{n_1-1} \binom{n_1-1}{n_2} \mathcal{C}_j^{(n_1-1-n_2)} \cdots \right.$$
$$\left. \sum_{n_L=0}^{n_{L-1}-1} \binom{n_{L-1}-1}{n_L} \mathcal{C}_j^{(n_{L-1}-1-n_L)} \right] \frac{\Delta_j}{(\beta_{i_j}-r)!} \tag{5.7}$$

with

$$\mathcal{C}_j^{(m)} = (-1)^{m+1} m! \sum_{\substack{k=1 \\ k \neq j}}^{L} \beta_{i_k} (\zeta_{i_k} - \zeta_{i_j})^{-(m+1)} \quad \text{and} \quad \Delta_j = \prod_{\substack{k=1 \\ k \neq j}}^{L} (\zeta_{i_k} - \zeta_{i_j})^{-\beta_{i_k}}$$

The CDF, $F_{\gamma^{Sum}}(\gamma)$, for $\gamma^{Sum}$ can be evaluated by inserting (5.6) into $F_\gamma(\gamma) =$

$\int_0^\gamma f_\gamma(\gamma)d\gamma$ with the aid of [127, eq. (3.381.1)]. Thus, this yields

$$F_{\gamma^{Sum}}(\gamma) = \sum_{i_1=1}^{N_1} \cdots \sum_{i_L=1}^{N_L} \left( \prod_{j=1}^{L} \alpha_{i_j} \Gamma(\beta_{i_j}) \right) \sum_{j=1}^{L} \sum_{r=1}^{\beta_{i_j}} \frac{b_{j_r}}{\zeta_{i_j}^r (r-1)!} G(r, \zeta_{i_j}\gamma) \qquad (5.8)$$

Substituting (5.6) in $\mathcal{M}_\gamma(s) = \int_0^\infty f_\gamma(\gamma)e^{-s\gamma}d\gamma$ with the help of [127, eq. (3.478.1)], the MGF for $\gamma^{Sum}$, $\mathcal{M}_{\gamma^{Sum}}(s)$, in (5.5) can be rewritten in another form as follows

$$\mathcal{M}_\gamma(s) = \sum_{i_1=1}^{N_1} \cdots \sum_{i_L=1}^{N_L} \left( \prod_{j=1}^{L} \alpha_{i_j} \Gamma(\beta_{i_j}) \right) \sum_{j=1}^{L} \sum_{r=1}^{\beta_{i_j}} \frac{b_{j_r}}{(s+\zeta_{i_j})^r} \qquad (5.9)$$

### 5.3.2  Statistics of the Maximum of *i.n.d* MG Variates

The statistics of the maximum of the SNRs in a fading channel are used in studying the behaviour of wireless communications systems with SC techniques.

By using the same assumptions in Subsection 5.3.1, the CDF of the maximum $\gamma^{Max} = \max\{\gamma_1, \gamma_2, \cdots, \gamma_L\}$ of *i.n.d* MG variates, $F_{\gamma^{Max}}(\gamma)$, is given by

$$F_{\gamma^{Max}}(\gamma) = \sum_{j=1}^{L} f_{\gamma_j}(\gamma) \prod_{\substack{k=1 \\ k\neq j}}^{L} F_{\gamma_j}(\gamma) = \sum_{j=1}^{L} \sum_{i_j=1}^{N_j} \boldsymbol{\alpha}_{i_j} \gamma^{\beta_{i_j}-1} e^{-\zeta_{i_j}\gamma} \prod_{\substack{k=1 \\ k\neq j}}^{L} \sum_{i_k=1}^{N_k} \boldsymbol{\alpha}_{i_k} \zeta_{i_k}^{-\beta_{i_k}} G(\beta_{i_k}, \zeta_{i_k}\gamma)$$

$$(5.10)$$

Supposing all values of $\beta_{i_j}$ are integer numbers and invoking the identity [127, eq. (8.352.1)], (5.10) can be expressed by

$$F_{\gamma^{Max}}(\gamma) = \sum_{j=1}^{L} \sum_{i_j=1}^{N_j} \boldsymbol{\alpha}_{i_j} \gamma^{\boldsymbol{\beta}_j-1} e^{-\boldsymbol{\zeta}_j\gamma} \underbrace{\sum_{i_1=1}^{N_1} \cdots \sum_{i_L=1}^{N_L}}_{i_1\neq i_2\neq\cdots\neq i_L\neq j} \left( \prod_{\substack{k=1 \\ k\neq j}}^{L} \boldsymbol{\alpha}_{i_k} \boldsymbol{\zeta}_k^{-\boldsymbol{\beta}_k} \Gamma(\boldsymbol{\beta}_k) \right)$$

$$\times \prod_{\substack{k=1 \\ k\neq j}}^{L} \left( 1 - e^{-\boldsymbol{\zeta}_k\gamma} \sum_{r=0}^{\boldsymbol{\beta}_k-1} \frac{(\boldsymbol{\zeta}_k\gamma)^r}{r!} \right) \quad (5.11)$$

where $\boldsymbol{\beta} = \beta_i$ and $\boldsymbol{\zeta} = \zeta_i$.

Now, by following a similar procedure in [128, Appendix I], the PDF of $\gamma^{Max}$,

$f_{\gamma^{Max}}(\gamma)$, is given by

$$f_{\gamma^{Max}}(\gamma) = \sum_{l=0}^{L-1} \frac{(-1)^l}{l!} \sum_{j=1}^{L} \sum_{i_j=1}^{N_j} \boldsymbol{\alpha}_{i_j} \underbrace{\sum_{i_1=1}^{N_1} \cdots \sum_{i_L=1}^{N_L}}_{i_1 \neq i_2 \neq \cdots \neq i_L \neq j} \left( \prod_{\substack{k=1 \\ k \neq j}}^{L} \boldsymbol{\alpha}_{i_k} \boldsymbol{\zeta}_k^{-\boldsymbol{\beta}_k} \Gamma(\boldsymbol{\beta}_k) \right)$$
$$\underbrace{\sum_{n_1=1}^{L} \cdots \sum_{n_l=1}^{L}}_{n_1 \neq n_2 \neq \cdots \neq n_l \neq j} \sum_{r_1=0}^{\boldsymbol{\beta}_{n_1}-1} \cdots \sum_{r_l=0}^{\boldsymbol{\beta}_{n_l}-1} \left( \prod_{t=1}^{l} \frac{\boldsymbol{\zeta}_{n_t}^{r_t}}{r_t!} \right) \gamma^{\psi-1} e^{-\rho\gamma} \qquad (5.12)$$

where

$$\psi = \sum_{t=1}^{l} r_t + \boldsymbol{\beta}_j, \quad \text{and} \quad \rho = \sum_{t=1}^{l} \boldsymbol{\zeta}_{n_t} + \boldsymbol{\zeta}_j \qquad (5.13)$$

Substituting (5.12) into $F_\gamma(\gamma) = \int_0^\gamma f_\gamma(\gamma)d\gamma$ with the aid of [127, eq. (3.381.1)], the CDF of $\gamma^{Max}$ in (5.10) can be represented in another form as follows

$$F_{\gamma^{Max}}(\gamma) = \sum_{l=0}^{L-1} \frac{(-1)^l}{l!} \sum_{j=1}^{L} \sum_{i_j=1}^{N_j} \boldsymbol{\alpha}_{i_j} \underbrace{\sum_{i_1=1}^{N_1} \cdots \sum_{i_L=1}^{N_L}}_{i_1 \neq i_2 \neq \cdots \neq i_L \neq j} \left( \prod_{\substack{k=1 \\ k \neq j}}^{L} \boldsymbol{\alpha}_{i_k} \boldsymbol{\zeta}_k^{-\boldsymbol{\beta}_k} \Gamma(\boldsymbol{\beta}_k) \right)$$
$$\underbrace{\sum_{n_1=1}^{L} \cdots \sum_{n_l=1}^{L}}_{n_1 \neq n_2 \neq \cdots \neq n_l \neq j} \sum_{r_1=0}^{\boldsymbol{\beta}_{n_1}-1} \cdots \sum_{r_l=0}^{\boldsymbol{\beta}_{n_l}-1} \left( \prod_{t=1}^{l} \frac{\boldsymbol{\zeta}_{n_t}^{r_t}}{r_t!} \right) \frac{G(\psi, \rho\gamma)}{\rho^\psi} \qquad (5.14)$$

The MGF of $\gamma^{Max}$, $\mathcal{M}_{\gamma^{Max}}(s)$, can be evaluated by using $\mathcal{M}_\gamma(s) = \int_0^\infty f_\gamma(\gamma)e^{-s\gamma}d\gamma$ and (5.12) with the help of [127, eq. (3.478.1)]. Thus, this yields

$$\mathcal{M}_{\gamma^{Max}}(s) = \sum_{l=0}^{L-1} \frac{(-1)^l}{l!} \sum_{j=1}^{L} \sum_{i_j=1}^{N_j} \boldsymbol{\alpha}_{i_j} \underbrace{\sum_{i_1=1}^{N_1} \cdots \sum_{i_L=1}^{N_L}}_{i_1 \neq i_2 \neq \cdots \neq i_L \neq j} \left( \prod_{\substack{k=1 \\ k \neq j}}^{L} \boldsymbol{\alpha}_{i_k} \boldsymbol{\zeta}_k^{-\boldsymbol{\beta}_k} \Gamma(\boldsymbol{\beta}_k) \right)$$
$$\underbrace{\sum_{n_1=1}^{L} \cdots \sum_{n_l=1}^{L}}_{n_1 \neq n_2 \neq \cdots \neq n_l \neq j} \sum_{r_1=0}^{\boldsymbol{\beta}_{n_1}-1} \cdots \sum_{r_l=0}^{\boldsymbol{\beta}_{n_l}-1} \left( \prod_{t=1}^{l} \frac{\boldsymbol{\zeta}_{n_t}^{r_t}}{r_t!} \right) \frac{\Gamma(\psi)}{(s+\rho)^\psi} \qquad (5.15)$$

## 5.4 Applications of MG Channel Model to Diversity Combining in Communications Systems

### 5.4.1 Outage Probability

The outage probability, $P_o$, is one of the most important performance criterion characteristic of wireless communications systems over fading channels. It is defined as the probability of exceeding the instantaneous error rate for a specified value or it is defined as the probability of crossing the output SNR, $\gamma$, for a certain predefined threshold, $\Upsilon$. Consequently, the $P_o$ is computed by $P_o = \int_0^\Upsilon f_\gamma(\gamma)d\gamma = F_\gamma(\Upsilon)$ [47].

**Maximal Ratio Combining (MRC)**

As demonstrated in Subsection 2.7.1, the received instantaneous SNR at the output of the MRC combiner is the sum of all received instantaneous SNRs by the branches. Therefore, the outage probability of MRC scheme over a variety of $i.n.d$ fading channels using MG distribution can be evaluated by (5.8).

**Selection Combining (SC)**

As explained in Subsection 2.7.4, the combiner in SC selects the receiver with largest SNR among all diversity receivers. Consequently, the outage probability for SC reception over any $i.n.d$ fading channels using MG distribution can be calculated by (5.10) or (5.14).

### 5.4.2 Average Bit Error Rate Probability

The ABEP, $P_e$ can be computed by using the PDF of the received instantaneous SNR, $\gamma$, as follows [129, eq. (9)]

$$P_e = \frac{1}{2\Gamma(p)} \int_0^\infty \Gamma(p, q\gamma) f_\gamma(\gamma) d\gamma \tag{5.16}$$

The parameters $p$ and $q$ represent the modulation dependent constants. Specifically, $p = 0.5$ and $q = 0.5$ for coherent binary frequency-shift keying (FSK), $p = 0.5$ and $q = 1$ for coherent BPSK, and $p = 1$ and $q = 1$ for binary differential phase-shift keying (DPSK).

**Maximal Ratio Combining (MRC)**

The ABEP for MRC, $P_{e_{MRC}}$, can be computed by inserting (5.6) into (5.16) with the aid of [127, eq. (6.455.1)] and performing some mathematical straightforward simplifications. Thus, this yields

$$P_{e_{MRC}} = \sum_{i_1=1}^{N_1} \cdots \sum_{i_L=1}^{N_L} \left( \prod_{j=1}^{L} \boldsymbol{\alpha}_{i_j} \Gamma(\beta_{i_j}) \right) \sum_{j=1}^{L} \sum_{r=1}^{\beta_{i_j}} \frac{b_{j_r}(p)_r}{2q^r \Gamma(1+r)(1+\zeta_{i_j}/q)^{p+r}}$$
$$\times {}_2F_1\left( 1, p+r; 1+r; \frac{\zeta_{i_j}}{q+\zeta_{i_j}} \right) \quad (5.17)$$

**Selection Combining (SC)**

The ABEP for SC, $P_{e_{SC}}$, can be evaluated by substituting (5.12) in (5.16) and invoking [127, eq. (6.455.1)]. Accordingly, the result is

$$P_{e_{SC}} = \sum_{l=0}^{L-1} \frac{(-1)^l}{l!} \sum_{j=1}^{L} \sum_{i_j=1}^{N_j} \boldsymbol{\alpha}_{i_j} \underbrace{\sum_{i_1=1}^{N_1} \cdots \sum_{i_L=1}^{N_L}}_{i_1 \neq i_2 \neq \cdots \neq i_L \neq j} \left( \prod_{\substack{k=1 \\ k \neq j}}^{L} \boldsymbol{\alpha}_{i_k} \boldsymbol{\zeta}_k^{-\boldsymbol{\beta}_k} \Gamma(\boldsymbol{\beta}_k) \right) \underbrace{\sum_{n_1=1}^{L} \cdots \sum_{n_l=1}^{L}}_{n_1 \neq n_2 \neq \cdots \neq n_l \neq j}$$
$$\sum_{r_1=0}^{\boldsymbol{\beta}_{n_1}-1} \cdots \sum_{r_l=0}^{\boldsymbol{\beta}_{n_l}-1} \left( \prod_{t=1}^{l} \frac{\boldsymbol{\zeta}_{n_t}^{r_t}}{r_t!} \right) \frac{(p)_\psi}{2\psi q^\psi (1+\rho/q)^{p+\psi}} {}_2F_1\left( 1, p+\psi; 1+\psi; \frac{\rho}{q+\rho} \right)$$
$$(5.18)$$

### 5.4.3 Average Channel Capacity

According to Shannon's theorem, the average channel capacity, $C$, is given by

$$C = B \int_0^\infty \log_2(1+\gamma) f_\gamma(\gamma) d\gamma \quad (5.19)$$

92

where $B$ is the channel bandwidth.

**Maximal Ratio Combining (MRC)**

Plugging (5.6) in (5.19) and invoking [123, eq. (47)], the average channel capacity for MRC, $C_{MRC}$, is obtained as follows

$$C_{MRC} = \sum_{i_1=1}^{N_1} \cdots \sum_{i_L=1}^{N_L} \left( \prod_{j=1}^{L} \boldsymbol{\alpha}_{i_j} \Gamma(\beta_{i_j}) \right) \sum_{j=1}^{L} \sum_{r=1}^{\beta_{i_j}} b_{j_r} e^{\zeta_{i_j}} \sum_{a=1}^{r} \frac{\Gamma(a-r, \zeta_{i_j})}{\zeta_{i_j}^a} \quad (5.20)$$

**Selection Combining (SC)**

The average channel capacity for the SC, $C_{SC}$, can be evaluated by inserting (5.12) into (5.19) and employing [123, eq. (47)]. Thus, this yields

$$C_{SC} = \sum_{l=0}^{L-1} \frac{(-1)^l}{l!} \sum_{j=1}^{L} \sum_{i_j=1}^{N_j} \boldsymbol{\alpha}_{i_j} \underbrace{\sum_{i_1=1}^{N_1} \cdots \sum_{i_L=1}^{N_L}}_{i_1 \neq i_2 \neq \cdots \neq i_L \neq j} \left( \prod_{\substack{k=1 \\ k \neq j}}^{L} \boldsymbol{\alpha}_{i_k} \boldsymbol{\zeta}_k^{-\boldsymbol{\beta}_k} \Gamma(\boldsymbol{\beta}_k) \right)$$

$$\underbrace{\sum_{n_1=1}^{L} \cdots \sum_{n_l=1}^{L}}_{n_1 \neq n_2 \neq \cdots \neq n_l \neq j} \sum_{r_1=0}^{\boldsymbol{\beta}_{n_1}-1} \cdots \sum_{r_l=0}^{\boldsymbol{\beta}_{n_l}-1} \left( \prod_{t=1}^{l} \frac{\boldsymbol{\zeta}_{n_t}^{r_t}}{r_t!} \right) (\psi-1)! e^{\rho} \sum_{a=1}^{\psi} \frac{\Gamma(a-\psi, \rho)}{\rho^a} \quad (5.21)$$

# 5.5 Applications of MG Channel Model to Diversity Combining in Energy Detector

## 5.5.1 Average Probability of Detection

**No Diversity Reception**

Substituting $P_d(\gamma, \lambda)$ of (2.11) and (2.31) in (3.1) and recalling the identity [127, eq. (8.354.2)], yielding

$$\overline{P_d}(\lambda) = \frac{1}{\Gamma(u)} \int_0^\infty \left( \Gamma(u) - \sum_{m=0}^{\infty} \frac{(-1)^m \left(\frac{\lambda}{2}\right)^{u+m}}{(u+m)(1+\gamma)^{(u+m)} m!} \right) \sum_{i=1}^{N} \boldsymbol{\alpha}_i \gamma^{\beta_i-1} e^{-\zeta_i \gamma} d\gamma \quad (5.22)$$

Employing the fact that $\int_0^\infty f_\gamma(\gamma)d\gamma \triangleq 1$ and [127, eq. (3.383.5)] to evaluate the integral in (5.22), the $\overline{P_d}(\lambda)$ is obtained as follows

$$\overline{P_d}(\lambda) = 1 - \sum_{i=1}^{N} \frac{\boldsymbol{\alpha}_i \Gamma(\beta_i)}{\Gamma(u)} \sum_{m=0}^{\infty} \frac{(-1)^m \left(\frac{\lambda}{2}\right)^{u+m}}{(u+m)m!} U\left(\beta_i; 1+\beta_i - u - m; \zeta_i\right) \quad (5.23)$$

where $U(.;.;.)$ is the confluent hypergeometric function of the second kind defined in [124, eq. (13.1.3)].

It can be noticed that (5.23) includes an infinite series that requires a convergence by limited number of terms, $R$, with truncation error, $|E_R^{\overline{P_d}(\lambda)}|$ as follows

$$|E_R^{\overline{P_d}(\lambda)}| = \sum_{i=1}^{N} \frac{\boldsymbol{\alpha}_i \Gamma(\beta_i)}{\Gamma(u)} \sum_{m=R}^{\infty} \frac{(-1)^m \left(\frac{\lambda}{2}\right)^{u+m}}{(u+m)m!} U\left(\beta_i; 1+\beta_i - u - m; \zeta_i\right) \quad (5.24)$$

It can be observed that $U(.;.;.)$ in (5.24) is monotonically decreasing with $m$. Accordingly, after doing similar mathematical operations to [130], yielding

$$|E_R^{\overline{P_d}(\lambda)}| \leq \sum_{i=1}^{N} \frac{\boldsymbol{\alpha}_i \Gamma(\beta_i)}{\Gamma(u)} U\left(\beta_i; 1+\beta_i - u - R; \zeta_i\right) \sum_{m=0}^{\infty} \frac{(-1)^{m+R} \left(\frac{\lambda}{2}\right)^{u+m+R}}{(u+m+R)(m+R)!} \quad (5.25)$$

Using the identities [39, eq. (1.2.1)] and [39, eq. (1.2.3)] with some mathematical straightforward simplifications, this yields

$$|E_R^{\overline{P_d}(\lambda)}| \leq \sum_{i=1}^{N} \frac{\boldsymbol{\alpha}_i \Gamma(\beta_i)(-1)^R \left(\frac{\lambda}{2}\right)^{u+R}}{\Gamma(u)(u+R)R!} U\left(\beta_i; 1+\beta_i - u - R; \zeta_i\right)$$

$$\sum_{m=0}^{\infty} \frac{(1)_m (u+R)_m}{(1+R)_m (1+u+R)_m m!} \left(-\frac{\lambda}{2}\right)^m$$

$$= \sum_{i=1}^{N} \frac{\boldsymbol{\alpha}_i \Gamma(\beta_i)(-1)^R \left(\frac{\lambda}{2}\right)^{u+R}}{\Gamma(u)(u+R)R!} U\left(\beta_i; 1+\beta_i - u - R; \zeta_i\right)$$

$$\times {}_2F_2\left(1, u+R; 1+R, 1+u+R; -\frac{\lambda}{2}\right) \quad (5.26)$$

where ${}_2F_2(.,.;.,.;.)$ is another form of the confluent hypergeometric function defined in [127, eq. (9.14.1)].

Similarly, the number of terms $R$ that needs to truncate the infinite series in all next equations with $|E_R|$ can be obtained.

**Maximal Ratio Combining (MRC)**

The average probability of detection for *i.n.d* MRC receivers, $\overline{P_d}^{MRC}(\lambda)$, over MG distribution can be computed by plugging $P_d(\gamma, \lambda)$ of (2.11) and (5.6) into (3.1) and following a similar procedure for no-diversity case. Consequently, $\overline{P_d}^{MRC}(\lambda)$ is expressed by

$$\overline{P_d}^{MRC}(\lambda) = 1 - \sum_{i_1=1}^{N_1} \cdots \sum_{i_L=1}^{N_L} \frac{\prod_{j=1}^{L} \boldsymbol{\alpha}_{i_j} \Gamma(\beta_{i_j})}{\Gamma(u)} \sum_{j=1}^{L} \sum_{r=1}^{\beta_{i_j}} \sum_{m=0}^{\infty} \frac{(-1)^m \left(\frac{\lambda}{2}\right)^{u+m} b_{j_r}}{(u+m)m!}$$
$$\times U\left(r; 1+r-u-m; \zeta_{i_j}\right) \quad (5.27)$$

The truncation error of an infinite series in (5.27), $|E_R^{\overline{P_d}^{MRC}(\lambda)}|$, is given by

$$|E_R^{\overline{P_d}^{MRC}(\lambda)}| \leq \sum_{i_1=1}^{N_1} \cdots \sum_{i_L=1}^{N_L} \frac{\prod_{j=1}^{L} \boldsymbol{\alpha}_{i_j} \Gamma(\beta_{i_j})}{\Gamma(u)} \sum_{j=1}^{L} \sum_{r=1}^{\beta_{i_j}} \frac{(-1)^R \left(\frac{\lambda}{2}\right)^{u+R} b_{j_r}}{(u+R)R!}$$
$$\times U\left(r; 1+r-u-R; \zeta_{i_j}\right){}_2F_2\left(1, u+R; 1+R, 1+u+R; -\frac{\lambda}{2}\right) \quad (5.28)$$

**Selection Combining (SC)**

The average probability of detection for SC with *i.n.d* branches, $\overline{P_d}^{SC}(\lambda)$, over MG distribution can be evaluated by inserting $P_d(\gamma, \lambda)$ of (2.11) and (5.12) into (3.1) and doing the same steps of no-diversity case. Accordingly, this yields

$$\overline{P_d}^{SC}(\lambda) = 1 - \sum_{l=0}^{L-1} \frac{(-1)^l}{l!} \sum_{j=1}^{L} \sum_{i_j=1}^{N_j} \boldsymbol{\alpha}_{i_j} \underbrace{\sum_{i_1=1}^{N_1} \cdots \sum_{i_L=1}^{N_L}}_{i_1 \neq i_2 \neq \cdots \neq i_L \neq j} \left( \prod_{\substack{k=1 \\ k \neq j}}^{L} \boldsymbol{\alpha}_{i_k} \boldsymbol{\zeta}_k^{-\boldsymbol{\beta}_k} \Gamma(\boldsymbol{\beta}_k) \right) \underbrace{\sum_{n_1=1}^{L} \cdots \sum_{n_l=1}^{L}}_{n_1 \neq n_2 \neq \cdots \neq n_l \neq j}$$
$$\sum_{r_1=0}^{\boldsymbol{\beta}_{n_1}-1} \cdots \sum_{r_l=0}^{\boldsymbol{\beta}_{n_l}-1} \left( \prod_{t=1}^{l} \frac{\boldsymbol{\zeta}_{n_t}^{r_t}}{r_t!} \right) \sum_{m=0}^{\infty} \frac{(-1)^m \left(\frac{\lambda}{2}\right)^{u+m} \Gamma(\psi)}{\Gamma(u)(u+m)m!} U\left(\psi; 1+\psi-u-m; \rho\right)$$
$$(5.29)$$

95

The error of truncation the infinite series in (5.29), $|E_R^{\overline{P_d}^{SC}(\lambda)}|$, can be evaluated by

$$
|E_R^{\overline{P_d}^{SC}(\lambda)}| \leq \sum_{l=0}^{L-1} \frac{(-1)^l}{l!} \sum_{j=1}^{L} \sum_{i_j=1}^{N_j} \boldsymbol{\alpha}_{i_j} \underbrace{\sum_{i_1=1}^{N_1} \cdots \sum_{i_L=1}^{N_L}}_{i_1 \neq i_2 \neq \cdots \neq i_L \neq j} \left( \prod_{\substack{k=1 \\ k \neq j}}^{L} \boldsymbol{\alpha}_{i_k} \boldsymbol{\zeta}_k^{-\boldsymbol{\beta}_k} \Gamma(\boldsymbol{\beta}_k) \right) \underbrace{\sum_{n_1=1}^{L} \cdots \sum_{n_l=1}^{L}}_{n_1 \neq n_2 \neq \cdots \neq n_l \neq j}
$$

$$
\sum_{r_1=0}^{\boldsymbol{\beta}_{n_1}-1} \cdots \sum_{r_l=0}^{\boldsymbol{\beta}_{n_l}-1} \left( \prod_{t=1}^{l} \frac{\boldsymbol{\zeta}_{n_t}^{r_t}}{r_t!} \right) \frac{(-1)^R \left(\frac{\lambda}{2}\right)^{u+R} \Gamma(\psi)}{\Gamma(u)(u+R)R!} U\big(\psi; 1+\psi-u-R; \rho\big)
$$

$$
\times {}_2F_2\left( 1, u+R; 1+R, 1+u+R; -\frac{\lambda}{2} \right) \tag{5.30}
$$

### 5.5.2   Average Area under the ROC (AUC)

In this chapter, the average AUC, $\bar{A}$, is computed by [110, eq. (33)]

$$
\bar{A} = \frac{1}{2^u \Gamma(u)} \int_0^\infty \lambda^{u-1} e^{-\frac{\lambda}{2}} \overline{P_d}(\lambda) d\lambda \tag{5.31}
$$

**No Diversity Reception**

The average area under the receiver operating characteristics curve, $\bar{A}$, over MG distribution with no diversity, can be evaluated by plugging (5.23) into (5.31) with the aid of [127, eq. (3.351.3)] as follows

$$
\bar{A} = 1 - \sum_{i=1}^{N} \frac{\boldsymbol{\alpha}_i \Gamma(\beta_i)}{[\Gamma(u)]^2} \sum_{m=0}^{\infty} \frac{(-1)^m \Gamma(2u+m)}{(u+m)m!} U\big(\beta_i; 1+\beta_i-u-m; \zeta_i\big) \tag{5.32}
$$

The truncation error, $|E_R^{\bar{A}}|$, for an infinite series in (5.32) is expressed by

$$
|E_R^{\bar{A}}| \leq \sum_{i=1}^{N} \frac{\boldsymbol{\alpha}_i \Gamma(\beta_i)(-1)^R \Gamma(2u+R)}{[\Gamma(u)]^2 (u+R)R!} U\big(\beta_i; 1+\beta_i-u-R; \zeta_i\big)
$$

$$
\times {}_3F_2\big(1, u+R, 2u+R; 1+R, 1+u+R; -1\big) \tag{5.33}
$$

where ${}_3F_2(.,.,.;.,.;.)$ is another model of the confluent hypergeometric function defined in [127, eq. (9.14.1)].

**Maximal Ratio Combining (MRC)**

Replacing (5.23) with (5.27) in no diversity case and following the same procedure, the average area under the receiver operating characteristics curve for MRC, $\bar{A}^{MRC}$, using MG distribution can be obtained as follows

$$
\bar{A}^{MRC} = 1 - \sum_{i_1=1}^{N_1} \cdots \sum_{i_L=1}^{N_L} \frac{\prod_{j=1}^{L} \boldsymbol{\alpha}_{i_j} \Gamma(\beta_{i_j})}{[\Gamma(u)]^2} \sum_{j=1}^{L} \sum_{r=1}^{\beta_{i_j}} \sum_{m=0}^{\infty} \frac{(-1)^m \Gamma(2u+m) b_{j_r}}{(u+m)m!}
$$
$$
U\big(r; 1+r-u-m; \zeta_{i_j}\big) \quad (5.34)
$$

The infinite series in (5.34) can be truncated by $R$ terms and error, $|E_R^{\bar{A}^{MRC}}|$, as follows

$$
|E_R^{\bar{A}^{MRC}}| \leq \sum_{i_1=1}^{N_1} \cdots \sum_{i_L=1}^{N_L} \frac{\prod_{j=1}^{L} \boldsymbol{\alpha}_{i_j} \Gamma(\beta_{i_j})}{[\Gamma(u)]^2} \sum_{j=1}^{L} \sum_{r=1}^{\beta_{i_j}} \frac{(-1)^R \Gamma(2u+R) b_{j_r}}{(u+R)R!}
$$
$$
\times U\big(r; 1+r-u-R; \zeta_{i_j}\big) {}_3F_2\big(1, u+R, 2u+R; 1+R, 1+u+R; -1\big)
$$
$$
(5.35)
$$

**Selection Combining (SC)**

Similar to no diversity, the average area under the receiver operating characteristics curve for SC, $\bar{A}^{MRC}$, over MG distribution can be calculated after employing (5.29) instead of (5.23) as follows

$$
\bar{A}^{SC} = 1 - \sum_{l=0}^{L-1} \frac{(-1)^l}{l!} \sum_{j=1}^{L} \sum_{i_j=1}^{N_j} \boldsymbol{\alpha}_{i_j} \underbrace{\sum_{i_1=1}^{N_1} \cdots \sum_{i_L=1}^{N_L}}_{i_1 \neq i_2 \neq \cdots \neq i_L \neq j} \left( \prod_{\substack{k=1 \\ k \neq j}}^{L} \boldsymbol{\alpha}_{i_k} \boldsymbol{\zeta}_k^{-\boldsymbol{\beta}_k} \Gamma(\boldsymbol{\beta}_k) \right) \underbrace{\sum_{n_1=1}^{L} \cdots \sum_{n_l=1}^{L}}_{n_1 \neq n_2 \neq \cdots \neq n_l \neq j}
$$
$$
\sum_{r_1=0}^{\boldsymbol{\beta}_{n_1}-1} \cdots \sum_{r_l=0}^{\boldsymbol{\beta}_{n_l}-1} \left( \prod_{t=1}^{l} \frac{\boldsymbol{\zeta}_{n_t}^{r_t}}{r_t!} \right) \sum_{m=0}^{\infty} \frac{(-1)^m \Gamma(2u+m) \Gamma(\psi)}{[\Gamma(u)]^2 (u+m)m!} U\big(\psi; 1+\psi-u-m; \rho\big)
$$
$$
(5.36)
$$

97

The truncation error of an infinite series in (5.36), $|E_R^{\bar{A}^{SC}}|$, is given by

$$
\begin{aligned}
|E_R^{\bar{A}^{SC}}| \leq & \sum_{l=0}^{L-1} \frac{(-1)^l}{l!} \sum_{j=1}^{L} \sum_{i_j=1}^{N_j} \boldsymbol{\alpha}_{i_j} \underbrace{\sum_{i_1=1}^{N_1} \cdots \sum_{i_L=1}^{N_L}}_{i_1 \neq i_2 \neq \cdots \neq i_L \neq j} \left( \prod_{\substack{k=1 \\ k \neq j}}^{L} \boldsymbol{\alpha}_{i_k} \boldsymbol{\zeta}_k^{-\boldsymbol{\beta}_k} \Gamma(\boldsymbol{\beta}_k) \right) \underbrace{\sum_{n_1=1}^{L} \cdots \sum_{n_l=1}^{L}}_{n_1 \neq n_2 \neq \cdots \neq n_l \neq j} \\
& \sum_{r_1=0}^{\boldsymbol{\beta}_{n_1}-1} \cdots \sum_{r_l=0}^{\boldsymbol{\beta}_{n_l}-1} \left( \prod_{t=1}^{l} \frac{\boldsymbol{\zeta}_{n_t}^{r_t}}{r_t!} \right) \frac{(-1)^R \Gamma(2u+R)\Gamma(\psi)}{[\Gamma(u)]^2 (u+R)R!} U\big(\psi; 1+\psi-u-R; \rho\big) \\
& \times {}_3F_2\bigg(1, u+R, 2u+R; 1+R, 1+u+R; -1\bigg) \qquad (5.37)
\end{aligned}
$$

## 5.6 Numerical Results

The numerical results for different performance metrics over $i.n.d$ composite $\alpha - \mu$/gamma fading channels of no diversity, MRC and SC schemes with dual and triple diversity branches that are given in this section, are numerically calculated using MATLAB. The simulation parameters are set to $(\alpha_1, \mu_1, k_1, N_1) = (3.2, 1.5, 2, 15)$, $(\alpha_2, \mu_2, k_2, N_2) = (0.9, 0.5, 3, 15)$ and $(\alpha_3, \mu_3, k_3, N_3) = (2.1, 2.4, 1, 15)$.

Fig. 5.1 (top of the next page) illustrates the OP of single, MRC, and SC diversity receptions over $i.n.d$ composite $\alpha - \mu$/gamma fading channels for $\Upsilon = -5$ dB. As seen, the MRC has less OP than the SC and no-diversity schemes. This is because the total received SNR in MRC is higher than the received SNR in both SC and no diversity. In addition to that, the increase in $\alpha$, $\mu$ or/and $k$ correspond to less non-linearity impact, high number of multipath clusters and less shadowing effect, respectively. For instance, when $\bar{\gamma} = 5$ dB (fixed), the $P_o$ for the MRC with $L = 3$ is approximately 74% and 99% less than the corresponding case of the SC and $L = 1$, respectively. It can be observed that in Fig. 5.1, when the number of diversity receivers increases, the diversity gain improves and thus, the OP reduces.
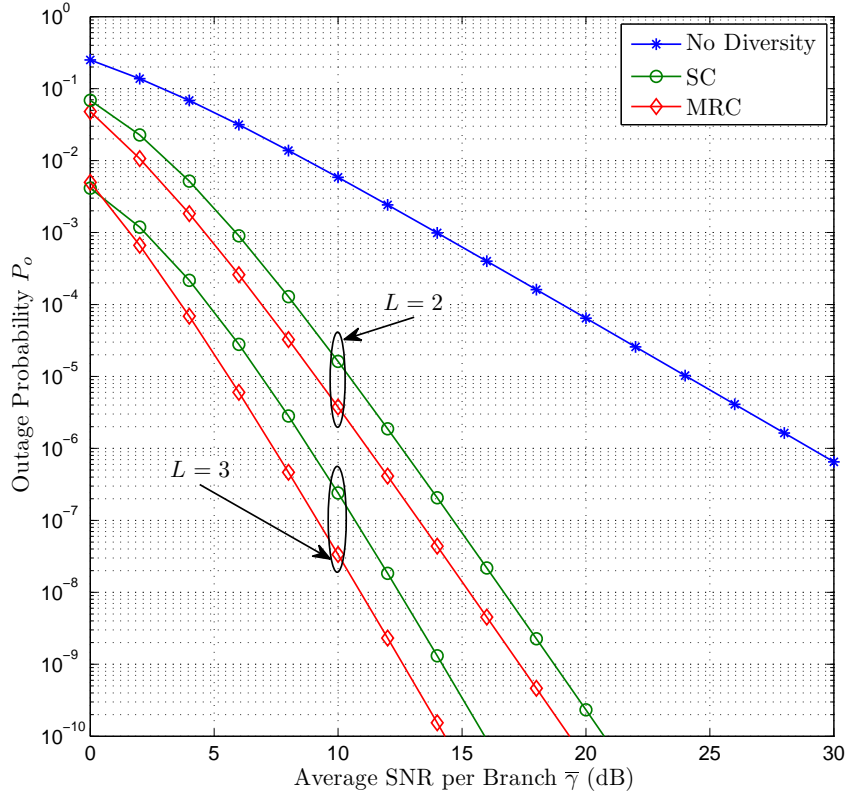
Figure 5.1: Comparison between the OP, $P_o$, of no-diversity, MRC, and SC schemes over $i.n.d$ composite $\alpha - \mu/$gamma fading channels for $\Upsilon = -5$ dB.

Fig. 5.2 (top of the next page) demonstrates the ABEP for single, MRC, and SC diversity receptions over $i.n.d$ composite $\alpha - \mu/$gamma fading channels for BPSK modulation. As expected, the results in Fig. 5.1 are affirmed by Fig. 5.2. For example, at $\bar{\gamma} = 15$ dB (fixed), the ABEP for the MRC with triple receivers is roughly 90% and 99% lower than the SC with $L = 3$ and $L = 1$, respectively.
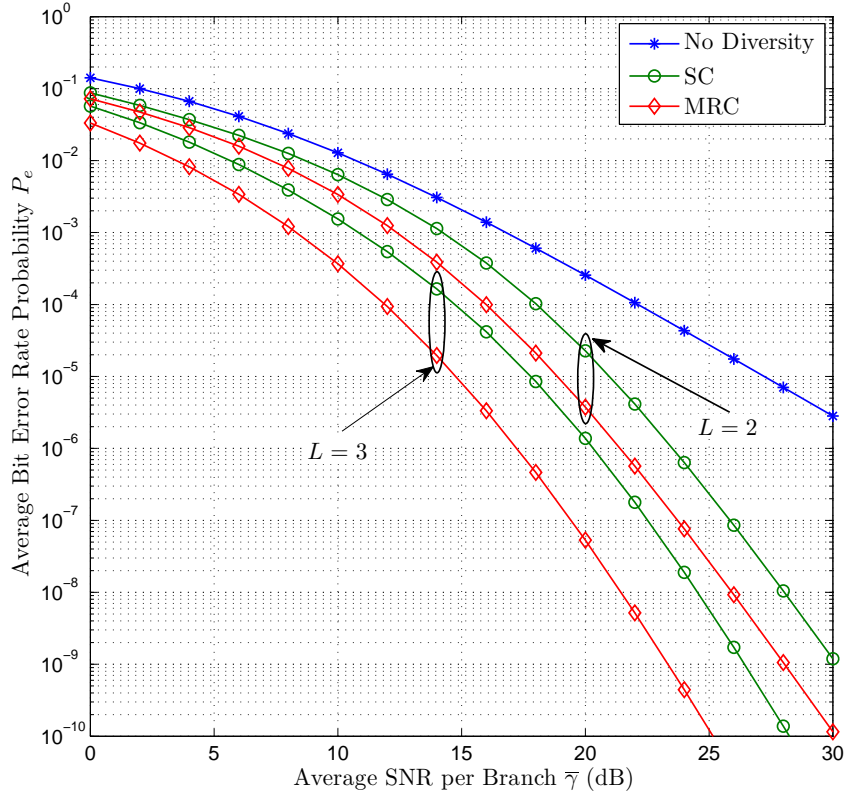
Figure 5.2: Comparison between the ABEP, $P_e$, of no-diversity, MRC, and SC schemes over $i.n.d$ composite $\alpha - \mu/$gamma fading channels for BPSK.

Fig. 5.3 (top of the next page) shows the normalized average channel capacity, $C$, for single, MRC, and SC diversity receptions over $i.n.d$ composite $\alpha - \mu/$gamma fading channels. In this figure, the values of $C$ for the MRC and the SC with dual branches are nearly 2.561 b/s/Hz and 2.414 b/s/Hz whereas the $C$ for no diversity is approximately 1.702 b/s/Hz at constant $\bar{\gamma} = 5$ dB.

100
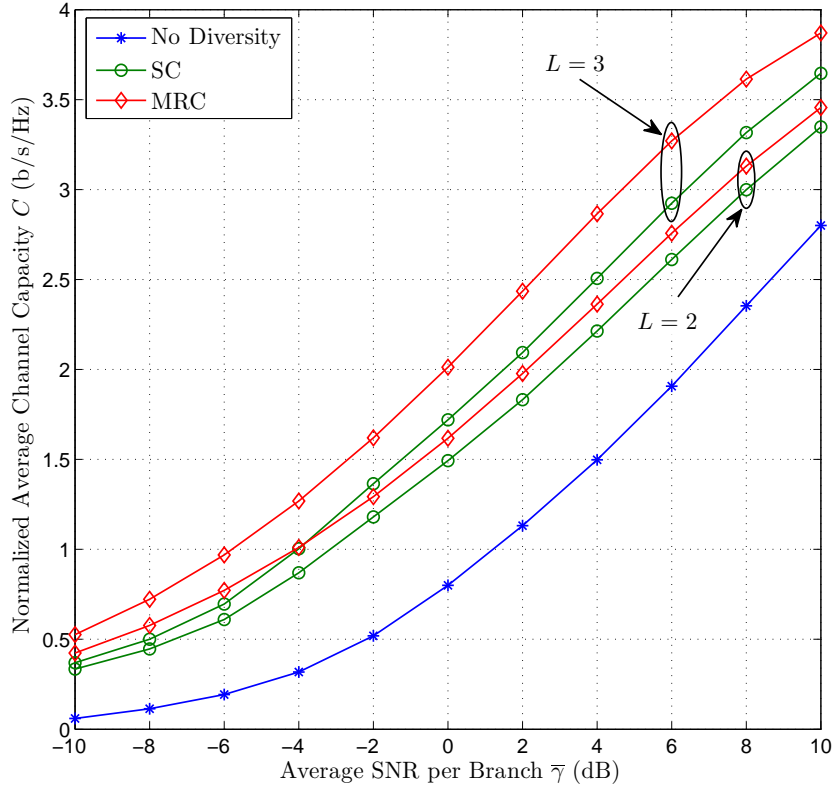
Figure 5.3: Comparison between the average channel capacity, $C$, of no-diversity, MRC, and SC schemes over $i.n.d$ composite $\alpha - \mu/$gamma fading channels.

Fig. 5.4 (top of the next page) depicts the complementary ROC of the energy detector with single, MRC, and SC schemes over $i.n.d$ composite $\alpha - \mu/$gamma fading channels with $u = 1.5$. The average SNR, $\bar{\gamma}_1$, $\bar{\gamma}_2$ and $\bar{\gamma}_3$ are set to 10 dB, 5 dB and 1 dB, respectively. Some examples that explain the required number of terms, $R$, to satisfy seven figure of accuracy for series convergences in (5.26), (5.28) and (5.30) are given in Table 5.1. As explained in Fig. 5.4, a substantial improvement in the performance of the energy detector can be noticed when the diversity reception is employed. For instance, the value of $\overline{P_{md}}$ for MRC with $L = 3$ and $P_f = 0.1$ (fixed) is approximately 78% and 99% smaller than the $\overline{P_{md}}$ of the corresponding SC and $L = 1$. In the same context, Fig. 5.5 (top of the page 103) portrays the complementary AUC curves of the energy detector.
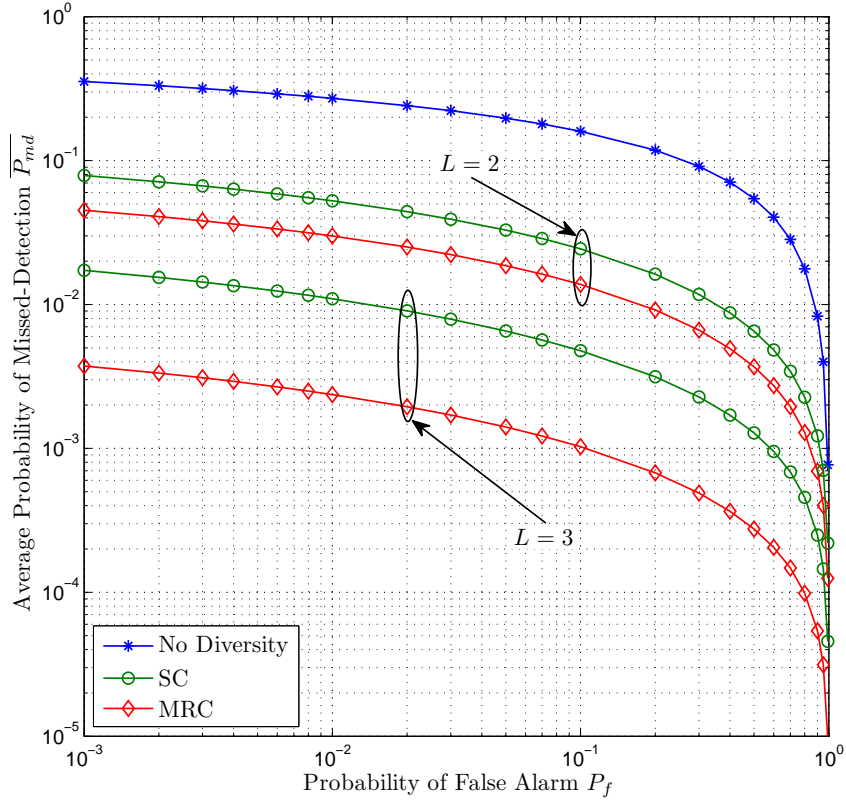
Figure 5.4: Comparison between the complementary ROC curves of the ED with no-diversity, MRC, and SC schemes over $i.n.d$ composite $\alpha - \mu/$gamma fading channels with $u = 1.5$.

Table 5.1: Number Of Terms, $R$, in (5.26), (5.28) and (5.30) for Evaluating (5.23), (5.27) and (5.29), Respectively With Accuracy of Seven Figure.

| $P_f$ | $i$ | $R$ in (5.26) | $R$ in (5.28) | | $R$ in (5.30) | |
|---|---|---|---|---|---|---|
| | | | $L = 2$ | $L = 3$ | $L = 2$ | $L = 3$ |
| 0.1 | 1 | 17 | 23 | 18 | 18 | 19 |
| 0.01 | 1 | 25 | 31 | 26 | 26 | 27 |
| 0.1 | 2 | 16 | 16 | 21 | 14 | 18 |
| 0.01 | 4 | 23 | 13 | 30 | 29 | 36 |

102
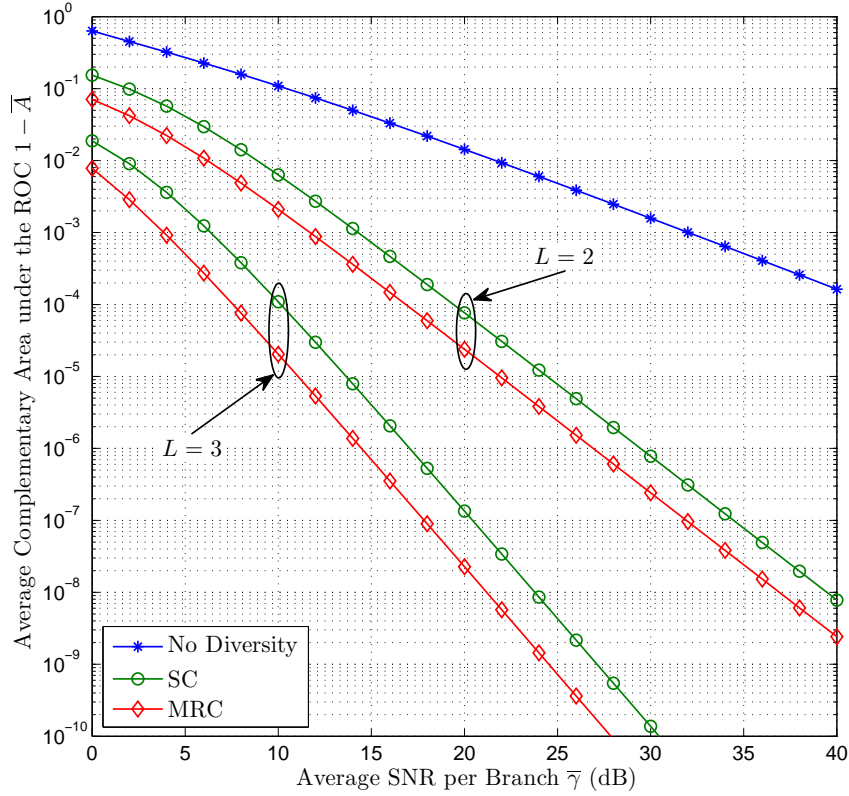
Figure 5.5: Comparison between the complementary AUC curves, $1 - \bar{A}$, of the ED with no-diversity, MRC, and SC schemes over $i.n.d$ composite $\alpha - \mu$/gamma fading channels with $u = 1.5$.

## 5.7 Conclusions

In this chapter, different performance metrics for communications systems and the energy detector with MRC and SC over $i.n.d$ composite $\alpha - \mu$/gamma fading channels were derived using a MG distribution. The parameters of MG distribution for the composite $\alpha - \mu$/gamma fading were evaluated first. Exact, closed-form and unified expressions for the PDF, the CDF and the MGF of the sum and the maximum of $i.n.d$ MG variates were then derived. The provided expressions can be employed to study the behaviour of communications systems and the energy detector with $i.n.d$ MRC and SC diversity receivers over any composite fading channel that has

intractable mathematical statistics. Furthermore, a great number of fading channels can be obtained from the composite $\alpha - \mu$/gamma fading channels by setting the fading parameters for a specific value, e.g., the statistical characterisations of $i.n.d$ $\alpha - \mu$ fading can be derived from $i.n.d$ composite $\alpha - \mu$/gamma fading by inserting $k \to \infty$.

# Chapter 6

# Statistical Characterizations of the Sum and the Maximum of I.N.D MG Random Variables

This chapter derives another model of the statistical characterizations of the sum and the maximum of $i.n.d$ MG RVs. In contrast to Chapter 5 in which the expressions are applicable when the shadowing factor is an integer number, the models of the PDF, the CDF and the MGF in this chapter are not limited by any condition. The analytic expressions of the OP, the average channel capacity, the ABEP, the average probability of detection and the average AUC curves for MRC and SC diversity receptions are then derived. The $\eta - \mu$ fading channel shadowed by gamma distribution is employed in this chapter.

## 6.1    Introduction

Diversity reception has been extensively employed to improve the performance of communications systems over different channel models. In [47], the OP and the ABEP for various diversity schemes such as MRC and SC over $i.n.d$ Rayleigh, Nakagami-$m$ and Nakagami-$n$ fading channels are derived. The average channel capacity over correlated Rician fading channels with MRC is analysed in [131].

Since wireless channels may undergo multipath fading and shadowing simultaneously, many studies for different communication systems have been investigated over composite fading channels. In [132], the statistical characterizations of $i.n.d\ K_G$ fading channels with MRC, SC and other diversity schemes are given with applications on performance analysis of communications systems. The generalized selection combining (GSC) with three receivers is employed in [133] to evaluate the OP and the ASEP over $i.n.d\ K_G$ fading channels. In [134], the analysis is based on the MGF of the SNR with GSC over $i.i.d\ K$ fading channels. In [135], the OP over exponentially correlated $K$ fading channel with SC is calculated. A closed-form analytic expression to compute the ABEP for different binary modulation formats with dual SC receivers over $i.n.d\ K_G$ fading channels is derived by [129]. Two different formats for the sum of the squared $i.n.d$ Rician-shadowed RVs are provided in [136, 137] with different applications to performance evaluation of communication systems.

Recently, the $\kappa-\mu$ and the $\eta-\mu$ distributions have been given special attention to model the multipath fading channels. The use of the $\kappa-\mu$ shadowed fading in different applications with various diversity combining is newly achieved in the open technical literature. For example, the statistical characterizations of the sum and the maximum of $i.n.d$ and $i.i.d\ \kappa-\mu$ shadowed RVs with applications to diversity receptions using MRC and SC are investigated by [111]. Moreover, the average channel capacity over composite $\kappa-\mu$/Nakagami-$m$ and $\kappa-\mu$/gamma fading channels with single receiver are derived in [138, 139], respectively. On the other hand, the performance of communication systems with diversity reception over $\eta-\mu$ fading channel with shadowing impact has not been yet studied in the literature. Thus, the previous works that are related to using the diversity combining with the $\eta-\mu$ fading channels as well as the composite $\eta-\mu$ fading and shadowing for no-diversity case are reviewed. In [140], the ASEP for various digital modulation schemes over $i.n.d\ \eta-\mu$ random variables with MRC diversity reception is derived by using the MGF approach. The OP, the channel capacity and the ABEP are calculated by [103] to study the behaviour of DS-CDMA systems using the PDF of $i.n.d\ \eta-\mu$ fading channels. Different studies of the performance of communication systems with MRC technique over correlated and co-channel interference in $\eta-\mu$ fading channels are given in [141, 142], respectively.

The expressions of the OP over $\alpha - \mu$, $\eta - \mu$ and $\kappa - \mu$ fading channels with EGC receivers in presence of co-channel interference are derived by [143]. In [144, 145], analytic expressions for the ABEP, the average channel capacity and the OP (in both [144, 145]) of digital communication systems over composite $\eta - \mu$/gamma fading channels are derived. Even though these expressions are for no-diversity, they are either limited by the values of fading parameters, i.e., $\mu$ should be an integer number or they are not closed form, i.e., with infinite series in [144] and with integrals in [145].

In this chapter, to overcome the previous problems in [144, 145] as well as to study the performance of communication systems over composite $\eta - \mu$/shadowing fading channels with diversity reception, a MG distribution is employed. The main contributions of this chapter are summarized as follows:

- In Chapter 5, the derived equations are applied to special cases i.e., the shadowing index should be an integer number. On the other hand, this chapter provides general closed-form expressions that are applicable to integer and non-integer values of the shadowing factor.

- The statistical properties of the sum and the maximum of composite $\eta - \mu$/gamma fading channels are not available in the open technical literature. Thus, the statistical characterizations of the MG can be used efficiently for this purpose.

## 6.2   MG Distribution for Composite $\eta - \mu$/gamma Fading Channel

The PDF of the instantaneous SNR $\gamma$ over composite $\eta-\mu$/gamma fading channels can be evaluated by integrating the $\eta - \mu$ fading channel (2.26) over [104, eq. (4)] to yield

$$f_\gamma(\gamma) = \frac{2\sqrt{\pi}h^\mu \mu^{\mu+\frac{1}{2}}\gamma^{\mu-\frac{1}{2}}}{\Gamma(\mu)\Gamma(k)\Omega^k H^{\mu-\frac{1}{2}}} \int_0^\infty y^{k-\mu-\frac{3}{2}} e^{-\frac{2\mu h\gamma}{y}-\frac{y}{\Omega}} I_{\mu-\frac{1}{2}}\left(\frac{2\mu H\gamma}{y}\right) dy \qquad (6.1)$$

By substituting $x = \frac{2\mu h \gamma}{y}$ in (6.1), this yields

$$f_\gamma(\gamma) = \vartheta_{\eta-\mu}\gamma^{k-1} \int_0^\infty e^{-x}g(x)dx \tag{6.2}$$

where $\vartheta_{\eta-\mu} = -\frac{\sqrt{\pi}2^{k-\mu+\frac{1}{2}}h^{k-\frac{1}{2}}}{\Gamma(\mu)\Gamma(k)H^{\mu-\frac{1}{2}}}\left(\frac{\mu}{\Omega}\right)^k$ and $g(x) = x^{\mu-k-\frac{1}{2}}e^{-\frac{2\mu h}{\Omega x}}I_{\mu-\frac{1}{2}}\left(\frac{H}{h}x\right)$.

Similar to (5.2), the integration in (6.2), $\mathcal{S} = \int_0^\infty e^{-x}g(x)dx$, can be approximately expressed as a Gaussian-Laguerre quadrature sum. Thus, (6.2) can be represented by the MG distribution with parameters

$$\boldsymbol{\alpha}_i = \frac{\theta_i}{\sum_{l=1}^N \theta_l \Gamma(\beta_l)\zeta_l^{-\beta_l}}, \quad \beta_i = k, \quad \zeta_i = \frac{2\mu h}{\Omega x_i}, \quad \theta_i = \vartheta_{\eta-\mu}w_i x_i^{\mu-k-\frac{1}{2}}I_{\mu-\frac{1}{2}}\left(\frac{H}{h}x_i\right) \tag{6.3}$$

## 6.3 Statistical Characterizations of MG Distribution with I.N.D RVs

In this section, the PDF, the CDF and the MGF of the sum and the maximum of $i.n.d$ MG random variables are derived. These functions are then used to study the performance of wireless communication systems over composite $\eta - \mu/$gamma fading channels.

### 6.3.1 Statistical Characterizations of the Sum of $i.n.d$ MG RVs

By using the same assumptions in Subsection 5.3.1, the MGF of the sum $\gamma^{Sum} = \sum_{j=1}^L \gamma_j$ of $i.n.d$ MG RVs, $\mathcal{M}_{\gamma^{Sum}}(s)$, can be evaluated by

$$\mathcal{M}_{\gamma^{Sum}}(s) = \prod_{j=1}^L \mathcal{M}_{\gamma_j}(s) = \prod_{j=1}^L \left[\sum_{i_j=1}^{N_j} \frac{\boldsymbol{\alpha}_{i_j}\Gamma(\beta_{i_j})}{(s+\zeta_{i_j})^{\beta_{i_j}}}\right] \tag{6.4}$$

The right hand side expression in (6.4) can be rewritten in another form as follows

$$\mathcal{M}_{\gamma^{Sum}}(s) = \sum_{i_1=1}^{N_1} \cdots \sum_{i_L=1}^{N_L} \prod_{j=1}^{L} \frac{\boldsymbol{\alpha}_{i_j} \Gamma(\beta_{i_j})}{(s + \zeta_{i_j})^{\beta_{i_j}}} \tag{6.5}$$

By plugging (6.5) into $f_{\gamma^{Sum}}(\gamma) = \mathcal{L}^{-1}\big[\mathcal{M}_{\gamma^{Sum}}(s); \gamma\big]^1$ where $f_{\gamma^{Sum}}(\gamma)$ is the PDF of $\gamma^{Sum}$, this yields

$$f_{\gamma^{Sum}}(\gamma) = \sum_{i_1=1}^{N_1} \cdots \sum_{i_L=1}^{N_L} \left( \prod_{j=1}^{L} \boldsymbol{\alpha}_{i_j} \Gamma(\beta_{i_j}) \right)$$
$$\times \mathcal{L}^{-1}\left[ (s + \zeta_{i_1})^{-\beta_{i_1}} (s + \zeta_{i_2})^{-\beta_{i_2}} \cdots (s + \zeta_{i_L})^{-\beta_{i_L}}; \gamma \right] \tag{6.6}$$

The inverse Laplace transform of (6.6) is available in [44, eq. (9.4.55)]. Accordingly, $f_{\gamma^{Sum}}(\gamma)$ is expressed by

$$f_{\gamma^{Sum}}(\gamma) = \sum_{i_1=1}^{N_1} \cdots \sum_{i_L=1}^{N_L} \left( \prod_{j=1}^{L} \boldsymbol{\alpha}_{i_j} \Gamma(\beta_{i_j}) \right) \frac{\gamma^{\sum_{j=1}^{L} \beta_{i_j} - 1}}{\Gamma\left(\sum_{j=1}^{L} \beta_{i_j}\right)}$$
$$\times \Phi_2^{(L)}\left( \beta_{i_1}, \cdots, \beta_{i_L}; \sum_{j=1}^{L} \beta_{i_j}; -\zeta_{i_1}\gamma, \cdots, -\zeta_{i_L}\gamma \right) \tag{6.7}$$

The CDF of $\gamma^{Sum}$ can be computed by using $F_{\gamma^{Sum}}(\gamma) = \mathcal{L}^{-1}\big[\mathcal{M}_{\gamma^{Sum}}(s)/s; \gamma\big]$ and [44, eq. (9.4.55)] to yield

$$F_{\gamma^{sum}}(\gamma) = \sum_{i_1=1}^{N_1} \cdots \sum_{i_L=1}^{N_L} \left( \prod_{j=1}^{L} \boldsymbol{\alpha}_{i_j} \Gamma(\beta_{i_j}) \right) \frac{\gamma^{\sum_{j=1}^{L} \beta_{i_j}}}{\Gamma\left(1 + \sum_{j=1}^{L} \beta_{i_j}\right)}$$
$$\times \Phi_2^{(L)}\left( \beta_{i_1}, \cdots, \beta_{i_L}; 1 + \sum_{j=1}^{L} \beta_{i_j}; -\zeta_{i_1}\gamma, \cdots, -\zeta_{i_L}\gamma \right) \tag{6.8}$$

---

[1]Here $\mathcal{L}^{-1}$ stands for inverse Laplace transform.

## 6.3.2 Statistical Characterizations of the Maximum of $i.n.d$ MG RVs

The CDF of the maximum $\gamma^{Max} = \max\{\gamma_1, \gamma_2, \cdots, \gamma_L\}$ of $i.n.d$ MG variates, $F_{\gamma^{Max}}(\gamma)$, is given by

$$F_{\gamma^{Max}}(\gamma) = \prod_{j=1}^{L} F_{\gamma_j}(\gamma) = \prod_{j=1}^{L} \left[ \sum_{i_j=1}^{N_j} \boldsymbol{\alpha}_{i_j} \zeta_{i_j}^{-\beta_{i_j}} G(\beta_{i_j}, \zeta_{i_j}\gamma) \right] \tag{6.9}$$

Using [124, eq. (6.5.12)] with some mathematical manipulations, the CDF of $\gamma^{Max}$, $F_{\gamma^{Max}}(\gamma)$, in (6.9) is rewritten as follows,

$$F_{\gamma^{Max}}(\gamma) = \sum_{i_1=1}^{N_1} \cdots \sum_{i_L=1}^{N_L} \left( \prod_{j=1}^{L} \frac{\boldsymbol{\alpha}_{i_j}}{\beta_{i_j}} \right) \left( \prod_{j=1}^{L} \gamma^{\beta_{i_j}} {}_1F_1(\beta_{i_j}; 1 + \beta_{i_j}; -\zeta_{i_j}\gamma) \right) \tag{6.10}$$

The MGF of $\gamma^{Max}$ can be computed by invoking $\mathcal{M}_{\gamma^{Max}}(s) = s\mathcal{L}[F_{\gamma^{Max}}(\gamma); s]$ with the aid of [44, eq. (9.4.35)]. Accordingly, the desired result is

$$\mathcal{M}_{\gamma^{Max}}(s) = \sum_{i_1=1}^{N_1} \cdots \sum_{i_L=1}^{N_L} \left( \prod_{j=1}^{L} \frac{\boldsymbol{\alpha}_{i_j}}{\beta_{i_j}} \right) \frac{\Gamma\left(1 + \sum_{j=1}^{L}\beta_{i_j}\right)}{s^{\sum_{j=1}^{L}\beta_{i_j}}}$$

$$\times F_A^{(L)}\left(1 + \sum_{j=1}^{L}\beta_{i_j}; \beta_{i_1}, \cdots, \beta_{i_L}; 1 + \beta_{i_1}, \cdots, 1 + \beta_{i_L}; -\frac{\zeta_{i_1}}{s}, \cdots, -\frac{\zeta_{i_L}}{s}\right) \tag{6.11}$$

Using $f_{\gamma^{Max}}(\gamma) = \mathcal{L}^{-1}[\mathcal{M}_{\gamma^{Max}}(s); \gamma]$ and [44, eq. (1.4.1)] with the help of the identity [123, eq. (12)], the following expression for the PDF of $\gamma^{Max}$, $f_{\gamma^{Max}}(\gamma)$, is obtained

$$f_{\gamma^{Max}}(\gamma) = \sum_{i_1=1}^{N_1} \cdots \sum_{i_L=1}^{N_L} \left( \prod_{j=1}^{L} \frac{\boldsymbol{\alpha}_{i_j}}{\beta_{i_j}} \right) \frac{\sum_{j=1}^{L}\beta_{i_j}}{\gamma^{1-\sum_{j=1}^{L}\beta_{i_j}}} \sum_{n_1,\dots,n_L=0}^{\infty} \frac{\left(1 + \sum_{j=1}^{L}\beta_{i_j}\right)_{n_1+n_2+\dots+n_L}}{\left(\sum_{j=1}^{L}\beta_{i_j}\right)_{n_1+n_2+\dots+n_L}}$$

$$\times \frac{(\beta_{i_1})_{n_1}\dots(\beta_{i_L})_{n_L}}{(1+\beta_{i_1})_{n_1}\dots(1+\beta_{i_L})_{n_L} n_1!\dots n_L!}(-\zeta_{i_1}\gamma)^{n_1}\dots(-\zeta_{i_L}\gamma)^{n_L} \tag{6.12}$$

It can be noticed that (6.12) can be exactly expressed as follows

$$f_{\gamma^{Max}}(\gamma) = \sum_{i_1=1}^{N_1} \cdots \sum_{i_L=1}^{N_L} \left( \prod_{j=1}^{L} \frac{\boldsymbol{\alpha}_{i_j}}{\beta_{i_j}} \right) \frac{\sum_{j=1}^{L} \beta_{i_j}}{\gamma^{1-\sum_{j=1}^{L} \beta_{i_j}}}$$
$$\times F_{1:1;\cdots;1}^{\overbrace{1:1;\cdots;1}^{L}} \left[ \begin{array}{c} (1+\sum_{j=1}^{L} \beta_{i_j}): (\beta_{i_1}) \; ;\cdots; \; (\beta_{i_L}) \; ; \\ (\sum_{j=1}^{L} \beta_{i_j}) \; :(1+\beta_{i_1});\cdots;(1+\beta_{i_L}); \end{array} -\zeta_{i_1}\gamma, \cdots, -\zeta_{i_L}\gamma \right] \quad (6.13)$$

where $F_{1:1;\cdots;1}^{1:1;\cdots;1}[.]$ is the Kampé de Fériet function [44, eq. (1.4.24)].

# 6.4 Performance Analysis of Communications Systems with Diversity Reception Using MG

## 6.4.1 Outage Probability

**Maximal Ratio Combining (MRC)**

The outage probability for MRC scheme can be calculated by (6.8).

**Selection Combining (SC)**

The outage probability for SC diversity reception can be computed by (6.9).

## 6.4.2 Average Bit Error Probability

The ABEP, $P_e$, can be expressed by the CDF of the received instantaneous SNR, $\gamma$, as follows [129, eq.(12)]

$$P_e = \frac{q^p}{2\Gamma(p)} \int_0^{\infty} \gamma^{p-1} e^{-q\gamma} F_\gamma(\gamma) d\gamma \quad (6.14)$$

**Maximal Ratio Combining (MRC)**

The ABEP for MRC, $P_{e_{MRC}}$, can be evaluated by substituting (6.8) into (6.14) as follows

$$P_{e_{MRC}} = \frac{q^p}{2\Gamma(p)} \sum_{i_1=1}^{N_1} \cdots \sum_{i_L=1}^{N_L} \frac{\left(\prod_{j=1}^{L} \boldsymbol{\alpha}_{i_j} \Gamma(\beta_{i_j})\right)}{\Gamma\left(1 + \sum_{j=1}^{L} \beta_{i_j}\right)}$$

$$\times \int_0^\infty \gamma^{p + \sum_{j=1}^{L} \beta_{i_j} - 1} e^{-q\gamma} \Phi_2^{(L)}\left(\beta_{i_1}, \cdots, \beta_{i_L}; 1 + \sum_{j=1}^{L} \beta_{i_j}; -\zeta_{i_1}\gamma, \cdots, -\zeta_{i_L}\gamma\right) d\gamma \quad (6.15)$$

The integral in (6.15) is given in [44, eq. (9.4.43)]. Accordingly, after some straightforward mathematical manipulations, this yields

$$P_{e_{MRC}} = \frac{1}{2\Gamma(p)} \sum_{i_1=1}^{N_1} \cdots \sum_{i_L=1}^{N_L} \frac{\left(\prod_{j=1}^{L} \boldsymbol{\alpha}_{i_j} \Gamma(\beta_{i_j})\right) \Gamma\left(p + \sum_{j=1}^{L} \beta_{i_j}\right)}{q^{\sum_{j=1}^{L} \beta_{i_j}} \Gamma\left(1 + \sum_{j=1}^{L} \beta_{i_j}\right)}$$

$$\times F_D^{(L)}\left(p + \sum_{j=1}^{L} \beta_{i_j}; \beta_{i_1}, \cdots, \beta_{i_L}; 1 + \sum_{j=1}^{L} \beta_{i_j}; -\frac{\zeta_{i_1}}{q}, \cdots, -\frac{\zeta_{i_L}}{q}\right) \quad (6.16)$$

**Selection Combining (SC)**

The ABEP of SC, $P_{e_{SC}}$, can be calculated by inserting (6.10) in (6.14) as follows

$$P_{e_{SC}} = \frac{q^p}{2\Gamma(p)} \sum_{i_1=1}^{N_1} \cdots \sum_{i_L=1}^{N_L} \left(\prod_{j=1}^{L} \frac{\boldsymbol{\alpha}_{i_j}}{\beta_{i_j}}\right)$$

$$\times \int_0^\infty \gamma^{p + \sum_{j=1}^{L} \beta_{i_j} - 1} e^{-q\gamma} \prod_{j=1}^{L} {}_1F_1(\beta_{i_j}; 1 + \beta_{i_j}; -\zeta_{i_j}\gamma) d\gamma \quad (6.17)$$

By invoking [44, eq. (9.4.35)] to compute the integral in (6.17), this obtains

$$P_{e_{SC}} = \frac{1}{2\Gamma(p)} \sum_{i_1=1}^{N_1} \cdots \sum_{i_L=1}^{N_L} \left(\prod_{j=1}^{L} \frac{\boldsymbol{\alpha}_{i_j}}{\beta_{i_j}}\right) \frac{\Gamma(p + \sum_{j=1}^{L} \beta_{i_j})}{q^{\sum_{j=1}^{L} \beta_{i_j}}}$$

$$\times F_A^{(L)}\left(p + \sum_{j=1}^{L} \beta_{i_j}; \beta_{i_1}, \cdots, \beta_{i_L}; 1 + \beta_{i_1}, \cdots, 1 + \beta_{i_L}; -\frac{\zeta_{i_1}}{q}, \cdots, -\frac{\zeta_{i_L}}{q}\right) \quad (6.18)$$

112

### 6.4.3  Average Channel Capacity

It can be noticed that (5.19) can not be employed in evaluating the channel capacity of both the MRC and the SC diversity receptions in this chapter. This is because the expressions of the PDF for both MRC and SC do not contain an exponential function that facilitates the integration process. Therefore, in this chapter, an approximated method in computing the average channel capacity is utilised. In this method, the average channel capacity is expressed in terms of the MGF of the received SNR as follows [131, eq. (8)],

$$C = \frac{B}{\ln 2} \int_0^\infty \frac{1 - \mathcal{M}_\gamma(z)}{z} e^{-z} dz \tag{6.19}$$

The integral in (6.19) can be computed approximately by using the Gauss Legendre quadrature approach as follows

$$C \approx \frac{B}{\ln 2} \sum_{l=1}^{M} w_l \frac{1 - \mathcal{M}_\gamma(x_l)}{x_l} \tag{6.20}$$

where $w_l$ and $x_l$ are the weights and the abscissas at $l$ point, respectively.

## 6.5  Performance of Energy Detector with Diversity Reception Using MG

In this subsection, the expressions of the $\overline{P_d}(\lambda)$ and the $\bar{A}$ with MRC and SC diversity receptions over $i.n.d$ MG fading channels are given.

### 6.5.1  Average Detection Probability

When $u \in \mathbb{R}$, i.e., $u$ is a real number, $P_d(\gamma, \lambda)$ of (2.8) can be expressed by [146, eq. (34)] as follows

$$P_d(\gamma, \lambda) = 1 - \left(\frac{\lambda}{2}\right)^u e^{-\frac{2\gamma+\lambda}{2}} \tilde{\Phi}_3\left(1; 1 + u; \frac{\lambda}{2}, \frac{\gamma\lambda}{2}\right) \tag{6.21}$$

where $\tilde{\Phi}_3(.;.;.,.)$ is the regularized bivariate confluent hypergeometric function defined in [146, eq. (4)].

**Maximal Ratio Combining (MRC)**

The average detection probability over MG fading channels with MRC diversity reception, $\overline{P_d}^{MRC}(\lambda)$, can be evaluated by plugging (6.7) and (6.21) into (3.1) to give

$$\overline{P_d}^{MRC}(\lambda) = 1 - \frac{\lambda^u 2^{-u} e^{-\frac{\lambda}{2}}}{\Gamma(1+u)} \sum_{i_1=1}^{N_1} \cdots \sum_{i_L=1}^{N_L} \left( \prod_{j=1}^{L} \boldsymbol{\alpha}_{i_j} \Gamma(\beta_{i_j}) \right) \Psi_1^{MRC} \qquad (6.22)$$

where

$$\Psi_1^{MRC} =$$

$$F_{2:0;\cdots;0;0}^{\overbrace{1:1;\ldots;1;0}^{L+2}} \left( \begin{array}{c} [\sum_{i=1}^{L} \beta_{i_j} : 1, ..., 1, 1, 0] \qquad : [\beta_{i_1} : 1]; ...; [\beta_{i_L} : 1]; [1 : 1]; -; \\ [\sum_{i=1}^{L} \beta_{i_j} : 1, ..., 1, 0, 0], [1 + u : 0, ..., 0, 1, 1] : \underline{\quad\quad}; ...; \underline{\quad\quad}; \underline{\quad\quad}; -; \\ -\zeta_{i_1}, ..., -\zeta_{i_L}, \frac{\lambda}{2}, \frac{\lambda}{2} \end{array} \right)$$

*Proof:* See Appendix C.1. ∎

**Selection Combining (SC)**

Under the condition $u \in \mathbb{R}$, the average detection probability over MG based channel modelling with SC diversity reception, $\overline{P_d}^{SC}(\lambda)$, can be calculated by inserting (6.13) and (6.21) into (3.1) and following the same procedure for (6.22). Accordingly, this yields

$$\overline{P_d}^{SC}(\lambda) = 1 - \frac{\lambda^u 2^{-u} e^{-\frac{\lambda}{2}}}{\Gamma(1+u)} \sum_{i_1=1}^{N_1} \cdots \sum_{i_L=1}^{N_L} \left( \prod_{j=1}^{L} \frac{\boldsymbol{\alpha}_{i_j}}{\Gamma(\beta_{i_j})} \right) \Gamma\left( 1 + \sum_{i=1}^{L} \beta_{i_j} \right) \Psi_1^{SC} \quad (6.23)$$

114

where

$$\Psi_1^{SC} = F_{2:1;\cdots;1;1;0}^{\overbrace{2:1;\ldots;1;1;0}^{L+2}}\left(\begin{array}{l}[\sum\limits_{i=1}^{L}\beta_{i_j}:1,...,1,1,0],[1+\sum\limits_{i=1}^{L}\beta_{i_j}:1,...,1,0,0]:\\[2mm][\sum\limits_{i=1}^{L}\beta_{i_j}:1,...,1,0,0]\quad,\quad[1+u:0,...,0,1,1]:\\[4mm][\beta_{i_1}:1]\;\;;...;\;\;[\beta_{i_L}:1]\;\;;[1:1];-;\\[2mm][1+\beta_{i_1}:1];...;[1+\beta_{i_L}:1];\underline{\quad\quad};-;\end{array}\right. \left.\begin{array}{l}\\[4mm]-\zeta_{i_j},\,...,\,-\zeta_{i_L},\frac{\lambda}{2},\frac{\lambda}{2}\\[4mm]\end{array}\right)$$

## 6.5.2 Average Area under the ROC (AUC)

**Maximal Ratio Combining (MRC)**

The average AUC under the MG distribution based channel representation with MRC receivers, $\bar{A}^{MRC}$, for $u \in \mathbb{R}$ can be computed by inserting (6.22) into (5.31) with the help of [43, eq. (3.351.3)]. Accordingly, this yields

$$\bar{A}^{MRC} = 1 - \frac{\Gamma(2u)}{u[2^u\Gamma(u)]^2}\sum_{i_1=1}^{N_1}\cdots\sum_{i_L=1}^{N_L}\left(\prod_{j=1}^{L}\boldsymbol{\alpha}_{i_j}\Gamma(\beta_{i_j})\right)\Lambda_1^{MRC} \tag{6.24}$$

where

$$\Lambda_1^{MRC} =$$

$$F_{2:0;\cdots;0;0}^{\overbrace{2:1;\ldots;1;0}^{L+2}}\left(\begin{array}{l}[\sum\limits_{i=1}^{L}\beta_{i_j}:1,...,1,1,0],\ \ [2u:0,...,0,1,1]\ \ :[\beta_{i_1}:1];...;[\beta_{i_L}:1];[1:1];-;\\[4mm][\sum\limits_{i=1}^{L}\beta_{i_j}:1,...,1,0,0],[1+u:0,...,0,1,1]:\underline{\quad\quad};...;\underline{\quad\quad};\underline{\quad\quad};-;\end{array}\right.$$

$$\left.\begin{array}{l}\\[4mm]-\zeta_{i_1},\,...,\,-\zeta_{i_L},\frac{1}{2},\frac{1}{2}\\[4mm]\end{array}\right)$$

*Proof:* See Appendix C.2. ∎

115

**Selection Combining (SC)**

The average AUC under composite fading channel modelled by MG distribution with SC diversity reception, $\bar{A}^{SC}$, and $u \in \mathbb{R}$ can be evaluated by

$$\bar{A}^{SC} = 1 - \frac{\Gamma(2u)}{u[2^u\Gamma(u)]^2} \sum_{i_1=1}^{N_1} \cdots \sum_{i_L=1}^{N_L} \left( \prod_{j=1}^{L} \frac{\boldsymbol{\alpha}_{i_j}}{\beta_{i_j}} \right) \Gamma\left( 1 + \sum_{i=1}^{L} \beta_{i_j} \right) \Lambda_1^{SC} \qquad (6.25)$$

where

$$\Lambda_1^{SC} = F_{2:1;\,\cdots;\,1;0;\,0}^{\overbrace{3:1;\,\cdots;\,1;1;0}^{L+2}} \left( \begin{array}{c} [\sum_{i=1}^{L} \beta_{i_j} : 1, ..., 1, 1, 0], [1 + \sum_{i=1}^{L} \beta_{i_j} : 1, ..., 1, 0, 0], [2u : 0, ..., 0, 1, 1] : \\[2mm] [\sum_{i=1}^{L} \beta_{i_j} : 1, ..., 1, 0, 0] \qquad , \qquad [1 + u : 0, ..., 0, 1, 1] \qquad : \\[4mm] [\beta_{i_1} : 1] \ \ ; ...; \ \ [\beta_{i_L} : 1] \ \ ; [1 : 1]; \_; \\[2mm] \qquad\qquad\qquad\qquad\qquad\qquad\qquad\qquad -\zeta_{i_j}, ..., -\zeta_{i_L}, \frac{1}{2}, \frac{1}{2} \\[2mm] [1 + \beta_{i_1} : 1]; ...; [1 + \beta_{i_L} : 1]; \_\_\_; \_; \end{array} \right)$$

The expression in (6.25) is calculated by plugging (6.23) into (5.31) with the aid of [43, eq. (3.35.3)] and doing some mathematical manipulations.

## 6.6   Numerical Results

In this section, the OP, the ABEP, the average channel capacity, the average probability of detection, and the average AUC for MRC and SC diversity receivers over *i.n.d* composite $\eta - \mu$/gamma fading channels are numerically computed using MATLAB software[2]. These results are given for single, dual and triple diversity branches. The set up parameters are $(\eta_1, \ \mu_1, \ k_1, \ N_1) = (0.1, 0.5, 1.5, 15)$, $(\eta_2, \ \mu_2, \ k_2, \ N_2) = (0.3, 1.5, 1.5, 15)$, and $(\eta_3, \ \mu_3, \ k_3, \ N_3) = (0.9, 2.5, 1.5, 15)$.

---

[2]In this chapter, Format 1 of the $\eta - \mu$ is used.

Fig. 6.1 shows the OP for single, MRC and SC diversity receptions with $\Upsilon = 0$ dB over $i.n.d$ composite $\eta - \mu/$gamma fading channels. As expected, the OP of the MRC is less than the OP of the SC and no-diversity cases. This is because the total received SNR in MRC scheme is based on summing of the SNR of all branches while in SC, the total received SNR is the largest SNR among all receivers. For example, in Fig. 6.1, when $\bar{\gamma} = 15$ dB (fixed), the $P_o$ for the MRC with $L = 2$ is nearly 73% and 99% lower than the SC with $L = 2$ and $L = 1$, respectively. Furthermore, one can see that the value of the OP reduces when the number of diversity branches increases. This also refers to increase in the total received SNR.
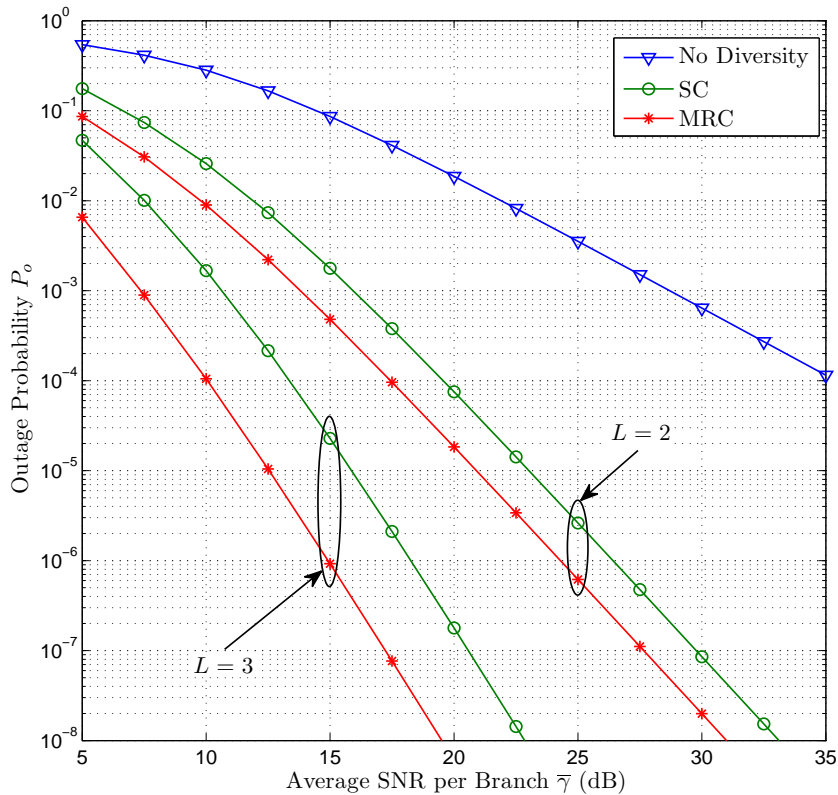


Figure 6.1: Comparison between the OP, $P_o$, of no-diversity, MRC, and SC schemes over $i.n.d$ composite $\eta - \mu/$gamma fading channels for $\Upsilon = 0$ dB.

Fig. 6.2 illustrates the ABEP for single, MRC and SC diversity receptions with BPSK modulation over $i.n.d$ composite $\eta - \mu$/gamma fading channels. The results in this figure confirm the results that are given in Fig. 6.1. For instance, in Fig. 6.2 at $\bar{\gamma} = 10$ dB (fixed), the ABEP for the MRC with double branches is approximately 48% and 95% less than the corresponding case of the SC and $L = 1$, respectively.

Fig. 6.3 (top of the next page) explains the normalized average channel capacity for single, MRC and SC diversity receptions over $i.n.d$ composite $\eta - \mu$/gamma fading channel. The number of terms, $M$, in (6.20) is chosen to be 15. The results in this figure show the superiority of the MRC over the SC and no-diversity schemes and for the same reasons that are mentioned for the previous figures. For example, in Fig.
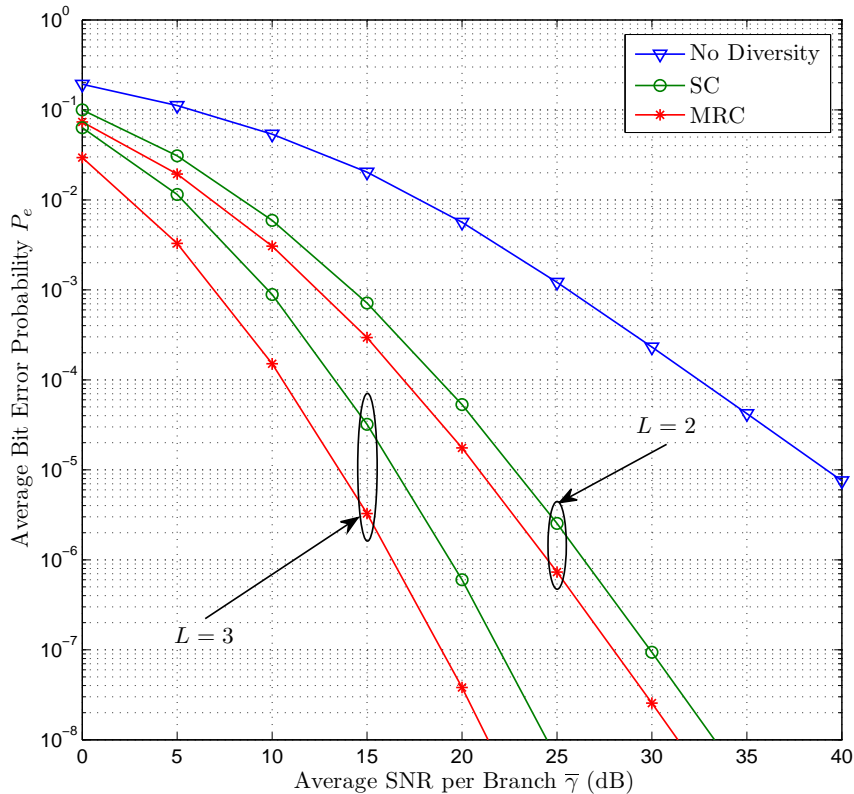


Figure 6.2: Comparison between the ABEP, $P_e$, of no-diversity, MRC, and SC schemes over $i.n.d$ composite $\eta - \mu$/gamma fading channels for BPSK.
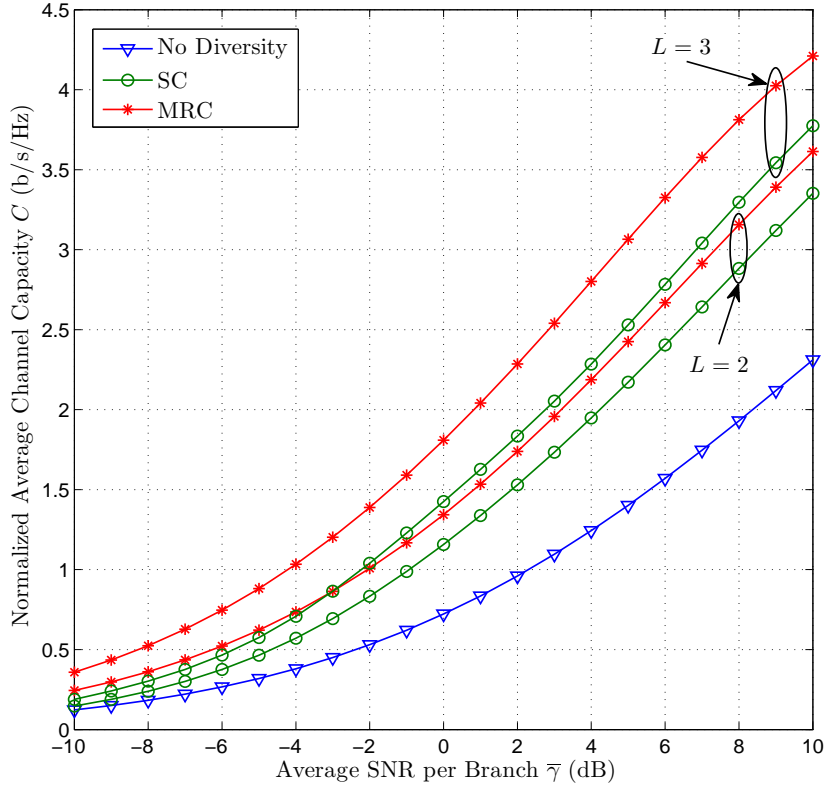
Figure 6.3: Comparison between the average channel capacity, $C$, of no-diversity, MRC, and SC schemes over $i.n.d$ composite $\eta - \mu/\text{gamma}$ fading channels.

6.3, when $\bar{\gamma} = 0$ dB (fixed), the $C$ for MRC with triple receivers is roughly 1.805 b/s/Hz whereas the $C$ for the corresponding SC and $L = 1$ are nearly 1.433 b/s/Hz and 0.6762 b/s/Hz, respectively.

Fig. 6.4 (top of the next page) depicts the CROC of energy detector with single, MRC and SC diversity receptions over $i.n.d$ composite $\eta - \mu/\text{gamma}$ fading channels. The values of the average SNR, $\gamma_1$, $\gamma_2$ and $\gamma_3$ are set to be 5 dB, 10 dB and 15 dB, respectively. Furthermore, $u$ is equal to 1.5. As shown in Fig. 6.4, the performance of ED becomes better when the diversity reception is used. For instance, the value of $\overline{P_{md}}$ for MRC with $L = 2$ at $P_f = 0.01$ (fixed) is approximately 41% and 80% smaller than the $\overline{P_{md}}$ of the corresponding SC and $L = 1$. In the same context, Fig. 6.5 (top of the page 121) explains the CAUC of energy detector by using the same scenarios of
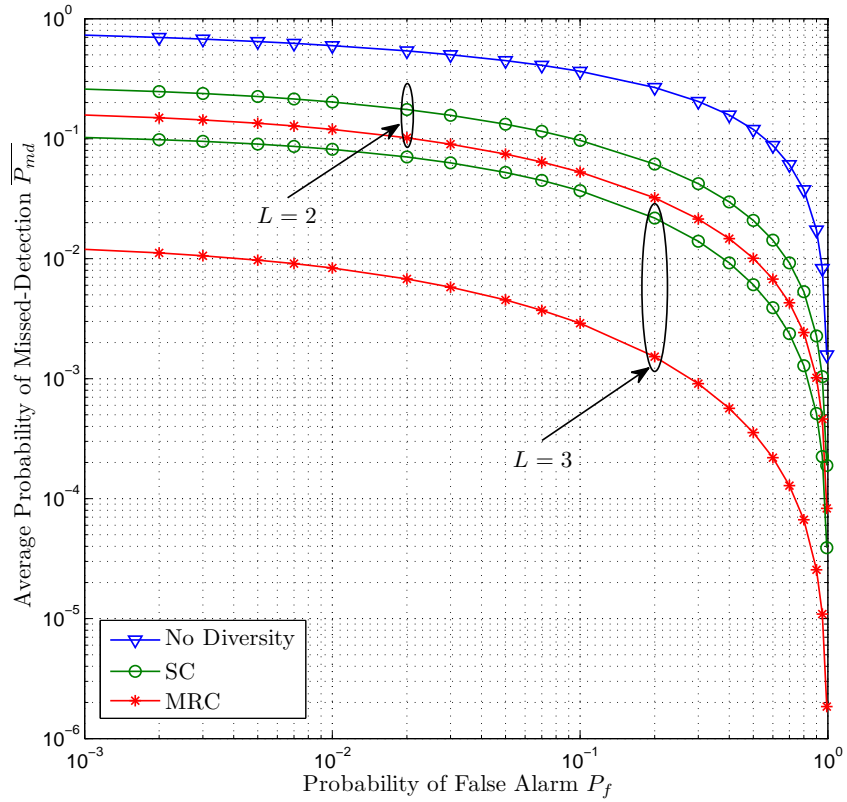
Figure 6.4: Comparison between the complementary ROC curves of the energy detector with no-diversity, MRC and SC schemes over *i.n.d* composite $\eta - \mu$/gamma fading channels with $u = 1.5$.

Fig. 6.4. Clearly, the CAUC demonstrates the behaviour of the ED over wide range of the SNR regardless the value of the $P_f$.
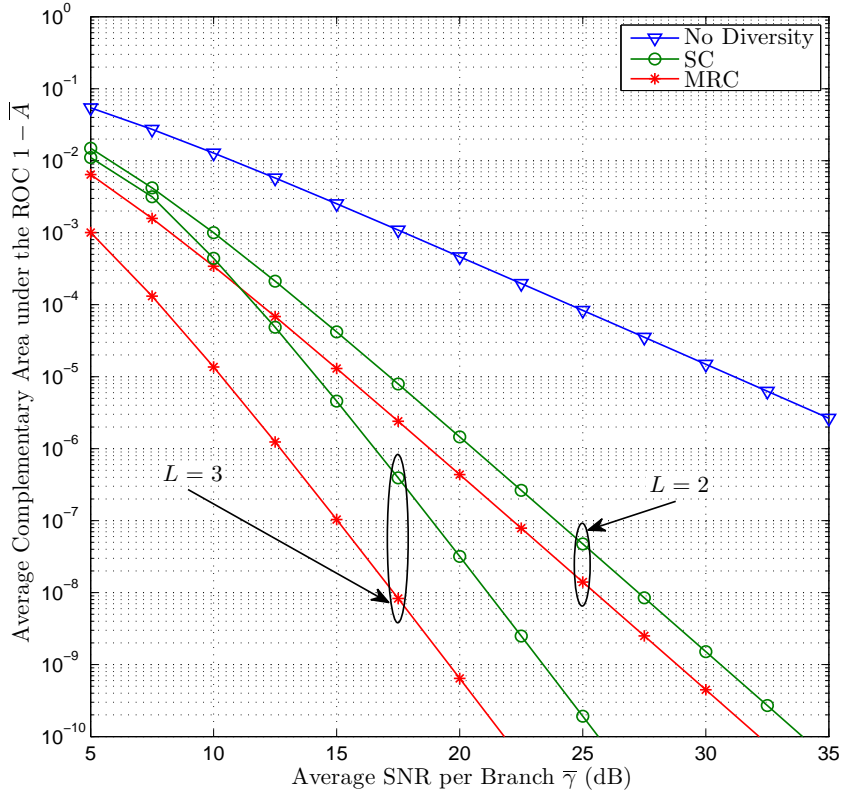
Figure 6.5: Comparison between the complementary AUC, $1 - \bar{A}$, of the energy detector with no-diversity, MRC and SC schemes over $i.n.d$ composite $\eta - \mu/\text{gamma}$ fading channels with $u = 1.5$.

## 6.7 Conclusions

In this chapter, the sum and the maximum of $i.n.d$ MG variates were statistically characterized. General exact analytic expressions for the PDF, the CDF and the MGF were derived. These expressions were employed as unified models in analysing the performance of communication systems with diversity reception. In particular, the outage probability, the average bit error probability and the average channel capacity with MRC and SC schemes were investigated. The composite $\eta - \mu/\text{gamma}$ was utilised in the study of the performance of these systems. The analysis of various communication scenarios with diversity receivers can be easily obtained from the

121

derived expressions. For example, the performance of communication systems over $\eta - \mu$ fading channels with MRC and SC can be deduced from $\eta - \mu$/gamma fading channels by setting $k \to \infty$. Moreover, these expressions can be used to evaluate the performance of different communication systems over any composite fading that is intractable to be studied by exact channel models.

# Chapter 7

# Filter bank Transforms Based Performance Enhancement of an Energy Detector

In this chapter, an improvement for energy detector performance is achieved by using DSP for the PU signal before taking the final decision by the SU. Firstly, signal denoising technique based on HST is applied on the noisy PU signal to reduce the noise effect on the ED technique. Secondly, the uncertain noise power is estimated by the SU using SPT to find the quantity of the noise that is included in the PU signal. Simulation results compare the detection performance of the proposed approach with wavelet transform based approaches. The results show the obvious superiority for proposed SPT-HST approach in comparison with wavelet approach in terms of improving the detection probability and reducing the computational complexity .

## 7.1 Introduction

The accuracy of energy detector is strongly influenced by the fluctuation of the noise power and would lead to degrading of the detection performance and especially at low SNR values. In addition, it suffers from the incorrect selection of the threshold value, which depends on the noise floor, for detecting PUs and cannot differentiate

interference from the PUs and noise [25]. Hence, many approaches have been proposed to minimize the effect of the noise on the detectability of energy detector. One of these techniques is based on employing tree-structured filter bank transforms to estimate the noise power. In [80, 82, 147], the performance of non-cooperative and CSS scenarios with DWT to reduce the noise impact at the SU and the FC is analysed. The behaviour of the energy detector based CSS under noise uncertainty condition is studied by [81] using DWT for signal denoising. In [85], an algorithm based on DWT is proposed to predict the noise variance of energy detector before calculating of the test statistic.

Other applications for wavelet transform using DWPT are implemented to improve the accuracy of energy detector. For example, in [86, 87, 148], a certain bandwidth is selected and then divided into several sub-bands by DWPT to check which sub-band is unoccupied by the PU. The DWPT is employed in [88] to estimate the noise power as well as to calculate the signal power for energy detector based SS. A combined DWPT and different infinite impulse response polyphase filtering schemes are proposed by [149, 150] to increase the accuracy of energy detector and to reduce the computational complexity.

As mentioned in Subsection 2.10, to achieve high degree of detection accuracy in the IEEE 802.22 WRAN, the number of samples should be large enough. Hence, DWPT and DWT that also require a large number of samples of PU can be used to improve the performance of ED based SS in the IEEE 802.22 WRAN standard. However, the computational complexity of ED with DWPT-DWT becomes higher than the conventional ED which would lead to an increase in the sensing time. Therefore, this chapter proposes a combined approach to provide SS in IEEE 802.22 WRAN with good detection sensitivity at both low SNR and acceptable number of samples.

The main contributions of this chapter are summarized as follows:

- The signal denoising technique based on HST is employed to reduce the noise impact on the detection performance of energy detector. A HST which is a set of digital filters is used rather than iterated DWT to enhance the performance of ED with less computational complexity.

- SPT is proposed as a tree-structure filter bank transform and then utilised to estimate the unknown noise power with higher detection accuracy and lower computational complexity in comparison with the iterated DWPT.

## 7.2 Hybrid Slantlet Transform

HST is a mixed transform between DWT and slantlet transform (ST) [151]. Moreover, it is an enhanced version of orthogonal iterated DWT using $D_2$ wavelet basis function by improving the time localization of the analysed signal with filters shorter than the iterated DWT filters. Therefore, HST is appropriate for analysing and processing the non-stationary PU signal with low computational complexity in comparison with the iterated DWT [152-154]. The two-levels of filter bank structures of iterated DWT and HST are explained in Fig. 7.1 and Fig. 7.2, respectively.



↓ 4 means selecting the fourth sample from each four samples.
↑ 4 means making each one sample as four samples by adding zeros.

(a) Two-level iterated DWT    (b) Two-level iterated IDWT
(signal analysis)    (signal synthesis)
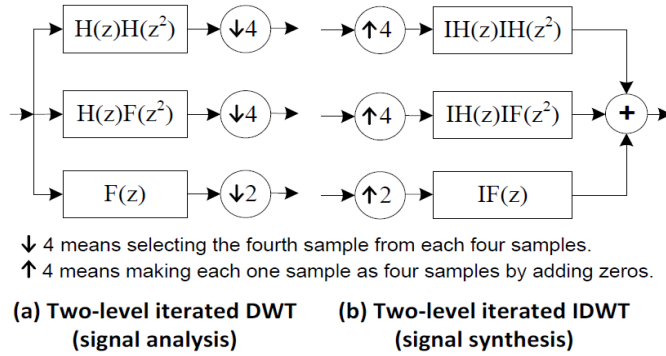
Figure 7.1: Filter-bank structure of iterated discrete wavelet transform [151].



(a) Two-level HST    (b) Two-level IHST
(signal analysis)    (signal synthesis)
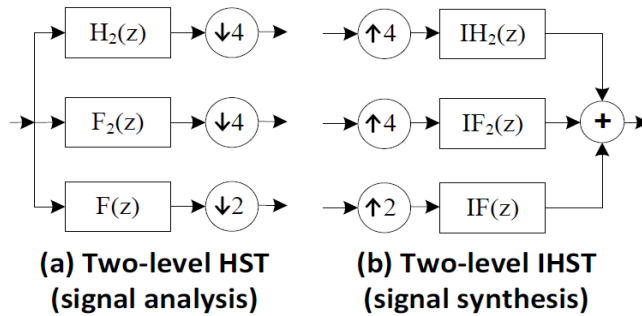
Figure 7.2: Filter-bank structure of hybrid slantlet transform.
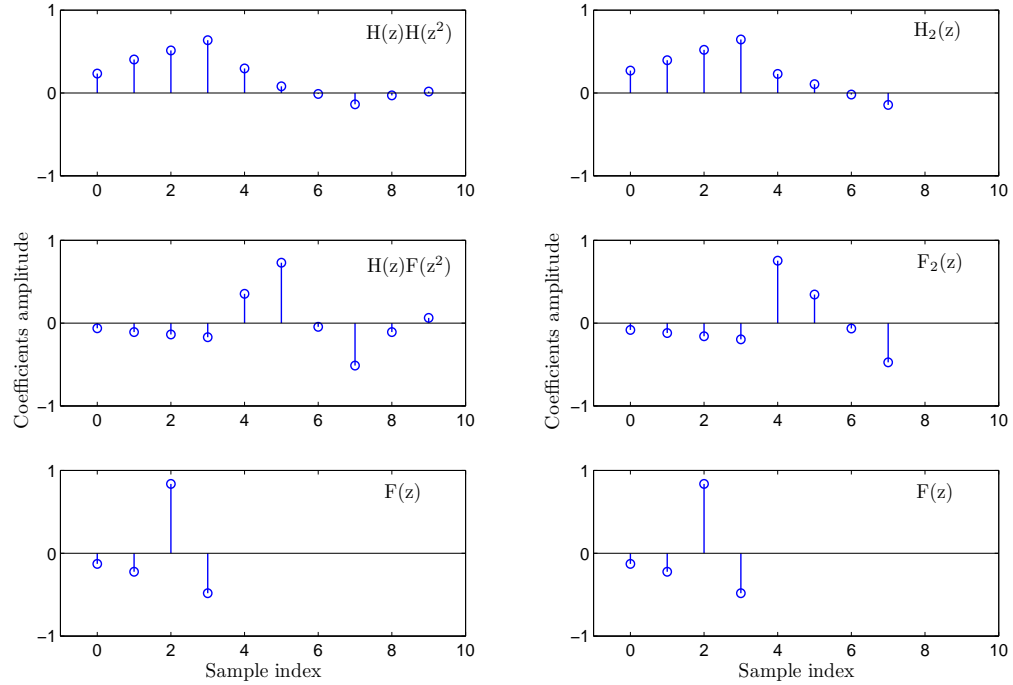
Figure 7.3: Comparison the number of filters' samples of iterated DWT and HST [151].

Fig. 7.3 and Fig 7.4 show comparisons between samples values and the filters response for two-level of iterated DWT and HST, respectively. From Fig 7.4, it is clear that the filters' response for both transforms are approximately similar. However, the number of samples for the first and second filters of the HST is less than the number of samples of the corresponding filters of the iterated DWT as depicted in Fig. 7.3.

## 7.3 Slantlet Packet Transform

SPT is an improved version of the DWPT as well as it is an extended version of the ST. In other words, SPT mixes some of the ST and DWPT features. Since there is a relation between SPT and DWPT, a brief information about the principle work of the DWPT is firstly provided.

DWPT is an extended version for the DWT by analyzing both the detailed and ap-

126
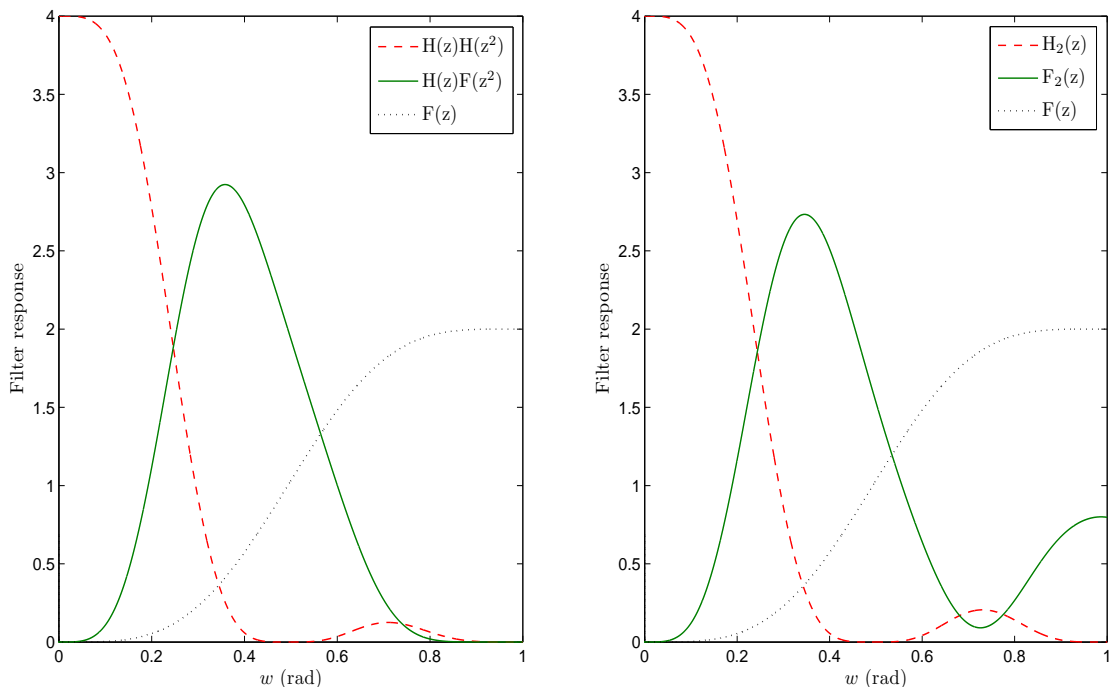
Figure 7.4: Comparison between the response of iterated DWT filters and HST filters [151].

proximation coefficients at each level. Thus, the DWPT gives more details about the analysing signal in comparison with the DWT. Moreover, it is appropriate to identify the signal information in both low and high frequency bands [79, 155]. The equivalent structure for the two-level decomposition of the DWPT filter banks (iterated DWPT) is demonstrated in Fig. 7.5.

As the DWPT is considered as an expanded version for the DWT, the SPT can also be suggested as an extended version for the ST. Therefore, SPT decomposes both the approximation and detailed coefficients in a complete tree structure, but with filters shorter than the iterated DWPT filters. Moreover, SPT enhances the time localization and the orthogonality of the DWPT. In other words, SPT is derived by using the same principle of deriving the ST from the DWT which it depends on the iterated form of the filter banks that result in the higher levels of the decompositions (two levels and above). Fig. 7.6 illustrates the two-levels of filter banks of the SPT.

**(a) Two-level iterated DWPT (signal analysis)**    **(b) Two-level iterated IDWPT (signal synthesis)**
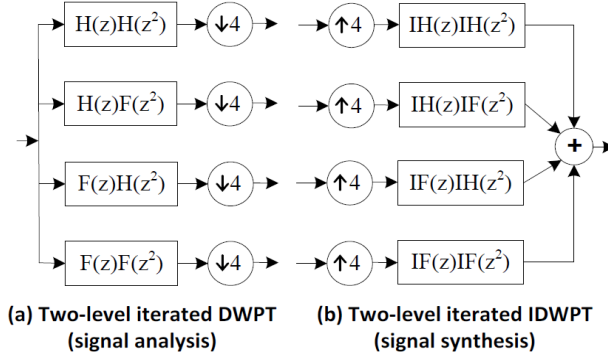
Figure 7.5: Filter-bank structure of iterated discrete wavelet packet transform.



**(a) Two-level SPT (signal analysis)**    **(b) Two-level ISPT (signal synthesis)**
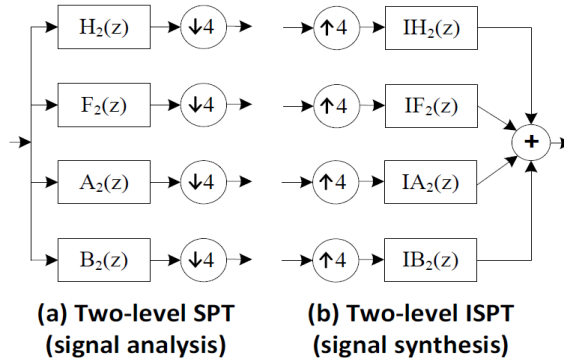
Figure 7.6: Filter-bank structure of slantlet packet transform.

The coefficients' amplitudes of the F(z) of the DWPT can be computed from the coefficients' amplitudes of the H(z), as follows [156]:

$$F(e^{jw}) = -e^{jdw}H^*(e^{j(w-\pi)}) \tag{7.1}$$

Or by using:

$$f(m) = (-1)^m h(d - m) \qquad m = 0, 1, \cdots, d \tag{7.2}$$

where $d$ is an odd integer number (for $D_2$, $d = 3$ for first level).

By using (7.1) or (7.2) and $d = 7$, the coefficients' amplitudes of the $B_2(z)$ and $A_2(z)$ can be evaluated from the coefficients' amplitudes of the $H_2(z)$ and $F_2(z)$, respectively.
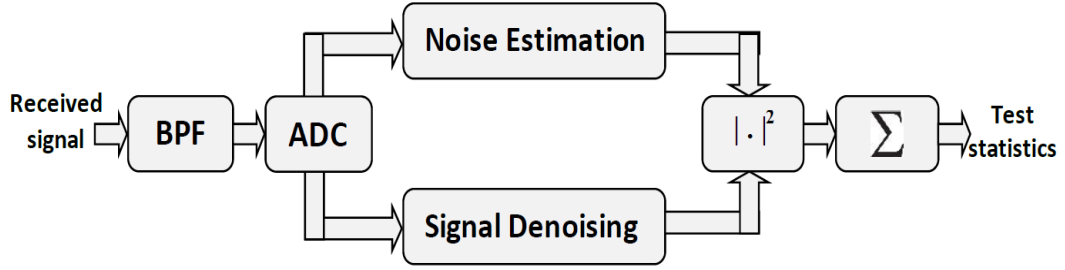
Figure 7.7: Block diagram of the proposed energy detector with signal denoising and noise estimation approaches using HST and SPT, respectively.

## 7.4 Hybrid Slantlet Transform Based Signal Denoising for Energy Detector

In the AWGN channel, the noise effects lead to an incorrect decision by the SU for the PU case. This degrades the accuracy of energy detection and thus a mutual interference between the PU and SU signals occurs. Therefore, the noisy PU signal should be manipulated at SU receiver before computing the test statistic, $\Xi$. In this thesis, a signal denoising approach based on HST is proposed to alleviate the noise impact on the energy detection technique as illustrated in Fig. 7.7 (top of this page).

As shown in Fig. 7.7, the input noisy PU signal is firstly limited by the BPF. Secondly, the band limited signal is converted from analog to digital using ADC. After that, the digital signal is processed by HST based signal denoising approach to reduce the noise. In this approach, the following steps that are explained in Fig. 7.8 are carried out on the PU signal:

1. The received PU signal is firstly decomposed by HST to convert the signal into a set of coefficients. These coefficients represent the scaling coefficients and hybrid slantlet coefficients. It should be noted that the highpass subbands are



Figure 7.8: Block diagram of the proposed signal denoising using HST or DWT.

129

called the hybrid slantlet coefficients instead of wavelet coefficients because the HST is used here.

2. The hybrid slantlet coefficients are used to eliminate the noise effect by thresholding. In this thresholding process, the data point value that is less than the threshold value is zeroed out. But, it is still without any change if the value is greater than this threshold. This type of thresholding is called hard thresholding and it allows for greater noise reduction in comparison with the other types of thresholding which is used in signal denoising approach such as soft thresholding. In this thesis, Stein's unbiased risk estimate (SURE) [157] approach has been employed to select a threshold value.

3. The denoisy hybrid slantlet coefficients together with the scaling coefficients are utilised as input to IHST to reconstruct the PU signal with very low noise.

Finally, the new signal that includes low noise impact is squared and summed to calculate the decision statistic, $\Xi$.

## 7.5 Slantlet Packet Transform Based Noise Power Estimation for Energy Detector

In the noise estimation part of Fig. 7.7, the SPT is used to estimate the unknown noise power by analysing the PU signal for the scaling coefficients and the slantlet coefficients. The slantlet coefficients are produced by decomposing the PU signal with the $A_2(z)$ and $B_2(z)$ filters. On the other hand, the scaling coefficients are already produced from the signal denoising by HST. Consequently, the power, $P$, of an analog PU signal can be computed by the SPT as follows [158, 159]

$$P = \frac{1}{M} \sum_{k=1}^{2^{i-1}} (c_{i,k}^2 + s_{i,k}^2) \tag{7.3}$$

where $i$, $c_{i,k}$ and $s_{i,k}$ are the number of the decomposition levels, scaling coefficients and slantlet coefficients at $i$th level, respectively.

It can be noted that the slantlet coefficients represent the transmitted signal with low noise whereas the scaling coefficients refer to the noise signal that is included in the received signal [80, 85, 158, 159]. Thus, the power of the transmitted signal, $P_t$, and the noise, $P_n$, can be evaluated as follows

$$P_t = \frac{1}{M} \sum_{k=1}^{2^{i-1}} s_{i,k}^2 \tag{7.4}$$

and

$$P_n = \frac{1}{M} \sum_{k=1}^{2^{i-1}} c_{i,k}^2 \tag{7.5}$$

By using (7.4) and (7.5), the SNR can be estimated.

Since, in this chapter, the model **P2** of energy detector is utilised to perform the SS for IEEE 802.22 WRAN at very low SNR, the $P_d(\gamma, \lambda)$ for this model can be further approximated by assuming $\sqrt{1+\gamma} \approx 1$. Thus, the $P_d(\gamma, \lambda)$ in (2.18) can be expressed by

$$P_d(\gamma, \lambda) \approx Q\left(\frac{\lambda - \sigma_w^2(1+\gamma)M}{\sqrt{2M}\sigma_w^2}\right) \tag{7.6}$$

It can be noted (7.6) is equal to [160, eq. (3)]. However, the approximated term in [161, eq. (3)] is $\sqrt{1+2\gamma} \approx 1$ which is larger than $\sqrt{1+\gamma} \approx 1$ at the same SNR. In another meaning, the approximation framework in this chapter is more acceptable than that given in [160] at very low SNR.

## 7.6 Computational Complexity of Iterated DWPT-DWT and SPT-HST Approaches

As mentioned previously, the lengths of HST and SPT filters are shorter than the lengths of iterated DWT and iterated DWPT filters respectively. Accordingly, the total number of real multiplications, $\mathbb{M}$, and additions, $\mathbb{A}$, in HST-SPT approach are

less than the iterated DWT-DWPT approach. This reduction leads to lower the TCC, $\mathbb{T}$, which depends on the number of addition and multiplication operations that are carried out between the signal, analysis and reconstructing filters. Consequently, the SU with HST-SPT approach has less system complexity, sensing time and handset power consumption in comparison with the SU who uses the iterated DWT-DWPT approach. Since the slantlet and wavelet coefficients that are employed in iterated DWPT and SPT are taken from iterated DWT and HST, respectively, the number of operations for evaluating these coefficients are computed for one time. Furthermore, the number of operations in thresholding stage of signal denoising part in both iterated DWT and HST is neglected.

### 7.6.1 Number of Multiplications

The number of real multiplications for any filter in filter bank transform is given by [150] [1]

$$\mathbb{M} = M \times L_F \tag{7.7}$$

where $L_F$ is the length of the filter.

**Number of Multiplications of Iterated DWPT-DWT Approach**

As given in [151], the length of H(z)H(z$^2$), H(z)F(z$^2$), F(z)H(z$^2$) and F(z)F(z$^2$) of Fig. 7.5 (a) can be calculated by $3.2^i - 2$. Thus, the number of real multiplications for iterated DWPT, $\mathbb{M}_{DWPT}$, based signal analysis can be expressed by:

$$\mathbb{M}_{DWPT} = 8(3.2^{i-1} - 1)M \tag{7.8}$$

The length of F(z) in Fig. 7.2 is 4 coefficients, i.e., $L_F = 4$ for F(z). Accordingly, the number of real multiplications for iterated DWT, $\mathbb{M}_{DWT}$, based signal analysis

---

[1]It can be noted that $M$ in all filter bank transforms should be power of 2.

and synthesis in Fig. 7.8 can be given by

$$\mathbb{M}_{DWT} = 4(3.2^{i-1} + 1)M \tag{7.9}$$

By summing (7.8) and (7.9) and substituting $i = 2$, the total number of real multiplications for DWPT-DWT approach, $\mathbb{M}_{DWPT-DWT}$, is obtained as follows

$$\mathbb{M}_{DWPT-DWT} = 4M(9.2^{i-1} - 1) \tag{7.10}$$

**Number of Multiplications of SPT-HST Approach**

The length of $H_2(z)$ and $F_2(z)$ of Fig 7.6 (a) can be computed by $2^{i+1}$ [151]. Consequently, the number of real multiplications for SPT, $\mathbb{M}_{SPT}$, based signal analysis is given by

$$\mathbb{M}_{SPT} = 2^{i+3}M \tag{7.11}$$

The number of real multiplications for HST, $\mathbb{M}_{HST}$, based signal analysis and synthesis in Fig. 7.8 can be evaluated by

$$\mathbb{M}_{HST} = 8(2^{i-1} + 1)M \tag{7.12}$$

The total real multiplications for SPT-HST approach at $i = 2$, $\mathbb{M}_{SPT-HST}$ can be obtained from (7.11) and (7.12) as follows

$$\mathbb{M}_{SPT-HST} = 8M(2^i + 2^{i-1} + 1) \tag{7.13}$$

## 7.6.2 Number of Additions

The number of real additions for any filter in filter bank transform can be evaluated by

$$\mathbb{A} = M \times L_F - (M + L_F - 1) \tag{7.14}$$

**Number of Additions of Iterated DWPT-DWT Approach**

By inserting $L_F = 3.2^i - 2$ into (7.14), the number of real additions for iterated DWPT, $\mathbb{A}_{DWPT}$, can be deduced as follows

$$\mathbb{A}_{DWPT} = 12(2^i - 1)(M - 1) \tag{7.15}$$

The number of real additions for iterated DWT, $\mathbb{A}_{DWT}$, that is utilised for signal denoising in Fig. 7.8 can be computed by

$$\mathbb{A}_{DWT} = 3.2^{i+1}(M - 1) \tag{7.16}$$

From (7.15) and (7.16), the number of real additions for iterated DWPT-DWT approach, $\mathbb{A}_{DWPT-DWT}$, can be calculated as follows

$$\mathbb{A}_{DWPT-DWT} = 12(3.2^{i-1} - 1)(M - 1) \tag{7.17}$$

**Number of Additions of SPT-HST Approach**

The number of real additions for SPT, $\mathbb{A}_{SPT}$, can be evaluated by plugging $L_F = 2^{i+1}$ into (7.14). Thus, this yields

$$\mathbb{A}_{SPT} = 4(2^{i+1} - 1)(M - 1) \tag{7.18}$$

Using $L_F = 4$ for F(z) and IF(z) that are employed for signal analysis and synthesis in signal denoising of HST, the number of real additions for HST, $\mathbb{A}_{HST}$, in Fig. 7.8 can be expressed by

$$\mathbb{A}_{HST} = 4(2^i + 1)(M - 1) \tag{7.19}$$

The total number of real additions for SPT-HST approach, $\mathbb{M}_{SPT-HST}$, can be computed by using (7.18) and (7.19) as follows

$$\mathbb{A}_{SPT-HST} = 12.2^i(M - 1) \tag{7.20}$$

## 7.7 Analytical Results

This section provides different comparisons between iterated DWPT-DWT approach and SPT-HST Approach. In Fig. 7.9 and Fig. 7.10, comparisons between the coefficients amplitude and the filters response of the iterated DWPT and SPT, respectively are given. From Fig. 7.10, it is clear that there is no huge difference
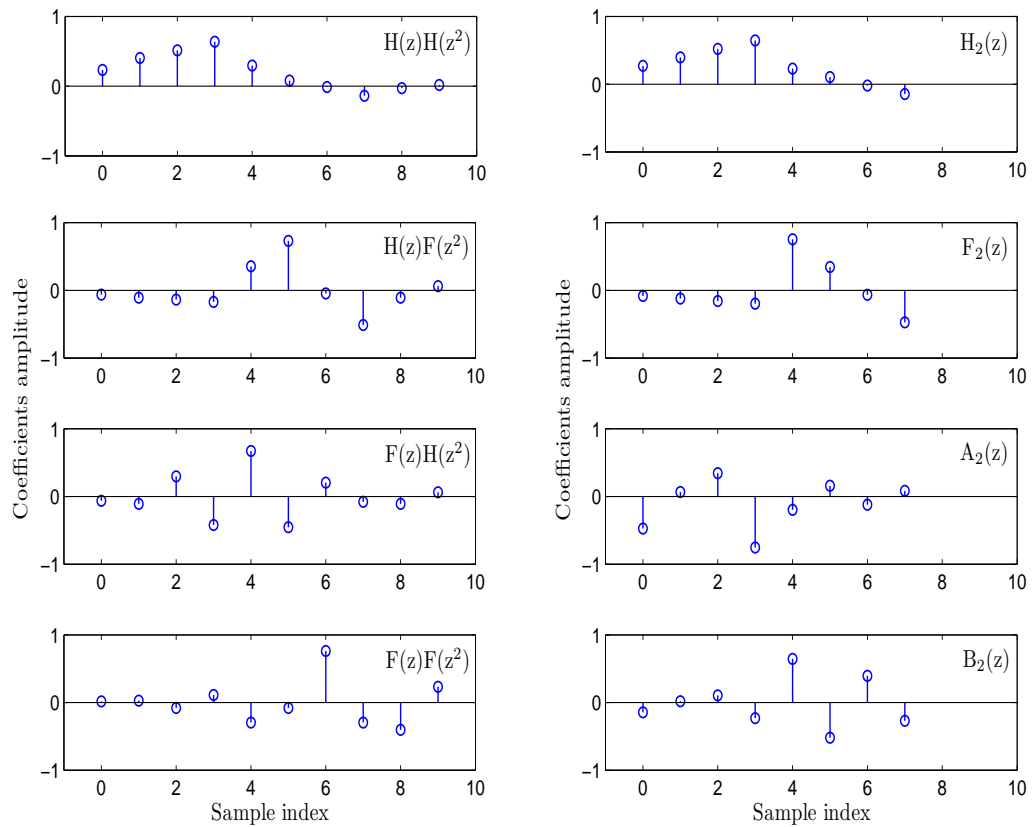


Figure 7.9: Comparison the number of filters' samples of iterated DWPT and SPT.

between the filters response of the iterated DWPT and SPT. However, it can be observed from Fig. 7.9 that the number of the coefficients of the SPT filters is less than its corresponding in the iterated DWPT. This minimization in the filters' length leads to reduce both $\mathbb{M}$ and $\mathbb{A}$ which lead to minimize the TCC, $\mathbb{T}$.

Fig. 7.11 (top of the next page) shows a comparison between the CROC of iterated
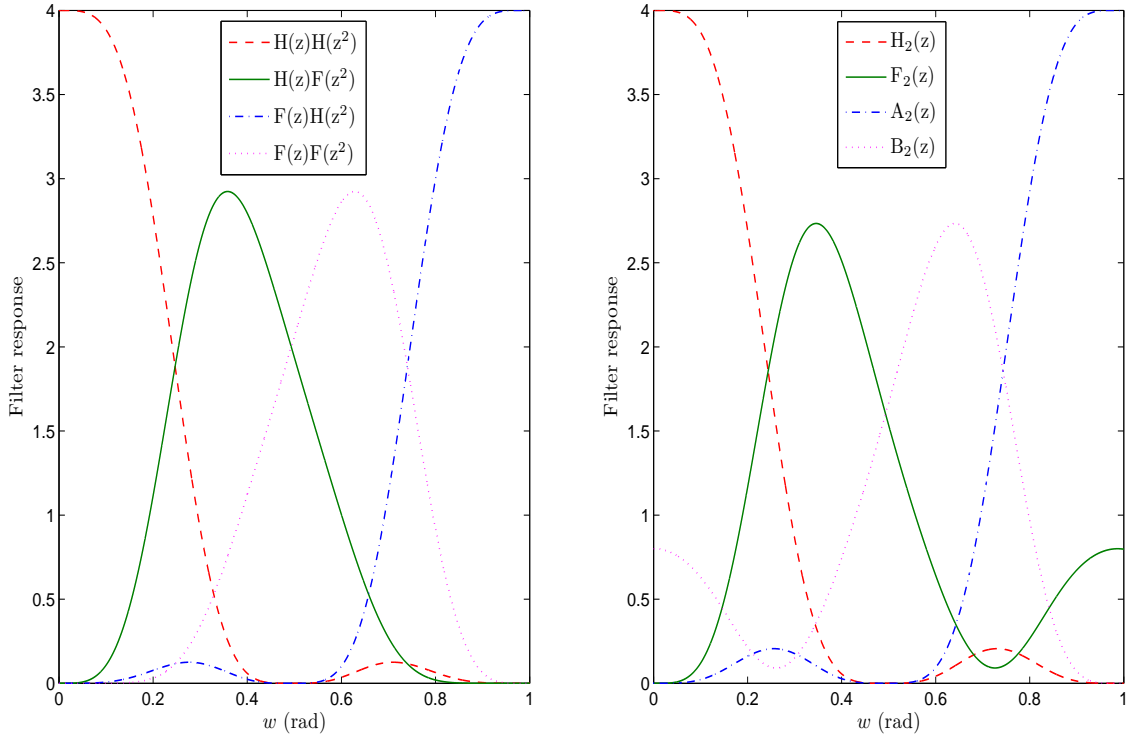
Figure 7.10: Comparison between the response of iterated DWPT and SPT filters

DWPT-DWT approach and SPT-HST approach for various $\gamma$. The input PU signal is chosen as quadrature phase shift keying (QPSK) signal with $M = 512$ and carrier frequency 3 kHz. The sampling frequency $(f_s)$ is equal to 62.5 kHz which is a typical fast Fourier transform (FFT) bin resolution of an experimental ED implementation [161]. From Fig 7.11, it is clear that the performance of the SPT-HST approach is better than the iterated DWPT-DWT approach at the same $P_f$. This is because the orthogonality of the filters for both SPT and HST is better than the orthogonality of corresponding filters in both DWPT and DWT, respectively. For example, when $P_f = 0.01$ dB (fixed), the $P_{md}$ for SPT-HST is roughly smaller than the $P_{md}$ for iterated DWPT-DWT by 97% at $\gamma = -5$ dB. One can see that the proposed SPT-HST can provide the SS at very low SNR with enough number of samples which is a critical case in IEEE 802.22 WRAN.

136
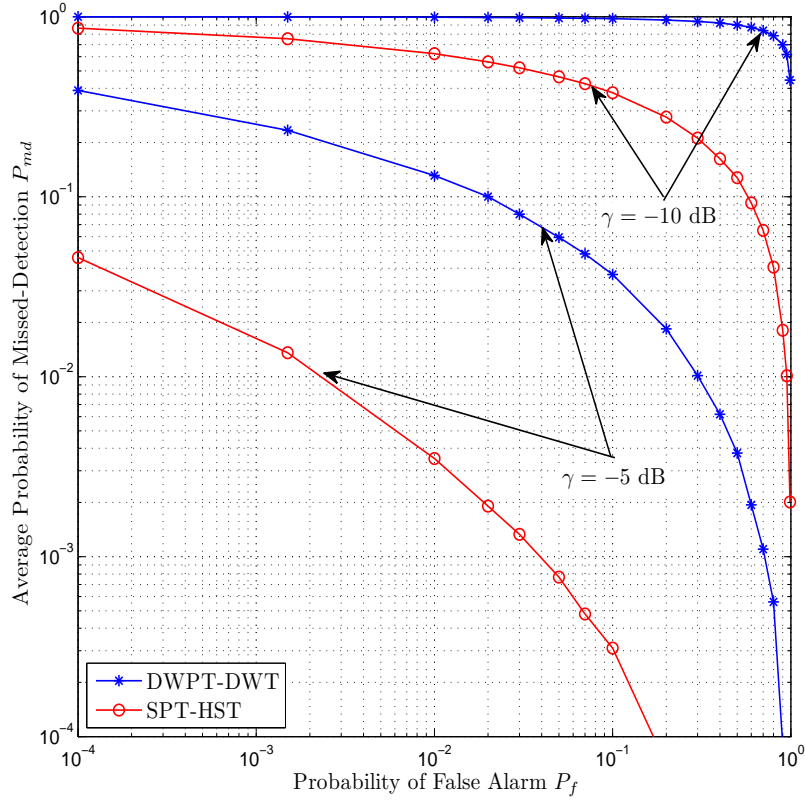
Figure 7.11: Comparison between the CROC of iterated DWPT-DWT approach and SPT-HST approach for various $\gamma$ and $M = 512$.

Fig. 7.12 (top of the next page) illustrates a comparison between the CROC of iterated DWPT-DWT approach and SPT-HST approach for various $M$ and $\gamma = -8$ dB. Similar to Fig. 7.11, Fig. 7.12 explains the superiority of SPT-HST approach over iterated DWPT-DWT approach for SS using the energy detector. For instance, when $M = 256$ and $P_f = 0.1$ dB (fixed), the $P_{md}$ for SPT-HST approach is nearly less by 97% than the $P_{md}$ for iterated DWPT-DWT approach. As it can be seen from Fig 7.12, when $M$ increases, a substantial degradation in the $P_{md}$ is noticed. This is because both the $P_{md}$ and the $P_f$ decrease when $M$ increases. But, the $P_{md}$ decreases faster than the $P_f$, thus causing an improvement in the performance of the energy detector.
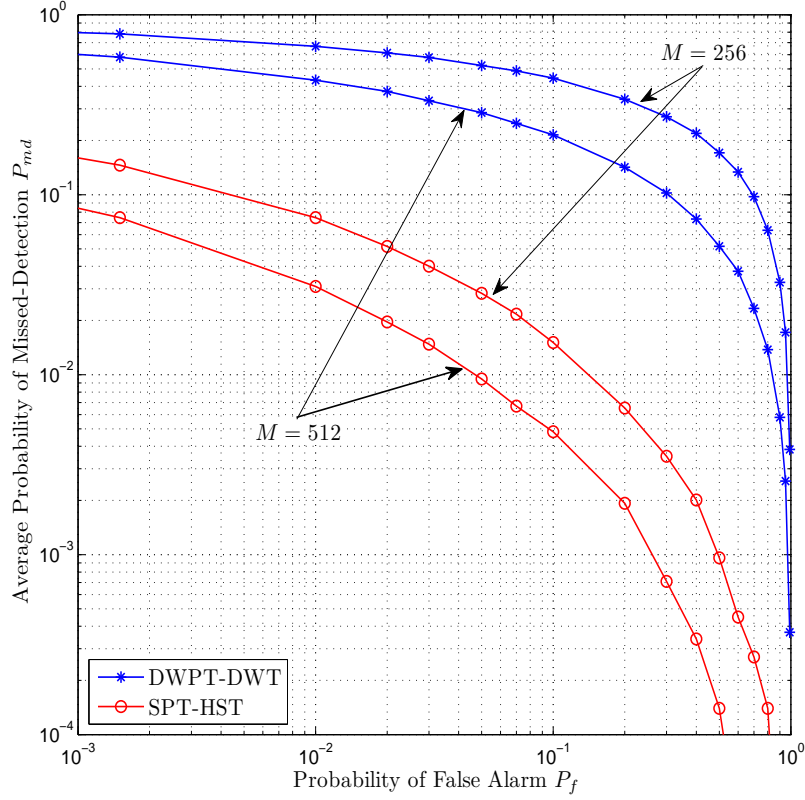
Figure 7.12: Comparison between the CROC of iterated DWPT-DWT approach and SPT-HST approach for various $M$ and $\gamma = -8$ dB.

Fig. 7.13 (top of the next page) highlights a comparison between the TCC, $\mathbb{T}$, of iterated DWPT-DWT approach and SPT-HST approach versus the number of the samples, $M$. The TCC for iterated DWPT-DWT approach, $\mathbb{T}_{DWPT-DWT}$, is computed by $\mathbb{T}_{DWPT-DWT} = \mathbb{M}_{DWPT-DWT} + \mathbb{A}_{DWPT-DWT}$. On the other side, the TCC for SPT-HST approach, $\mathbb{T}_{SPT-HST}$, is evaluated by $\mathbb{T}_{SPT-HST} = \mathbb{M}_{SPT-HST} + \mathbb{A}_{SPT-HST}$. Hence, when $i = 2$, the total complexity order for DWPT-DWT and SPT-HST approaches are $\mathcal{O}(128M - 60)$, and $\mathcal{O}(104M - 48)$, respectively. Accordingly, the difference between both the total complexity orders is $\mathcal{O}(24M - 12)$. As expected, the iterated DWPT-DWT approach has higher TCC (i.e., complexity order) than SPT-HST approach. For example, at $M = 512$, the $\mathbb{T}_{DWPT-DWT}$ and the $\mathbb{T}_{SPT-HST}$ are 65476 operations and 53200 operations, respectively. In other words, the $\mathbb{T}_{SPT-HST}$
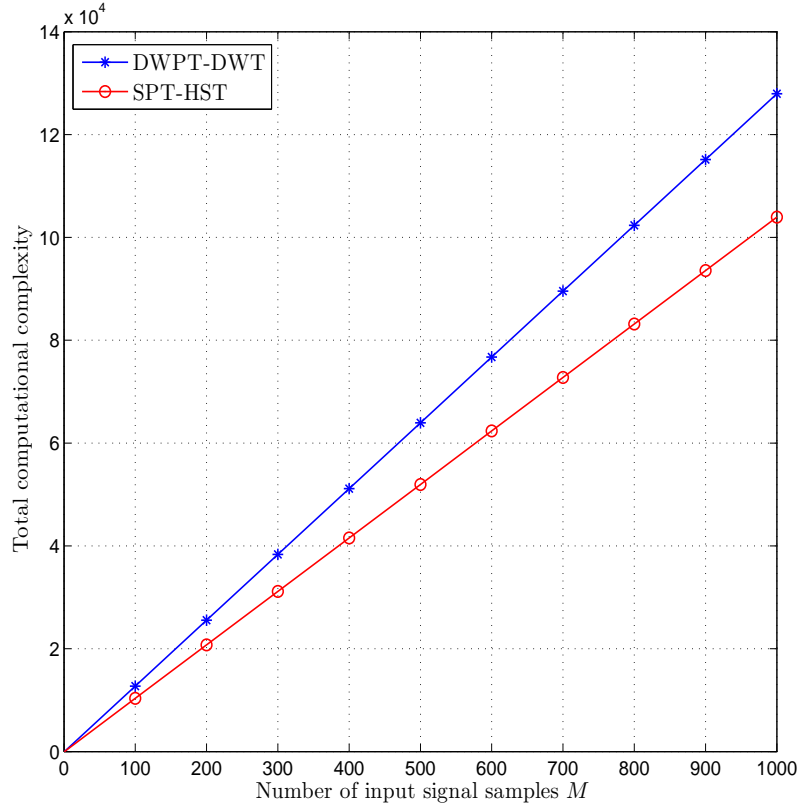
Figure 7.13: Comparison between the total computational complexity, $\mathbb{T}$, of iterated DWPT-DWT approach and SPT-HST approach versus number of samples, $M$.

is approximately 19% lower than $\mathbb{T}_{DWPT-DWT}$. This decrease in the number of operations leads to reduce the sensing time for cascaded SS framework. Consequently, the sensing time, $T$, which is obtained from $T \approx M/f_s + \tau$ where $\tau$ is the consumed time by $\mathbb{T}$ of SPT-HST approach is less than the sensing time of iterated DWPT-DWT approach.

## 7.8    Conclusions

A combined approach using both SPT and HST was employed in this chapter to enhance the performance of energy detector. Signal denoising was applied by using HST to alleviate the impact of noise. Thereafter, the SPT was proposed and utilised

to estimate the noise power. The main advantage of the SPT-HST approach against the iterated DWPT-DWT approach, which was greatly employed in the literature, is improving the detectability of energy detector at minimum total computational complexity. The validation for possibility of using the SPT-HST for SS in IEEE 802.22 WRAN standard was verified. Different simulation results were shown to compare between iterated DWPT-DWT and SPT-HST approaches for different values of $P_f$, $\gamma$ and $M$. In all results, the SPT-HST approach has exceeded the iterated DWPT-DWT in detecting the case of the PU by the SU receiver with low computational complexity. This reduction in the TCC leads to reducing the total system complexity, sensing time and consumed handset power by the SU.

# Chapter 8

# Conclusion and Future Work

This chapter is divided into two sections. In the first section, the conclusions of the whole thesis are highlighted while in the second section, some non-treated problems that are related to this thesis are suggested as future works.

## 8.1   Conclusion

The main conclusions of this thesis are summarised as follows:

- Chapter 3 studies the behaviour of an energy detector over $\eta - \mu$ fading channel without and with $i.n.d$ diversity receptions using PDF approach. This study reveals that a degradation in the detectability of energy detector happens when $\eta$ and/or $\mu$ decrease. Furthermore, the diversity combining schemes such as MRC, SLC and SLS can help to reduce the impacts of the multipath fading parameters.

- Chapter 4 analyses the performance of an energy detector over $\kappa - \mu$ shadowed fading channel without and with $i.n.d$ diversity receptions. This analysis finds out that the increasing in the multipath and/or shadowing severity indices leads to improved detection performance. Similar to Chapter 3, different diversity receptions can assist to alleviate the dropping of the performance of energy detector at low values for multipath and/or shadowing severity indices.

141

- Chapter 5 provides the statistical characterisations for the sum and the maximum $i.n.d$ composite $\alpha - \mu$/gamma variates using MG distribution. The MG distribution close approximation of the $\alpha - \mu$/gamma distribution, helps to overcome the intractability of mathematical expressions of exact composite fading model. Therefore, the performance of an energy detector as well as the communications systems are evaluated with MRC and SC under $i.n.d$ receivers.

- Although Chapter 5 derives the PDF, the CDF and the MGF for the sum and the maximum $i.n.d$ composite $\alpha - \mu$/gamma variates using MG distribution, these expressions are limited by some conditions, e.g., the shadowing index for $\alpha - \mu$/gamma should be an integer number. Thus, Chapter 6 provides other statistical properties for the sum and the maximum of $i.n.d$ MG RVs. The derived expressions are employed to analyse performance of an energy detector and the communication systems over composite $\eta - \mu$/gamma fading channels.

The $\kappa - \mu$ shadowed, $\alpha - \mu$/gamma, and $\eta - \mu$/gamma fading channel models do not have clear relationships among each other. However, a comparison between the performance of energy detector over $\kappa - \mu$ shadowed, $\alpha - \mu$/gamma, and $\eta - \mu$/gamma fading channels can be achieved by using Nakagami-$m$/gamma, Nakagami-$m$ and Rayleigh fading channels which are common fading channels between these channels. As mentioned in Chapter 4, Chapter 5, and Chapter 6, Nakagami-$m$/gamma is obtained from $\kappa - \mu$ shadowed, $\alpha - \mu$/gamma, and $\eta - \mu$/gamma by using $\kappa \to 0$, $\alpha = 2$, and $\eta \to \infty$, respectively. Moreover, when $m \to \infty$ (shadowing index in $\kappa - \mu$ shadowed) and $k \to \infty$ (shadowing index in both $\alpha - \mu$/gamma, and $\eta - \mu$/gamma), Nakagami-$m$/gamma is converted to Nakagami-$m$. Furthermore, Nakagami-$m$ fading channel becomes Rayleigh fading channel when $m = 1$ as explained in Table 2.1, Table 2.2, and Table 2.3.

Fig. 8.1 shows a comparison between the performance of energy detector over $\kappa - \mu$ shadowed, $\alpha - \mu$/gamma, and $\eta - \mu$/gamma fading channels with $u = 1.5$, $\bar{\gamma} = 15$, $m = 0.5$ (for Nakagami-$m$/gamma and Nakagami-$m$),$\alpha = 2.5$, $\eta = 0.9$, and $\kappa = 1.5$. In this figure, it can be observed that when $\kappa - \mu$ shadowed, $\alpha - \mu$/gamma, and $\eta - \mu$/gamma fading channels are used to model
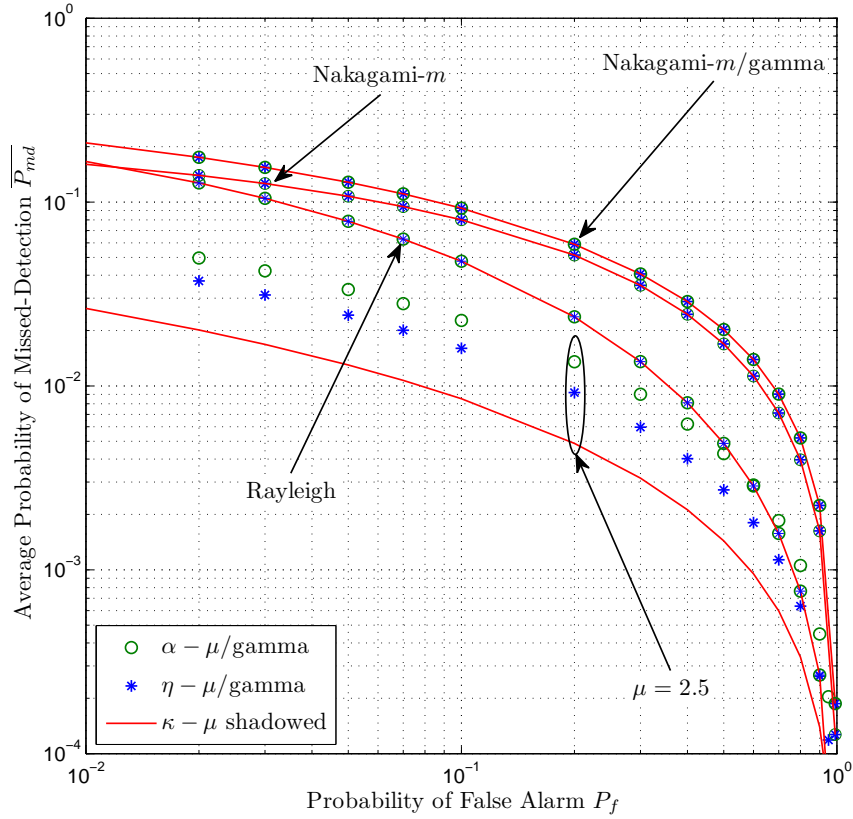
Figure 8.1: Comparison between the complementary ROC of the energy detector over composite $\kappa - \mu$ shadowed, $\alpha - \mu$/gamma, and $\eta - \mu$/gamma fading channels with $u$ = 1.5, $\bar{\gamma}$ = 15 dB, $m$ = 0.5 (for Nakagami-$m$/gamma and Nakagami-$m$), $\alpha$ = 2.5, $\eta$ = 0.9, and $\kappa$ = 1.5.

the composite Nakagami-$m$/gamma fading channel, the performances of the energy detector are similar. Similarly, when these generalised fading channels are employed to model Nakagami-$m$ and Rayleigh fading channels. Moreover, one can see that the performance of the energy detector over Rayleigh fading is better than the Nakagami-$m$. This is because $m = 1$ in Rayleigh fading while $m = 0.5$ in Nakagami-$m$ fading channel.

- Chapter 7 proposes a constructed approach from SPT and HST to predict the noise power and to reduce the noise effects, respectively for IEEE 802.22

WRAN standard. From the provided comparisons with iterated DWPT-DWT approach, the results demonstrate that the energy detector with SPT-HST approach outperforms the DWPT-DWT approach in enhancing the performance with low total computational complexity.

## 8.2 Future Work

Even though this thesis has addressed different problems that are related to energy detector based spectrum sensing for cognitive radio, there are still some issues that need to be studied in future work.

- Use real data sets for $u$ (i.e., $T$ and $W$) and other parameters to compare the performance of an energy detector over composite $\kappa - \mu$/gamma, $\eta - \mu$/gamma, and $\alpha - \mu$/gamma fading channels.

- The behaviour of an energy detector over generalised multipath/shadowing fading channels was extensively analysed in this thesis. Further analysis for the performance of an energy detector over composite generalised multipath/shadowing fading with co-channel interference can be considered.

- The average AUC curve has been widely used in this thesis and in the open technical literature as single figure of merit for studying the performance of an energy detector. Nevertheless, this performance metric has not been yet derived for other SS techniques such as cyclostationary detection as well as for CSS scenarios.

- The statistics of the MG random variables can be derived and employed to evaluate different performance metrics with EGC scheme. Moreover, these expressions can be utilised to evaluate the performance of energy detector over composite $\alpha - \kappa - \mu$/gamma fading channel.

- In this thesis, the SPT was derived for two-level of signal decomposition and has provided good results in energy detection. Therefore, higher level of signal de-

composition by SPT is necessary to achieve better performance. Moreover, the SPT can be employed in other applications such as image denoising technique.

# Bibliography

[1] United States Government Accountability Office, "Spectrum management: NTIA planning and processes need strengthening to promote the efficient use of spectrum by federal agencies," GAO-11-352, Apr. 2011.

[2] X. Tao, X. Xu, and Q. Cui,"An overview of cooperative communications," *IEEE Commun. Mag.*, vol. 50, no. 6, pp. 65-71, June 2012.

[3] C.-X. Wang, X. Hong, X. Ge, X. Cheng, G. Zhang, and J. S. Thompson, "Cooperative MIMO channel models: A survey," *IEEE Commun. Mag.*, vol. 48, no. 2, pp. 80-87, Feb. 2010.

[4] D. Gesbert, S. Hanly, H. Huang, S. S. Shitz, O. Simeone, and W. Yu, "Multi-cell MIMO cooperative networks: A new look at interference," *IEEE J. Sel. Areas Commun.*, vol. 28, pp. 1380-1408, Dec. 2010.

[5] E. Larsson, F. Tufvesson, O. Edfors, and T. Marzetta, "Massive MIMO for next generation wireless systems," *IEEE Commun. Mag.*, vol. 52, no. 2, pp. 186-195, Feb. 2014.

[6] T. L. Marzetta, "Noncooperative cellular wireless with unlimited numbers of base station antennas," *IEEE Trans. Wireless Commun.* , vol.9, no. 11, pp. 3590-3600, Nov. 2010.

[7] L. Lu, G. Y. Li, A. L. Swindlehurst, A. Ashikhmin, and R. Zhang, "An Overview of Massive MIMO: Benefits and Challenges," *IEEE J. Sel. Topics Signal Process.*, vol. 8, no. 5, pp. 742-758, Oct. 2014.

[8] Federal Communications Commission, "Spectrum Policy Task Force," Rep. ET Docket no. 02-135, Nov. 2002.

[9] J. Mitola, and G. Q. Maguire, "Cognitive radio: making software radios more personal," *IEEE Pers. Commun.*, vol. 6, pp. 13-18, Aug. 1999.

[10] S. Haykin, "Cognitive radio: brain-empowered wireless communications," *IEEE J. Select. Areas Commun.*, vol. 23, pp. 201-220, Feb. 2005.

[11] Measuring the TV "White Space" Available for Unlicensed Wireless Broadband, New America Foundation, Nov. 2005.

[12] R. E. D. Borth, and B. Oberlie, "Considerations for successful cognitive radio systems in US TV white space," *Proc. IEEE Symp. New Frontiers in Dynamic Spectrum Access Networks (DySPAN08)*, pp. 1-5, Oct. 2008.

[13] T. Yücek, and H Arslan, "A survey of spectrum sensing algorithms for cognitive radio applications," *IEEE Commun. Surveys Tuts.*, vol. 11, no. 1, pp. 116-130, first quarter 2009.

[14] J. Wang, M. Ghosh, and K. Challapali, "Emerging cognitive radio applications: A survey," *IEEE Commun. Mag.*, vol. 49, no. 3, pp. 74-81, Mar. 2011.

[15] T. Doumi, "Spectrum considerations for public safety in the United States," *IEEE Commun. Mag.*, vol. 44, no. 1, pp. 30-37, Jan. 2006.

[16] C.-S. Sum, H. Harada, F. Kojima, Z. Lan, and R. Funada, "Smart utility networks in TV white space," *IEEE Commun. Mag.*, vol. 49, no. 7, pp. 132-139, Jul. 2011.

[17] K. Shin, H. Kim, A. Min and A. Kumar, "Cognitive radios for dynamic spectrum access: From concept to reality," *IEEE Wireless Commun.*, vol. 17, no. 6, pp.64-74, Dec. 2010.

[18] F. Granelli, P. Pawelczak, R. V. Prasad, K. P. Subbalakshmi, R. Chandramouli, J. A. Hoffmeyer, and H. S. Berger, "Standardization and research in cognitive and

dynamic spectrum access networks: IEEE SCC41 efforts and other activities," *IEEE Commun. Mag.*, vol. 48, no. 1, pp.71-79, 2010.

[19] A. Flores, R. Guerra, E. Knightly, P. Ecclesine, and S. Pandey, "IEEE 802.11 af: A standard for TV white space spectrum sharing," *IEEE Commun. Mag.*, vol. 51, no. 10, pp. 92-100, 2013.

[20] Y.-C. Liang, K. Chen, Y. Li, and P. Mähönen, "Cognitive radio networking and communications: An overview," *IEEE Trans. Veh. Technol.*, vol. 60, no. 7, pp. 3386-3407, Sep. 2011.

[21] R. Tandra, and A. Sahai, "Fundamental limits on detection in low SNR under noise uncertainty," in *Proc. IEEE Int. Conf. Wireless Networks, Commun. and Mobile Computing*, vol. 1, June 2005, pp. 464-469.

[22] D. Cabric, and R. W. Brodersen, "Physical layer design issues unique to cognitive radio systems," in *Proc. IEEE Int. Symp. Personal, Indoor, Mobile Radio Commun. (PIMRC)*, vol. 2, Sept. 2005, pp. 759-763.

[23] J. Lundén, V. Koivunen, A. Huttunen, and H. V. Poor, "Spectrum sensing in cognitive radios based on multiple cyclic frequencies," in *Proc. IEEE Int. Conf. Cognitive Radio Oriented Wireless Netw. Commun. (CrownCom)*, July/Aug. 2007, pp. 37-43.

[24] H. Urkowitz, "Energy detection of unknown deterministic signals," *Proc. IEEE*, vol. 55, pp. 523-531, Apr. 1967.

[25] H. Tang, "Some physical layer issues of wide-band cognitive radio systems," in *Proc. IEEE Int. Symposium on New Frontiers in Dynamic Spectrum Access Networks (DySPAŃ05)*, Nov. 2005, pp. 151-159.

[26] R. Tandra, and A. Sahai, "SNR walls for signal detection," *IEEE J. Sel. Topics Signal Process.*, vol. 2, no. 1, pp. 4-17, Feb. 2008.

[27] Y.-C. Liang, E. P. Y. Zeng, and A. T. Hoang, "Sensing-throughput tradeoff for cognitive radio networks," *IEEE Trans. Wireless Commun.*, vol. 7, no. 4, pp. 1326-1337, Apr. 2008.

[28] V. I. Kostylev, "Energy detection of a signal with random amplitude," in *Proc. IEEE Int. Conf. Commun. (ICC)*, Apr. 2002, pp. 1606-1610.

[29] F. F. Digham, M. S. Alouini, and M. K. Simon, "On the energy detection of unknown signals over fading channels," in *Proc. IEEE Int. Conf. Commun. (ICC)*, May 2003, pp. 3575-3579.

[30] ——, "On the energy detection of unknown signals over fading channels," *IEEE Trans. Commun.*, vol. 55, no. 1, pp. 21-24, Jan. 2007.

[31] C. Stevenson, G. Chouinard, Z. Lei, W. Hu, S. Shellhammer, and W. Caldwell, "IEEE 802.22: The first cognitive radio wireless regional area network standard," *IEEE Commun. Mag.*, vol. 47, no. 1, pp. 130-138, Jan. 2009.

[32] Unlicensed operations in the TV broadcast bands, second memorandum opinion and order, FCC 10-174, Sept. 2010.

[33] T.-H. Yu, O. Sekkat, S. Rodriguez-Parera, D. Marković, and D. Cabrić, "A wideband spectrum-sensing processor with adaptive detection threshold and sensing time," *IEEE Trans. Circuits Syst. I, Reg. Papers*, vol. 58, no. 11, pp. 2765-2775, 2011.

[34] F. Paisana, N. Marchetti, and L. A. Dasilva, "Radar, TV and Cellular Bands: Which Spectrum Access Techniques for which Bands?," *IEEE Commun. Surveys Tuts.*, vol. 16, no. 3, pp. 1193-1220, Third Quarter 2014.

[35] V. M. Kapinas, S. K. Mihos, and G. K. Karagiannidis, "On the monotonicity of the generalized Marcum and Nuttall Q-functions," *IEEE Trans. Inf. Theory*, vo. 55, no. 8, pp. 3701-3710, Aug. 2009.

[36] J. Salt, and H. Nguyen, "Performance prediction for energy detection of unknown signals," *IEEE Trans. Veh. Technol.*, vol. 57, no. 6, pp. 3900-3904, Nov. 2008.

[37] Y. Chen, "Improved energy detector for random signals in Gaussian noise," *IEEE Trans. Wireless Commun.*, vol. 9, no. 2, pp. 558-563, Feb. 2010.

[38] D. J. Torrieri, *Principles of Secure Communication Systems*, Boston: Artech House, 1992.

[39] S. Ciftci, and M. Torlak, "A comparison of energy detectability models for spectrum sensing," in *Proc. IEEE Global Telecommun. Conf. (GLOBECOM)*, Nov. 2008, pp. 1-5.

[40] J. Edell, "Wideband, non-coherent, frequency-hopped waveforms and their hybrids in low-probability of intercept communications," *Report Naval Research Laboratory (NRL) 8025*, Nov. 1976.

[41] S. Atapattu, C. Tellambura, and H. Jiang, "Analysis of area under the ROC curve energy detection," *IEEE Trans. Wireless Commun.*, vol. 9, no. 3, pp. 1216-1225, Mar. 2010.

[42] ——, "Performance of energy detection: A complementary AUC approach," in *Proc. IEEE Global Commun. Conf. (GLOBECOM)*, Dec. 2010.

[43] I. S. Gradshteyn, and I. M. Ryzhik, *Table of Integrals, Series and Products*, 7th ed. Academic Press Inc., 2007.

[44] H. M. Srivastava, and P. W. Karlsson, *Multiple Gaussian Hypergeometric Series*, John Wiley & Sons, 1985.

[45] M. Nakagami, "The $m$-distribution-a general formula of intensity distribution of rapid fading," in *Statistical Methods in Radio Wave Propagation*, W. C. Hoffman, Ed. Elmsford, NY: Pergamon, 1960.

[46] H. Suzuki, "A statistical model for urban radio propagation," *IEEE Trans. Commun.*, vol. 25, no. 7, pp.673-679, July 1977.

[47] M. K. Simon, and M.-S. Alouini, *Digital Communication over Fading Channels*, 2nd ed. New York: Wiley, 2005.

[48] G. L. Stüber, *Principles of Mobile Communication*, 3rd ed. Springer, 2012.

[49] M. D. Yacoub, "The $\eta - \mu$ distribution: A general fading distribution," in *Proc. IEEE Veh. Technol. Conf. (VTC Fall)*, Sep. 2000.

[50] ——, "The $\kappa - \mu$ distribution: A general fading distribution," in *Proc. IEEE Veh. Technol. Conf. (VTC Fall)*, Oct. 2001.

[51] ——, "The $\kappa - \mu$ distribution and the $\eta - \mu$ distribution," *IEEE Antennas Propag. Mag.*, vol. 49, no. 1, pp. 68-81, Feb. 2007.

[52] ——, "The $\alpha - \mu$ distribution: A general fading distribution," in *Proc. IEEE Pers. Ind. and Mob. Rad. Commun. (PIMRC)*, Sep. 2002, vol. 2, pp. 629-633.

[53] ——, "The $\alpha - \mu$ distribution: a physical fading model for the Stacy distribution," *IEEE Trans. Veh. Technol.*, vol. 56, no. 1, pp. 27-34, Jan. 2007.

[54] G. S. Rabelo, U. S. Dias, and M. D. Yacoub, "The $\kappa - \mu$ extreme distribution: Characterizing severe fading conditions," in *Proc. SBMO/IEEE MTT-S IMOC*, Nov. 2009, pp.244-248.

[55] ——, "The $\kappa - \mu$ extreme distribution," *IEEE Trans. Commun.*, vol. 59, no. 10, pp. 2776-2785, Oct. 2011.

[56] N. Ermolova, "Moment generating functions of the generalized $\eta - \mu$ and $\kappa - \mu$ distributions and their applications to performance evaluations of communication systems," *IEEE Commun. Lett.*, vol. 12, no. 7, pp. 502-504, July 2008.

[57] D. Morales-Jiménez, and J. F. Paris, "Outage probability analysis for $\eta - \mu$ fading channels," *IEEE Commun. Lett.*, vol. 14, no. 6, pp. 521-523, June 2010.

[58] A. M. Magableh, and M. M. Matalgah, "Moment generating function of the generalized $\alpha - \mu$ distribution with applications," *IEEE Commun. Lett.*, vol. 13, no. 6, pp. 411-413, June 2009.

[59] S. Atapattu, C. Tellambura, and Hai Jiang, "Representation of composite fading and shadowing distributions by using mixtures of gamma distributions," in *Proc. IEEE Wireless Commun. Net. Conf. (WCNC)*, Apr. 2010, pp. 1-5.

[60] ——, "A mixture gamma distribution to model the SNR of wireless channels," *IEEE Trans. Wireless Commun.*, vol. 10, no. 12, pp. 4193-4203, Dec. 2011.

[61] S. P. Herath, N. Rajatheva, and C. Tellambura, "Energy detection of unknown signals in fading and diversity reception," *IEEE Trans. Commun.*, vol. 59, no. 9, pp. 2443-2453, Sep. 2011.

[62] K. B. Letaief, and W. Zhang, "Cooperative communications for cognitive radio networks," *Proc. IEEE*, vol. 97, no. 5, pp. 878-893, May 2009.

[63] A. Ghasemi, and E. S. Sousa, "Collaborative spectrum sensing for opportunistic access in fading environments," *Proc. IEEE Symp. New Frontiers in Dynamic Spectrum Access Networks (DySPAN05)*, pp. 131-136, Nov. 2005.

[64] G. Ganesan, and Y. G. Li, "Cooperative spectrum sensing in cognitive radio-part I: two user networks," *IEEE Trans. Wireless Commun.*, vol. 6, pp. 2204-2213, 2007.

[65] G. Ganesan, and L. Ye, "Cooperative spectrum sensing in cognitive radio, Part II: Multiuser networks," *IEEE Trans. Wireless Commun.*, vol. 6, no. 6, pp. 2214-2222, 2007.

[66] S. Chaudhari, J. Lunden, V. Koivunen, and H. V. Poor, "Cooperative sensing with imperfect reporting channels: Hard decisions or soft decisions?," *IEEE Trans. Signal Process.*, vol. 60, no. 1, pp. 18-28, 2012.

[67] W. Zhang, R. K. Mallik, and K. B. Letaief, "Optimization of cooperative spectrum sensing with energy detection in cognitive radio networks," *IEEE Trans. Wireless Commun.*, vol. 8, no. 12, pp. 5761-5766, Dec. 2009.

[68] S. Atapattu, C. Tellambura, and H. Jiang, "Energy detection based cooperative spectrum sensing in cognitive radio networks," *IEEE Trans. Wireless Commun.*, vol. 10, no. 4, pp.1232-1241, Apr. 2011.

[69] W. Zhang, and K. B. Letaief, "Cooperative spectrum sensing with transmit and relay diversity in cognitive radio networks," *IEEE Trans. Wireless Commun.*, vol. 7, no. 12, pp. 4761-4766, 2008.

[70] S. Shankar, C. Cordeiro, and K. Challapali, "Spectrum agile radios: utilization and sensing architectures," in *Proc. IEEE Int',l Symp. Dynamic Spectrum Access Networks (DySPAŃ05)*, pp. 160-169, Nov. 2005.

[71] K. G. Smitha, and A. P. Vinod, "A multi-resolution fast filter bank for spectrum sensing in military radio receivers," *IEEE Trans. Very Large Scale Integ. (VLSI) Sys.*, vol. 20, no. 7, pp. 1323-1327, June 2011.

[72] ——, "A multi-resolution digital filter bank for spectrum sensing in military radio receivers," in *Proc. IEEE Int. Conf. Signal Process. Commun. (SPCOM)*, July 2010, pp. 1-5.

[73] S. Dikmese, M. Renfors, and H. Dincer, "FFT and filter bank based spectrum sensing for WLAN signals," in *Proc. 20th European Conf. Circuit Theory, Design (ECCTD)*, Aug. 2011, pp. 781-784.

[74] S. Dikmese, S. Srinivasan, and M. Renfors, "FFT and filter bank based spectrum sensing and spectrum utilization for cognitive radios," in *Proc. IEEE Int. Symp. Commun. Control, Signal Process. (ISCCSP)*, May 2012, pp. 1-5.

[75] S. Dikmese, A. Gokceoglu, and M. Renfors, "Optimized FFT and filter bank based spectrum sensing for Bluethooth signals," in *Proc. IEEE Wireless Commun. Net. Conf. (WCNC)*, Apr. 2012, pp. 792-797.

[76] T. Schlechter, and M. Huemer, "Generic low complex filter bank based spectrum sensing approach for LTE cognitive radio," in *Proc. Asilomar Conf. on Signals, Systems and Computers (ACSSC)*, Nov. 2012, pp. 168-172.

[77] M. Narendar, A. P. Vinod, A. S. Madhukumar, and A. K. Krishna, "An algorithm for spectrum sensing in cognitive radio using tree-structured filter bank," in *Proc. IEEE Int. Conf. Telecommun. (ICT)*, Apr. 2010, pp. 418-424.

[78] ——, "A tree-structured DFT filter bank based spectrum detector for estimation of radio channel edge frequencies in cognitive radios," *Elsevier Physical Commun.*, vol. 9, pp. 45-60, 2013.

[79] S. G. Mallat, *A wavelet tour of signal processing*, 2nd ed. Academic Press, Sep. 1999.

[80] H. Wang, Y. Xu, X. Su, and J. Wang, "Cooperative spectrum sensing with wavelet denoising in cognitive radio," in *Proc. IEEE Veh. Technol. Conf. (VTC Spring)*, May 2010, pp. 1-5.

[81] ——, "Cooperative spectrum sensing in cognitive radio under noise uncertinaty," in *Proc. IEEE Veh. Technol. Conf. (VTC Spring)*, May 2010, pp. 1-5.

[82] V. Guptaa, and A. Kumar, "Wavelet based dynamic spectrum sensing for cognitive radio under noisy environment," in *Proc. Elsevier Int. Conf. Modelling Optimization, Computing (ICMOC)*, 2012, pp. 3228-3234.

[83] E. P. L. de Almeida, P. H. P. de Carvalho, P. A. B. Cordeiro, and R. D. Vieira, "Experimental study of a wavelet-based spectrum sensing technique," in *Proc. Asilomar Conf. on Signals, Systems and Computers (ACSSC)*, Oct. 2008, pp. 1552-1556.

[84] D. D. Ariananda, M. K. Lakshmanan, and H. Nikookar, "A study on application of wavelets and filter banks for cognitive radio spectrum estimation," in *Proc. European Wireless Technol. Conf. (EWTC)*, 2009, pp. 218-221.

[85] C. Bektas, A. Akan, and N. Odabasioglu, "Energy based spectrum sensing using wavelet transform for fading channels," in *Int. Congress on Ultra Modern Telecommun. (ICUMT)*, Oct. 2012, pp. 207-211.

[86] D. D. Ariananda, M. K. Lakshmanan, and H. Nikookar, "A study on the application of wavelet packet transforms to cognitive radio spectrum estimation," in *Proc. Int. Conf. Cognitive Radio Oriented Wireless Netw., Commun. (CROWNCOM)*, 22-24 June 2009, pp. 1-6.

[87] M. K. Lakshmanan, D. D. Ariananda, and H. Nikookar, "Cognitive radio transmission and spectrum sensing using a wavelet packet transceiver," in *Proc. IEEE Int. Symp. Personal, Indoor, Mobile Radio Commun. (PIMRC)*, 2009, pp. 142-146.

[88] S. B. Zhang, and J. J. Qin, "Energy detection algorithm based on wavelet packet transform under uncertain noise for spectrum sensing," in *Proc. IEEE Int. Conf. Wireless Networks, Commun. and Mobile Computing (WiCOM)*, Sept. 2010, pp. 1-4.

[89] C. Cordeiro, K. Challapali, D. Birru, and S. S. N., "IEEE 802.22: An introduction to the first wireless standard based on cognitive radios," *J. of Commun. (JCM)*, vol. 1, no. 1, pp. 38-47, Apr. 2006.

[90] S. J. Shellhammer, "Spectrum sensing in IEEE 802.22," in *Proc. 1st IAPR Workshop on Cognitive Information Process.*, June 2008.

[91] H. Sun, A. Nallanathan, J. Jiang, and C.-X. Wang, "Cooperative spectrum sensing with diversity reception in cognitive radios," in *Proc. IEEE Int. Conf. Commun. and Net. (ICST)*, 17-19 Aug. 2011, pp. 216-220.

[92] A. Shahini, A. Bagheri, and A. Shahzadi, "A unified approach to performance analysis of energy detection with diversity receivers over Nakagami-$m$ fading channels," in *Proc. IEEE Int. Conf. Connected Veh. and Expo (ICCVE)*, 2-6 Dec. 2013, pp. 707-712.

[93] S. Atapattu, C. Tellambura, and H. Jiang, "MGF based analysis of area under the ROC curve in energy Detection," *IEEE Commun. Lett.*, vol. 15, no. 12, pp. 1301-1303, Dec. 2011.

[94] ——, "Energy detection of primary signals over $\eta - \mu$ fading channels," in *Proc. IEEE Int. Conf. Industrial Inf. Syst. (ICIIS)*, Dec. 2009, pp. 118-122.

[95] P. Sofotasios, E. Rebeiz, L. Zhang, T. Tsiftsis, D. Cabric, and S. Freear, "Energy detection based spectrum sensing over $\kappa - \mu$ and $\kappa - \mu$ extreme fading channels," *IEEE Trans. Veh. Technol.*, vol. 62, no. 3, pp. 1031-1040, Mar. 2013.

[96] H. Y. Darawsheh, and A. Jamoos, "Performance analysis of energy detector over $\alpha - \mu$ fading channels with selection combining," *Wireless Pers. Commun.*, vol. 77, no. 2, pp. 1507-1517, Jan. 2014.

[97] Q. Shi, "A unified MGF based approach to the analysis of area under the ROC curve of energy detection over generalized fading channels," in *Proc. IEEE Int. Conf. Sig. Process. Commun. Computing (ICSPCC)*, 5-8 Aug. 2013, pp. 1-4.

[98] A. Annamalai, and A. Olaluwe, "On the energy detection of unknown signals in $\kappa - \mu$ and $\eta - \mu$ fading channels with diversity receivers," in *Proc. IEEE Int. Conf. Connected Veh. and Expo. (ICCVE)*, 2-6 Dec. 2013, pp. 127-132.

[99] E. Adebola, and A. Annamalai, "Unified analysis of diversity average energy detectors over generalized fading channels," in *Proc. IEEE Int. Conf. Connected Veh. and Expo (ICCVE)*, 2-6 Dec. 2013, pp. 121-126.

[100] A. Annamalai, and A. Olaluwe, "Energy detection of unknown deterministic signals in $\kappa - \mu$ and $\eta - \mu$ generalized fading channels with diversity receivers," in *Proc. IEEE Computing Net. Commun. (ICNC)*, 3-6 Feb. 2014, pp. 761-765.

[101] Y. Wang, M. Zhang, and Q. Shi, "Unified approach to performance analysis of energy detection in generalised fading channels," *Elect. Lett.*, vol. 50, no. 11, pp. 837-839, May 2014.

[102] E. Adebola, and A. Annamalai, "Unified analysis of energy detectors with diversity reception in generalized fading channels," *IET Commun.*, vol. 8, no. 17, pp. 3095-3104.

[103] K. P. Peppas, F. Lazarakis, T. Zervos, A. Alexandridis, and K. Dangakis, "Sum of non-identical independent squared $\eta - \mu$ variates and applications in the performance analysis of DS-CDMA systems," *IEEE Trans. Wireless Commun.*, vol. 9, no. 9, pp. 2718-2723, Sep. 2010.

[104] S. Atapattu, C. Tellambura, and H. Jiang, "Performance of an energy detector over channels with both multipath fading and shadowing," *IEEE Trans. Wireless Commun.*, vol. 9, no. 12, pp. 3662-3670, Dec. 2010.

[105] H. Rasheed, F. Haroon, and F. Adachi, "On the energy detection over generalized-K ($K_G$) fading," in *Proc. IEEE Int. Multi-topic Conf. (INMIC)*, 22-24 Dec. 2011, pp. 367-371.

[106] S. Alam, and A. Annamalai, "Energy detector's performance analysis over the wireless channels with composite multipath fading and shadowing effects using the AUC approach," in *Proc. IEEE Consumer Commun. Net. Conf. (CCNC)*, 14-17 Jan. 2012, pp. 771-775.

[107] A. Bagheri, A. Shahini, and A. Shahzadi, "Analytical and learning-based spectrum sensing over channels with both fading and shadowing," in *Proc. IEEE Int. Conf. Connected Veh. and Expo. (ICCVE)*, 2-6 Dec. 2013, pp. 699-706.

[108] Q. Shi, "On the performance of energy detection for spectrum sensing in cognitive radio over Nakagami-lognormal composite channels," in *Proc. IEEE China Sig. and Inf. Process. (ChinaSIP)*, 6-10 July 2013, pp. 566-569.

[109] K. P. Peppas, G. Efthymoglou, V. A Aalo, M. Alwakeel, and S. Alwakeel, "On the performance analysis of energy detection of unknown signals in Gamma shadowed Ricean fading environments," in *Proc. IEEE Pers. Ind. and Mob. Rad. Commun. (PIMRC)*, 8-11 Sept. 2013, pp. 756-760.

[110] ——, "Energy detection of unknown signals in Gamma-shadowed Rician fading environments with diversity reception," *IET Commun.*, vol. 9, no. 2, pp. 196-210, Jan. 2015.

[111] J. Paris, "Statistical Characterization of $\kappa - \mu$ Shadowed fading," *IEEE Trans. Veh. Technol.*, vol. 63, no. 2, pp. 518-526, Feb. 2014.

[112] G. S. Rabelo, U. S. Dias, and M. D. Yacoub, "The $\kappa - \mu$ extreme distribution: Characterizing severe fading conditions," in *Proc. SBMO/IEEE MTT-S IMOC*, Nov. 2009, pp.244-248.

[113] ——, "The $\kappa - \mu$ extreme distribution," *IEEE Trans. Commun.*, vol. 59, no. 10, pp. 2776-2785, Oct. 2011.

[114] D. B. da Costa, M. D. Yacoub, and J. C. S. S. Filho, "Highly accurate closed-form approximations to the sum of $\alpha - \mu$ variates and applications," *IEEE Trans. Wireless Commun.*, vol. 7, no. 9, pp. 3301-3306, Sept. 2008.

[115] R. A. A. de Souza, and M. D. Yacoub, "The multivariate $\alpha - \mu$ distribution," *IEEE Trans. Wireless Commun.*, vol. 9, no. 1, pp. 45-50, Jan. 2010.

[116] G. S. Rabelo, M. D. Yacoub, and R. A. A. de Souza, "On the multivariate $\alpha - \mu$ distribution: New exact analytical formulations," *IEEE Trans. Veh. Technol.*, vol. 60, no. 8, pp. 4063-4070, Oct. 2011.

[117] M. M. H. El Ayadi, and M. H. Ismail, "On the cumulative distribution function of the sum and harmonic mean of two-random variables with applications," *IET Commun.*, vol. 6, no. 18, pp. 3122-3130, Dec. 2012.

[118] R. Mohamed, M. H. Ismail, F. A. Newagy, and H. M. Mourad, "Capacity of the $\alpha - \mu$ fading channel with SC diversity under adaptive transmission techniques," in *Proc. IEEE Int. Conf. Telecommun. (ICT)*, April 2012, pp. 1-6.

[119] S. Krithiga, and V. Bhaskar, "Capacity and BER performance of independent and identically distributed $\alpha - \mu$ fading channel under absolute SNR scheduling," in *Proc. IEEE Int. Conf. Commun. Sig. Process. (ICCSP)*, April 2013, pp. 387-391.

[120] M. M. H. El Ayadi, and M. H. Ismail, "Novel closed-form exact expressions and asymptotic for the symbol error rate of single- and multiple-branch MRC and

EGC receivers over $\alpha - \mu$ fading," *IEEE Trans. Veh. Technol.*, vol. 63, no. 9, pp. 4277-4291, Nov. 2014.

[121] H. Y. Darawsheh, and A. Jamoos, "Selection diversity combining analysis of energy detector over $\alpha - \mu$ generalized fading channels," in *Proc. IEEE Int. Conf. Technol. Advances Electric. Electron. Comp. Engineering (TAEECE)*, May 2013, pp. 563-567.

[122] E. J. Leonardo, and M. D. Yacoub, "The product of two $\alpha - \mu$ variates and the composite $\alpha - \mu$ multipath-shadowing Model," *IEEE Trans. Veh. Technol.*, to be published, July 2014.

[123] J. Jung, S.-R. Lee, H. Park, S. Lee, and I. Lee, "Capacity and error probability analysis of diversity reception schemes over generalized-$K$ fading channels using a mixture gamma distribution," *IEEE Trans. Wireless Commun.*, vol. 13, no. 9, pp.4721-4730, Sept. 2014.

[124] M. Abramowitz, and I. A. Stegun, editors, *Handbook of Mathematical Functions: With Formulas, Graphs, and Mathematical Tables.* Dover Publications, 9th ed. 1972.

[125] S. Hussain, and X. N. Fernando, "Closed-form analysis of relay-based cognitive radio networks over Nakagami-$m$ fading channels," *IEEE Trans. Veh. Technol.*, vol. 63, no. 3, pp. 1193-1203, March 2014.

[126] ——, "Performance analysis of relay-based cooperative spectrum sensing in cognitive radio networks over non-identical Nakagami-$m$ channels," *IEEE Trans. Commun.*, vol. 62, no. 8, pp. 2733-2746, Aug. 2014.

[127] I. S. Gradshteyn, and I. M. Ryzhik, *Table of Integrals, Series and Products*, 6th ed. Academic Press Inc., 2000.

[128] R. Kwan, and C. Leung, "Selection diversity in non-identically distributed Nakagami fading channels," in *Proc. IEEE Sarnoff Symp.*, Apr. 2005, pp. 192-195.

[129] I. S. Ansari, S. Al-Ahmadi, F. Yilmaz, M.-S. Alouini, and H. Yanikomeroglu, "A new formula for the BER of binary modulations with dual-branch selection over generalized-$K$ composite fading channels," *IEEE Trans. Commun.*, vol. 59, no. 10, pp. 2654-2658, Oct. 2011.

[130] C. C. Tan, and N. C. Beaulieu, "Infinite series representation of the bivariate Rayleigh and Nakagami-$m$ distributions," *IEEE Trans. Commun.*, vol. 45, no. 10, pp. 1159-1161, Oct. 1997.

[131] K. A. Hamdi, "Capacity of MRC on correlated Rician fading channels," *IEEE Trans. Commun.*, vol. 56, no. 5, pp. 708-711, May 2008.

[132] P. S. Bithas, P. T. Mathiopoulos, and S. A. Kotsopoulos, "Diversity reception over generalized-$K$ ($K_G$) fading channels," *IEEE Trans. Wireless Commun.*, vol. 6, no. 12, pp. 4238-4243, Dec. 2007.

[133] K. P. Peppas, "Performance evaluation of triple-branch GSC diversity receivers over generalized-$K$ fading channels," *IEEE Commun. Lett.*, vol. 13, no. 11, pp. 829-831, Nov. 2009.

[134] P. Theofilakos, A. G. Kanatas, and G. P. Efthymoglou, "Performance of generalized selection combining receivers in $K$ fading channels," *IEEE Commun. Lett.*, vol. 12, no. 11, pp. 816-818, Nov. 2008.

[135] T. S. B. Reddy, R. Subadar, and P. R. Sahu, "Outage probability of SC receiver over exponentially correlated $K$ fading channels," *IEEE Commun. Lett.*, vol. 14, no. 2, pp. 118-120, Feb. 2010.

[136] G. Alfano, and A. D. Maio, "Sum of squared shadowed-Rice random variables and its application to communication systems performance prediction," *IEEE Trans. Wireless Commun.*, vol. 6, no. 10, pp. 3540-3545, Oct. 2007.

[137] M. C. Clemente, and J. F. Paris, "Closed-form statistics for sum of squared Rician shadowed variates and its application," *Electronics Lett.*, vol. 50, no. 2, pp. 120-121, Jan. 2014.

[138] Z. Lingwen, Z. Jiayi, and L. Liu, "Average channel capacity of composite $\kappa - \mu$/gamma fading channels," *China Commun.*, vol. 10, no. 6, pp. 28-34, June 2013.

[139] C. G.-C., F. J. Cañete, and J. F. Paris, "Capacity of $\kappa - \mu$ Shadowed Fading Channels," *Int. J. of Antennas and Propag.*, vol. 2014, pp. 1-8, July 2014.

[140] K. Peppas, F. Lazarakis, A. Alexandridis, and K. Dangakis, "Error performance of digital modulation schemes with MRC diversity reception over $\eta - \mu$ fading channels," *IEEE Trans. Wireless Commun.*, vol. 8, no. 10, pp. 4974-4980, Oct. 2009.

[141] R. Subadar, and P. R. Sahu, "Performance of a L-MRC receiver over equally correlated $\eta - \mu$ fading channels," *IEEE Trans. Wireless Commun.*, vol. 10, no. 5, pp. 1351-1355, May 2011.

[142] D. Morales-Jimenez, J. F. Paris, and A. Lozano, "Outage probability analysis for MRC in $\eta - \mu$ fading channels with co-channel interference," *IEEE Commun. Lett.*, vol. 16, no. 5, pp. 674-677, May 2012.

[143] A. C. Moraes, D. B. da Costa, and M. D. Yacoub, "An outage analysis of multibranch diversity receivers with cochannel interference in $\alpha - \mu$, $\eta - \mu$, and $\kappa - \mu$ fading scenarios," *Wireless Pers. Commun.*, vol. 64, no. 1, pp. 3-19, Jan. 2012.

[144] J. Zhang, M. Matthaiou, Z. Tan, and H. Wang, "Performance analysis of digital communication systems over composite $\eta - \mu$/gamma fading channels," *IEEE Trans. Veh. Technol.*, vol. 61, no. 7, pp. 3114-3124, Sep. 2012.

[145] N. Y. Ermolova, and O. Tirkkonen, "Outage probability over composite $\eta - \mu$ fading-shadowing radio channels," *IET Commun.*, vol. 6, no. 13, pp. 1898-1902, Sep. 2012.

[146] D. Morales-Jimenez, F. J. Lopez-Martinez, E. Martos-Naya, J. F. Paris, and A. Lozano, "Connections between the generalized Marcum-$Q$ function and a class of

hypergeometric functions," *IEEE Trans. Inf. Theory*, vol. 60, no. 2, pp. 1077-1082, Feb. 2014.

[147] H. Kobeissi, O. Bazzi, and Y. Nasser, "Wavelet denoising in cooperative and non-cooperative spectrum sensing," in *Proc. IEEE Int. Conf. Telecommun. (ICT)*, May 2013, pp. 1-5.

[148] T. A. Devi, and S. Sagar, "Discrete wavelet packet transform based cooperative spectrum sensing for cognitive radios," in *Proc. IEEE Computational Systems Commun. (ICCSC)*, Dec. 2014, pp. 226-231.

[149] Y. Youn , H. Jeon, and H. Lee, "Discrete wavelet packet transform based energy detector for cognitive radios," in *Proc. IEEE Veh. Technol. Conf. (VTC Spring)*, Apr. 2007, pp. 2641-2645.

[150] S. Kim, Y. Yoon, H. Jeon, M. Kim, and H. Lee, "Selective discrete wavelet packet transform-based energy detector for cognitive radios," in *Proc. IEEE Conf. Military Commun. (MILCOM)*, Nov. 2008, pp. 1-6.

[151] I. W. Selesnick, "The slantlet transform," *IEEE Trans. Signal Process.*, vol. 47, no. 5, pp. 1304-1313, May 1999.

[152] P. K. Kundu, A. Chatterjee, and P. C. Panchariya, "Electronic tongue system for water sample authentication: A slantlet-transform-based approach," *IEEE Trans. Instrum. Meas.*, vol. 60, no. 6, pp. 1959-1966, June 2011.

[153] J. L. Semmlow, *Biosignal and biomedical image processing: MATLAB–based applications*, Marcel Dekker, 14 Jan. 2004.

[154] I. Daubechies, *Ten Lectures on Wavelets*. Philadelphia, PA: SIAM, 1992.

[155] X. Zhou, C. Zhou, and B. G. Stewart, "Comparisons of discrete wavelet transform, wavelet packet transform and stationary wavelet transform in denoising PD measurement data," in *Proc. IEEE Int. Symp. Electrical Insulation (ISEI)*, June 2006, pp. 237-240.

[156] I. Bayram, and I. W. Selesnick, "On the dual-tree complex wavelet packet and M-band transforms," *IEEE Trans. Sig. Process.*, vol. 56, no. 6, pp. 2298-2310, June 2008.

[157] X. P. Zhang, and M. D. Desai, "Adaptive denoising based on SURE risk," *IEEE Signal Process. Lett.*, vol. 5, pp. 265-267, Oct. 1998.

[158] W.-K. Yoon, and Michael J. D., "Power measurement using the wavelet transform," *IEEE Trans. Instrum. Meas.*, vol. 47, no. 5, October 1998.

[159] ——, "Reactive power measurement using the wavelet transform" *IEEE Trans. Instrum. Meas.*, vol. 49, no. 2, Apr. 2000.

[160] S. Atapattu, C. Tellambura, and H. Jiang, "Spectrum sensing via energy detector in low SNR," in *Proc. IEEE Int. Conf. Commun. (ICC)*, 2011, pp. 1-5.

[161] D. Cabric, A. Tkachenko, and R. W. Brodersen, "Experimental study of spectrum sensing based on energy detection and network cooperation," in *Proc. First Int. Workshop on Technology and Policy for Accessing Spectrum (TAPAS)*, Aug. 2006.

[162] A. Erdélyi, W. Magnus, F. Oberhettinger, and F. G. Tricomi, *Tables of Integral Transforms*, vol. I. McGraw-Hill Book Company, Inc., New York-Toronto-London, 1954.

[163] A. P. Prudnikov, Y. A. Brychkov, and O. I. Marichev, *Integrals and Series*, vol. 4. Gordon and Breach Science Publishers, 1992.

# Appendix A

# Proofs for Chapter 3

## A.1    Derivation of $\overline{P_d}(\lambda)$ in (3.2)

After using (2.9) and [43, eq. (8.445)] to express $P_d(\gamma, \lambda)$ of (2.8) and $I_{\mu-\frac{1}{2}}\left(\frac{2\mu H}{\bar{\gamma}}\gamma\right)$ of (2.26), respectively into a series form and substituting that in (3.1), this yields

$$\overline{P_d}(\lambda) = \frac{2\sqrt{\pi}\mu^{\mu+\frac{1}{2}}h^{\mu}}{\Gamma(\mu)H^{\mu-\frac{1}{2}}\bar{\gamma}^{\mu+\frac{1}{2}}} \sum_{j,n=0}^{\infty} \frac{\Gamma(u+n, \frac{\lambda}{2})}{\Gamma(n+1)\Gamma(u+n)\Gamma(\mu+j+\frac{1}{2})j!}$$
$$\times \int_0^{\infty} \gamma^{2\mu+n+2j-1} e^{-\frac{2\mu h+\bar{\gamma}}{\bar{\gamma}}\gamma} d\gamma \qquad (A.1)$$

The integral in (A.1) can be evaluated by [43, eq. (3.351.3)] as follows,

$$\overline{P_d}(\lambda) = \frac{2\sqrt{\pi}\mu^{\mu+\frac{1}{2}}h^{\mu}}{\Gamma(\mu)H^{\mu-\frac{1}{2}}\bar{\gamma}^{\mu+\frac{1}{2}}} \sum_{j,n=0}^{\infty} \frac{\Gamma(u+n, \frac{\lambda}{2})}{\Gamma(n+1)\Gamma(u+n)\Gamma(\mu+j+\frac{1}{2})j!} \frac{\Gamma(2\mu+n+2j)}{\left(\frac{2\mu h+\bar{\gamma}}{\bar{\gamma}}\right)^{2\mu+n+2j}}$$
$$(A.2)$$

By invoking $\Gamma(a, b) = \Gamma(a) - \sum_{k=0}^{\infty} \frac{(-1)^k}{(a+k)k!}(b)^{a+k}$ [43, eq. (8.354.2)] and $\Gamma(a+b) = (a)_b\Gamma(a)$ [44, eq. (1.2.3)], the following expression is deduced

$$\overline{P_d}(\lambda) = \frac{2\sqrt{\pi}\mu^{\mu+\frac{1}{2}}h^\mu}{\Gamma(\mu)H^{\mu-\frac{1}{2}}\bar{\gamma}^{\mu+\frac{1}{2}}}\left(\frac{\sqrt{\mu H\bar{\gamma}}}{2\mu h+\bar{\gamma}}\right)^{2\mu}\left(\sqrt{\frac{\bar{\gamma}}{\mu H}}\right)\left[\sum_{j,n=0}^{\infty}\frac{(2\mu)_{2j+n}\Gamma(2\mu)}{(\mu+\frac{1}{2})_j\Gamma(\mu+\frac{1}{2})j!n!}\right.$$

$$\times\left(\frac{(\mu H)^2}{(2\mu h+\bar{\gamma})^2}\right)^j\left(\frac{\bar{\gamma}}{2\mu h+\bar{\gamma}}\right)^n-\frac{\lambda}{2}\sum_{j,n,k=0}^{\infty}\frac{(2\mu)_{2j+n}\Gamma(2\mu)}{\Gamma(u+n)\Gamma(\mu+\frac{1}{2})(\mu+\frac{1}{2})_j(u+n+k)n!j!k!}$$

$$\left.\times\left(\frac{(\mu H)^2}{(2\mu h+\bar{\gamma})^2}\right)^j\left(\frac{\bar{\gamma}\lambda}{2(2\mu h+\bar{\gamma})}\right)^n\left(-\frac{\lambda}{2}\right)^k\right] \tag{A.3}$$

With the aid of the identities $(a+b)_c = \frac{(a)_{b+c}}{(a)_b}$ [44, eq. (1.2.9)] and $a+b+c = a\frac{(1+a)_{b+c}1}{(a)_{b+c}}$, (A.3) can be further simplified to become

$$\overline{P_d}(\lambda) = \frac{2\sqrt{\pi}\Gamma(2\mu)\mu^{\mu+\frac{1}{2}}h^\mu}{\Gamma(\mu)\Gamma(\mu+\frac{1}{2})H^{\mu-\frac{1}{2}}\bar{\gamma}^{\mu+\frac{1}{2}}}\left(\frac{\sqrt{\mu H\bar{\gamma}}}{2\mu h+\bar{\gamma}}\right)^{2\mu}\left(\sqrt{\frac{\bar{\gamma}}{\mu H}}\right)\left[\sum_{j,n=0}^{\infty}\frac{(2\mu)_{2j+n}}{(\mu+\frac{1}{2})_j j!n!}\right.$$

$$\times\left(\frac{(\mu H)^2}{(2\mu h+\bar{\gamma})^2}\right)^j\left(\frac{\bar{\gamma}}{2\mu h+\bar{\gamma}}\right)^n-\frac{\lambda}{2u!}\sum_{j,n,k=0}^{\infty}\frac{(2\mu)_{2j+n}(u)_{n+k}}{(u)_n(1+u)_{n+k}(\mu+\frac{1}{2})_j n!j!k!}$$

$$\left.\times\left(\frac{(\mu H)^2}{(2\mu h+\bar{\gamma})^2}\right)^j\left(\frac{\bar{\gamma}\lambda}{2(2\mu h+\bar{\gamma})}\right)^n\left(-\frac{\lambda}{2}\right)^k\right] \tag{A.4}$$

After some mathematical simplifications and employing the multiple variables hypergeometric functions, the desired result in (3.2) is deduced from (A.4).

## A.2  Derivation of $\bar{A}$ in (3.4)

Substituting (2.21) into (3.3), this yields

$$\bar{A} = \overbrace{\int_0^\infty f_\gamma(\gamma)d\gamma}^{\mathcal{I}_1} - \sum_{n=0}^{u-1}\frac{1}{2^n n!}\overbrace{\int_0^\infty \gamma^n e^{-\frac{\gamma}{2}}f_\gamma(\gamma)d\gamma}^{\mathcal{I}_2} + \sum_{n=1-u}^{u-1}\frac{(u)_n}{2^{u+n}}$$

$$\overbrace{\int_0^\infty e^{-\gamma}{}_1\tilde{F}_1\left(u+n;1+n;\frac{\gamma}{2}\right)f_\gamma(\gamma)d\gamma}^{\mathcal{I}_3} \tag{A.5}$$

---

[1]This identity can be easily calculated by using [44, eq. (1.2.1)], [44, eq. (1.2.3)] and [44, eq. (1.2.9)].

Since $\int_0^\infty f_\gamma(\gamma)d\gamma \triangleq 1$, $\mathcal{I}_1 = 1$.

By plugging (2.26) in (A.5) and employing [43, eq.(3.351.3)], $\mathcal{I}_2$ in (A.5) can be evaluated as follows

$$\mathcal{I}_2 = \frac{2\sqrt{\pi}\mu^{\mu+\frac{1}{2}}h^\mu}{\Gamma(\mu)H^{\mu-\frac{1}{2}}\bar{\gamma}^{\mu+\frac{1}{2}}} \sum_{j=0}^\infty \frac{\Gamma(2\mu+2j+n)}{\Gamma(j+\mu+\frac{1}{2})j!} \left(\frac{2\bar{\gamma}}{4\mu h + \bar{\gamma}}\right)^{2\mu+2j+n} \left(\frac{\mu H}{\bar{\gamma}}\right)^{\mu+2j-\frac{1}{2}} \quad \text{(A.6)}$$

Now, recalling the identity $\Gamma(a+b) = (a)_b\Gamma(a)$ and then using the identity $(a)_{2b} = 2^{2b}(\frac{a}{2})_b(\frac{a+1}{2})_b$ [44, eq. (1.2.13)] to rewrite $\mathcal{I}_2$ in (A.6) in the following form

$$\mathcal{I}_2 = \frac{2\sqrt{\pi}\mu^{\mu+\frac{1}{2}}h^\mu\Gamma(2\mu+n)}{\Gamma(\mu)\Gamma(\mu+\frac{1}{2})H^{\mu-\frac{1}{2}}\bar{\gamma}^{\mu+\frac{1}{2}}} \left(\frac{\sqrt{\mu H\bar{\gamma}}}{2\mu h + \bar{\gamma}}\right)^{2\mu} \left(\sqrt{\frac{\bar{\gamma}}{\mu H}}\right) \left(\frac{2\bar{\gamma}}{4\mu h + \bar{\gamma}}\right)^n$$
$$\times \sum_{j=0}^\infty \frac{(\mu+\frac{n}{2})_j(\mu+\frac{n}{2}+\frac{1}{2})_j}{(\mu+\frac{1}{2})j!} \left(\frac{(2\mu H)^2}{(4\mu h + \bar{\gamma})^2}\right)^j \quad \text{(A.7)}$$

Utilising [44, eq. (1.2.23)] to express (A.7) in exact form as in (3.4).

Substituting (2.26) in (A.5) and using [41, eq. (27)], and [43, eq. (8.445)], $\mathcal{I}_3$ becomes

$$\mathcal{I}_3 = \frac{2\sqrt{\pi}\mu^{\mu+\frac{1}{2}}h^\mu}{\Gamma(\mu)H^{\mu-\frac{1}{2}}\bar{\gamma}^{\mu+\frac{1}{2}}} \sum_{l=0}^\infty \frac{1}{\Gamma(l+\mu+\frac{1}{2})n!l!} \left(\frac{\mu H}{\bar{\gamma}}\right)^{\mu+2l-\frac{1}{2}}$$
$$\times \int_0^\infty \gamma^{2\mu+2l-1}e^{-\frac{2\mu h+\bar{\gamma}}{\bar{\gamma}}\gamma} {}_1F_1\left(u+n; 1+n; \frac{\gamma}{2}\right)d\gamma \quad \text{(A.8)}$$

The integral in (A.8) can be computed by [43, eq. (7.522.9)] as follows

$$\mathcal{I}_3 = \frac{2\sqrt{\pi}\mu^{\mu+\frac{1}{2}}h^\mu}{\Gamma(\mu)H^{\mu-\frac{1}{2}}\bar{\gamma}^{\mu+\frac{1}{2}}} \sum_{l=0}^\infty \frac{\Gamma(2\mu+2l)}{\Gamma(l+\mu+\frac{1}{2})n!l!} \left(\frac{\mu H}{\bar{\gamma}}\right)^{\mu+2l-\frac{1}{2}} \left(\frac{\bar{\gamma}}{2\mu h\bar{\gamma}}\right)^{2\mu+2l}$$
$$\times {}_2F_1\left(u+n; 1+n; \frac{\gamma}{2}\right) \quad \text{(A.9)}$$

After invoking [44, eq. (1.2.23)] to rewrite ${}_2F_1(.)$ into series form, $a+b+c = a\frac{(1+a)_{b+c}}{(a)_{b+c}}$ and $(a+b)_{2c} = 2^{2c}(\frac{a+b}{2})_c(\frac{a+b+2}{2})_c$, this yields

166

$$\mathcal{I}_3 = \frac{2\sqrt{\pi}\Gamma(u+n)\Gamma(2\mu)\mu^{\mu+\frac{1}{2}}h^\mu}{\Gamma(\mu)\Gamma(u)\Gamma(\mu+\frac{1}{2})H^{\mu-\frac{1}{2}}\bar{\gamma}^{\mu+\frac{1}{2}}n!}\left(\frac{\sqrt{\mu H\bar{\gamma}}}{2\mu h + \bar{\gamma}}\right)^{2\mu}\left(\sqrt{\frac{\bar{\gamma}}{\mu H}}\right)$$

$$\times \sum_{l,k=0}^{\infty}\frac{(2\mu)_{2l+k}(u+n)_k}{(\mu+\frac{1}{2})_l(1+n)_k l! k!}\left(\frac{(\mu H)^2}{(2\mu h + \bar{\gamma})^2}\right)^l\left(\frac{\bar{\gamma}}{2(2\mu h + \bar{\gamma})}\right)^k \quad \text{(A.10)}$$

After putting $\mathcal{I}_1 = 1$, (A.7) and (A.10) in (A.5) and performing some mathematical straightforward simplifications, the final expression for $\bar{A}$ is deduced as given in (3.4).

## A.3   Derivation of $\overline{P}_{d_{i.n.d}}^{MRC}(\lambda)$ in (3.7) and Proof of Corollary 1

Substitute $P_d(\gamma,\lambda)$ of (2.8) and (3.5) in (3.1) with the help of (2.9), yielding

$$\overline{P}_{d_{i.n.d}}^{MRC}(\lambda) = \frac{\left(\prod_{i=1}^{L}\left(\frac{4\mu_i^2 h_i}{\bar{\gamma}_i^2}\right)^{\mu_i}\right)}{\Gamma\left(2\sum_{i=1}^{L}\mu_i\right)}\sum_{n=0}^{\infty}\frac{\Gamma(u+n,\frac{\lambda}{2})}{\Gamma(n+1)\Gamma(u+n)}$$

$$\times \int_0^{\infty}\gamma^{2\sum_{i=1}^{L}\mu_i+n-1}e^{-\gamma}\Phi_2^{(2L)}\left(\mu_1,\mu_1,...,\mu_L,\mu_L; 2\sum_{i=1}^{L}\mu_i; -\frac{2\mu_1(h_1-H_1)\gamma}{\bar{\gamma}_1},\right.$$

$$\left. -\frac{2\mu_1(h_1+H_1)\gamma}{\bar{\gamma}_1}, ..., -\frac{2\mu_L(h_L-H_L)\gamma}{\bar{\gamma}_L}, -\frac{2\mu_L(h_L+H_L)\gamma}{\bar{\gamma}_L}\right)d\gamma$$

$$\text{(A.11)}$$

The integral in (A.11) can be evaluated by [44, eq. (9.4.43)] as follows

$$\overline{P}_{di.n.d}^{MRC}(\lambda) = \frac{\left(\prod_{i=1}^{L}\left(\frac{4\mu_i^2 h_i}{\bar{\gamma}_i^2}\right)^{\mu_i}\right)}{\Gamma\left(2\sum_{i=1}^{L}\mu_i\right)}\sum_{n=0}^{\infty}\frac{\Gamma(u+n,\frac{\lambda}{2})}{\Gamma(n+1)\Gamma(u+n)}\Gamma\left(2\sum_{i=1}^{L}\mu_i+n\right)$$

$$\times F_D^{(2L)}\left(2\sum_{i=1}^{L}\mu_i+n;\mu_1,\mu_1,...,\mu_L,\mu_L;2\sum_{i=1}^{L}\mu_i;-\frac{2\mu_1(h_1-H_1)}{\bar{\gamma}_1},\right.$$

$$\left.-\frac{2\mu_1(h_1+H_1)}{\bar{\gamma}_1},...,-\frac{2\mu_L(h_L-H_L)}{\bar{\gamma}_L},-\frac{2\mu_L(h_L+H_L)}{\bar{\gamma}_L}\right) \qquad (A.12)$$

By using [44, eq. (1.4.4)] and following the same procedure for (A.2) and (A.3), (A.12) can be rewritten as follows

$$\overline{P}_{di.n.d}^{MRC}(\lambda) = \left(\prod_{i=1}^{L}\left(\frac{4\mu_i^2 h_i}{\bar{\gamma}_i^2}\right)^{\mu_i}\right)\left[\sum_{j_1,\cdots,j_L,k_1,\cdots,k_L,n=0}^{\infty}\frac{\left(2\sum_{i=1}^{L}\mu_i\right)_{k_1+j_1\cdots+k_L+j_L+n}}{\left(2\sum_{i=1}^{L}\mu_i\right)_{k_1+j_1\cdots+k_L+j_L}}\right.$$

$$\frac{(\mu_1)_{k_1}(\mu_1)_{j_1}...(\mu_L)_{k_L}(\mu_L)_{j_L}}{k_1!\cdots k_L!j_1!\cdots j_L!n!}\left(-\frac{2\mu_1(h_1-H_1)}{\bar{\gamma}_1}\right)^{k_1}\left(-\frac{2\mu_1(h_1+H_1)}{\bar{\gamma}_1}\right)^{j_1}$$

$$\cdots\left(-\frac{2\mu_L(h_L-H_L)}{\bar{\gamma}_L}\right)^{k_L}\left(-\frac{2\mu_L(h_L+H_L)}{\bar{\gamma}_L}\right)^{j_L}$$

$$-\frac{\lambda^u}{u!2^u}\sum_{j_1,\cdots,j_L,k_1,\cdots,k_L,n,l=0}^{\infty}\frac{\left(2\sum_{i=1}^{L}\mu_i\right)_{k_1+j_1\cdots+k_L+j_L+n}}{\left(2\sum_{i=1}^{L}\mu_i\right)_{k_1+j_1\cdots+k_L+j_L}}\frac{(u)_{n+l}(\mu_1)_{j_1}(\mu_1)_{k_1}...(\mu_L)_{j_L}(\mu_L)_{k_L}}{(1+u)_{n+l}(u)_n j_1!\cdots j_L!k_1!\cdots k_L!n!l!}$$

$$\times\left(-\frac{2\mu_1(h_1-H_1)}{\bar{\gamma}_1}\right)^{k_1}\left(-\frac{2\mu_1(h_1+H_1)}{\bar{\gamma}_1}\right)^{j_1}$$

$$\cdots\left(-\frac{2\mu_L(h_L-H_L)}{\bar{\gamma}_L}\right)^{k_L}\left(-\frac{2\mu_L(h_L+H_L)}{\bar{\gamma}_L}\right)^{j_L}\left(\frac{\lambda}{2}\right)^n\left(-\frac{\lambda}{2}\right)^l\right] \qquad (A.13)$$

The $\overline{P}_{di.n.d}^{MRC}(\lambda)$ in (A.13) can be expressed exactly as in (3.7).

Corollary 1 can be proved by substituting (2.8) and (3.6) in (3.1) with the aid of

(2.9). Accordingly, this yields

$$
\overline{P}_{d.i.i.d}^{MRC}(\lambda) = \frac{\left(\frac{4\mu^2 h}{\bar{\gamma}^2}\right)^{L\mu}}{\Gamma(2L\mu)} \sum_{n=0}^{\infty} \frac{\Gamma(u+n,\frac{\lambda}{2})}{\Gamma(n+1)\Gamma(u+n)}
$$
$$
\times \int_0^{\infty} \gamma^{2L\mu+n-1} e^{-\gamma} \Phi_2\left(L\mu, L\mu; 2L\mu; -\frac{2\mu(h-H)\gamma}{\bar{\gamma}}, -\frac{2\mu(h+H)\gamma}{\bar{\gamma}}\right) d\gamma \quad \text{(A.14)}
$$

The integral in (A.14) can be computed by [162, eq. (4.24.4)], as follows

$$
\overline{P}_{d.i.i.d}^{MRC}(\lambda) = \frac{\left(\frac{4\mu^2 h}{\bar{\gamma}^2}\right)^{L\mu}}{\Gamma(2L\mu)} \sum_{n=0}^{\infty} \frac{\Gamma(u+n,\frac{\lambda}{2})\Gamma(2L\mu+n)}{\Gamma(n+1)\Gamma(u+n)}
$$
$$
\times F_1\left(2L\mu+n, L\mu, L\mu; 2L\mu; -\frac{\mu(h-H)}{\bar{\gamma}}, -\frac{2\mu(h+H)}{\bar{\gamma}}\right) \quad \text{(A.15)}
$$

where $F_1(.)$ is the double variables Appell hypergeometric function [43, eq. (9.180.1)][2].

By using [43, eq. (9.180.1)] and following a similar procedure for (A.12) with some mathematical operations, this yields

$$
\overline{P}_{d.i.i.d}^{MRC}(\lambda) = \left(\frac{4\mu^2 h}{\bar{\gamma}^2}\right)^{L\mu} \left[ \sum_{n,k,j=0}^{\infty} \frac{(2L\mu)_{n+k+j}(L\mu)_k(L\mu)_j}{(2L\mu)_{k+j}n!k!j!} \left(-\frac{2\mu(h-H)}{\bar{\gamma}}\right)^k \right.
$$
$$
\left(-\frac{2\mu(h+H)}{\bar{\gamma}}\right)^j - \frac{\lambda^u}{u!2^u} \sum_{n,k,j,l=0}^{\infty} \frac{(2L\mu)_{n+k+j}(u)_{n+l}(L\mu)_k(Lm)_j}{(2L\mu)_{k+j}(1+u)_{n+l}(u)_n n!k!j!l!} \left(-\frac{2\mu(h-H)}{\bar{\gamma}}\right)^k
$$
$$
\left. \times \left(-\frac{2\mu(h+H)}{\bar{\gamma}}\right)^j \left(\frac{\lambda}{2}\right)^n \left(-\frac{\lambda}{2}\right)^l \right] \quad \text{(A.16)}
$$

The $\overline{P}_{d.i.i.d}^{MRC}(\lambda)$ in (A.16) can be expressed in exact form as given in (3.8).

---

[2]It can be noted that $F_1(.)$ is a special case of $F_D^{(M)}(.)$ where $F_1(.) = F_D^{(2)}(.)$

## A.4 Derivation of $\bar{A}_{i.n.d}^{MRC}$ in (3.9) and Proof of Corollary 2

Plugging (3.5) in (3.3), the result is

$$
\bar{A} = \overbrace{\int_0^\infty f_{\gamma,i.n.d}^{MRC}(\gamma)d\gamma}^{\mathcal{I}_{1,i.n.d}} - \sum_{n=0}^{u-1} \frac{1}{2^n n!} \overbrace{\int_0^\infty \gamma^n e^{-\frac{\gamma}{2}} f_{\gamma,i.n.d}^{MRC}(\gamma)d\gamma}^{\mathcal{I}_{2,i.n.d}} + \sum_{n=1-u}^{u-1} \frac{(u)_n}{2^{u+n}}
$$

$$
\overbrace{\int_0^\infty e^{-\gamma} {}_1\tilde{F}_1\left(u+n; 1+n; \frac{\gamma}{2}\right) f_{\gamma,i.n.d}^{MRC}(\gamma)d\gamma}^{\mathcal{I}_{3,i.n.d}} \qquad (A.17)
$$

Similar to $\mathcal{I}_1$ in Appendix A.2, $\mathcal{I}_{1,i.n.d} = 1$. Moreover, $\mathcal{I}_{2,i.n.d}$ can be evaluated by employing (3.5) and [44, eq. (9.4.43)] as follows

$$
\mathcal{I}_{2,i.n.d} = \frac{\left(\prod_{i=1}^L \left(\frac{4\mu_i^2 h_i}{\bar{\gamma}_i^2}\right)^{\mu_i}\right)}{\Gamma\left(2\sum_{i=1}^L \mu_i\right)} 2^{n+2\sum_{i=1}^L \mu_i} \Gamma\left(n+2\sum_{i=1}^L \mu_i\right) F_D^{(2L)}\left(n+2\sum_{i=1}^L \mu_i; \mu_1, \mu_1, ..., \mu_L,\right.
$$

$$
\left. \mu_L; 2\sum_{i=1}^L \mu_i; -\frac{4\mu_1(h_1-H_1)}{\bar{\gamma}_1}, -\frac{4\mu_1(h_1+H_1)}{\bar{\gamma}_1}, ..., -\frac{4\mu_L(h_L-H_L)}{\bar{\gamma}_L}, -\frac{4\mu_L(h_L+H_L)}{\bar{\gamma}_L}\right)
$$

$$
(A.18)
$$

Using (3.5) and [44, eq. (9.4.43)] and following a similar procedure for $\mathcal{I}_3$ in Appendix A.2, $\mathcal{I}_{3,i.n.d}$ of (A.17) becomes

$$
\mathcal{I}_{3,i.n.d} = \frac{\left(\prod_{i=1}^L \left(\frac{4\mu_i^2 h_i}{\bar{\gamma}_i^2}\right)^{\mu_i}\right)}{\Gamma\left(2\sum_{i=1}^L \mu_i\right)\Gamma(1+n)} \sum_{j=0}^\infty \frac{(u+n)_j}{(1+n)_j j!} \left(\frac{1}{2}\right)^j \Gamma\left(2\sum_{i=1}^L \mu_i + j\right)
$$

$$
\times F_D^{(2L)}\left(j+2\sum_{i=1}^L \mu_i; \mu_1, \mu_1, ..., \mu_L, \mu_L; 2\sum_{i=1}^L \mu_i; -\frac{2\mu_1(h_1-H_1)}{\bar{\gamma}_1}, -\frac{2\mu_1(h_1+H_1)}{\bar{\gamma}_1}, ...,\right.
$$

$$
\left. -\frac{2\mu_L(h_L-H_L)}{\bar{\gamma}_L}, -\frac{2\mu_L(h_L+H_L)}{\bar{\gamma}_L}\right) \qquad (A.19)
$$

Invoking [44, eq. (1.4.4)] and utilizing the same steps for (A.2) and (A.3) with some mathematical operations, (A.19) can be written as follows

$$
\mathcal{I}_{3,i.n.d} = \frac{\left(\prod_{i=1}^{L}\left(\frac{4\mu_i^2 h_i}{\bar{\gamma}_i^2}\right)^{\mu_i}\right)}{\Gamma(1+n)} \sum_{k_1,\cdots,k_L,l_1,\cdots,l_L,j=0}^{\infty} \frac{\left(2\sum_{i=1}^{L}\mu_i\right)_{k_1+l_1\ldots+k_L+l_L+j}}{\left(2\sum_{i=1}^{L}\mu_i\right)_{k_1+l_1\cdots+k_L+l_L}} \frac{(u+n)_j}{(1+n)_j}
$$

$$
\times\frac{(\mu_1)_{k_1}(\mu_1)_{l_1}\ldots(\mu_L)_{k_L}(\mu_L)_{l_L}}{k_1!\cdots k_L!l_1!\cdots l_L!j!}\left(-\frac{2\mu_1(h_1-H_1)}{\bar{\gamma}_1}\right)^{k_1}\left(-\frac{2\mu_1(h_1+H_1)}{\bar{\gamma}_1}\right)^{l_1}\cdots
$$

$$
\left(-\frac{2\mu_L(h_L-H_L)}{\bar{\gamma}_L}\right)^{k_L}\left(-\frac{2\mu_L(h_L+H_L)}{\bar{\gamma}_L}\right)^{l_L} \tag{A.20}
$$

Using the exact form for (A.20) that is recorded in [44, eq. (1.4.21)] and inserting that together with $\mathcal{I}_{1,i.n.d} = 1$ and (A.18) in (A.17), the desired result in (3.9) is obtained.

The expression that is given in Corollary 2 can be derived from (A.18) and (A.20). Consequently, this yields

$$
\mathcal{I}_{2,i.i.d} = \frac{\left(\frac{4\mu^2 h}{\bar{\gamma}^2}\right)^{L\mu}}{\Gamma(2L\mu)} 2^{n+2L\mu}\Gamma(n+2L\mu)
$$

$$
\times F_D^{(2)}\left(n+2L\mu, L\mu, L\mu; 2L\mu; -\frac{4\mu(h-H)}{\bar{\gamma}}, -\frac{4\mu(h+H)}{\bar{\gamma}}\right) \tag{A.21}
$$

and

$$
\mathcal{I}_{3,i.i.d} = \frac{\left(\prod_{i=1}^{L}\left(\frac{4\mu_i^2 h_i}{\bar{\gamma}_i^2}\right)^{\mu_i}\right)}{\Gamma(1+n)} \sum_{k,l,j=0}^{\infty} \frac{(2L\mu)_{j+k+l}(L\mu)_k(L\mu)_l(u+n)_j}{(2L\mu)_{j+k}(1+n)_j k!l!j!}
$$

$$
\times\left(-\frac{2\mu(h-H)}{\bar{\gamma}}\right)^k\left(-\frac{2\mu(h+H)}{\bar{\gamma}}\right)^l\left(\frac{1}{2}\right)^j \tag{A.22}
$$

Substituting $\mathcal{I}_{1,i.i.d} = 1$, (A.21) and (A.22) instead of $\mathcal{I}_{1,i.n.d}$, $\mathcal{I}_{2,i.n.d}$ and $\mathcal{I}_{3,i.3.d}$, respectively into (A.17), the expression in (3.10) is obtained.

# A.5   Derivation of $\bar{A}_{i.n.d}^{SLS}$ in (3.14)

To compute the average AUC for SLS diversity reception, the unfaded AUC for SLS should be firstly derived. Accordingly, from (2.38), the derivative of the probability of false alarm $P_f^{SLS}(\lambda)$ is expressed by

$$\frac{\partial P_f^{SLS}(\lambda)}{\partial \lambda} = -\frac{L\lambda^{u-1}e^{-\frac{\lambda}{2}}}{2^u[\Gamma(u)]^L}[G(u,\lambda/2)]^{L-1} \tag{A.23}$$

Substituting (A.23) and (2.39) in (2.19), this yields

$$A^{SLS}(\gamma) = \frac{L}{2^u[\Gamma(u)]^L}\left[\overbrace{\int_0^\infty \lambda^{u-1}e^{-\frac{\lambda}{2}}[G(u,\lambda/2)]^{L-1}d\lambda}^{\xi_1}\right.$$
$$\left.-\underbrace{\int_0^\infty \lambda^{u-1}e^{-\frac{\lambda}{2}}[G(u,\lambda/2)]^{L-1}\prod_{i=1}^L(1-Q_u(\sqrt{2\gamma_i},\sqrt{\lambda}))d\lambda}_{\xi_2}\right] \tag{A.24}$$

Using [124, eq. (6.5.12)], $\xi_1$ can be represented as follows

$$\xi_1 = \frac{1}{[u2^u]^{L-1}}\int_0^\infty \lambda^{uL-1}e^{-\frac{\lambda}{2}}\prod_{i=1}^{L-1}{}_1F_1\left(u;1+u;-\frac{\lambda}{2}\right)d\lambda \tag{A.25}$$

Recalling [44, eq. (9.4.35)] to evaluate the integral in (A.25), $\xi_1$ becomes

$$\xi_1 = \frac{2^u\Gamma(Lu)}{u^{L-1}}F_A^{(L-1)}(Lu;u,...,u;1+u,...,1+u;-1,...,-1) \tag{A.26}$$

By invoking [124, eq. (6.5.12)] and [91, eq. (6)], the following series form for $\xi_2$ yields,

$$\xi_2 = \frac{2^{u(1-2L)}}{u^{L-1}}\sum_{n_1,...,n_L=0}^\infty \frac{\gamma_1^{n_1}...\gamma_L^{n_L}e^{-(\gamma_1+\cdots+\gamma_L)}}{(n_1+u)\cdots(n_L+u)\Gamma(n_1+u)\cdots\Gamma(n_L+u)n_1!\cdots n_L!}\left(\frac{1}{2}\right)^{n_1+...+n_L}$$
$$\times \int_0^\infty \lambda^{n_1+\cdots+n_L+2Lu-1}e^{-\frac{\lambda}{2}}\prod_{i=1}^L{}_1F_1(n_i+u,n_i+1+u,-\frac{\lambda}{2})\prod_{i=1}^{L-1}{}_1F_1(u,1+u,-\frac{\lambda}{2})d\lambda \tag{A.27}$$

By employing [44, eq. (9.4.35)] to calculate the integral in (A.27) with some mathematical manipulations, the following expression yields,

$$\xi_2 = \frac{2}{u^{L-1}} \sum_{n_1,...,n_L=0}^{\infty} \frac{\gamma_1^{n_1}...\gamma_L^{n_L} e^{-(\gamma_1+...+\gamma_L)}}{(n_1+u)\cdots(n_L+u)\Gamma(n_1+u)\cdots\Gamma(n_L+u)n_1!\cdots n_L!}$$
$$\times \Gamma(n_1+...+n_L+2Lu)F_A^{(2L-1)}(n_1+...+n_L+2Lu; u, ..., u, n_1+u, ..., n_L+u;$$
$$1+u, ..., 1+u, n_1+1+u, ..., n_L+1+u; -1, ..., -1) \qquad (A.28)$$

Using [44, eq. (1.4.1)] and then employing the identities $\Gamma(a+b) = (a)_b\Gamma(a)$, $(a+b)_c = \frac{(a)_{b+c}}{(a)_b}$ and $a+b+c = a\frac{(1+a)_{b+c}}{(a)_{b+c}}$, (A.28) can be expressed as follows

$$\xi_2 = \frac{2^u\Gamma(2Lu)e^{-\sum_{i=1}^{L}\gamma_i}}{u^{(L-1)}[\Gamma(1+u)]^L} \sum_{n_1,...,n_L,l_1,...,l_{2L-1}=0}^{\infty} \frac{(2Lu)_{n_1+...+n_L+l_1+...+l_{2L-1}}(u)_{n_1+l_1}...(u)_{n_L+l_L}}{(1+u)_{n_1+l_1}...(1+u)_{n_L+l_L}(u)_{n_1}...(u)_{n_L}}$$
$$\frac{(u)_{l_{L+1}}...(u)_{l_{2L-1}}}{(1+u)_{l_{L+1}}...(1+u)_{l_{2L-1}}n_1!\cdots n_L!l_1!\cdots l_{2L-1}!}\gamma_1^{n_1}...\gamma_L^{n_L}(-1)^{l_1}...(-1)^{l_{2L-1}} \qquad (A.29)$$

Substituting (A.26) and (A.29) in (A.24) with some mathematical manipulations, $A^{SLS}(\gamma)$ can be exactly expressed as follows

173

$$A^{SLS}(\gamma) = \frac{\Gamma(1+Lu)}{[\Gamma(1+u)]^L}\left[ F_A^{(L-1)}(Lu; u, ..., u; 1+u, ..., 1+u; -1, ..., -1) - \frac{(Lu)_{Lu}}{[\Gamma(1+u)]^L}\right.$$

$$\times e^{-\sum_{i=1}^{L}\gamma_i} F_L^{L+1:\overbrace{0;\cdots;0;\,0;\cdots;0;\,1;\cdots;1}^{3L-1}}_{\quad L\;\;:1;\cdots;1;\,0;\cdots;0;\,1;\cdots;1}\left( \begin{array}{c} [u:1,1,0,0,...,0,0] \quad , \quad [u:0,0,1,1,...,0,0] \quad , \\[6pt] [1+u:1,1,0,0,...,0,0], [1+u:0,0,1,1,...,0,0], \end{array}\right.$$

$$..., [u:0,0,...,0,0,1,1], [2Lu:1,1,...,1,1] : \underline{\quad}; ...; \underline{\quad}; \underline{\quad}; ...; \underline{\quad};$$

$$..., [1+u:0,0,...,0,0,1,1] \qquad : [u:1]; ...; [u:1]; \underline{\quad}; ...; \underline{\quad};$$

$$[u:1]\;\;;...;\;\;[u:1]\;\;;$$

$$\left.\left.\begin{array}{c} \\ \gamma_1, ..., \gamma_L, -1, ..., -1 \end{array}\right)\right]$$

$$[1+u:1]; ...; [1+u:1];$$

$$\tag{A.30}$$

To calculate the average AUC for $i.n.d$ SLS diversity over $\eta - \mu$ fading channels, $\bar{A}_{i.n.d}^{SLS}$, $A^{SLS}(\gamma)$ should be averaged over (2.26) for $L$ times, i.e.,

$$\bar{A}_{i.n.d}^{SLS} = \overbrace{\int_0^\infty ... \int_0^\infty}^{L} A^{SLS}(\gamma) f_{\gamma_1}(\gamma_1) d\gamma_1 \cdots f_{\gamma_L}(\gamma_L) d\gamma_L \tag{A.31}$$

It can be noted that the integral in (A.31) is applied on the second term only. Hence, the average of $\xi$ can be called $\bar{\xi}$ that can be computed from integrating (A.29) over (2.26) for $i$th diversity branch. Accordingly, this yields

$$\Lambda_i = \frac{2\sqrt{\pi}\mu_i^{\mu_i+\frac{1}{2}}h_i^{\mu_i}}{\Gamma(\mu_i)H_i^{\mu_i-\frac{1}{2}}\bar{\gamma}_i^{\mu_i+\frac{1}{2}}} \int_0^\infty \gamma_i^{n_i+\mu_i-\frac{1}{2}} e^{-\frac{2\mu_i h_i+\bar{\gamma}_i}{\bar{\gamma}_i}\gamma_i} I_{\mu_i-\frac{1}{2}}\left(\frac{2\mu_i H_i}{\bar{\gamma}_i}\gamma_i\right) d\gamma_i \tag{A.32}$$

With the aid of [43, eq. (8.445)], the integral in (A.32) can be evaluated by [43,

174

eq. (3.351.3)] as follows,

$$\Lambda_i = \frac{2\sqrt{\pi}\Gamma(2\mu_i)\mu_i^{2\mu_i}h_i^{\mu_i}\bar{\gamma}_i^{n_i}}{\Gamma(\mu_i)\Gamma(\mu_i+\frac{1}{2})(2\mu_i h_i+\bar{\gamma}_i)^{n_i+2\mu_i}}\sum_{j=0}^{\infty}\frac{(2\mu_i)_{n_i+2j}}{(\mu_i+\frac{1}{2})_j j!}\left(\frac{(\mu_i H_i)^2}{(2\mu_i h_i+\bar{\gamma}_i)^2}\right)^j \quad (A.33)$$

Plugging (A.33) for $i=1,....,L$ in (A.29) with the aid of the identities $\Gamma(a+b) = (a)_b\Gamma(a)$ and $\Gamma(a+b) = (a)_b\Gamma(a)$, $\bar{\xi}$ is deduced as follows

$$\bar{\xi}_2 = \frac{2^u\Gamma(2Lu)}{u^{(L-1)}[\Gamma(1+u)]^L}\left(\prod_{i=1}^{L}\frac{2\sqrt{\pi}\Gamma(2\mu_i)\mu_i^{2\mu_i}h_i^{\mu_i}}{\Gamma(\mu_i)\Gamma(\mu_i+\frac{1}{2})(2\mu_i h_i+\bar{\gamma})^{2\mu_i}}\right)\sum_{n_1,...,n_L,j_1,...,j_L,l_1,...,l_{2L-1}=0}^{\infty}$$

$$\frac{(2Lu)_{n_1+...+n_L+l_1+...+l_{2L-1}}(u)_{n_1+l_1}...(u)_{n_L+l_L}(2\mu_1)_{n_1+2j_1}...(2\mu_L)_{n_L+2j_L}}{(1+u)_{n_1+l_1}...(1+u)_{n_L+l_L}(u)_{n_1}...(u)_{n_L}(1+u)_{l_{L+1}}...(1+u)_{l_{2L-1}}(\mu_1+\frac{1}{2})_{j_1}...(\mu_L+\frac{1}{2})_{j_L}}$$

$$\times\frac{(u)_{l_{L+1}}...(u)_{l_{2L-1}}}{n_1!\cdots n_L!l_1!\cdots l_{2L-1}!j_1!\cdots j_L!}\left(\frac{\bar{\gamma}_1}{2\mu_1 h_1+\bar{\gamma}_1}\right)^{n_1}\cdots\left(\frac{\bar{\gamma}_L}{2\mu_L h_L+\bar{\gamma}_L}\right)^{n_L}\left(\frac{(\mu_1 H_1)^2}{(2\mu_1 h_1+\bar{\gamma}_1)^2}\right)^{j_1}$$

$$\cdots\left(\frac{(\mu_L H_L)^2}{(2\mu_L h_L+\bar{\gamma}_L)^2}\right)^{j_L}(-1)^{l_1}...(-1)^{l_{2L-1}} \quad (A.34)$$

Using [44, eq. (1.4.21)] to express (A.34) in exact form and then inserting (A.34) into (A.30), $\bar{A}_{i.n.d}^{SLS}$ is obtained as given in (3.14).

# Appendix B

# Proofs for Chapter 4

## B.1  Derivation of $\overline{P_d}(\lambda)$ in (4.2)

Substituting (2.8) and (4.1) in (3.1) with the aid of (2.9), this yields

$$\overline{P_d}(\lambda) = \frac{\mu^\mu m^m (1+\kappa)^\mu}{\Gamma(\mu)\bar{\gamma}^\mu(\mu\kappa+m)^m}\sum_{n=0}^{\infty}\frac{\Gamma(u+n,\frac{\lambda}{2})}{\Gamma(n+1)\Gamma(u+n)}$$
$$\times \int_0^{\infty}\gamma^{\mu+n-1}e^{-\frac{\mu(1+\kappa)+\bar{\gamma}}{\bar{\gamma}}\gamma}{}_1F_1\left(m;\mu;\frac{\mu^2\kappa(1+\kappa)}{(\mu\kappa+m)}\frac{\gamma}{\bar{\gamma}}\right)d\gamma \qquad \text{(B.1)}$$

Employing [163, eq. (3.35.1.2)] to calculate the integral in (B.1), $\overline{P_d}(\lambda)$ can be obtained as

$$\overline{P_d}(\lambda) = \frac{\mu^\mu m^m (1+\kappa)^\mu}{\Gamma(\mu)\bar{\gamma}^\mu(\mu\kappa+m)^m}\sum_{n=0}^{\infty}\frac{\Gamma(u+n,\frac{\lambda}{2})\Gamma(\mu+n)}{\Gamma(n+1)\Gamma(u+n)}\left(\frac{\bar{\gamma}}{\mu(1+\kappa)+\bar{\gamma}}\right)^{\mu+n}$$
$$\times{}_2F_1\left(m,\mu+n;\mu;\frac{\mu^2\kappa(1+\kappa)}{(\mu\kappa+m)(\mu(1+\kappa)+\bar{\gamma})}\right) \qquad \text{(B.2)}$$

By recalling [44, eq. (1.2.23)] to express ${}_2F_1(.)$ of (B.2) in a series form and following the same steps for (A.2) and (A.3) in Appendix A.1, the following expression for $\overline{P_d}(\lambda)$ is deduced

$$\overline{P_d}(\lambda) = \frac{\mu^\mu m^m (1+\kappa)^\mu}{\bar{\gamma}^\mu (\mu\kappa + m)^m} \left[ \sum_{n,j=0}^{\infty} \frac{(\mu)_{n+j}(m)_j}{(\mu)_j n! j!} \left( \frac{\mu^2 \kappa (1+\kappa)}{(\mu\kappa + m)(\mu(1+\kappa) + \bar{\gamma})} \right)^j \right.$$

$$\times \left( \frac{\bar{\gamma}}{(\mu(1+\kappa) + \bar{\gamma})} \right)^n - \frac{\lambda^u}{u\Gamma(u) 2^u} \sum_{n,j,i=0}^{\infty} \frac{(m)_j (u)_{i+n} (\mu)_{j+n}}{(1+u)_{n+i}(u)_n (\mu)_j n! j! i!}$$

$$\left. \left( \frac{\mu^2 \kappa (1+\kappa)}{(\mu\kappa + m)(\mu(1+\kappa) + \bar{\gamma})} \right)^j \left( \frac{\bar{\gamma}\lambda}{2(\mu(1+\kappa) + \bar{\gamma})} \right)^n \left( -\frac{\lambda}{2} \right)^i \right] \quad \text{(B.3)}$$

Using multivariate hypergeometric functions, the exact representation for $\overline{P_d}(\lambda)$ is obtained as in (4.2).

## B.2 Derivation of $\bar{A}$ in (4.3)

Similarly to (A.5) in Appendix A.2, the $\bar{A}$ can be computed by inserting (4.1) into (A.5). Accordingly, $\mathcal{I}_1 = 1$.

The exact solution for $\mathcal{I}_2$ can be evaluated by invoking [163, eq. (3.35.1.2)] as follows

$$\mathcal{I}_2 = \frac{\Gamma(\mu + n)\mu^\mu m^m (1+\kappa)^\mu}{\Gamma(\mu)\bar{\gamma}^\mu (\mu\kappa + m)^m} \left( \frac{2\bar{\gamma}}{2\mu(1+\kappa) + \bar{\gamma}} \right)^{\mu+n}$$

$$\times {}_2F_1\left( m, \mu + n; \mu; \frac{2\mu^2 \kappa (1+\kappa)}{(\mu\kappa + m)(2\mu(1+\kappa) + \bar{\gamma})} \right) \quad \text{(B.4)}$$

With the aid of [41, eq. (27)], $\mathcal{I}_3$ can be expressed as follows

$$\mathcal{I}_3 = \frac{\mu^\mu m^m (1+\kappa)^\mu}{\Gamma(\mu)(\mu\kappa + m)^m \bar{\gamma}^\mu} \sum_{l=0}^{\infty} \frac{(u+n)_l}{2^l (1+n)_l n! l!}$$

$$\times \int_0^{\infty} \gamma^{\mu+l-1} e^{-\frac{\mu(1+\kappa)+\bar{\gamma}}{\bar{\gamma}}\gamma} {}_1F_1\left( m; \mu; \frac{\mu^2 \kappa (1+\kappa)}{(\mu\kappa + m)\bar{\gamma}}\gamma \right) d\gamma \quad \text{(B.5)}$$

Using [163, eq. (3.35.1.2)] to calculate (B.5) and following a similar procedure for (A.9) in Appendix A.2, this yields

$$\mathcal{I}_3 = \frac{\mu^\mu m^m (1+\kappa)^\mu}{(\mu\kappa + m)^m \bar{\gamma}^\mu} \left( \frac{\bar{\gamma}}{\mu(1+\kappa) + \bar{\gamma}} \right)^\mu \sum_{l,j=0}^{\infty} \frac{(\mu)_{j+l}(m)_j(u+n)_l}{(\mu)_j(1+n)_l j! l!}$$

$$\times \left( \frac{\mu^2 \kappa(1+\kappa)}{(\mu\kappa + m)(\mu(1+\kappa) + \bar{\gamma})} \right)^j \left( \frac{\bar{\gamma}}{2(\mu(1+\kappa) + \bar{\gamma})} \right)^l \quad \text{(B.6)}$$

By plugging $\mathcal{I}_1 = 1$, (B.4) and (B.6) in (A.5) and doing some mathematical manipulations, the exact representation for $\bar{A}$ over $\kappa - \mu$ shadowed fading channels is obtained as in (4.3).

# B.3   Derivation of $\overline{P}_{d\,i.n.d}^{MRC}(\lambda)$ in (4.6) and Proof of Corollary 3

After utilising (2.9) to express $P_d(\gamma, \lambda)$ of (2.8) into series form and substituting that together with (4.1) in (3.1), this yields

$$\overline{P}_{d\,i.n.d}^{MRC}(\lambda) = \frac{\Psi}{\Gamma\left(\sum_{i=1}^{L} \mu_i\right)} \sum_{n=0}^{\infty} \frac{\Gamma(u+n, \frac{\lambda}{2})}{\Gamma(n+1)\Gamma(u+n)}$$

$$\times \int_0^\infty \gamma^{\sum_{i=1}^{L} \mu_i + n - 1} e^{-\gamma} \Phi_2^{(2L)} \left( \mu_1 - m_1, ..., \mu_L - m_L, m_1, ..., m_L; \sum_{i=1}^{L} \mu_i; -\frac{\mu_1(1+\kappa_1)\gamma}{\bar{\gamma}_1}, ..., \right.$$

$$\left. -\frac{\mu_L(1+\kappa_L)\gamma}{\bar{\gamma}_L}, -\frac{\mu_1(1+\kappa_1)}{\bar{\gamma}_1} \frac{m_1\gamma}{\mu_1\kappa_1 + m_1}, ..., -\frac{\mu_L(1+\kappa_L)}{\bar{\gamma}_L} \frac{m_L\gamma}{\mu_L\kappa_L + m_L} \right) d\gamma$$

$$\text{(B.7)}$$

where $\Psi = \prod_{i=1}^{L} \frac{\mu_i^{\mu_i} m_i^{m_i} (1+\kappa_i)^{\mu_i}}{(\mu_i\kappa_i + m_i)^{m_i} \bar{\gamma}_i^{\mu_i}}$.

Clearly, the integral in (B.7) is similar to (A.11). Thus, by using the same steps for (A.13) in Appendix A.3, the following expression for $\overline{P}_{d\,i.n.d}^{MRC}(\lambda)$ is deduced

$$\overline{P}_{d.i.n.d}^{MRC}(\lambda) = \Psi$$

$$\times \Bigg[ \sum_{j_1,\cdots,j_L,k_1,\cdots,k_L,n=0}^{\infty} \frac{\left(\sum\limits_{i=1}^{L}\mu_i\right)_{k_1+j_1\cdots+k_L+j_L+n}}{\left(\sum\limits_{i=1}^{L}\mu_i\right)_{k_1+j_1\cdots+k_L+j_L}} \frac{(\mu_1-m_1)_{k_1}...(\mu_L-m_L)_{k_L}(m_1)_{j_1}...(m_L)_{j_L}}{k_1!\cdots k_L!j_1!\cdots j_L!n!}$$

$$\times \left(-\frac{\mu_1(1+\kappa_1)}{\bar{\gamma}_1}\right)^{k_1}\cdots\left(-\frac{\mu_L(1+\kappa_L)}{\bar{\gamma}_L}\right)^{k_L}$$

$$\times \left(-\frac{\mu_1(1+\kappa_1)}{\bar{\gamma}_1}\frac{m_1}{\mu_1\kappa_1+m_1}\right)^{j_1}\cdots\left(-\frac{\mu_L(1+\kappa_L)}{\bar{\gamma}_L}\frac{m_L}{\mu_L\kappa_L+m_L}\right)^{j_L}$$

$$-\frac{\lambda^u}{u!2^u}\sum_{j_1,\cdots,j_L,k_1,\cdots,k_L,n,l=0}^{\infty}\frac{\left(\sum\limits_{i=1}^{L}\mu_i\right)_{k_1+j_1\cdots+k_L+j_L+n}}{\left(\sum\limits_{i=1}^{L}\mu_i\right)_{k_1+j_1\cdots+k_L+j_L}}\frac{(u)_{n+l}(\mu_1-m_1)_{k_1}...(\mu_L-m_L)_{k_L}}{(1+u)_{n+l}(u)_n n!k_1!\cdots k_L!}$$

$$\times\frac{(m_1)_{j_1}\cdots(m_L)_{j_L}}{j_1!\cdots j_L!}\left(-\frac{\mu_1(1+\kappa_1)}{\bar{\gamma}_1}\right)^{k_1}\cdots\left(-\frac{\mu_L(1+\kappa_L)}{\bar{\gamma}_L}\right)^{k_L}$$

$$\times\left(-\frac{\mu_1(1+\kappa_1)}{\bar{\gamma}_1}\frac{m_1}{\mu_1\kappa_1+m_1}\right)^{j_1}\cdots\left(-\frac{\mu_L(1+\kappa_L)}{\bar{\gamma}_L}\frac{m_L}{\mu_L\kappa_L+m_L}\right)^{j_L}\left(\frac{\lambda}{2}\right)^n\left(-\frac{\lambda}{2}\right)^l\Bigg]$$

(B.8)

It can be noticed, (B.8) can be expressed in similar form for (A.13) as given in (4.6).

To derive the $\overline{P}_{d.i.i.d}^{MRC}(\lambda)$ that is given in corollary 3, (2.8) and (4.5) are substituted in (3.1) with the aid of (2.9). Accordingly, the result is as follows

$$\overline{P}_{d.i.i.d}^{MRC}(\lambda) = \frac{\mu^{L\mu}m^{Lm}(1+\kappa)^{L\mu}}{\Gamma(L\mu)\bar{\gamma}^{L\mu}(\mu\kappa+m)^{Lm}}\sum_{n=0}^{\infty}\frac{\Gamma(u+n,\frac{\lambda}{2})}{\Gamma(n+1)\Gamma(u+n)}$$

$$\times\int_{0}^{\infty}\gamma^{L\mu+n-1}e^{-\gamma}\Phi_2\left(L\mu-Lm,Lm;L\mu;-\frac{\mu(1+\kappa)\gamma}{\bar{\gamma}},-\frac{\mu(1+\kappa)}{\bar{\gamma}}\frac{m\gamma}{\mu\kappa+m}\right)d\gamma \quad \text{(B.9)}$$

Now, by following the same procedure for corollary 1 in Appendix A.3, the $\overline{P}_{d.i.i.d}^{MRC}(\lambda)$ becomes

$$\overline{P}_{d_{i.i.d}}^{MRC}(\lambda) = \left( \frac{\mu^{\mu} m^m (1+\kappa)^{\mu}}{\bar{\gamma}^{\mu} (\mu\kappa + m)^m} \right)^L$$

$$\times \left[ \sum_{n,k,j=0}^{\infty} \frac{(L\mu)_{n+k+j}(L\mu - Lm)_k (Lm)_j}{(L\mu)_{k+j} n! k! j!} \left( -\frac{\mu(1+\kappa)}{\bar{\gamma}} \right)^k \left( -\frac{\mu(1+\kappa)}{\bar{\gamma}} \frac{m}{\mu\kappa + m} \right)^j \right.$$

$$- \frac{\lambda^u}{u! 2^u} \sum_{n,k,j,l=0}^{\infty} \frac{(L\mu)_{n+k+j}(u)_{n+l}(L\mu - Lm)_k (Lm)_j}{(L\mu)_{k+j}(1+u)_{n+l}(u)_n n! k! j! l!} \left( -\frac{\mu(1+\kappa)}{\bar{\gamma}} \right)^k$$

$$\left. \times \left( -\frac{\mu(1+\kappa)}{\bar{\gamma}} \frac{m}{\mu\kappa + m} \right)^j \left( \frac{\lambda}{2} \right)^n \left( -\frac{\lambda}{2} \right)^l \right] \qquad \text{(B.10)}$$

Using [44, eq. (1.4.21)] and [44, eq. (1.5.3)], the desired expression in (4.7) is obtained.

## B.4 Derivation of $\bar{A}_{i.n.d}^{MRC}$ in (4.8) and Proof of Corollary 4

By inserting (4.4) in (A.17) and employing the same procedure for calculating $\mathcal{I}_{2,i.n.d}$ in Appendix A.4, $\mathcal{I}_{2,i.n.d}$ for $\kappa - \mu$ shadowed fading channel is given by

$$\mathcal{I}_{2,i.n.d} = \frac{\Psi}{\Gamma\left( \sum_{i=1}^{L} \mu_i \right)} 2^{\sum_{i=1}^{L} \mu_i + n} \Gamma\left( \sum_{i=1}^{L} \mu_i + n \right)$$

$$\times F_D^{(2L)} \left( \sum_{i=1}^{L} \mu_i + n; \mu_1 - m_1, \cdots, \mu_L - m_L, m_1, \cdots, m_L; \sum_{i=1}^{L} \mu_i; -\frac{2\mu_1(1+\kappa_1)}{\bar{\gamma}_1}, \cdots, \right.$$

$$\left. -\frac{2\mu_L(1+\kappa_L)}{\bar{\gamma}_L}, -\frac{2\mu_1(1+\kappa_1)}{\bar{\gamma}_1} \frac{m_1}{\mu_1\kappa_1 + m_1}, \cdots, -\frac{2\mu_L(1+\kappa_L)}{\bar{\gamma}_L} \frac{m_L}{\mu_L\kappa_L + m_L} \right) \qquad \text{(B.11)}$$

It can be observed that $\mathcal{I}_{3,i.n.d}$ for $\kappa - \mu$ shadowed fading channel can be computed in a way similar to $\mathcal{I}_{3,i.n.d}$ in Appendix A.4. Accordingly, this yields

$$\mathcal{I}_{3,i.n.d} = \frac{\Psi}{n!} \sum_{k_1,\cdots,k_L,l_1,\cdots,l_L,j=0}^{\infty} \frac{\left(\sum_{i=1}^{L}\mu_i\right)_{j+k_1+l_1\cdots+k_L+l_L}}{\left(\sum_{i=1}^{L}\mu_i\right)_{k_1+l_1\cdots+k_L+l_L}} \frac{(u+n)_j(\mu_1-m_1)_{k_1}\cdots}{(1+n)_j j! k_1! \cdots k_L!}$$

$$\times \frac{(\mu_L-m_L)_{k_L}(m_1)_{l_1}\cdots(m_L)_{l_L}}{l_1!\cdots l_L!} \left(-\frac{\mu_1(1+\kappa_1)}{\bar{\gamma}_1}\right)^{k_1} \cdots \left(-\frac{\mu_L(1+\kappa_L)}{\bar{\gamma}_L}\right)^{k_L}$$

$$\left(-\frac{\mu_1(1+\kappa_1)}{\bar{\gamma}_1}\frac{m_1}{\mu_1\kappa_1+m_1}\right)^{l_1} \cdots \left(-\frac{\mu_L(1+\kappa_L)}{\bar{\gamma}_L}\frac{m_L}{\mu_L\kappa_L+m_L}\right)^{l_L}\left(\frac{1}{2}\right)^{j} \qquad \text{(B.12)}$$

Invoking [44, pp. 454] to express (B.12) in exact form and plugging that together with $\mathcal{I}_{1,i.n.d}=1$ and (B.11) in (A.17), the desired result in (4.8) is deduced.

The $\bar{A}_{i.i.d}^{MRC}$ that is given in Corollary 4 can be computed by doing the same steps in Corollary 2. Consequently, the following expressions yield

$$\mathcal{I}_{2,i.i.d} = \frac{\vartheta^L}{\Gamma(L\mu)} 2^{L\mu+n}\Gamma(L\mu+n)$$

$$\times F_D^{(2)}\left(L\mu+n, L\mu-Lm, Lm; L\mu; -\frac{2\mu(1+\kappa)}{\bar{\gamma}}, -\frac{2\mu(1+\kappa)}{\bar{\gamma}}\frac{m}{\mu\kappa+m}\right) \qquad \text{(B.13)}$$

and

$$\mathcal{I}_{3,i.i.d} = \frac{\vartheta^L}{n!} \sum_{k,l,j=0}^{\infty} \frac{(L\mu)_{j+k+l}(L\mu-Lm)_k(Lm)_l}{(L\mu)_{j+k}(1+n)_j} \frac{(u+n)_j}{k!l!j!}$$

$$\times \left(-\frac{\mu(1+\kappa)}{\bar{\gamma}}\right)^{k}\left(-\frac{\mu(1+\kappa)}{\bar{\gamma}}\frac{m}{\mu\kappa+m}\right)^{l}\left(\frac{1}{2}\right)^{j} \qquad \text{(B.14)}$$

Substituting $\mathcal{I}_{1,i.i.d}=1$, (B.13) and (B.14) in (A.17) and performing some mathematical manipulations, the exact form for $\bar{A}_{i.i.d}^{MRC}$ in Corollary 2 is the result.

# B.5 Derivation of $\bar{A}_{i.n.d}^{SLS}$ in (4.12)

As explained in Appendix A.5, the integral in (A.31) is applied on the second term only. Thus, by replacing (2.25) in (A.32) by (4.1), this yields

$$\Lambda_i = \frac{\mu_i{}^{\mu_i} m_i{}^{m_i} (1 + \kappa_i)^{\mu_i}}{\Gamma(\mu_i) \bar{\gamma}_i{}^{\mu_i} (\mu_i \kappa_i + m_i)^m}$$
$$\int_0^\infty \gamma_i^{n_i + \mu_i - 1} e^{-\frac{\mu_i(1+\kappa_i) + \bar{\gamma}_i}{\bar{\gamma}_i} \gamma_i} {}_1F_1\left(m_i; \mu_i; \frac{\mu_i^2 \kappa_i (1 + \kappa_i)}{(\mu_i \kappa_i + m_i) \bar{\gamma}_i} \gamma_i\right) d\gamma_i \quad \text{(B.15)}$$

The integral in (A.15) can be calculated by [163, eq. (3.35.1.2)] as follows

$$\Lambda_i = \frac{\mu_i{}^{\mu_i} m_i{}^{m_i} (1 + \kappa_i)^{\mu_i} (\mu_i)_{n_i}}{\bar{\gamma}_i{}^{\mu_i} (\mu_i \kappa_i + m_i)^m} \left(\frac{\bar{\gamma}_i}{(\mu_i(1 + \kappa_i) + \bar{\gamma}_i)}\right)^{n_i + \mu_i}$$
$$\times {}_2F_1\left(m_i, n_i + \mu_i; \mu_i; \frac{\mu_i^2 \kappa_i (1 + \kappa_i)}{(\mu_i \kappa_i + m_i)(\mu_i(1 + \kappa_i) + \bar{\gamma}_i)}\right) \quad \text{(B.16)}$$

Substituting (A.16) for $i = 1, ..., L$ in (A.29) and recalling [44, eq. (1.2.23)] to express ${}_2F_1(.)$ in series form, after some mathematical operations in a way similar to (A.34), yielding

$$\bar{\xi}_2 = \frac{2^u \Gamma(2Lu)}{u^{(L-1)} [\Gamma(1 + u)]^L} \left(\prod_{i=1}^L \frac{\mu_i{}^{\mu_i} m_i{}^{m_i} (1 + \kappa_i)^{\mu_i}}{(\mu_i(1 + \kappa_i) + \bar{\gamma}_i)^{\mu_i} (\mu_i \kappa_i + m_i)^{m_i}}\right) \sum_{n_1,...,n_L,l_1,...,l_{2L-1},j_1,...,j_L=0}^\infty$$
$$\frac{(2Lu)_{n_1+...+n_L+l_1+...+l_{2L-1}} (u)_{n_1+l_1}...(u)_{n_L+l_L} (\mu_1)_{n_1+j_1}...(\mu_L)_{n_L+j_L}}{(1 + u)_{n_1+l_1}...(1 + u)_{n_L+l_L} (u)_{n_1}...(u)_{n_L} (\mu_1)_{n_1}...(\mu_L)_{n_L} (1 + u)_{l_{L+1}}...(1 + u)_{l_{2L-1}}}$$
$$\times \frac{(u)_{l_{L+1}}...(u)_{l_{2L-1}} (m_1)_{j_1}...(m_L)_{j_L}}{(\mu_1)_{j_1} \cdots (\mu_L)_{j_L} n_1! \cdots n_L! l_1! \cdots l_{2L-1}! j_1! \cdots j_L!} \left(\frac{\bar{\gamma}_1}{\mu_1(1 + \kappa_1) + \bar{\gamma}_1}\right)^{n_1}$$
$$...\left(\frac{\bar{\gamma}_L}{\mu_L(1 + \kappa_L) + \bar{\gamma}_L}\right)^{n_L} \left(\frac{\mu_1^2 \kappa_1 (1 + \kappa_1)}{(\mu_1 \kappa_1 + m_1)(\mu_1(1 + \kappa_1) + \bar{\gamma}_1)}\right)^{j_1}$$
$$...\left(\frac{\mu_L^2 \kappa_L (1 + \kappa_L)}{(\mu_L \kappa_L + m_L)(\mu_L(1 + \kappa_L) + \bar{\gamma}_L)}\right)^{j_L} (-1)^{l_1}...(-1)^{l_{2L-1}} \quad \text{(B.17)}$$

With the aid of [44, pp. (1.4.21)], $\bar{\xi}_2$ can be expressed in exact representation which is substituted in (A.30) to give (4.12).

# Appendix C

# Proofs for Chapter 6

## C.1   Derivation of $\overline{P_d}^{MRC}(\lambda)$ in (6.22)

After substituting (6.7) and (6.21) into (3.1) with the aid of [146, eq. (4)] and $\int_0^\infty f_\gamma(\gamma)d\gamma \triangleq 1$, this yields

$$
\overline{P_d}^{MRC}(\lambda) = 1 - \frac{\lambda^u e^{-\frac{\lambda}{2}}}{2^u \Gamma(1+u)} \sum_{i_1=1}^{N_1} \cdots \sum_{i_L=1}^{N_L} \frac{\left( \prod_{j=1}^L \boldsymbol{\alpha}_{i_j} \Gamma(\beta_{i_j}) \right)}{\Gamma\left( \sum_{j=1}^L \beta_{i_j} \right)} \sum_{l=0}^\infty \sum_{m=0}^\infty \frac{(1)_l}{(1+u)_{l+m} l! m!}
$$

$$
\times \left( \frac{\lambda}{2} \right)^l \left( \frac{\lambda}{2} \right)^m \int_0^\infty \gamma^{m+\sum_{j=1}^L \beta_{i_j}-1} e^{-\gamma} \Phi_2^{(L)}\left( \beta_{i_1}, \cdots, \beta_{i_L}; \sum_{j=1}^L \beta_{i_j}; -\zeta_{i_1}\gamma, \cdots, -\zeta_{i_L}\gamma \right) d\gamma
$$

$$(\text{C.1})$$

The integral in (C.1) can be evaluated by [44, eq. (9.4.43)] as follows

$$
\overline{P_d}^{MRC}(\lambda) = 1 - \frac{\lambda^u e^{-\frac{\lambda}{2}}}{2^u \Gamma(1+u)} \sum_{i_1=1}^{N_1} \cdots \sum_{i_L=1}^{N_L} \frac{\left( \prod_{j=1}^L \boldsymbol{\alpha}_{i_j} \Gamma(\beta_{i_j}) \right)}{\Gamma\left( \sum_{j=1}^L \beta_{i_j} \right)} \sum_{l=0}^\infty \sum_{m=0}^\infty \frac{(1)_l}{(1+u)_{l+m} l! m!}
$$

$$
\times \left( \frac{\lambda}{2} \right)^l \left( \frac{\lambda}{2} \right)^m \Gamma\left( m + \sum_{j=1}^L \beta_{i_j} \right) F_D^{(L)}\left( m + \sum_{j=1}^L \beta_{i_j}, \beta_{i_1}, \cdots, \beta_{i_L}; \sum_{j=1}^L \beta_{i_j}; -\zeta_{i_1}, \cdots, -\zeta_{i_L} \right)
$$

$$(\text{C.2})$$

Recalling the identity $\Gamma(a+b) = (a)_b \Gamma(a)$ [44, eq. (1.2.3)] and [44, eq. (1.4.4)],

183

$\overline{P_d}^{MRC}(\lambda)$ becomes

$$\overline{P_d}^{MRC}(\lambda) = 1 - \frac{\lambda^u e^{-\frac{\lambda}{2}}}{2^u \Gamma(1+u)} \sum_{i_1=1}^{N_1} \cdots \sum_{i_L=1}^{N_L} \left( \prod_{j=1}^{L} \boldsymbol{\alpha}_{i_j} \Gamma(\beta_{i_j}) \right)$$

$$\sum_{n_1=0}^{\infty} \cdots \sum_{n_L=0}^{\infty} \sum_{l=0}^{\infty} \sum_{m=0}^{\infty} \frac{\left( m + \sum_{j=1}^{L} \beta_{i_j} \right)_{n_1+\cdots+n_L} (\beta_{i_1})_{n_1} \cdots (\beta_{i_L})_{n_L} (1)_l \left( \sum_{j=1}^{L} \beta_{i_j} \right)_m}{\left( \sum_{j=1}^{L} \beta_{i_j} \right)_{n_1+\cdots+n_L} (1+u)_{l+m} n_1! \cdots n_L! l! m!}$$

$$\times (-\zeta_{i_1})^{n_1} \cdots (-\zeta_{i_L})^{n_L} \left( \frac{\lambda}{2} \right)^l \left( \frac{\lambda}{2} \right)^m \qquad (C.3)$$

Invoking the identity $(a)_{b+c} = (a)_b (a+b)_c$ [44, eq. (1.2.9)], this yields

$$\overline{P_d}^{MRC}(\lambda) = 1 - \frac{\lambda^u e^{-\frac{\lambda}{2}}}{2^u \Gamma(1+u)} \sum_{i_1=1}^{N_1} \cdots \sum_{i_L=1}^{N_L} \left( \prod_{j=1}^{L} \boldsymbol{\alpha}_{i_j} \Gamma(\beta_{i_j}) \right)$$

$$\sum_{n_1=0}^{\infty} \cdots \sum_{n_L=0}^{\infty} \sum_{l=0}^{\infty} \sum_{m=0}^{\infty} \frac{\left( \sum_{j=1}^{L} \beta_{i_j} \right)_{n_1+\cdots+n_L+m} (\beta_{i_1})_{n_1} \cdots (\beta_{i_L})_{n_L} (1)_l}{\left( \sum_{j=1}^{L} \beta_{i_j} \right)_{n_1+\cdots+n_L} (1+u)_{l+m} n_1! \cdots n_L! l! m!}$$

$$\times (-\zeta_{i_1})^{n_1} \cdots (-\zeta_{i_L})^{n_L} \left( \frac{\lambda}{2} \right)^l \left( \frac{\lambda}{2} \right)^m \qquad (C.4)$$

Using [44, eq. (1.4.21)], the desired result in (6.22) is obtained.

## C.2   Derivation of $\bar{A}^{MRC}$ in (6.24)

By plugging (C.4) in (5.31), this yields

$$\bar{A}^{MRC} = 1 - \frac{1}{2^{2u} \Gamma(u) \Gamma(1+u)} \sum_{i_1=1}^{N_1} \cdots \sum_{i_L=1}^{N_L} \left( \prod_{j=1}^{L} \boldsymbol{\alpha}_{i_j} \Gamma(\beta_{i_j}) \right)$$

$$\sum_{n_1=0}^{\infty} \cdots \sum_{n_L=0}^{\infty} \sum_{l=0}^{\infty} \sum_{m=0}^{\infty} \frac{\left( \sum_{j=1}^{L} \beta_{i_j} \right)_{n_1+\cdots+n_L+m} (\beta_{i_1})_{n_1} \cdots (\beta_{i_L})_{n_L} (1)_l}{\left( \sum_{j=1}^{L} \beta_{i_j} \right)_{n_1+\cdots+n_L} (1+u)_{l+m} n_1! \cdots n_L! l! m!}$$

$$\times (-\zeta_{i_1})^{n_1} \cdots (-\zeta_{i_L})^{n_L} \left( \frac{1}{2} \right)^l \left( \frac{1}{2} \right)^m \int_0^{\infty} \lambda^{l+m+2u-1} e^{-\lambda} d\lambda \qquad (C.5)$$

With the help of [43, eq. (3.351.3)], the integral in (C.5) is calculated as follows

$$
\bar{A}^{MRC} = 1 - \frac{1}{2^{2u}\Gamma(u)\Gamma(1+u)} \sum_{i_1=1}^{N_1} \cdots \sum_{i_L=1}^{N_L} \left( \prod_{j=1}^{L} \boldsymbol{\alpha}_{i_j} \Gamma(\beta_{i_j}) \right)
$$

$$
\sum_{n_1=0}^{\infty} \cdots \sum_{n_L=0}^{\infty} \sum_{l=0}^{\infty} \sum_{m=0}^{\infty} \frac{\left( \sum_{j=1}^{L} \beta_{i_j} \right)_{n_1+\cdots+n_L+m} (\beta_{i_1})_{n_1} \cdots (\beta_{i_L})_{n_L} (1)_l}{\left( \sum_{j=1}^{L} \beta_{i_j} \right)_{n_1+\cdots+n_L} (1+u)_{l+m} n_1! \cdots n_L! l! m!}
$$

$$
\times \Gamma(l+m+2u)(-\zeta_{i_1})^{n_1} \cdots (-\zeta_{i_L})^{n_L} \left( \frac{1}{2} \right)^l \left( \frac{1}{2} \right)^m \tag{C.6}
$$

Using the identity $\Gamma(a+b) = (a)_b \Gamma(a)$ [44, eq. (1.2.3)], this yields

$$
\bar{A}^{MRC} = 1 - \frac{\Gamma(2u)}{2^{2u}\Gamma(u)\Gamma(1+u)} \sum_{i_1=1}^{N_1} \cdots \sum_{i_L=1}^{N_L} \left( \prod_{j=1}^{L} \boldsymbol{\alpha}_{i_j} \Gamma(\beta_{i_j}) \right)
$$

$$
\sum_{n_1=0}^{\infty} \cdots \sum_{n_L=0}^{\infty} \sum_{l=0}^{\infty} \sum_{m=0}^{\infty} \frac{\left( \sum_{j=1}^{L} \beta_{i_j} \right)_{n_1+\cdots+n_L+m} (2u)_{l+m} (\beta_{i_1})_{n_1} \cdots (\beta_{i_L})_{n_L} (1)_l}{\left( \sum_{j=1}^{L} \beta_{i_j} \right)_{n_1+\cdots+n_L} (1+u)_{l+m} n_1! \cdots n_L! l! m!}
$$

$$
\times (-\zeta_{i_1})^{n_1} \cdots (-\zeta_{i_L})^{n_L} \left( \frac{1}{2} \right)^l \left( \frac{1}{2} \right)^m \tag{C.7}
$$

By utilising [44, eq. (1.4.21)], the provided expression in (6.24) is deduced.